Advanced Regional Aircraft

Final Report

DSE group 13

Delft University of Technology

TU Delft

AQUILA

This page is intentionally left blank

Advanced Regional Aircraft

Final Report

by

DSE group 13

to obtain the degree of Bachelor of Science

at the Delft University of Technology

Group members:	P. Bijl	4492102
	R. Coenen	4378563
	B. Harrison	4556828
	B. van Manen	4549465
	R. Nelen	4533186
	S. Nolet	4535677
	E. Peeters	4547322
	T. Stolk	4488458
	M. Torsij	4533399
	V. Vloeberghs	4547144

Project duration: April 23, 2019 – July 5, 2019

Supervisor:	ir. J. Sinke,	TU Delft, tutor
	B. della Corte,	TU Delft, coach
	L. Laguarda Sanchez,	TU Delft, coach

Version	Purpose/Change	Responsibility	Date
0.1	Final draft	S. Nolet	25/06/2019
1.0	Final version	S. Nolet	02/07/2019

TU Delft AQUILA

Preface

"You cannot fly like an eagle with the wings of a mockingbird."

As global temperatures and sea levels are rising, the world comes to accept that we cannot continue on this road, that something has to change. The aviation industry on its own accounts for 2% of human induced CO_2 emissions and as this industry keeps on growing, that percentage is not likely to decrease with the current class of aircraft soaring through the skies. It is time then for a new type of aircraft, one that combines slender, strutted wings with advanced, innovative engines, to give aviation a new face. Project Aquila aims to be just that, and more. Because not only is the Aquila 60 the most sustainable regional aircraft to this day and for many years to come, it also has the potential of connecting more and smaller airports, thanks to its short take-off and landing distances. Aiming at low cost carriers that want to maximise the time the aircraft is in the air, the block time of the Aquila has been optimised. This, together with the demise of the hub-and-spoke system and the increasing demand for regional aircraft means that the Aquila 60 will not only be the most sustainable, but also economically the best option out there for low cost carriers.

As a team of ten aspiring engineers, we have worked hard over the last ten weeks to present the reader with, what we believe to be, the future of aviation. This report is the product of those ten challenging, but inspiring weeks that will no doubt be of great influence on all of us during the duration of our engineering careers.

This project would not have been possible without the help of some dedicated people. We would like to thank our mentor Jos Sinke for his commitment and support throughout the project. Furthermore, we want to express our gratitude to our tutors Biagio della Corte and Luis Laguarda Sanchez, for providing us with feedback and helping us with our analysis. Furthermore, we would like to thank A.H. Van Zuijlen, S.J. Hulshoff, E.J. van den Bos and A. Gangoli Rao, for their help. Finally, we want to thank everyone who supported us in any other way during the past ten weeks.

Team Aquila
Delft, June 2019

Executive Overview

After decades of aircraft innovation, the industry has converged to the typical conventional aircraft. Although this proven concept has shown its great potential, its limits in terms of efficiency are showing. This becomes evident in several of the many diverse aspects that the ever-growing aviation industry comprises of. One of these aspects is the high need for sustainable innovation, given that obsolete, polluting aircraft are still widely used. Because of this, a new design is required to satisfy this need. By using the latest technologies and integrate sustainability in the design process, it was believed the market for regional aircraft can be re-energised. This report explains the steps that were taken to develop this regional aircraft, using innovative technologies which will be more sustainable than current competitors: the Aquila 60.

Market Analysis

Around the world, the commercial aviation market is growing. The International Air transport Association (IATA) forecasts the passenger number could be doubled to 8.2 billion passengers by 2037. Due to this fast growth, lots of large airports are getting saturated. For airlines to bypass this problem, regional airports are to be connected. Another trend is the increase in popularity of low cost carriers, which thrive on keeping operational cost as low as possible, and therefore demand the most fuel efficient aircraft. In general, a threat to the aviation is the possible increase in environmental taxes. If these taxes are increased, ticket prices will rise, which then again increases the demand for a decrease in the emission of aircraft.

For turboprop aircraft, ATR holds the majority of the market, even though Bombardier's Q400 series has a higher cruise speed and lower cabin noise. Due to the lower unit cost and fuel efficiency, the ATR has driven Bombardier to give up on the turboprop market and put their focus on jet aircraft. The goal is to match the ATR 72 in terms of order size in the upcoming years: 630 aircraft by 2037. This will be done by using ATR's own strategy. The European market shows to be the most promising, with rapid expansion of the regional airports and regional routes.

Mission

The requirements for this mission were based on five stakeholders: airports, authorities, passengers, airlines, and the client: the manufacturer. The client itself provided the following requirements:

- The aircraft shall be designed using the latest technologies.
- The production factory of the aircraft shall be able to produce 5 aircraft per month, with an option to increase the production to 10 aircraft per month.
- The maximum take-off length at sea level for MTOW is set at 1400 m.
- The design range at maximum payload of the aircraft shall be 1850 km.
- The number of passengers shall be in the range of 60-65 passengers.
- The aircraft shall comply with noise and emission regulations.
- The aircraft shall have a 10% lower fuel burn on a 1000 km trip when compared to reference aircraft.
- The new aircraft shall be implementable within 8 years time.
- The aircraft shall include at least two innovations in its design.

The needs of the other stakeholders were satisfied by additional requirements, which can be found in the full report. The client indicated to have a preference for the smaller amount of passengers, which is why the passenger amount was set to 60. It was assumed that the optimal cruise Mach number for the turboprop engines would be 0.55 and therefore the optimum cruise altitude would be about 8000 m. Later, it was verified that this combination together with the full design was indeed optimal. Table 1 contains the top level mission characteristics from which the design was further worked out.

Table 1: Mission profile characteristics

Characteristic	Value	Unit
PAX	60	-
Range	1850	km
Cruise Mach	0.55	-
Cruise altitude	8000	m

Sustainable Development Strategy

Sustainability is becoming more and more important in recent years; therefore a sustainable development strategy was implemented throughout every part of the design. Aviation is responsible for 12% of the total CO_2 emissions of the transport sector and around 2% of total human induced CO_2[1]. This number is expected to increase, since aviation is a fast growing industry. The design team decided to focus on several types of sustainability to achieve the maximum impact this design can make on a more sustainable world.

In terms of environmental sustainability, the goal of this design was to improve the fuel efficiency and reduce emissions, to show that regional aviation can comply with the Paris accords in the near future. Additionally, the focus of the noise emissions was to reduce noise levels under all circumstances with respect to reference aircraft. The main focus of sustainability in production was the reduction of emissions and negating the use of dangerous chemicals. Finally, it was the goal of the design team to achieve at least 85% recyclability of the aircraft. Improvements on this can primarily be gained by making the traditionally non recyclable parts of the aircraft more recyclable, such as the furnishings and carbon composites.

Environmental economic and social sustainability come together with practical sustainability. It is important for the project to be economically viable, but it also needs to be socially and environmentally sustainable. By balancing these three factors, maximum impact on sustainability in the regional aviation market can be achieved.

Design Characteristics

With the requirements and mission characteristics known, the aircraft was designed. The sizing and design of all the relevant subsystems have been described below to provide some insight in the design process.

Aerodynamic Wing Characteristics

The required surface area of the wing was determined by means of a wing-loading diagram. With the cruise speed of the aircraft set at Mach 0.55, at an cruise altitude of 8000 m, the available design space was rather limited. The optimal point in the diagram corresponds with a design wing-loading of 3,625 N/m2, which results in a required wing surface area of 49.21 m^2.

The aspect ratio of a wing has a significant influence on the aerodynamic efficiency of an aircraft, which is the reason a high aspect ratio was chosen for this design in the first place. A strut was introduced to account for the structural drawback of a slender wing. 'The aspect ratio of the wing has a significant influence on the aerodynamic efficiency of an aircraft, as a large aspect ratio greatly reduces the lift induced drag of the wing. For this reason, a long, slender wing was chosen. This results in a wing span of 31.37 m, excluding any wingtip devices and 32.65 m including the raked wingtips. The taper ratio mainly affects the lift distribution and the stall characteristics. The most optimal lift distribution, i.e. as close as possible to an elliptical one, can be achieved with a taper ratio of 0.4 [1]. Sweep was not introduced, given that the aircraft has a design cruise speed of Mach 0.55. A small dihedral angle of 1° was applied to the wing to increase the stability in case of wing gusts and unwanted motions.

A wing profile was chosen by taking into account the lift-over-drag ratio, drag bucket, and angle of attack at which stall occurs. The root airfoil was chosen to be NACA 4415 and the tip airfoil was selected to be NACA 4412. The most important advantage of these profiles is their low drag at cruise conditions for a lift

[1] Retrieved from https://www.sustainableaviation.co.uk/ (consulted on 24/04/2019).

coefficient of approximately 0.5. A twist angle of 2 degrees was applied to the wing in order to prevent tip stall.

For the high lift devices, single Fowler flaps were chosen because they can provide a high δC_L, while remaining relatively simple. No slats are used since the δC_L required can be obtained with flaps, and slats add weight and complexity to the wing design. Using computational fluid dynamics (CFD) in ANSYS Fluent, raked wingtips were found to increase the L/D the most of the devices that are currently used in the industry. Table 2 shows an overview of the design parameters of the wing.

Table 2: Final Design Parameters of the Wing

Parameter	**Symbol**	**Value**	**Unit**
Surface Area	S	49.21	m^2
Root Chord	c_r	2.24	m
Tip Chord	c_t	0.90	m
Mean Aerodynamic Chord	MAC	1.66	m
Taper Ratio	λ	0.4	-
Span	b	32.65	m
Quarter Chord Sweep	$\Lambda_{c/4}$	0	deg
Dihedral	Γ	1	deg
Twist	ϕ	-2	deg

Empennage Design

The empennage consists of the horizontal tail and the vertical tail. The purpose of the horizontal tail is to provide longitudinal stability and control, while the vertical tail provides lateral stability and control. By using a scissor plot the horizontal tail was sized. This plot takes into account the boundaries for stability and controllability, as well as the c.g. range, as shown in Figure 1.

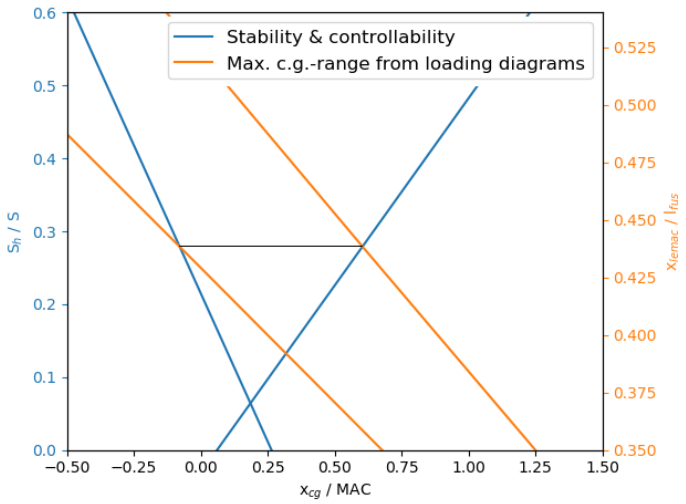

Figure 1: Scissor Plot

A dorsal fin was introduced to stabilise the flow causing a low pressure region over the vertical tail, which increases the stall angle for the vertical tail. The horizontal tail must lie outside of the wake of the main wing. As a high wing configuration was chosen for the main wing, this results in a T-tail configuration at the tail.

Material Characteristics

Over the years, weight reduction of aircraft has been achieved by applying new, advanced materials and improving on the production processes. Using composite material allows a significant weight reduction, but introduces an increase in cost of both the material and production. In the long term, this may be countered by the savings in fuel as a result of the weight reduction. When looking at metals, the third generation of Al-Li alloys offers significant weight savings with respect to older aluminium alloys, while having none of the disadvantages of composites, e.g. complex failure prediction or poor recyclability.

The weight and cost difference for the structures was the basis for the ultimate decision per component, while taking the advantages and disadvantages of the considered materials into account. Therefore, alloys from the third generation Al-Li alloys were selected for the wing box and fuselage. The strut was made out of quasi isotropic carbon-fibre-reinforced-polymer, because of its superior stiffness.

Structural Characteristics

Three components of the aircraft were subjected to a structural analysis: the fuselage, the wing box, and the strut. During the structural analyses, failure modes related to both materials and structures were considered.

Wing Box Characteristics

The wing was analysed first, which resulted in a wing box stiffened by hat stiffeners on the upper skin and Z-stiffeners on the lower skin. Using composites for the wing box would result in a weight reduction of 15% with respect to Al-Li alloys, which reduced the fuel weight by 1%. However, the cost would increase by a factor 19. Taking into account the disadvantages of using composite material, such as the poor recyclability, it was decided to use the latest generation of Al-Li alloys instead, resulting in the parameters as shown in Table 3 per wing box, with the skin thickness constant throughout the span of the wing.

Table 3: Wing box parameters

Skin material	AA2055-T84
Stiffener material	AA2099-T83
Amount of stiffeners	24
Amount of ribs	10
Skin thickness [mm]	3.7
Weight [kg]	553.4
Cost [USD]	2,105.87

Strut Design

The structural part of the strut will have a circular shape in order to transfer the loads as efficiently as possible. To improve manufacturability and the ability to fit an airfoil around the strut, the strut was designed hollow. The outer diameter will be 80 mm and the inner diameter will be 69.2 mm. Similar to the wing, a box will transfer the loads to the fuselage. This box was placed below the floor and attached to the fuselage at two points.

The effect of using a strut becomes evident when looking at Table 4. To counter for these increase in stresses when the strut is removed, reinforcing the wing box configuration would result in a weight increase of 517%.

Table 4: Ultimate stresses along the wing box.

Parameter	**Value with strut**	**Value without strut**	**Unit**
Tensile stress	445.4	936.6	MPa
Compressive stress	-422.9	-841.7	MPa
Shear stress	179.3	170.7	MPa
Von Mises stress	345.8	810.9	MPa

Fuselage Characteristics

The pressure inside the cabin will be equivalent to the pressure at 1800 m (81200 Pa), which is a relatively high pressure, to increase passenger comfort. By including a safety factor, the skin thickness of the fuselage was set at 1.6 mm and is made of AA2060-T8E30, a third generation Al-Li alloy. In terms of corrosion resistance this alloy outperforms previous generations, having a 140% increase in corrosion resistance with respect to the AA2024-T351[2].

Propulsion System Design

One of the goals of the aircraft was to design it with sustainability and fuel efficiency in mind. To choose an engine three engines were analysed, by calculating their fuel efficiency if they were to use methane as fuel by using the real Brayton cycle. The GE T6E was selected, since it offered the best compromise between power and weight and had the best fuel consumption characteristics.

To let the engine run on LNG, some modifications were made. By using high heat resistant materials for the turbine blades, the temperature at the turbine can be increased. To mitigate potential incomplete combustion catalysts and swirl flameholders were used. This has the effect of lower NO_x emissions and increase the percentage of combusted LNG.

Fuel System

Each wing was provided with a detachable fuel tank, suspended beneath the wing. The total fuel stored for a normal mission profile is 1967 kg, so each fuel tank will be designed to carry 1000 kg of LNG, with the surplus amount to account for trapped fuel. To store the LNG at cryogenic temperatures, a vacuum insulated tank was chosen for the design, because of its superior insulation, which allowed for a lighter design. Furthermore, the tank is not susceptible to fuel sloshing effects, is able to contain the fuel and the evaporated gasses up to 5 days, and allows for simple operation. In order to transfer the fuel into the fuel system, the fuel is pumped out of the tank using booster pumps, of which two are located at each fuel tank. This fuel feeding systems delivers the appropriate amount of LNG to the engines. It was found to be more complex for this aircraft than for a conventional aircraft, as it deals with cryogenic liquids and high pressure gasses. So a more extensive analysis has been performed to make sure a viable and implementable design was made. Naturally, the design includes a backup system with cross-feed capability.

Operations

For airlines, flexibility during loading is the key to a short turnaround time and thus high efficiency of aircraft use. Hence, the aircraft is designed to allow for loading in any order; that is, it does not matter whether passengers board first, or cargo is loaded before the passengers. The same holds for the attachment of the fuel tanks, which can theoretically happen at any moment during the turnaround, even when passengers are on board. However, in terms of safety this requires the refuelling equipment to be placed outside possible emergency exit routes. The additional flexibility in this design is in particular interesting for low cost carriers, which are expected to be the primary customers of the aircraft.

Regarding the operations and logistics of LNG, it is already being produced on a large scale and the production is still increasing, with more and more LNG being used for road vehicles, ships and for power generation. The infrastructure for LNG distribution is already present in a large part of the world, but is mainly focused on ports and terminals that are near the sea. Some airports, such as Brussels Airport and Schiphol Airport also offer LNG fuelled transport busses. These facilities could be used to store LNG for LNG powered aircraft.

In conclusion, the minimal turnaround time of the Aquila comes at just under 20 minutes; this is the case when boarding processes takes place via both doors, both fuel tanks can be replaced simultaneously and the cabin replenishment is finished within 12 minutes. This results in a short turnaround time and therefore improves its competitiveness on the regional aviation market.

[2] Retrieved from: https://www.constellium.com/sites/default/files/markets/airware_2198_t8_fuselage_sheet.pdf (consulted on 18-6-2019)

Design Analysis

In order to verify that the design met all the requirements a design analysis was made. If a certain subsystem failed to meet a requirement it would be redesigned and the performance would be checked again.

Mass Budget Breakdown

Figure 2 shows the resource allocation of the maximum take-off mass of the aircraft. As visible in Figure 7.1, most of the mass is allocated to the operational mass weight. The rest of the maximum take-off mass was allocated to the payload and fuel. The payload consists of 60 passengers including their luggage. A value of 105 kg per passenger was used to estimate this value. The fuel mass was determined by calculating the amount of fuel needed for the design range of 1850 km. Adding these weights brings the MTOM of the aircraft at 18,536 kg, as shown in Figure 3.

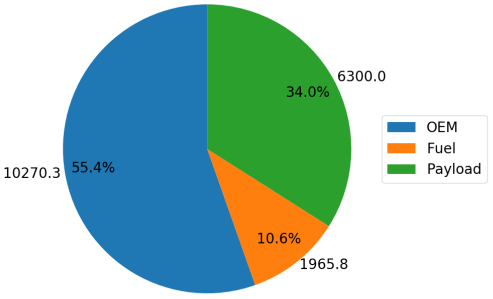

Figure 2: Masses as percentage of MTOM

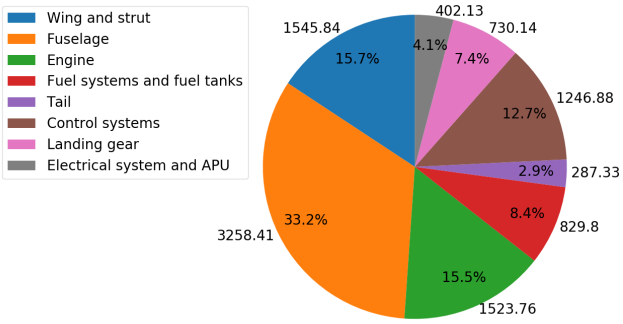

Figure 3: Component masses as percentage of empty mass

Performance Analysis

Both the ground and flight performance were assessed. The ground performance consists of the manoeuvrability of the aircraft on the ground. A low turning radius allows the aircraft to be manoeuvrable at small, narrow runways, which is why the nose landing gear is able to turn with a maximum angle of 70 degrees. The take-off field length (TOFL) was calculated to be 1213 m at sea-level, while the landing field length for maximum landing weight was found to be 1083 m. Only after altitudes higher than 1220 m, the requirement for a maximum TOFL of 1400 m was no longer satisfied.

The payload range diagram for the mission was plotted as shown in Figure 4. The design point is indicated with the dotted line that corresponds with 60 passengers for a range of 1850 km. When flying at maximum payload, i.e. including 300 kg cargo, the range decreases to 1281 km, while the ferry range of the aircraft is 4112 km.

When combining the manoeuvring envelope and the gust envelope and implementing the stall limit, the service flight envelope was determined as displayed in Figure 5. The full line basically shows the total limits in which the aircraft can operate. Outside these limits, hazards such as stall and structural failure are more likely to occur.

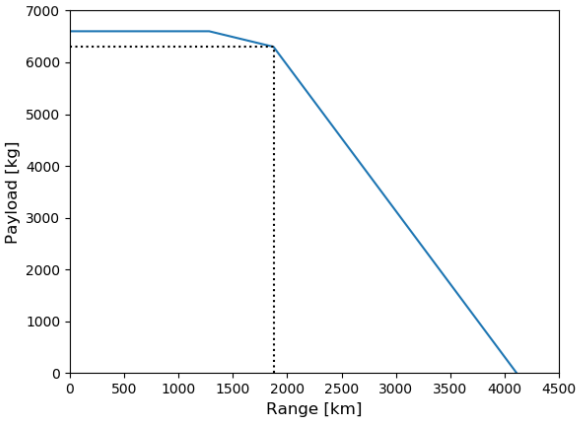

Figure 4: Payload-Range Diagram

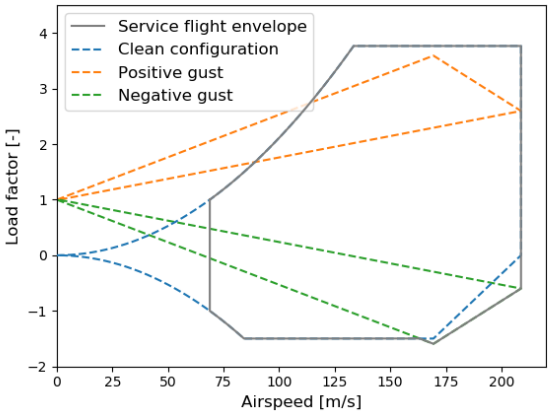

Figure 5: Service flight envelope

Noise and Emission

One of the requirements of Aquila was to comply with the noise regulations that are set by the International Civil Aviation Organization or ICAO for short. The goal was to not only meet these requirements, but to improve on them, thereby beating the competition. By taking into account both the noise generated by the airframe and engine, the Aquila shows to be more silent in every category, as shown in Table 5. These results were obtained by using a method from NASA and JPL for noise estimation [2] [3]

Table 5: Maximum noise of the Aquila and the ATR 72

Situation	**Aquila**	**ATR 72**
Lateral [EPNdB]	71.1	73.1
Approach [EPNdB]	85.8	89.1
Fly-over [EPNdB]	72.9	73.5

To estimate the impact in terms of greenhouse gas emissions both LNG and kerosene were considered. An overview of the emissions for the two types of fuel that were considered has been provided in Table 6, from which the benefits of using LNG in terms of emission become evident.

Table 6: Emissions of CO_2 and NO_x for kerosene and LNG [2, 3]

Parameter	**Aquila (LNG)**	**ATR 72 (Kerosene)**
CO_2 (kg/kg fuel)	2.75	3.00
NO_x (kg/kg fuel)	0.001	0.003
Fuel used (kg/1000 km flight)	1494.1	2159.0
CO_2 (kg/1000 km flight)	4108.7	6477.0
NO_x (kg/1000 km flight)	1.5	6.5
CO_2 (kg/pax/1000 km flight)	68.5	83.0
NO_x (kg/pax/ 1000 km flight)	0.025	0.108

Sensitivity Analysis

In the sensitivity analysis, three outputs were analysed as a result of a change in number of passengers and design range, as shown in Figure 6 and Figure 7. An increase in the amount of passengers would result in the design still outperforming the ATR 72 in terms on sustainability, although the TOFL would be increased

[2] Retrieved from: https://www.engineeringtoolbox.com/co2-emission-fuels-d_1085.html (Consulted on 21/06/2019)
[3] Retrieved from: https://www.engineeringtoolbox.com/nox-emission-combustion-fuels-d_1086.html (Consulted on 21/06/2019)

by almost 20%. Decreasing the number of passengers would allow the aircraft to be operable at even smaller airports. Although, inevitably, the fuel efficiency would go down in terms of fuel burned per passenger. Figure 7.21 shows that the sensitivity of the outputs when varying the range is minimal. The most sensitive output is the TOFL, which still only is increased by 4%, or 50 meters. The OEM and fuel burned per passenger show almost no variation by a change in the design range. From this analysis, it can be concluded that adapting the design range would require a minimal amount of redesigning, based on the varied inputs.

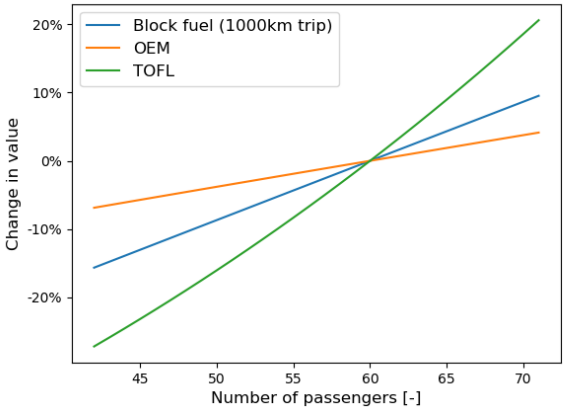

Figure 6: Sensitivity analysis of the number of passengers

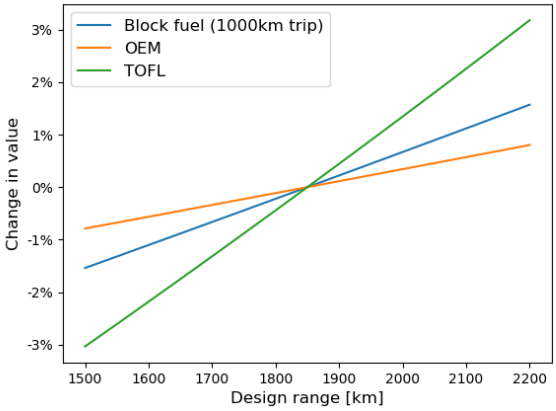

Figure 7: Sensitivity analysis of the design range

RAMS Analysis

The biggest challenge for Aquila in terms of reliability results from the fact that for several systems there exists few to no technical experience at this point. These systems are mainly the fuel system, the high aspect ratio wing and the strut. The Aquila was designed to be in-service for at least 300 days a year, with a block time on a 1000 km mission of 2.17 hours. This comes down to flying up to 5 times a day, which results in a total amount of 1500 flight cycles a year. If the airline chooses to operate the aircraft over shorter distances, the amount of daily flight cycles will increase accordingly. In order to make these processes as efficient as possible, the maintainability aspect was kept in mind during the design phase of Aquila.

Production Plan

The production of Aquila is of key importance to the client. It is required that 5 Aquila aircraft will be produced each month, with an option to increase the production rate to 10 aircraft a month. For the manufacturing of components, additive manufacturing will be used to decrease weight and cost for heavy components that are only used in small quantities. As for the majority of the parts metal alloys are used, conventional tools can be widely used.

In order to reach the break-even point sooner, there are two ways to increase the production: more assembly lines can be created or the same assembly line can be used for more hours during the day. Since the original assembly line is not used throughout the whole day, the design team opted for increasing the number of shifts to two shifts a day to increase production. While increasing the amount of shifts is the easiest solution to increasing the production rate it also makes the main bottleneck of production worse, which is finding extra people to fill the extra man-hours. A way to solve this is to increase the wages of the employees or by promoting working at the company through the use of ads. Subcontractors are also used so it should be investigated if they can also increase the production of the parts that they produce. If these bottlenecks can be solved, the increase of production rate should not meet significant obstacles and the break-even-point can be reached sooner.

Financial Analysis

Besides defining the next advancement in regional aircraft, the Aquila project also aims at making a profit. Based on the prices of the direct competitors that are manufactured by ATR and Bombardier, a regression of the price versus number of passengers resulted in a retail price 24.5 million USD, which is about 2 million USD less than the ATR 72-600. Ultimately, when selling 630 aircraft, this would result in an ROI of 13% for the manufacturer. In terms of direct operational cost (DOC), the Aquila showed to be 15% cheaper. Even if the ATR brings 12 more passengers, the Aquila is cheaper in DOC per passenger.

Sustainability and Risk Assessment

The sustainability was analysed and compared to the main competitor: the ATR 72. By being able to use recycled materials, the environmental impact of the Aquila in terms of CO_2 emission during production is 20% of the ATR's, which is mainly due to the fact that less composites are used. When the aircraft is in operation, the total environmental impact of the Aquila is 36.5% less in CO_2 emission, and 76.9% less in NO_x emission. As most of the aircraft is made out of aluminium, it is relatively easy to recycle. In order to visualise the improvements of the Aquila with respect to the ATR, a spider diagram was made as shown in Figure 8. Here, both aircraft were scored on several aspects from 1 to 5, with 1 being the lowest score in the center point of the diagram. Throughout the project, risks have been assessed per subject and mitigation was conducted on those that showed to be most significant.

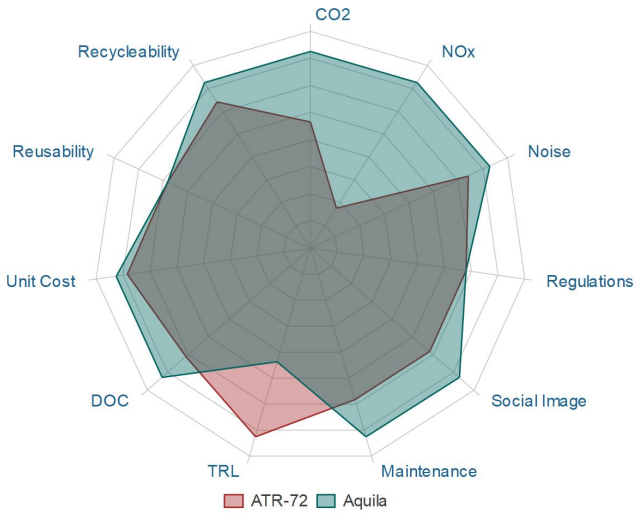

Figure 8: Spider diagram of the sustainability comparison between the ATR 72 and the Aquila

Future Development

Upon completion of the DSE project, the aircraft will not be ready to fly yet; a large team of engineers will be employed to complete these last steps. The main design phase is expected to be closed in March 2021. At the same time the existing production facilities need to be prepared to build five complete test aircraft. The production of these aircraft is estimated to take 3.5 years and needs to be done in parallel with building the production facilities for normal production. The aircraft production facilities for the large-scale production need to meet the requirements for production facilities, as stated in CS 21 (subpart G). Setting up these permanent facilities was estimated to take two years. Before the production of aircraft can start, a manufacturer is required to obtain a Production Certificate. In case of Aquila, this is issued by EASA and follows the guidelines as outlined in CS-21. The certification process of the entire aircraft is estimated to last from 2023 until the start of 2027. The first aircraft for normal operations is expected for late 2025.

Conclusion and Recommendations

Findings throughout the report suggest the Aquila is able to form serious competition for current competitors in regional aviation. The adaptability needs to be further evaluated, considering regional airports might have been built in landscapes at high altitudes or limited runway lengths. A more elaborate flutter analysis will also have to be performed, as the used method did not provide conclusive answers. To implement LNG, airports will have to be motivated and supported to create the suited environment for it, while new engines should also be designed to optimise its use for the aviation industry. To reduce the carbon footprint of this project even further, biomethane can be potentially be used as fuel. In conclusion, the Aquila was found to be a possible foundation to make aviation fit in the environmental friendly future that the world is yearning for.

Contents

List of Abbreviations

Abbreviation	Meaning
APU	Auxiliary Power Unit
AR	Aspect Ratio
ATC	Air Traffic Control
c.g.	Centre of Gravity
CAD	Computer-Aided Design
CASK	Cost per Available Seat Kilometer
CFD	Computational Fluid Dynamics
DOC	Direct Operational Costs
EHA	Electro-Hydrostatic Actuators
ELT	Emergency Location Transmitter
EMA	Electro-Mechanical Actuators
EOL	End-Of-Life
HA	Hydraulic Actuators
ICAO	International Civil Aviation Organization
ILS	Instrument Landing System
LCC	Life Cycle Cost
LEMAC	Leading Edge of the Mean Aerodynamic Chord
LFL	Landing Field Length
LNG	Liquid Natural Gas
MAC	Mean Aerodynamic Chord
MLG	Main Landing Gear
MLW	Maximum Landing Weight
MTOM	Maximum Take-Off Mass
MTOW	Maximum Take-Off Weight
NLG	Nose Landing Gear
OEM	Operational Empty Mass
OEW	Operational Empty Weight
RAMS	Reliability, Availability, Maintainability and Safety
RDTE	Research Development Testing and Evaluation
ROI	Return on Investment
SATCOM	Satellite Communication
SFC	Specific Fuel Consumption
TCAS	Traffic Collision Avoidance System
TOFL	Take-Off Field Length
UHF	Ultra High Frequency
USD	United States Dollar
VHF	Very High Frequency

List of Symbols

Symbol	Meaning	Unit
A	Aspect Ratio	-
a	Acceleration	m/s^2
b	Wing Span	m
C	Buckling Coefficient	-
C_D	Drag Coefficient	-
C_{D_0}	Zero-Lift Drag Coefficient	-
C_L	Lift Coefficient	-
C_l	Rolling Moment Coefficient	-
C_{l_a}	Lift Curve Slope	rad^{-1}
C_p	Pressure Coefficient	-
c	Chord Length	m
c_j	Specific fuel consumption of a jet engine	-
c_p	Specific fuel consumption of a propeller engine	-
D	Drag	N
D	Diameter	m
E	Endurance	s
E	Young's Modulus	Pa
e	Oswald Efficiency Factor	-
F	Force	N
f	Fuel Fraction	-
G	Modulus of Rigidity	Pa
H	Altitude	m
h	Height	m
I	Moment of Inertia	m^4
J	Torsional Constant	m^4
K_θ	Torsional Stiffness	Nm/rad
L	Lift	N

Symbol	Meaning	Unit
M	Mach Number	-
M	Moment	N/m
m	Mass	kg
n	Load Factor	-
P	Power	W
p	Pressure	Pa
p	Roll Rate	rad/s
Q	First Moment of Area	m^3
Q	The Q-criterion	s^{-2}
q	Dynamic Pressure	Pa
q	Shear Flow	N/m
R	Radius	m
R	Range	m
R	Reaction Force	N
Re	Reynolds Number	-
S	Wing Area	m^2
S	Rate-of-Strain	s^{-1}
s	Length	m
T	Temperature	K
T	Thrust	N
t	Thickness	m
V	Shear Force	N
V	Speed	m/s
V_C	Cruise Speed	m/s
V_D	Diving Speed	m/s
V_S	Stall Speed	m/s
v	Deflection	m
v	Poisson's Ratio	-
W	Weight	N

Greek Symbol	Meaning	Unit
α	Angle of Attack	-
Γ	Dihedral Angle	deg
γ	Path Angle	deg
γ	Specific Heat Ratio	-
δ	Deflection Angle	deg
ϵ	Downwash Angle	deg
θ	Angle	deg
Λ	Sweep Angle	deg
λ	Taper Ratio	-
λ	Temperature Lapse Rate	-
μ	Friction Coefficient	-
ρ	Density	kg/m^3
σ	Stress	Pa
τ	Effectiveness Factor	-
τ	Shear Stress	Pa
ϕ	Roll Angle	deg
ϕ	Angle of Twist	deg
Ω	Vorticity	s^{-1}

Subscript	Meaning
∞	Free Stream
0	At Sea-Level
A	Aircraft
A	Approach
a	Aileron
ac	Aerodynamic Center
c	Chord
cg	Center of Gravity
cr	Critical Value
dA	Approach
E	Elevator
F	Fin
g	Ground
h	Horizontal Tail
MAC	Mean Aerodynamic Chord
r	Root
r	Rudder
T	Touch Down
TO	Take-Off
t	Tip
v	Vertical Tail

1 Introduction

The end of the Airbus A380 production proved to be a turning point in the aviation industry: the hub-and-spoke system is becoming more and more obsolete. In the future, the demand for point-to-point transport will grow significantly. Considering intracontinental aviation, flights between two remote airports are carried out by regional aircraft. Currently, the regional turboprop market is dominated by the newly upgraded ATR 72-600. This aircraft is the most fuel efficient in its class. While this aircraft is a great step forward in terms of sustainability, the carbon footprint of the regional aviation industry is still growing.

After decades of aircraft innovation, the industry has clearly converged to the typical conventional aircraft. This proven concept has shown its great potential, but also its limits in terms of fuel efficiency. A new, more sustainable configuration is needed to push the boundaries of both cost and sustainable efficiency. Current aircraft manufacturers need to be encouraged to envision and embrace it.

This report was part of the Design Synthesis Exercise for the Bachelor's Degree in Aerospace Engineering at Delft University of Technology. The aim of this report is to show the steps taken in the design of an advanced regional aircraft for an aircraft manufacturer. The client provided several requirements, on which the design was ultimately based. Following these requirements, the Mission Need Statement was set up: *To develop a regional aircraft using innovative technologies which will be more sustainable than current competitors.* With the given constraints and requirements, a trade-off was performed to design an aircraft that is able to comply with all these requirements.

An extensive research was performed to come up with an innovative concept, resulting in the Aquila. With the addition of a strut, the wings are allowed to be long and slender, heavily reducing the lift-induced drag. This in itself increases the fuel efficiency, but in order for Aquila to be even more sustainable, this configuration was combined with an innovative fuel for aircraft: Liquid Natural Gas (LNG) for turboprop engines. This new type of aviation fuel has already proven itself in a variety of industries and using this fuel for aircraft could be a breakthrough in CO_2 and NO_x emissions produced by the aviation industry.

To meet the market demand, a market analysis was performed in chapter 2. Based on this market analysis and the requirements set by the client, a detailed mission analysis was carried out as a baseline for the design, which is presented in chapter 3. Since sustainability was found to be of great importance, a sustainable development strategy was developed. Together with the risks that are present with an innovative design, this is reported in chapter 4. Taking all these factors into account, the aircraft was designed. The complete design process can be found in chapter 5. Furthermore, a new design comes with new operational activities, which are then elaborated on in chapter 6. Next, a complete analysis of the aircraft is presented in chapter 7. This includes a resource allocation, performance analysis, sensitivity analysis and a RAMS analysis. The production of the aircraft was assessed in chapter 8. After all technical aspects of the aircraft are outlined, the financial analysis was performed in chapter 9. This includes return on investment, as well as a cost breakdown. After the financial analysis, an assessment of all risks and sustainability measures is given in chapter 10. In chapter 11, the compliance matrix is given. In this chapter, all requirements were checked whether they are met or not by the design. If requirements were found to be not met, an elaboration or a recommended change is given. The future project development and timeline are given in chapter 12, which includes future certification and production procedures. Finally, a conclusion of the report is given with recommendations for further project and design development.

2
Market Analysis

With more and more people using aircraft as a means of transportation all over the world, the large airports are becoming overcrowded. Because of this, the general focus is shifting more towards the airports that are often under-served: the regional airports. While aircraft manufacturers nowadays tend to focus on building aircraft that have a capacity of at least 70 seats, the regional routes are operated by older aircraft which entered service during the 1980's and 1990's. In this chapter, the opportunity to re-energise this market was investigated, starting with the trends in regional aviation in section 2.1. Subsequently, section 2.2 discusses the competition that Aquila is dealing with, followed by the found opportunities in section 2.3. Finally, the stakeholders are identified in section 2.4.

2.1. Regional Aviation Trends

Around the world, the market for commercial aviation is growing. The International Air Transport Association (IATA) forecasts the passenger number could double to 8.2 billion passengers by 2037[1]. This increase is mainly driven by the new passengers that the Asia-Pacific region will provide, where China will even displace the United States as largest aviation market around the world. Due to this increase in popularity for commercial aviation, the infrastructure of the industry is facing the challenge of handling such growth[2]. Another trend that is evident when considering the global aviation industry, is the increase of passenger capacity per aircraft. Both these trends will be discussed more elaborately in this section.

Airport Saturation

Due to the fast growth of the industry, many airports will experience difficulties at keeping up with the growth in demand. Lots of large airports, especially in Europe, are getting saturated. One of the reasons for this is that at some of the airports the runways are operating almost at the max of their capacity for most of the time. One example for this is Heathrow, which is largest airport for passenger traffic in Europe[3]. By 2030, the twenty largest European airports are expected to be fully saturated[4]. This trend is not only noticed in Europe, but also in the rest of the world, for example in India [4]. One way for airports to cope with this is increasing their operating prices, possibly resulting in higher ticket prices for the passengers. To bypass this problem and in general relieve the bigger, international airports, airlines are likely to connect the smaller, regional airports.

Increasing number of passengers

According to a forecast by Bombardier of 2016, the global 60-150 seat segment will increase from 6,900 aircraft to 14,250 aircraft by 2036 [5]. One of the reasons for this is that many regional old low-seat aircraft are to be replaced by new, higher-seat aircraft. This allows to reduce the cost per seat for the airline. Therefore, newer, bigger aircraft are appealing for low cost carriers. However, larger aircraft can usually not be operated

[1] Retrieved from: https://www.iata.org/pressroom/pr/Pages/2018-10-24-02.aspx (consulted on 20-6-2019)

[2] Retrieved from: https://aci.aero/news/2019/01/31/major-investments-in-airport-infrastructure-vital-to-meeting-future-travel-demand/ (consulted on 20-6-2019)

[3] Retrieved from https://www.itf-oecd.org/sites/default/files/docs/expanding-airport-capacity-competition-connectivity-gatwickheathrow.pdf (consulted on 20-6-2019)

[4] Retrieved from: https://centreforaviation.com/analysis/reports/20-european-airports-to-be-saturated-by-2030---eurocontrol-4309 (consulted on 20-6-2019)

in regional airports, limiting their operability.

2.2. Competition

In regional aviation, both turboprop and jet aircraft are used. Currently, North America is dominated by regional jet aircraft. Operating in a hub-and-spoke network, these aircraft often fly relatively large distances in comparison with for example Europe, which is why jet aircraft are preferred[5]. Turboprop aircraft are usually operated at a lower altitude and airspeed, which is why they are preferred in a dense network, like Europe's.

For small regional aircraft up to 60 passengers, the jet aircraft CRJ100 and ERJ145 of Bombardier and Embraer respectively are the most popular designs, having a market share of 39% and 31% respectively in North and South America. Together with the ATR 42 series and Saab 340 they make up the majority of the European market for small regional aircraft, as shown in Figure 2.1.

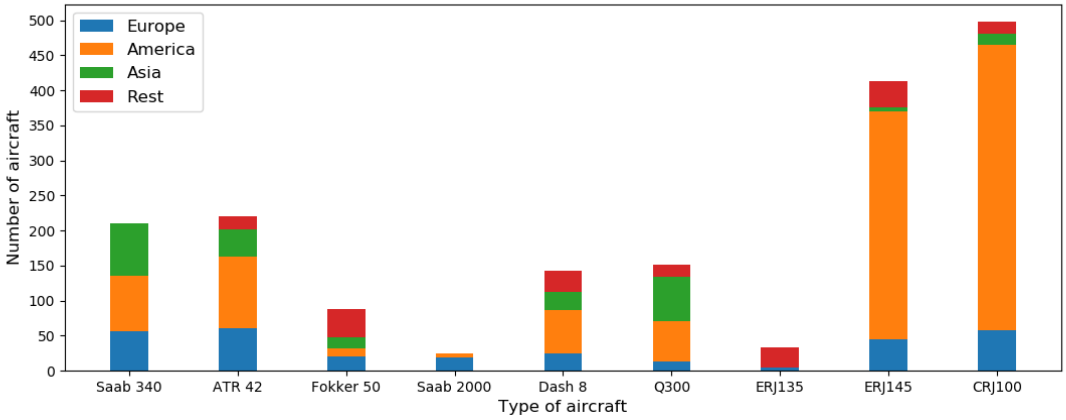

Figure 2.1: The market for regional aircraft up to 60 passengers

When considering aircraft up to 100 passengers, the same manufacturers hold the majority of the market. The Embraer ERJ170, ERJ175 and ERJ190 hold 47% of the regional market share, followed by Bombardier's CRJ700, CRJ900, CRJ1000, and Q400-series holding 45%. The ATR only holds about 7% of the market in America. In Asia, the ATR 72 is particularly popular, holding 50% of the market there on its own. These numbers are summarised and displayed in Figure 2.2.

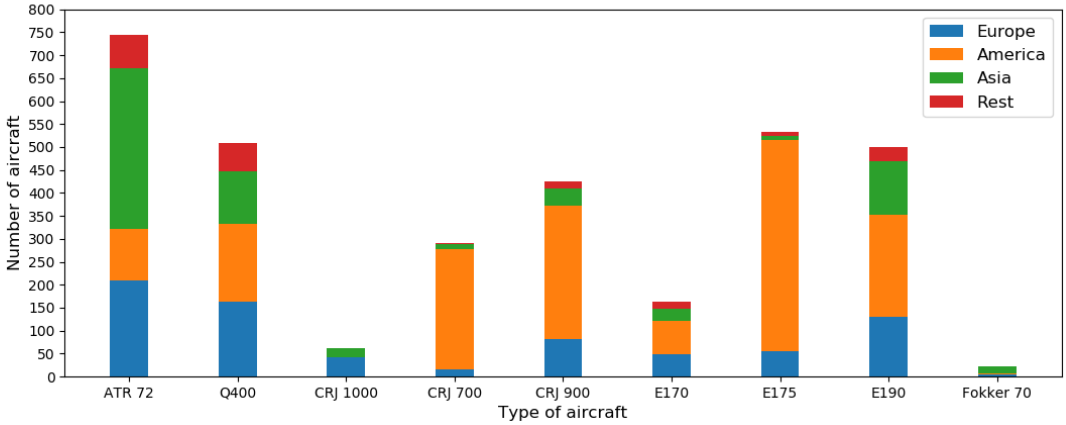

Figure 2.2: The market for regional aircraft up to 100 passengers

[5]Retrieved from: https://science.howstuffworks.com/transport/flight/modern/airline3.htm (consulted on 20-6-2019)

For turboprop aircraft specifically, the market is as shown in Figure 2.3, according to data from the World Airliner Directory [6]. ATR holds the majority of the market, even though Bombardier's Q400 has a higher cruise speed and lower cabin noise. This is due to the ATR's lower unit cost and better fuel efficiency, which has led to Bombardier to get out of the turboprop market and hand over the Q400 to the Longview Aviation Capital Corp[6]. A result from this is that the Q400 is expected to leave a gap in the market.

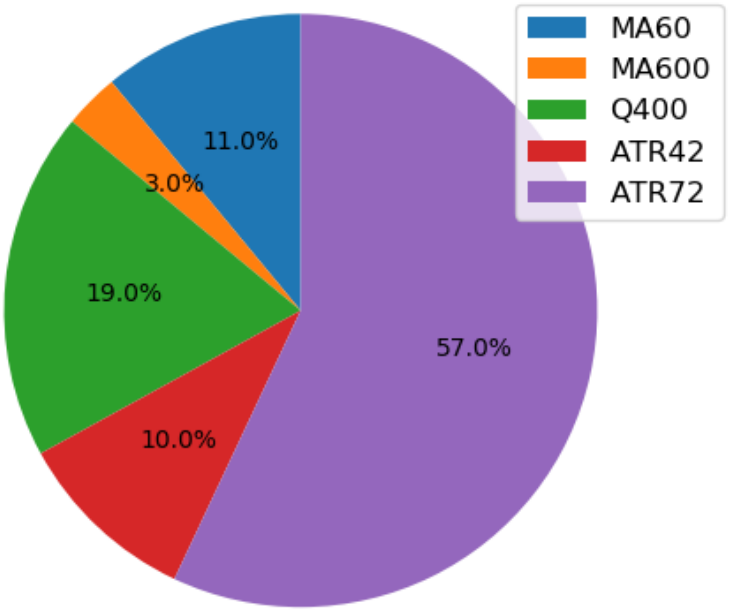

Figure 2.3: Turboprop market analysis

In the upcoming 20 years, both ATR and Bombardier forecast the demand in the above-60-seat segment regional aircraft to increase [5, 7]. Bombardier expects that the below-60-segment turboprops are to be replaced by bigger regional jets. However, ATR believes that the higher flexibility and more fuel efficient turboprops will still play a role. ATR forecast to sell 630 more turboprop aircraft in the coming 20 years. This project aims at competing with ATR in the 60-passenger market by proposing an aircraft design which has a lower unit cost and a better fuel efficiency (hence lower operating costs). By reaching this goal, it is expected that Aquila can steal some of the market share of ATR and other competitors and match the same forecast order size as ATR by selling 630 aircraft in the upcoming 20 years.

2.3. Opportunities

In order to enter the most promising market to limit the financial risks of the project, an analysis was performed on the opportunities in each continent. The analysed continents are North America, Europe, and Asia. The outcome of this analysis will determine on what market the focus will lie, although this does not imply that the design is unfit to serve other markets.

North America

North America holds the largest air fleet in the world, and has a strong and growing economy. However, some risks lie in the renegotiation of the NAFTA, a trade agreement between Canada, USA, and Mexico. Also, a pilot shortage has been existent since the 1500-flight-hour rule was introduced in 2013. This rule requires First Officers to have 1500 flight-hours before they can fly commercially. This withholds pilots from joining the commercial aviation industry.

[6] Retrieved from: https://www.forbes.com/sites/jeremybogaisky/2018/11/08/bombardier-selling-q400-turboprop-line-cutting-5000-jobs-as-it-moves-to-strengthen-balance-sheet/ (consulted on 20-6-2019)

Asia

When looking at Asia, there is a large imbalance in the composition of its fleet, having very few regional aircraft in comparison with the bigger aircraft. That is where the opportunity lies: small regional aircraft that are operable at smaller airports but can compete with bigger aircraft in terms of cost per passenger. Introducing Aquila here, would increase the connectivity between regions, and allows airlines to operate a cost-effective aircraft. For example in India, regional air travel is already being promoted [4]. The outcome might also provide interesting perspectiveS for this project.

Europe

Looking at the small regional aircraft fleet, Europe is at a point where soon a significant part has to be replaced: 49% of its aircraft is in service for 10 years or longer. [7]. As mentioned earlier in this chapter, low cost carriers are experiencing a growth in traffic. This is especially the case in Europe [8]. Next to this, 47% of all flown routes in Europe are over a distance lower than 1100 km [5], and regional airports have grown by 39.1% [9]. When comparing this to the growth of international airports (19.7%), it becomes evident that regional aviation is growing in Europe.

Conclusion

Europe and Pacific-Asia seems to show the greatest promise. In Europe this is due to the old age of the fleet, while in Asia the imbalance suggests introducing and stimulating regional aviation. Additionally, both regions are having trouble with the big, international airports getting saturated, which amplifies the growth of the regional airports. North America shows less promise despite the potential of a huge replacement market, due to the decrease in demand for regional aircraft and the fact that jet aircraft are more popular there.

2.4. Stakeholder Identification

There are two categories of stakeholders: primary and secondary stakeholders. These are defined based on how much influence they have on the project. Primary stakeholders are more crucial to the project, but the secondary stakeholder cannot be overlooked as they can still have a significant interest.

To be able to identify and categorise all stakeholders, a stakeholder map was made. This map is shown in Figure 2.4 and plots the influence of the stakeholder versus their interest. The regulating authorities and the manufacturer are the primary stakeholders and the passengers, airports and airlines the secondary stakeholders.

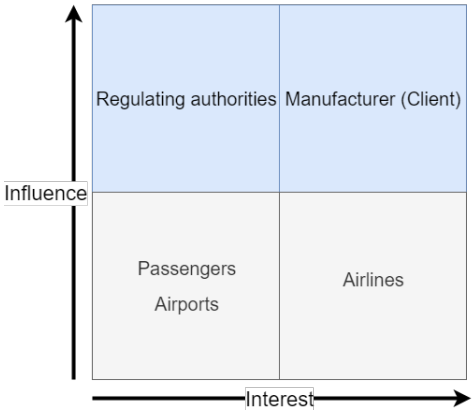

Figure 2.4: Stakeholder Map

After the stakeholders had been identified, the interests of the different stakeholders were determined and

[7] Retrieved from: https://ec.europa.eu/eurostat/web/products-eurostat-news/-/EDN-20171207-1?inheritRedirect=true&redirect=%2Feurostat%2F (consulted on 20-6-2019)

are described in the following sections.

Manufacturer (Client)

The client initiated the project and is financing it. That is why the client is the most important stakeholder, or key stakeholder, and why the main focus lies here. The requirements as provided directly by the client formed the basis of the design and are further addressed in chapter 3. The client was consulted regularly during the whole design project. Ultimately, the client needs a profitable product with which it can outperform competition.

Regulating Authorities

The regulating authorities are also a primary stakeholder. Although they don't show specific interest in this project, they do define the regulations with which this aircraft design has to comply. Therefore, they drive the limits of the design of the product.

Airlines

Although they end up as the buyer of the aircraft, they do not have a direct influence on the entire design. They do, however, indirectly drive the design as their needs are of primary concern for the manufacturers. It is therefore interesting to consult them on their needs in the low-risk areas. Low operational cost and retail price are of primary interest together with economical viability.

Airports

The airports offer services for the aircraft, but they do not affect the design as much as the client and authorities. Airports do not care which aircraft are operated as long as they are still compatible with them and the people living around the airports are satisfied. However, it is interesting to seek out their current capabilities in order to enhance the integration of the new aircraft with the current infrastructure. Especially since we are dealing with a regional aircraft, it needs to fit within the acceptable sizes and be able to be operated by regional airports as well.

Passengers

In the end, the passengers are the users of the aircraft, so for the airlines they are of utmost importance. To attract as many passengers as possible, the ticket prices need to be as low as possible. Additionally, the cabin should be comfortable enough and easily accessible during entering and leaving the aircraft both in case of emergency and everyday use. As these needs will not drive major design choices such as the engine, the passengers are classified as a secondary stakeholder.

3
Mission Analysis

The design was based on a certain mission for which the aircraft will be used by an airline. This mission consists of all requirements and constraints that were used to design the aircraft. In this chapter, firstly the mission requirements are elaborated. The next section consists of the mission characteristics that were concluded from the requirements. Lastly, the functional flow diagram and functional breakdown structure are given. These diagrams include all functions that the aircraft should perform in its lifetime.

3.1. Mission Requirements

The mission is determined by the stakeholders. The task of the design team is to fulfil the needs of these stakeholders. The stakeholders for Aquila are identified and their needs are noted. Next, these needs are transformed into system requirements that are driving for the aircraft design. The technical aspect is divided into; performance, production and operations. The mission aspect is divided into; cost, schedule and PESTLE.

Performance

- **AQ-PERF-01:** The aircraft shall have a design range of 1850 km for nominal payload.
- **AQ-PERF-02:** The fuel burn of the aircraft on a 1000 km trip shall be less than 1943 kg.
- **AQ-PERF-03:** The aircraft shall produce a maximum of 94 dB during take-off.
- **AQ-PERF-04:** The aircraft shall produce a maximum of 89 dB during cruise.
- **AQ-PERF-05:** The aircraft shall produce a maximum of 98 dB during landing.
- **AQ-PERF-06:** The emissions of the aircraft shall comply to the ICAO regulations for 2020-2050.
- **AQ-PERF-07:** The aircraft shall be able to take-off on a runway of 1400 m at sea level at MTOW.
- **AQ-PERF-08:** The aircraft shall be able to land on a runway of 1400 m at sea level at MLW.
- **AQ-PERF-09:** The number of passengers shall be in the range of 60-65 passengers.

Production

- **AQ-PROD-01:** The production factory of the aircraft shall be able to produce 5 aircraft per month.
- **AQ-PROD-02:** The production shall have an option to increase to 10 aircraft a month.
- **AQ-PROD-03:** The system shall be manufactured according to the lean manufacturing philosophy.

Operations

- **AQ-OPS-01** At least 2 cabin seating configurations shall be designed for the aircraft.
- **AQ-OPS-02** The average noise in the cabin during cruise shall be less than 78 dB.
- **AQ-OPS-03** The cabin pressure shall be at least 75.3 kPa during cruise operation.
- **AQ-OPS-04** The nominal CO2 concentration in the cabin shall be less than 1000 ppm.
- **AQ-OPS-05** The cabin temperature shall be in the range of 15-30 ° C in nominal flight.
- **AQ-OPS-06** There shall be at least one toilet on board.
- **AQ-OPS-07** There shall be at least one galley on board.
- **AQ-OPS-08** The MTOW shall not exceed 28,000 kg.
- **AQ-OPS-09** The minimum turning radius for ground manoeuvres for the point furthest from the pivot point shall be less than 19.74 m.

- **AQ-OPS-10** The wing span shall be less than 36 m.
- **AQ-OPS-11** The tail height shall be less than 13.5 m.
- **AQ-OPS-12** The turnaround time shall be less than 45 min.
- **AQ-OPS-13** The aircraft shall be able to perform 72,000 flight cycles.
- **AQ-OPS-14** The passengers shall be able to board the aircraft without the use of external stairs.
- **AQ-OPS-15** The aircraft shall have at least 5.2 m^3 cargo volume.

Cost

- **AQ-COST-01:** The retail price of the aircraft shall be 30% of the LCC.
- **AQ-COST-02:** The production cost shall be less than 80% of the retail price (after inflation).
- **AQ-COST-03:** The monthly operational cost shall be less than 56% of the LCC.
- **AQ-COST-04:** The EOL cost shall be less than 4% of the LCC.
- **AQ-COST-05:** The CASK shall be less than 0.106 USD (FY2019).

Schedule

- **AQ-SCHED-01:** The aircraft shall be operational in 2027.
- **AQ-SCHED-02:** The certification shall take 5 years or less.

PESTLE

- **AQ-PESTLE-01** The aircraft shall comply with the current FAA regulations.
- **AQ-PESTLE-02** The aircraft shall comply with the current EASA regulations.
- **AQ-PESTLE-03** The aircraft shall include at least two innovations (yet to be certified technologies).

3.2. Mission Characteristics

Regarding the requirements from the previous section a set of mission characteristics have been defined. These characteristics are the cornerstones of the design and make sure that some of the most basic requirements are met. First of all, the number of passengers had to be chosen. The requirements suggested 60-65 passengers. As the client preferred to have a smaller number of passengers, the number of passengers was set at 60. After this the mission profile was defined, which determined the design range, the flight level and cruise velocity. The design range was predefined in the requirements, and equal to 1850 km. The flight level and cruise velocity go hand in hand. It was assumed that the optimal cruise mach for the wing of the aircraft would be 0.55 and therefor the optimum cruise altitude would be about 8000 m. Later it was verified that this combination together with the full design was indeed optimal.

Table 3.1: Mission profile characteristics

Characteristic	Value	Unit
PAX	60	-
Range	1850	km
Cruise Mach	0.55	-
Cruise altitude	8000	m

3.3. Functional Flow Diagram and Functional Breakdown Structure

The functional flow diagram and functional breakdown structure were set up to make sure no functions would be forgotten when designing the aircraft. These diagrams were both created before the design process started. The flow diagram can be found in Figure 3.1. The resulting functional breakdown structure can be found in Figure 3.2.

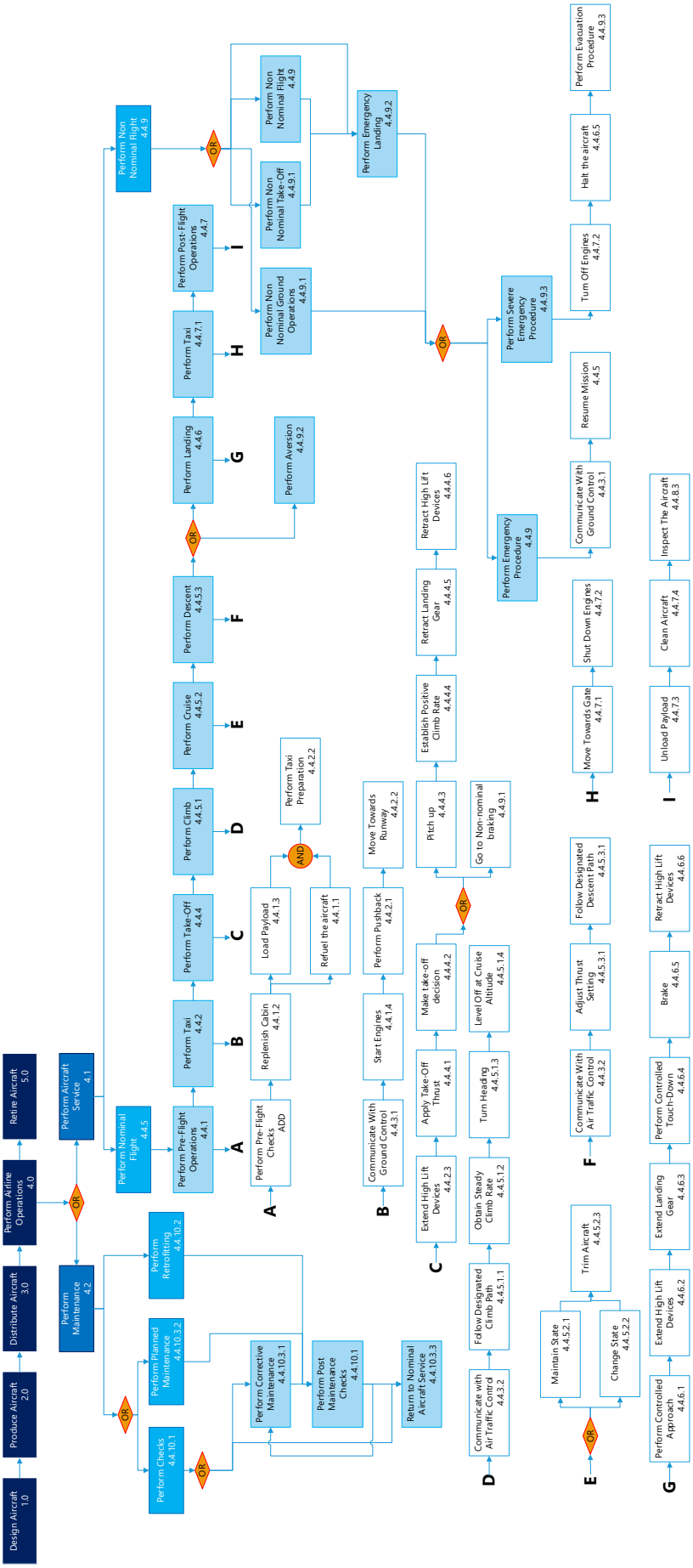

Figure 3.1: Functional Flow Diagram

Figure 3.2: Functional Breakdown Structure

4

Sustainable Development & Risk Strategies

Sustainability has become more and more important in recent years and as such it was found to be important that this project had a sound sustainable development strategy, which was used during the design process and the analysis of the aircraft. Section 4.1 focuses on the different kinds of sustainability and how they affect the design choices and the eventual performance of the aircraft. The capability that systems function reliably is a fundamental requirement of safe operation of the aircraft. The strategy concerning the risk for this reliability is discussed in section 4.2. In the final part of chapter 10, an overview is given of the major risks.

4.1. Sustainable Development Strategy

Aviation is responsible for 12% of the total CO_2 emissions caused by transportation. This causes the aviation industry to be responsible for around 2% of all human induced CO_2 emissions[1]. This number is expected to increase, since aviation is still a fast growing industry. Current improvements in fuel efficiency are not able to cope this rapid growth of aviation. Therefore, it goes without saying that a sustainable strategy is crucial when designing an aircraft.

Sustainability can be implemented in many ways and allows various approaches to make the design of aircraft more sustainable. The philosophy and strategy behind sustainability of the design group was of 'realistic and practical sustainability'. This strategy aims to minimise the impact on the environment by also factoring in the economics and feasibility of the design into the analysis of sustainability. It is important to look at the full picture of the project and not just the performance of the design.

This strategy has been set not just for the performance and production of the aircraft, but also for the process of designing and selecting the concepts. Options in the design option tree that did not comply with the sustainable design philosophy were scrapped and removed from the possible options. Requirements were set both for performance, social and economic sustainability. It was also decided by the team that for selecting the recommended concept, sustainability would be one of the main, if not the most important, factors.

The main approach to verify the results of the design team is to compare them with a reference aircraft. This reference aircraft would need to be one of the most fuel efficient and sustainable aircraft in order to set ambitious goals. This reference aircraft was chosen to be the ATR 72, since it is of similar size and would be one of the main competitors of the Aquila, both in terms of fuel efficiency as well as cost. Since the ATR 72 is at this point the most cost effective and fuel efficient aircraft it is sufficient to prove that the Aquila can beat the competition in terms of sustainability by comparing it to the ATR 72.

4.1.1. Environmental Sustainability

The first aspect of sustainability that was analysed is the environmental aspect. This deals with the direct impact of the aircraft during production, operations and disposal on the environment. The impact was divided into the following four aspects:

- The operational emission and pollution by CO_2 and NO_x.
- The noise emission of the aircraft.

[1] Retrieved from https://www.sustainableaviation.co.uk/ (consulted on 24/04/2019).

- The emission and pollution during the production phase of the aircraft.
- The end-of-life recycling process of the aircraft.

The CO_2 and NO_x emissions were calculated in terms of kilogram per passenger for a trip of 1000 km. For the ATR 72 this was also done, but with 60 passengers instead of the usual 70 passengers to make the comparison fair. The goal of this design was to improve the fuel efficiency and reduce emissions, to show that regional aviation can comply with the Paris accords in the near future [2].

The focus of the noise emissions was to reduce noise levels under all circumstances with respect to reference aircraft. Special care was given to the selection of the engine and the propeller, which are two of the main contributors to noise. By reducing the top speed at which the aircraft flies, as well as trying to minimise the approach speed at landing, the noise level was reduced. This has all been documented in chapter 7.

The sustainability strategy with regard to production was the reduction of emissions and negating the use of dangerous chemicals. Reducing the emissions can be done by using green energy from sustainable resources and reducing the number of energy intensive processes. Reducing the use of dangerous chemicals can be done by choosing alternative methods where possible, even if these options are more expensive.

To make sure that the least amount of waste is created at the end-of-life of an aircraft, recyclability needs to be taken into account already during the design and production of the aircraft. It was the goal of the design team to achieve at least 85% recyclability of the aircraft. Improvements on this can primarily be gained by making the traditionally non-recyclable parts of the aircraft more recyclable, such as the furnishings, titanium parts and carbon composites.

In the short term (within 10 years) this project aims to reduce emissions and other pollutants by a significant amount in order to comply with climate accords. In the long term this project aims to make aviation as much carbon neutral as possible. This can be done by consideren the use of biomethane as a fuel. This will be further discussed in chapter 12.

4.1.2. Economic and Social Sustainability

Economics is the main driver for the success of this project. It is important to show that the design will make a profit for the manufacturer as well as for the airliner. The primary strategy for this is to beat the competition in terms of direct operational cost (DOC for short) and a low unit cost. The main strategy to decrease operational cost is by decreasing fuel consumption by increasing the fuel efficiency of the aircraft. To keep the unit cost low it is important to make the plane easy to manufacture and keep the development cost as low as possible. This strategy also helped ATR to take large portions of the turboprop market in the 80s and 90s.

An increasingly important factor in the aviation industry is the demand of the public for more sustainable aircraft. In recent years the demand from the public and government for a ban or at least a discouragement for short air trips (under 500 km) has been growing. It is therefore important to show that Aquila can be a sustainable competitor for other modes of transport, both in terms of emission and noise.

Economic and social sustainability come together with practical sustainability; together they make the project sustainable. It is important for the project to be economically viable, but it also needs to be socially and environmentally sustainable. By balancing these three factors one can achieve the maximum impact on sustainability in the regional aviation market.

4.2. Risk Management Strategy

As presented in earlier reports [10], risk is a probability or threat of damage, injury, liability, loss, or any other negative occurrence that is caused by external or internal vulnerabilities, and that may possibly be avoided through preemptive action [11].

Risk affects all aspects of the design. Therefore risk was addressed at different parts of the project, like the design, the operation, the production, the financial aspect and the future development of Aquila. Not all

[2] Retrieved from: https://unfccc.int/resource/bigpicture/#content-the-paris-agreemen (Consulted on 24/06/2019)

risks can be accounted for. However, the most prominent ones, and their related mitigation, are addressed in subsequent chapters.

4.2.1. Risk Classification

In order to better understand and mitigate risks, risks can be quantified in terms of the likelihood of the occurrence and the magnitude of the impact. The clarification of both classifications are presented below. Especially for the graphical representation of risks, shown in section 10.4, the classification below is useful to get a overview of the risks and to directly indentify which risks require more attention if both the likelihood and impact is significant.

The *Likelihood of Occurence* was categorised in the following five degrees, in descending order of likelihood. An event with a likelihood which is *very high* is an event that will occur almost certainly (75% - 100%). An event with a *high* likelihood might or might not happen (25% - 75%). An event with a *medium* likelihood is an event that will probably not occur (5% - 25%). An event that has a *low* probability to occur is almost not likely to occur (0.5% - 5%). Finally, an event with a *very low* likelihood is an event that will very likely never occur (0% - 0.5%). It is important to note that the presented probabilities indicate the likelihood over the entire project duration.

The *Magnitude of Impact* was categorised in the following five degrees, in descending order of impact. A *catastrophic* event will lead to the end of development or the end of production of Aquila. A *critical* event will result in the loss of life or in a halt in production over a long time ($\pm$ 3 months). A *moderate* event will lead to injury, an unusable product in operation, or a delay in production ($\pm$ 1 month). A *marginal* event will lead to a minor delay in production or operation. And finally, a *negligible* event will have a result which is barely noticeable in terms of production or operation. It should be stressed that although some events will be catastrophic for the human perspective, for example the loss of life, it will not be catastrophic for the continuation of the project, in the eyes of the manufacturer.

5
Detailed Concept Design

With the requirement and mission characteristics identified, the aircraft was designed. In this chapter, the actual design of the aircraft will be elaborated. The first section will focus on the fuselage sizing and cabin lay-out. Secondly, the aerodynamics of the aircraft will be investigated and designed. This section mainly involves the wing design. The next system that is designed is the empennage. This section consists of stability and control assessment, as well as control system design and the determination of the empennage size. The undercarriage is designed afterwards. Mainly, the required height and width of the main landing gear is determined in this section. In the material and structural characteristics section, structural components of the aircraft are designed and materials are chosen. The propulsion and fuel system design involve the adaption of LNG to the aircraft. The last section describes aircraft systems such as the actuator system and communication system of the aircraft. Lastly, the design methods are verified.

5.1. Fuselage Design

The first step was to size the fuselage in order to facilitate the passengers and their cargo. This process was already described in detail in the midterm report [12].

Fuselage Top View

The top view and side view of the aircraft are presented in Figure 5.1. There is a lavatory situated in the front of the aircraft and a galley is situated in the end. the length of these items is shown in Figure 5.1. The seat pitch is taken to be 31 inch or 0.787 m.

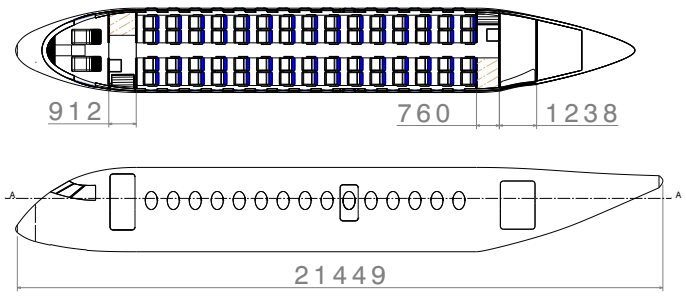

Figure 5.1: Fuselage top view and side view

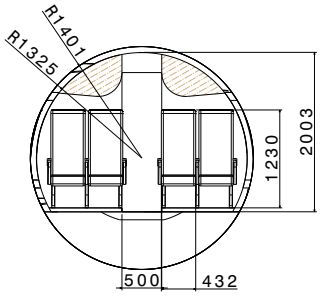

Figure 5.2: Fuselage cross section of the Aquila

Cross Section

In Figure 5.2, the seat width, aisle width and aisle height are presented. Also the inner and outer diameter of the fuselage are highlighted.

Cargo Compartment

For the payload, a mass of 20 kg per passenger for luggage was assumed[1]. From this, 10 kg must be stored into the cargo compartment in the end of the aircraft due to the limiting volume of the overhead bins. The cargo compartment has an available volume of 5.3 m^3. For a cargo density of 170 kg/m^3, this results in a total cargo capacity of 900 kg. Thus, the AQ60 is able to transport 300 kg of extra cargo. This also enables the decrease of cargo stored in the overhead bins.

5.2. Aerodynamic Wing Design

This section describes the design process of the wing. Firstly, the wing planform design is explained in subsection 5.2.1. Then, the remaining geometric properties of the wing are outlined in subsection 5.2.2. Furthermore, a description of the high lift devices is provided in subsection 5.2.3, and subsection 5.2.4 shows the design of the ailerons. Several wingtip devices are analysed in subsection 5.2.5, after which some design considerations are made in subsection 5.2.6. A brief summary of the geometric properties is given in subsection 5.2.7 and an initial aerodynamic analysis is done in subsection 5.2.8. Finally, the risk of the aerodynamic design is assessed in subsection 5.2.9.

5.2.1. Wing Planform Design

The wing planform design affects the aerodynamic efficiency of the wing and depends highly on operating conditions of the aircraft, such as the cruise speed and altitude. This subsection provides an explanation of the methods and assumptions used for the wing planform design, starting with the wing loading and continuing with design parameters such as aspect ratio, span, taper ratio, sweep and dihedral angle.

Wing Loading

The required surface area of the wing was determined by means of a wing-loading diagram. This is a visual representation of a set of constraints, which results in a range of probable wing-loading cases. This diagram can be found in Figure 5.3. It includes lines representing constraints on take-off, landing, cruise and climb. The red areas show the non-feasible domains, while the white part is the available design space. As described in section 3.2, the cruise speed of the aircraft is set at Mach 0.55, at an cruise altitude of 8000 m.

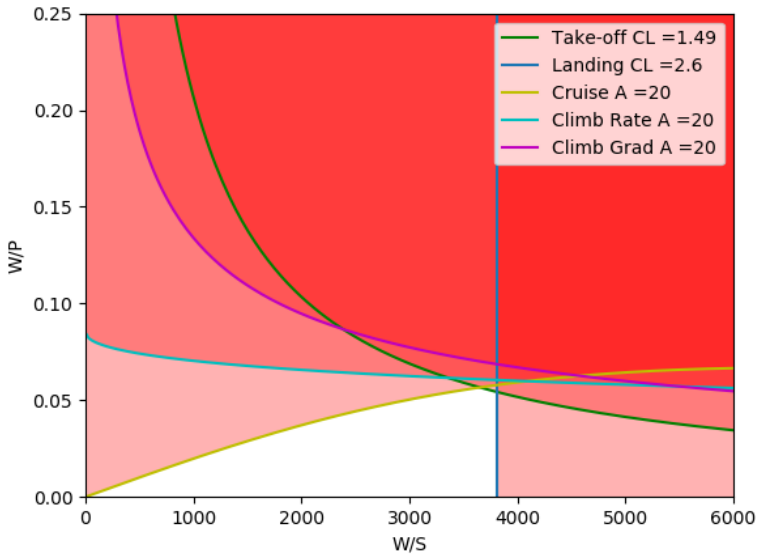

Figure 5.3: Wing loading diagram

[1]Retrieved from https://www.easa.europa.eu/sites/default/files/dfu/Weight%20Survey%20R20090095%20Final.pdf (consulted on 01/07/2019).

As shown in Figure 5.3, the available design space is rather limited. The optimal point is located in the top right corner of the available, white, domain. This would result in the smallest wing and engine for the required performance. Therefore, the design wing-loading was chosen to be 3625 N/m^2. This resulted in a required wing surface area of 49.21 m^2.

Aspect Ratio and Wing Span

The aspect ratio of a wing has a significant influence on the aerodynamic efficiency of an aircraft, which is the reason a high aspect ratio was chosen for this design in the first place. However, it should be noted that a high aspect ratio also has two major drawbacks. Firstly, from an operational point of view, a higher aspect ratio leads to a longer wing. It must, however, still adhere to AQ-OPS-10. The second drawback is structural; a longer, more slender wing can cause structural related issues regarding bending moments and flutter.

Therefore, a trade-off between increased efficiency and aforementioned disadvantages was performed by means of a sensitivity analysis. This analysis looked into the increase of lift over drag for different aspect ratios, as well as the corresponding wing span. In this trade-off, the addition of a strut was taken into account. An aspect ratio of 20 turned out to be close to the optimum and was therefore selected for this design. As a result, the wing span was determined using Equation 5.1. From this equation, it follows that the total wingspan is 31.37 m, excluding any wingtip devices.

$$b = \sqrt{SA} \tag{5.1}$$

Taper Ratio

The taper ratio mainly affects the lift distribution and the stall characteristics. The most optimal lift distribution, i.e. as close as possible to an elliptical one, can be achieved with a taper ratio of 0.4 [1]. Therefore, this taper ratio was selected for the design. However, it should be taken into account that, for a smaller taper-ratio, the span-wise position of initial stall moves outboard [13]. This is undesirable, as it makes the aileron more prone to stall. This could lead to a sudden loss of control in roll and must therefore be prevented. Hence, a negative twist is introduced, as discussed later in this section.

Sweep and Dihedral Angle

Sweep is generally used for aircraft flying close to or at transonic speeds or faster. Given that this aircraft is designed for a cruise speed of Mach 0.55, there is no sweep required for this condition. Sweep could still be introduced for optimisation of performance and stability. However, more sweep requires a heavier wing structure and thus makes the entire aircraft heavier. It was decided not to use sweep at the quarter chord line of the wing; $\Lambda_{c/4} = 0$.

The dihedral angle mainly affects the roll stability of the aircraft; the higher the dihedral angle, the more stable the aircraft. This is beneficial in case of wind gusts and unwanted motions, but limits the controllability of the aircraft. Adhering to conventional designs for unswept, high wing configurations, the dihedral angle was taken to be 1 degree [14].

5.2.2. Wing Profile Design

The planform design does not completely define the wing geometry; the wing profile and twist must also be defined. Thus, in this section, an airfoil selection is described, as well as the determination of the twist and incidence angles, to complete the description of the wing geometry.

Airfoil Selection

Because there are many different airfoils, all of them designed with a certain mission and flight condition in mind, a selection of airfoils was taken from *airfoiltools* [2] to analyse and compare.

[2] Retrieved from: http://airfoiltools.com/ (consulted on 29-5-2019)

For this comparison, several NACA 4- and 5-digit series airfoils were used. The selection of the most optimal airfoils was based mainly on the following aspects:

- The lift-over-drag ratio in the designed flight condition shall be as high as possible.
- The drag bucket around the designed lift coefficient shall be sufficiently wide to cover the nominal flight conditions.
- The angle of attack at which the airfoil stalls shall be as large as possible.

After evaluating these points, the root airfoil was chosen to be NACA 4415 and the tip airfoil was selected to be NACA 4412. These profiles only differ in thickness, which decreases linearly from root to tip. The most important advantage of these profiles is their low drag at cruise conditions for a lift coefficient of approximately 0.5. The lift curves for both profiles can be found in Figure 5.4. Here, the third (green) curve shows the airfoil at the tip when a twist of 2 degrees is applied. One of the reasons to include a twist angle of 2 degrees, as explained in Figure 5.2.2, is to avoid tip stall.

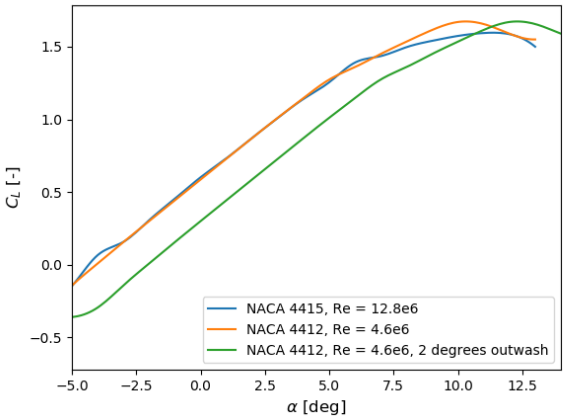

Figure 5.4: Lift curves for the root and tip airfoils

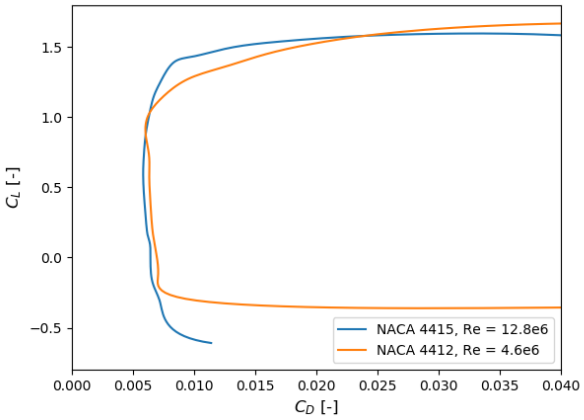

Figure 5.5: Drag polars for the root and tip airfoils

As mentioned before, one of the criteria to select an airfoil on is the availability of a so-called 'drag bucket', which is a range of angles of attack at which the drag is significantly lower than for other angles of attack. In Figure 5.5, one can see that both airfoils have a low drag region when the lift coefficient is around $C_L = 0.5$. This is the design lift coefficient and hence these airfoils were very convenient as they are both optimised for this condition. They also provide sufficient lift during take-off and landing (in case the proper flap setting is chosen), as will be described later in this report.

Twist and Incidence Angle

Because the ailerons are located near the tip of the wing, the outboard stall of the wing must be avoided to ensure controllability, even close to stall conditions. One way to do this is to include negative twist for the wing tip. This means that the airfoil at the tip of the wing has a lower angle of attack compared to the airfoil at the root of the wing. This ensures that the tip reaches its stall later, as a larger increase of angle of attack is required for this to happen. Generally, the twist is between 0 and -5 degrees [15].

For this design, a twist angle of -2 degrees was chosen. This value was based on a comparison between the root and tip airfoils. The twist must be sufficient to let the tip of the wing stall later than the root. As shown in Figure 5.4, the airfoil with the 2 degrees downwash has its stall point at a higher angle of attack than the airfoil at the root, while the original airfoil at the tip (the orange line) has its stall point at a smaller angle of attack than the root. Furthermore, the root and tip have similar lift over drag properties for the regular flight domain, which means that they are both optimised for the same conditions. This leads to a more efficient flight and reduced drag.

5.2.3. High Lift Devices

High Lift Devices (HLDs) increase the value that the maximum lift coefficient of the aircraft ($C_{L_{max}}$) can attain. The HLDs were sized by calculating the extra lift (ΔC_L) that the wing has to produce to meet the

landing and take-off criteria, using the methods described by Roskam [16]. ΔC_L is the difference between the clean $C_{L_{max}}$ and the $C_{L_{max}}$ with HLDs deployed. $C_{L_{max_{TO}}}$ and $C_{L_{max_L}}$ were set at 1.8 and 2.6 respectively, in order for the aircraft to meet its take-off and landing requirements. The $C_{L_{max}}$ of the clean wing was calculated to be 1.43. Single Fowler flaps were chosen because they can provide a high ΔC_L, while remaining relatively simple. No slats were used since the ΔC_L required can be obtained with flaps only, and slats add weight and complexity to the wing design. To maximise the available space on the wing, the flaps start as close to the root as possible, just after the fairing has ended at 1.4 m from the centre line of the aircraft. The flaps then run for 6.8 m and end at 8.2 m from the centre line of the aircraft. A cut of 0.75 m is made at the location of the engine. The flaps take up 37% of the chord length and have eight settings, ranging from 0 to 35 degrees. At take-off the flaps are deflected to an angle of 10 degrees and at landing to an angle of 35 degrees. The flap sizing and positioning can be seen in Figure 5.6.

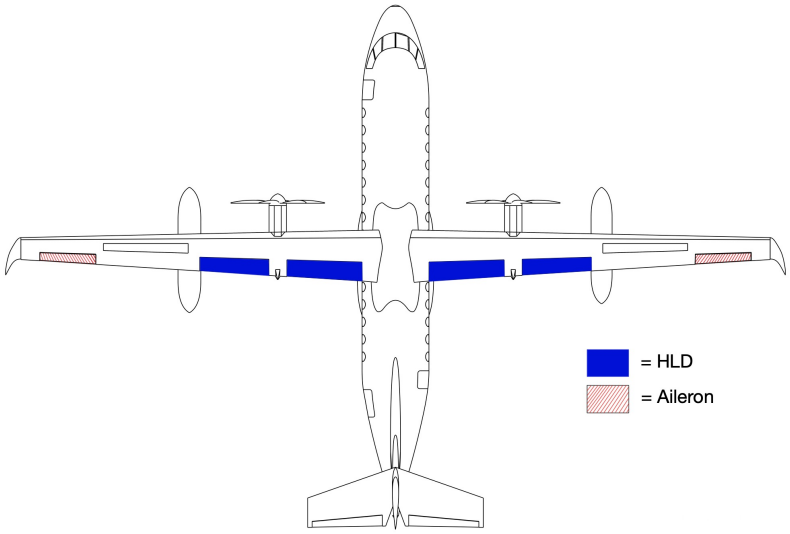

Figure 5.6: HLD and Aileron locations top view

5.2.4. Aileron Design

The aileron allows the aircraft to roll and thereby obtain lateral control. They are designed according to a set of requirements. The most prominent of these is the roll requirement, which states that *for transport aircraft, a roll angle of 30 degrees shall be obtained within 1.5 seconds* [17]. As the roll performance depends on the velocity, it must be specified for which speed this requirement must be met. Since the landing condition is most critical, the landing speed was used for this analysis. Then, the roll rate p was determined by using Equation 5.2 [17].

$$p = -\frac{C_{l_{\delta_a}}}{C_{l_p}} \frac{2V}{b} \delta_{a_{max}} \tag{5.2}$$

Here, $C_{l_{\delta_a}}$ and C_{l_p} are defined in Equation 5.3 and Equation 5.4, respectively, and $\delta_{a_{max}}$ is the maximum aileron deflection. This is decided to be 25 degrees up and 20 degrees down, to minimise the adverse yaw effect. To include a safety margin in the design, the latter value is taken as $\delta_{a_{max}}$ in Equation 5.2.

The aileron control derivative $C_{l_{\delta_a}}$ is given by Equation 5.3.

$$C_{l_{\delta_a}} = \frac{2C_{l_\alpha}\tau}{Sb} \int_{b_1}^{b_2} c(y) y dy \tag{5.3}$$

Here, C_{l_α} is the slope of the lift curve for the airfoil in rad^{-1}; τ is the aileron effectiveness, which depends on the aileron chord and has a value of 0.57; b_1 and b_2 are the inboard and outboard limits of the aileron in span-wise direction in m, respectively; y is the span-wise location in m; $c(y)$ is the chord in m as a function

of the span-wise location.

Furthermore, the roll damping coefficient is given by Equation 5.4.

$$C_{l_p} = -\frac{4(C_{l_\alpha} + C_{d_0})}{Sb} \int_0^{b/2} c(y) y^2 dy \tag{5.4}$$

Here, C_{d_0} is the zero-lift drag coefficient of the airfoil.

Once the aileron control derivative and roll damping coefficient were determined, the roll rate could be found using Equation 5.2. Then, the time required to roll 30 degrees could be calculated using Equation 5.5.

$$\Delta t = \frac{\Delta \phi}{p} \tag{5.5}$$

Here, $\Delta\phi$ is the roll angle (i.e. 30 degrees) an p is the roll rate. If $\Delta t < 1.5$, then the roll requirement is met. Otherwise, the geometry should be adjusted to improve the roll performance. Using this method, the inboard side of the aileron was positioned at 80% of the half-span and the outboard side at 95% of the half-span. The sizing and positioning of the ailerons can be seen in Figure 5.6.

5.2.5. Wingtip devices

Wingtip devices are used to decrease the wingtip-vortices produced by a wing and to increase the efficiency of that wing. Several different wingtip devices are currently used in the industry. In this section, three different wingtip devices are compared to each other and to a wing without any wingtip device. The wingtip devices considered here are a blended winglet, a raked wingtip and a wingtip fence. They can be seen in Figures 5.7 to 5.10. These figures were created using ANSYS Fluent, the software used to perform the computational fluid dynamics (CFD) analysis. The wingtip devices were compared using the value of L/D of each wing and the wingtip-vortices that are produced. The following table shows the L/D value of each of the four wings, as well as the lift and drag values obtained. These values were obtained by subjecting the wings to cruise conditions, so flying at Mach 0.55 at 8000 m altitude. The values are the combined lift and drag of both wings.

Table 5.1: Results of ANSYS CFD analysis

Wingtip device	**Lift [N]**	**Drag [N]**	**L/D**
No wingtip device	203377.1	9146.1	22.2
Blended winglet	238725.4	9934.0	24.0
Raked wingtip	236884.1	9545.1	24.8
Wingtip fence	232080.2	9604.4	24.2

It can be seen that the addition of the wingtip devices adds both lift and drag. The blended winglet adds the most lift, but the drag also increases the most. The drag values for the raked wingtip and the wingtip fence are very similar, but the lift when adding the raked wingtip increases more than the lift of the wing with a wingtip fence. In an attempt to see where these differences come from, Figures 5.7 to 5.10 show the different wingtip devices with the Q-criterion plotted. The equation for the Q-criterion can be seen in Equation 5.6, where Ω is the vorticity and S is the rate-of-strain [18].

$$Q = \frac{1}{2}\|\Omega\|^2 - \|S\|^2 \tag{5.6}$$

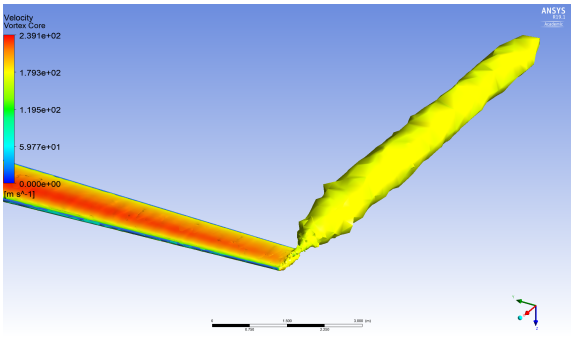

Figure 5.7: CFD analysis of a wing without wingtip device

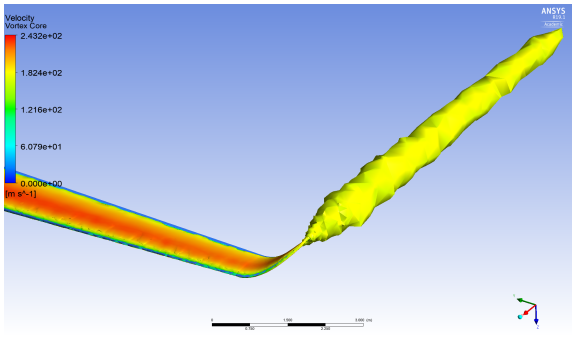

Figure 5.8: CFD analysis of a wing with a blended winglet

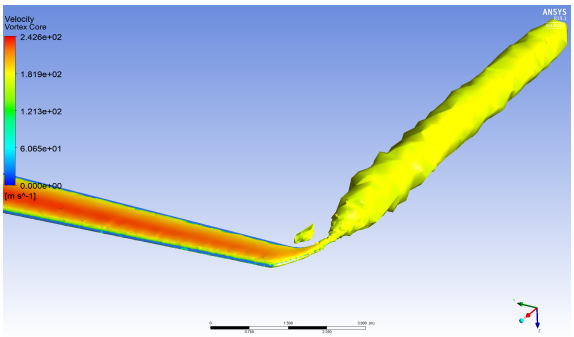

Figure 5.9: CFD analysis of a wing with a raked wingtip

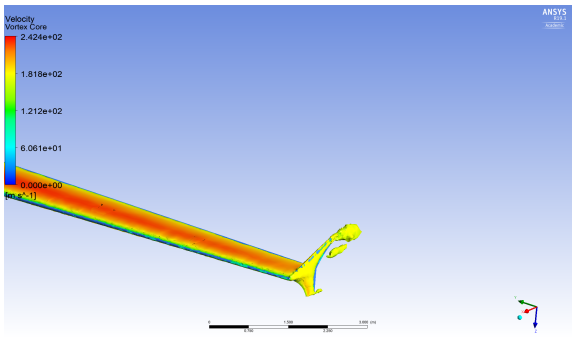

Figure 5.10: CFD analysis of a wing with a wingtip fence

Visual inspection of the above figures does not show why the raked wingtip has a higher L/D than the other wingtip devices. It does however show an interesting property of the wingtip fence; it creates significantly less vorticity than the other wingtip devices. This explains why the L/D is increased, even though the effective aspect ratio is not increased as opposed to the other wingtip devices. In theory, the wingtip fence does what a wingtip device should do the best; it reduces the wingtip vortices the most. Nevertheless, the raked wingtip was selected for this aircraft because it provides the highest L/D increase. It was hypothesised that even though the wingtip fence reduces the wingtip vortices more than the raked wingtip, it does not increase the lift of the wing. The raked wingtip, on the other hand, not only reduces the induced drag on the wing, it also increase the lift. Apparently, for this wing configuration, these changes in drag and lift happen in such a way that the L/D of the raked wingtip increases more than the L/D of the wingtip fence. The span of the aircraft is increased by the addition of the raked wingtip from 31.37 m to 32.65 m. In the future development of this aircraft, a more extensive analysis of wingtip devices should be performed.

Mesh Refinement

To ensure that the quality of the mesh used in the CFD analysis is good enough to get reliable results, a brief analysis was done. For the model of the raked wingtip, a range of different meshes was created, all with a different level of refinement. Figure 5.11 shows the number of cells in each of the meshes versus the lift of the wing with a raked wingtip that was calculated.

The value for the lift does not seem to settle around or converge to a specific value as the number of cells increases. Instead, the lift seems to increase with increased cell numbers. This indicates that the mesh used for the wingtip device analysis might have been too coarse. However, given that the differences in lift for this range of cell numbers fall within 1%, it was decided to be good enough for the initial analysis. All analyses were performed with cell numbers between 1 and 1.5 million, as the given computing power did not allow for effective analysis for cell numbers higher than that. Using higher cell numbers resulted in computing times of hours at best. Many times the simulation could not even be run at these high cell numbers. For future aerodynamic analysis, it is recommended to do an extensive analysis of the mesh refinement necessary and to make sure more computing power is available.

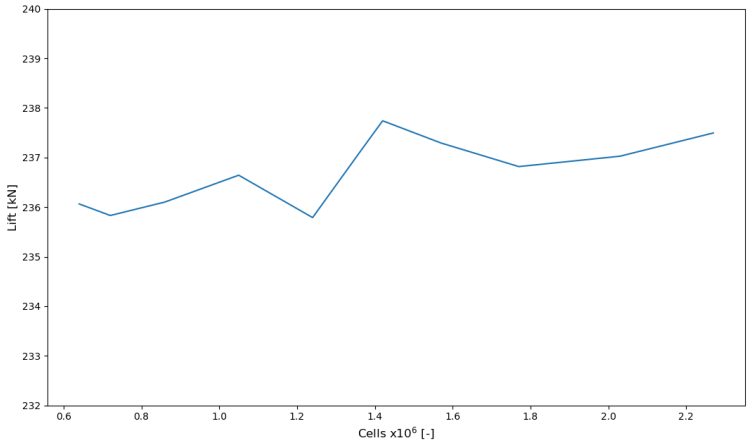

Figure 5.11: Mesh refinement versus lift for the wing with raked wingtip

5.2.6. Design Considerations

After the aerodynamic design of the wing was completed, some additional analyses were performed. Each analysis in this section had the potential of changing the design of the wing, but after careful consideration, it was found that this was not necessary. First the critical Mach number of the airfoils was analysed, after which the propeller-wing interaction was analysed.

Critical Mach Number

Finding the critical Mach number of the airfoils was important because flying at a Mach number higher than the critical one creates supersonic regions over the surface of the wing. This, in turn, has a negative effect on the performance of the wing and thus the overall aircraft. The critical Mach number of an airfoil can be found using Equation 5.7, where $C_{p_{min}}$ is calculated using Equation 5.8 and $C_{p_{cr}}$ can be found using Equation 5.9 [19].

$$C_{p_{min}} = C_{p_{cr}} \tag{5.7}$$

$$C_{p_{min}} = \frac{C_{P0min}}{\sqrt{1 - M_\infty^2}} \tag{5.8}$$

$$C_{p_{cr}} = \frac{2}{\gamma M_{cr}^2}\left(\left(\frac{1 + \frac{\gamma+1}{2} M_{cr}^2}{1 + \frac{\gamma-1}{2}}\right)^{\frac{\gamma}{\gamma-1}} - 1\right) \tag{5.9}$$

The critical Mach number (M_{cr}) was only calculated for both the root and the tip airfoil, since the critical Mach numbers of the intermediate airfoils will be in between the critical Mach numbers of the root and tip airfoils. M_∞ is equal to 0.55 for both airfoils and γ is also the same for both aifoils, with a value of 1.4. For the tip airfoil (NACA 4412), C_{P0min} is equal to -1.0199 and for the root airfoil (NACA 4415), C_{P0min} is equal to -1.1844. This results in a M_{cr} for the tip airfoil of 0.603 and 0.577 for the root airfoil. Because the aircraft is flying at Mach 0.55, there will be no supersonic regions on the wing and no alterations to the design had to be made. The margin between the cruise Mach number and the critical Mach numbers of the airfoils is quite small. Therefore, in future design phases, airfoils with higher critical Mach numbers can be analysed.

Propeller-Wing Interaction

Placing the propeller in front of the wing has an effect on the flow that the wing encounters. Both the velocity and the vorticity of the flow increase and concerns arose that this would cause the HLDs to become less efficient and the wing to stall sooner. However, the opposite turns out to be the case. Ananda et al. conclude that the stall characteristics of the wing in the wake of a propeller improve and that the lift of this wing section improves as well [20]. Furthermore, Veldhuis concludes that the L/D of the aircraft can be increased by having the propeller rotate inboard up [21]. Despite these positive effects, a further investigation has to be performed into the effects of the propeller wake on the wing surface. The most pressing issue is the

possibility of the flow exceeding the critical Mach number of the airfoil, due to the increased velocity of the flow.

5.2.7. Results

In Table 5.2, the final design parameters for the wing are summarised. The geometry of the HLD's and the aileron are also included to provide a clear overview.

Table 5.2: Final Design Parameters of the Wing

Parameter	Symbol	Value	Unit
Surface Area	S	49.21	m^2
Root Chord	c_r	2.24	m
Tip Chord	c_t	0.90	m
Mean Aerodynamic Chord	MAC	1.66	m
Taper Ratio	λ	0.4	-
Span	b	32.65	m
Quarter Chord Sweep	$\Lambda_{c/4}$	0	deg
Dihedral	Γ	1	deg
Twist	ϕ	-2	deg
Flap chord w.r.t. local wing chord	c_{flap}/c	0.37	-
Inbourd flap limit w.r.t. half-span	$b_{flap_{in}}/(b/2)$	0.09	-
Outbourd flap limit w.r.t. half-span	$b_{flap_{out}}/(b/2)$	0.52	-
Aileron chord w.r.t. local wing chord	c_{ail}/c	0.36	-
Inbourd aileron limit w.r.t. half-span	$b_{ail_{in}}/(b/2)$	0.80	-
Outbourd aileron limit w.r.t. half-span	$b_{ail_{out}}/(b/2)$	0.95	-

5.2.8. Preliminary Aerodynamic Analysis

In order to design the wing and the strut, the aerodynamic forces on the wing and strut such as the lift and the drag have to be known. To calculate the lift distribution along the span of the wing and strut, a software called AVL[3] was used. AVL uses vortex lattice models to simulate lifting surfaces (such as the wing and strut) and a slender-body model to simulate bodies (such as the fuselage, nacelles and fuel pods). AVL assumes inviscid flow in its calculations, which means that the drag calculated is lower than it would be in a more realistic model. This is why the drag calculated by AVL was not used. The lift on the other hand was used, as the assumption of inviscid flow only has a minor effect on the calculated lift values. To calculate the drag on the wing and strut, Equation 5.10 was used.

$$C_D = C_{D_0} + \frac{{C_L}^2}{\pi A e} \tag{5.10}$$

C_{D_0} is the drag coefficient when the wing produces no lift and the second term on the right hand side of the equation is the induced drag, with A being the aspect ratio and e the Oswald efficiency factor. C_{D_0} was calculated using a different software called XFOIL[4], which uses panel methods to evaluate airfoils for inviscid flows, but uses viscous formulations to get a reliable drag for the airfoil. Using Equation 5.10, the C_{D_0} from XFOIL and the values for C_L at every section from AVL, the C_D at every section along the wing was calculated. Figure 5.12 shows the model in AVL that was used to calculate the lift distribution over the wing and strut. In this model, the fuel tanks and engines are modelled in the same way as the fuselage. The effects of the propeller and its wake are not taken into account in this model.

It should be noted that the lift produced by the wing alone, computed using the software AVL, increases when a strut is added. As expected, the lift on the inboard side of the strut was decreased by the presence of the strut, but the lift was increased on the outboard side of the strut, which was not expected. As a result the total lift produced by the wing increased. Even though this is highly unlikely, since there was no other lift dis-

[3]Retrieved from: http://web.mit.edu/drela/Public/web/avl/ (consulted on 3-6-2019)
[4]Retrieved from: https://web.mit.edu/drela/Public/web/xfoil/ (consulted on 3-6-2019)

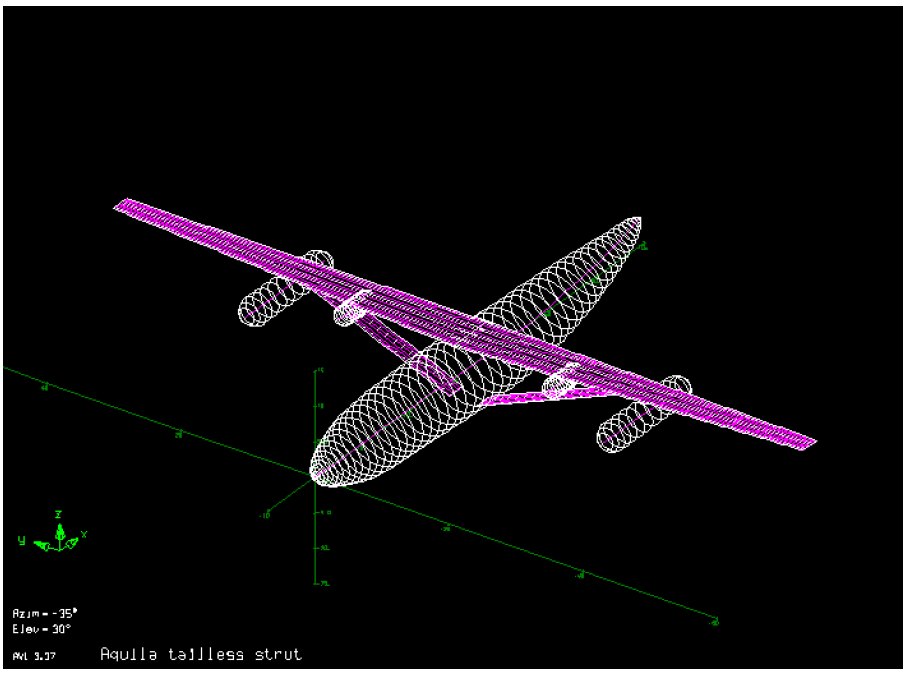

Figure 5.12: AVL model of the wing section and fuselage

tribution available, the lift distribution shown in Figure 5.13 was used for the structural design of the wing. One justification for this decision is that this lift distribution results in higher forces applied on the wing. This means that designing for this condition has the potential of ending up with an overdesigned wing, but using the lift distribution of the wing without strut-effect might lead to an underdesigned wing. From a safety perspective, an overdesigned wing is preferable to an underdesigned wing, so the overdesigned wing was chosen. This does, however, also have an effect on the overall design of the aircraft and decreases the accuracy of the design. Given that further design phases will follow after this, it was decided to leave the numerical simulations, needed to accurately model the forces on the wing, to one of these later design phases.

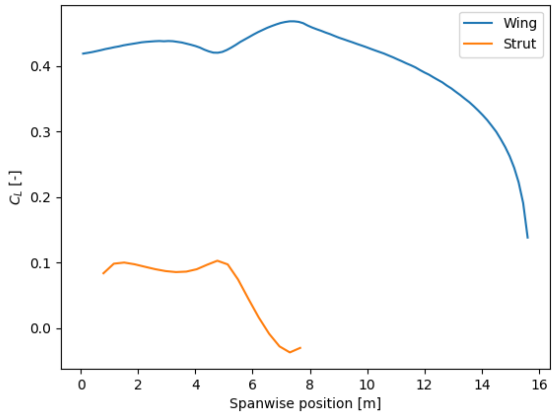

Figure 5.13: Spanwise C_L

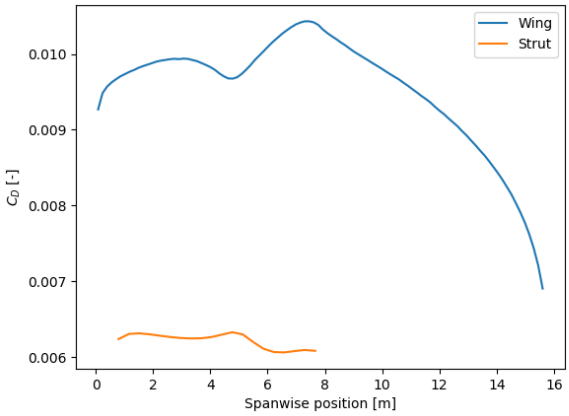

Figure 5.14: Spanwise C_D

Validation

To validate the results from AVL, a CFD analysis was performed in ANSYS. This was done in two steps; first the wings without struts were compared, then the wings with struts. For the wings without struts, the total lift produced by the wings was compared. The lift from the CFD analysis was 203,377.1 N and from AVL 201,410.2 N. That is a 0.97% difference and it was decided that this was good enough to get valid results from the AVL model of a single wing. To validate the wing-strut interaction results from AVL, two wings

were compared using CFD; one with and one without a strut. The results can be seen in Table 5.3. The values were obtained by placing the wings in cruise condition; 8000 m altitude at Mach 0.55.

Table 5.3: CFD results for single wing and wing-strut combination

Section	**Lift [N]**	**Drag [N]**	**Section**	**Lift [N]**	**Drag [N]**
Wing	189,594.1	10,010.1	Wing	182,148.0	10,663.7
			Strut	15,879.1	3,071.1
Total	**189,594.1**	**10,010.1**	**Total**	**198,027.1**	**13,734.8**

It can be seen from this table that unlike in the AVL analysis, the lift that the wing produces decreases when the strut is added. Figure 5.15 shows how this happens; the presence of the low pressure region on the top of the strut creates a low pressure area on the bottom of the wing, the blue area. This reduces the pressure difference between the top and bottom surface of the wing, decreasing the lift. From the AVL analysis it would follow that the pressure on the lower wing surface outboard of the strut would increase. However, as can be seen in the figure, this does not happen. This means that AVL does not accurately predict the behaviour of the flow where two surfaces interact with each other. The obtained lift distribution is thus not correct, but, as stated before, it was still used because it only slightly overdesigns the wingbox.

A second conclusion that can be drawn from the CFD analysis is that even though the wing loses lift due to the presence of the strut, the overall system actually gains lift because the strut also generates lift. It should be noted that the wing analysed here is not the full wing; the wing considered is shorter than in reality and the wingtip devices are omitted. This explains why the values for the lift and the drag presented here differ from the ones presented in subsection 5.2.5.

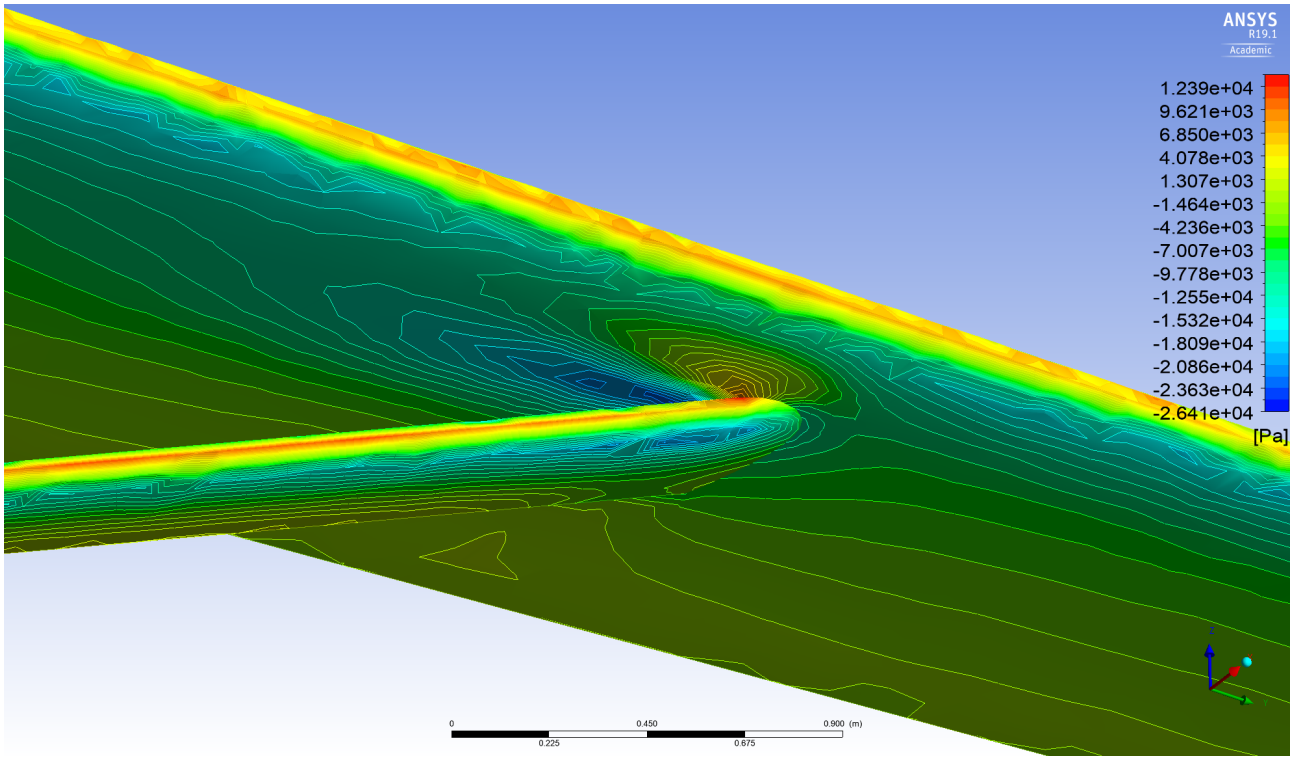

Figure 5.15: Pressure distribution on wing-strut intersection

5.2.9. Risk Assessment

During the design and sizing of the wing, it was of the utmost importance that the wing provided enough lift. One of the most critical flight phases was the landing phase since the speed was very low. The aircraft is equipped with high lift devices to provide lift at these low speeds. However, in case of failure of the high lift devices, the aircraft is still able to land. If this occurs, the aircraft has to land at a higher speed which requires a longer runway, possibly at a different airport.

Another risk which should be considered is the loss of lift at the point where the strut is connected to the wing. This risk was mitigated by fitting an airfoil around the strut such that it creates lift. By doing this, a margin was created regarding the lift.

5.3. Empennage Design

The empennage consists of the horizontal tail and the vertical tail. The purpose of the horizontal tail is to provide longitudinal stability and control, while the vertical tail provides lateral stability and control. First, the stability and control constraints of the aircraft are calculated. These result in a wing surface of the horizontal tail. In the next section, the total planform of the horizontal wing is given. This is followed up by the calculation of the vertical tail area and planform. Finally, the total resulting empennage is presented.

5.3.1. Stability and Control

The main purpose of the horizontal tail is to stabilise and control the aircraft in longitudinal direction. Therefore, the stability and control constraints are driving the sizing and design of the horizontal tail. Firstly, the stability of the aircraft is assessed. After that, the controllability is evaluated. This is done using a so-called "scissor plot". In this plot, the region in which the aircraft is both stable and controllable will be analysed.

Stability

The stability equation can be found in Equation 5.11 [22]. It can be seen that the centre of gravity is dependent on two factors: the aerodynamic centre and the influence of the horizontal tail. The stability margin (S.M.) is the safety factor on the centre of gravity, and is usually 5% of the MAC [22].

$$\bar{x}_{cg} = \bar{x}_{ac} + \frac{C_{L\alpha_h}}{C_{L\alpha_{A-h}}}\left(1 - \frac{d\epsilon}{d\alpha}\right)\frac{S_h l_h}{S\bar{c}}\left(\frac{V_h}{V}\right)^2 - S.M. \tag{5.11}$$

To determine the $C_{L\alpha_h}$ and $C_{L\alpha_{A-h}}$ of the aircraft, the *DATCOM* method is used [22]. This method is based on the wing geometry and on Mach number effects.

$$C_{L\alpha_h} = \frac{2\pi A_h}{2 + \sqrt{4 + \left(\frac{A_h \beta}{\eta}\right)^2 \left(1 + \frac{tan^2 \Lambda_{0.5c_h}}{\beta^2}\right)}} \tag{5.12}$$

In Equation 5.12, A_h is the aspect ratio of the horizontal tail. Furthermore, η is the airfoil efficiency and $\Lambda_{0.5c_h}$ is the wing sweep at the half chord line. The value is corrected for the Mach number with a correction factor β, which is equal to $\beta = \sqrt{1 - M^2}$.

For the computation of $C_{L\alpha_{A-h}}$, Equation 5.13 is used. This equation is dependent on the main wing geometry and on the fuselage diameter. For $C_{L\alpha_w}$, Equation 5.12 can be used. Parameters of the main wing should be used instead of parameters of the horizontal tail.

$$C_{L\alpha_{A-h}} = C_{L\alpha_w}\left(1 + 2.15\frac{b_f}{b}\right)\frac{S_{net}}{S} + \frac{\pi}{2}\frac{b_f^2}{S} \tag{5.13}$$

Here, b_f is the width of the fuselage and b is the span of the entire aircraft. S_{net} is the surface area without the fuselage attached part and S is the total surface area.

Control

Now that the stability constraint can be calculated, controllability should be assessed. This is done with equation Equation 5.14. In this equation, the centre of gravity is calculated by the aerodynamic moment and the moment created by the horizontal tail.

$$\bar{x}_{cg} = \bar{x}_{ac} - \frac{C_{m_{ac}}}{C_{L_{A-h}}} + \frac{C_{L_h}}{C_{L_{A-h}}} \frac{S_h l_h}{S\bar{c}} \left(\frac{V_h}{V}\right)^2 \tag{5.14}$$

The most crucial situation for controllability is the landing. Therefore, the C_L of the aircraft during landing is used. The lift coefficient of the horizontal tail during landing can be approximated using Equation 5.15.

$$C_{L_{h_L}} = -0.35 A_h^{1/3} \tag{5.15}$$

Loading Diagram

Loading diagrams are a crucial tool when operating the aircraft. They present the minimum and maximum centre of gravity location for all the possible loading cases. The wing position and the according c.g. position of the OEW were used to create the loading diagram, presented in Figure 5.16.

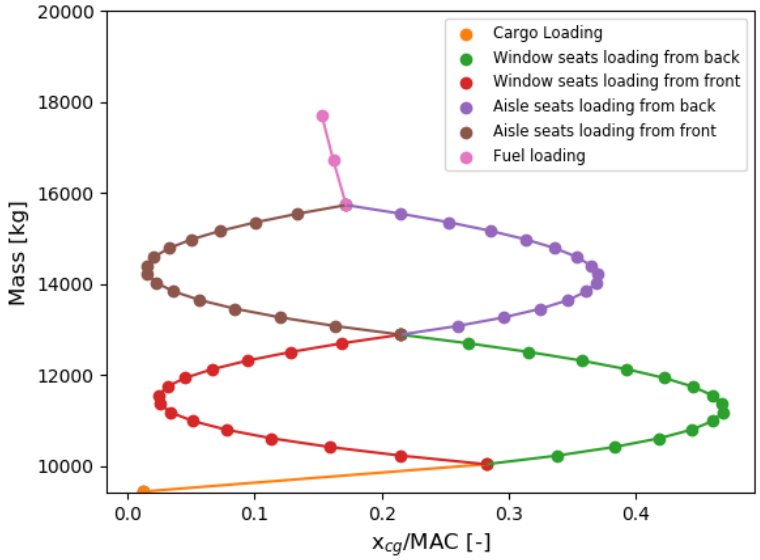

Figure 5.16: Loading Diagram of the aircraft

The diagram consists of three main parts; the loading of the payload in the cargo bay, the loading of the passengers, and the attachments of the fuel pods. The loading of the passengers was split into the loading of the window seats and the loading of the aisle seats. For each of these cases, forward loading and backward loading were both considered. This resulted in the two oval shapes in Figure 5.16. For the minimum and maximum value of the c.g., a safety margin of 2% was applied to compute the centre of gravity limits. This is done to account for inaccuracies in the passenger weights and location of the weights.

Scissor Plot

Now that the control and stability constraints and the centre of gravity shift are known, a scissor plot can be made. In this plot, the area between the blue lines represents the what combination of horizontal tail area and c.g. range the aircraft is both controllable and stable. The area between the yellow lines represents the stable c.g. ranges for several wing positions. The optimal line is where both c.g. ranges overlap. From this horizontal line, the size of the horizontal tail and the longitudinal position of the wing can be determined. The scissor plot can be found in Figure 5.17. As can be seen, the horizontal tail ratio is determined to be 0.274 and the position of the LEMAC wing is at 42.83% of the fuselage.

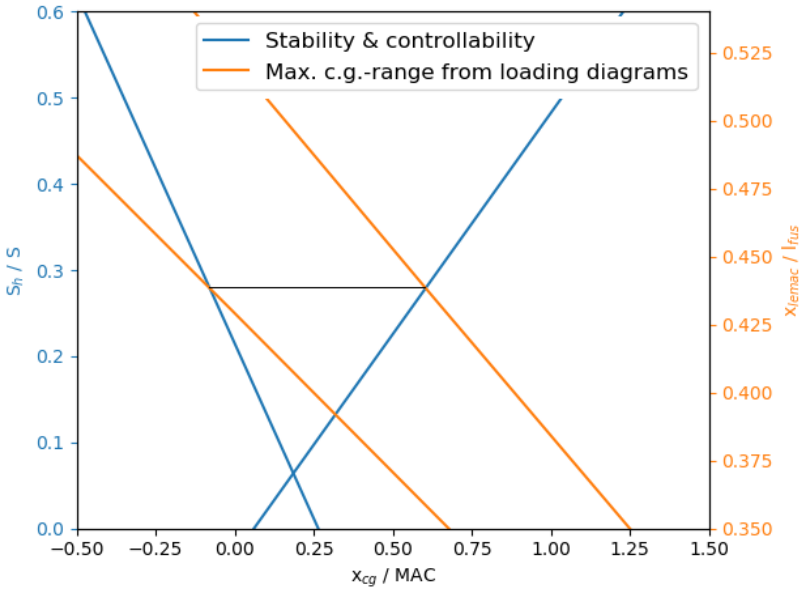

Figure 5.17: Scissor Plot

5.3.2. Horizontal Tail

The next step is to decide the horizontal tail wing parameters. Parameters, such as the aspect ratio and taper ratio, have a great influence on the effectiveness of the horizontal tail. Furthermore, an elevator needs to be designed to control the aircraft.

Wing Planform

The taper ratio, wing sweep and aspect ratio are decided based on statistical data and desired wing characteristics [23]. The most crucial factor in this case was the T-tail configuration. In order to fit the horizontal safely to the vertical tail, the root chord of the horizontal tail could not exceed the tip chord of the vertical tail. It was later decided to fit the horizontal tail close to the tip of the vertical tail, instead of on top of the vertical tail. As a result, weight was saved in the connection between the two tail surfaces. The horizontal tail can have a higher taper ratio, though. This increases the C_{L_α} of the horizontal tail.

Elevator design

The primary function of the elevators is to ensure longitudinal control of the aircraft. This is done by changing the elevator angle δ_E, in order to change the lift generated by the horizontal tail. For the design of the elevators, three main parameters must be considered; the elevator chord-to-tail-chord ratio ($\frac{C_E}{C_h}$), the elevator-span-to-tail-span ratio ($\frac{b_E}{b_h}$), and the maximum elevator deflection ($\pm\delta_{E_{max}}$). The design steps were based on the design algorithm presented in [24].

The maximum deflection angle was taken to be ±25°, based on values of modern reference aircraft. The elevators are designed to span 80% of the entire horizontal tail, so $\frac{b_E}{b_h} = 0.8$. Thus, the only parameter left to be calculated was $\frac{C_E}{C_h}$.

It was found that the take-off rotation was the most limiting factor for the elevator sizing, as the elevator must ensure a minimum pitch acceleration for take-off. From [24], this minimum pitch acceleration was found to be $7\frac{deg}{s^2}$ for an twin turboprop airliner. The required lift generated by the horizontal tail L_h was calculated using Equation 5.16.

$$L_h = \frac{L_{wf}\left(x_{mg} - x_{ac_{wf}}\right) + M_{ac_{wf}} + ma\left(z_{cg} - z_{mg}\right) - W\left(x_{mg} - x_{cg}\right) + D\left(z_D - z_{mg}\right) - T\left(z_T - z_{mg}\right) - I_{yy_{mg}}\ddot{\theta}}{x_{ac_h} - x_{mg}} \tag{5.16}$$

From L_h, the C_{L_h} to ensure take-off rotation was found to be -0.465, using Equation 5.17

$$C_{L_{h_{TO}}} = C_{L_{\alpha_h}} \alpha_h + C_{L_{\alpha_h}} \tau_e \delta_E = C_{L_{c_h}} (\alpha_h + \tau_e \delta_E) \tag{5.17}$$

The next step was to calculate the angle of attack effectiveness of the elevator by use of Equation 5.18, resulting in a value of 0.32.

$$\tau_e = \frac{\alpha_h + \left(C_{L_h} / C_{L_{a_b}}\right)}{\delta_{E_{\max}}} \tag{5.18}$$

This value was used to determine the elevator-area-to-vertical-tail-area ratio $\frac{S_e}{S_h}$ from Figure 5.18.

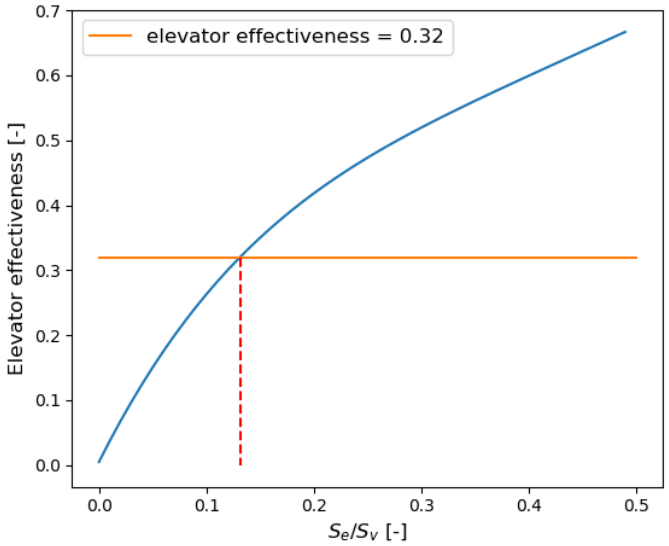

Figure 5.18: Elevator effectiveness as a function of the surface area ratio

The relation presented in Figure 5.18 is constructed by Equation 5.19.

$$\tau_e = -6.624\left(\frac{S_a}{S}\right)^4 + 12.07\left(\frac{S_a}{S}\right)^3 - 8.292\left(\frac{S_a}{S}\right)^2 + 3.295\left(\frac{S_a}{S}\right) + 0.004942 \tag{5.19}$$

This results in a $\frac{S_e}{S_h}$ of 0.132. Accounting for the fact that only 80% of the horizontal tail span is available for the elevator, because of the space needed for the rudder, this translates to a $\frac{C_e}{C_h}$ of 0.376.

5.3.3. Vertical Tail

The function of the vertical tail is to control the aircraft in lateral direction. This is mainly done by the rudder which deflects in order to create lift, and thus a resulting yawing moment. The design of the vertical tail consists of three main items; the wing planform, the vertical tail surface S_v, and the rudder-chord-to-fin-chord ratio $\frac{C_R}{C_F}$.

Wing Planform

Because the aircraft has a T-tail configuration, the vertical tail can not be heavily tapered. When selecting a taper ratio, statistical data of T-tailed aircraft was consulted. A higher taper ratio will decrease the structural weight, but can result in premature tip stall of the vertical tail. Using this statistical data, the taper ratio was chosen to be 0.6.

As one of the requirements states that the total height of the aircraft shall not exceed 13.5 meters. With the vertical tail designed as such, the total height of the aircraft will be 7.62 m. This means that the requirement is met.

Dorsal Fin

A dorsal fin is a wing structure in front of the vertical tail. The main goal of this structure is to stabilise the flow causing a low pressure region over the vertical tail. This results in a higher stall angle for the vertical tail. The dorsal fin of Aquila was sized by use of statistically based relationships [25], resulting in a dorsal fin leading edge sweep angle of 11 degrees and a height of 0.516 m. After this, the dynamic vertical tail stall angle was found to be 40.1 degrees[26].

Surface Area and Rudder Sizing

The rudder is used to control the lateral attitude of the aircraft. The rudder-span-to-fin-span ratio was taken to be 0.8, which is a maximal value due to geometry of the empennage. Therefore, the only parameter that influences the size, and thus the performance, is the vertical fin surface area S_v, and the rudder-chord-to-fin-chord ratio $\frac{C_R}{C_F}$. These must be designed to meet the following requirements for the yawing moment coefficient due to rudder deflection N_ζ [27]:

- The rudder must enable the aircraft to change its heading against the failed engine. This results in the boundary condition in Equation 5.20.

$$N_\zeta \geq 1.35 N_E / \zeta_{\text{MAX}} \tag{5.20}$$

  Here, N_E is the engine failed moment coefficient at take-off, calculated by Equation 5.21 [28].

$$C_{n_e} = k \frac{\Delta T_{TO} y_e}{\frac{1}{2}\rho_0 V_{TO}^2 S b} \tag{5.21}$$

  Where $k = 1.3$ for a high wing configuration and an inward rotating propeller.
- The full rudder deflection must never cause the vertical fin to stall. This can be translated to the boundary equation in Equation 5.22.

$$-N_\zeta \leq 0.7 N_V / \zeta_{\text{MAX}} \tag{5.22}$$

  The factor of 0.7 represents the dynamic fin stall angle, resulting from the dorsal fin.
- The rudder must ensure the aircraft to maintain its heading in the presence of cross-wind. The ratio of the cross-wind velocity to the forward velocity of the aircraft was taken to be 0.2. This boundary condition for N_ζ was computed using Equation 5.23:

$$-N_\zeta \geq 0.375 N_v / \zeta_{MAX} \tag{5.23}$$

  Here, the factor of 0.375 accounts for a heading change of 0.175 rad due to the cross-wind condition.

These will all result in boundary conditions for the yawing moment coefficients due to the rudder deflection, as a function of $\frac{S_v}{S}$ and a fixed value of $\frac{C_R}{C_F}$. These conditions are plotted in Figure 5.19. Also, using equation Equation 5.24,the actual yawing moment coefficient due to the rudder deflection is plotted in Figure 5.19.

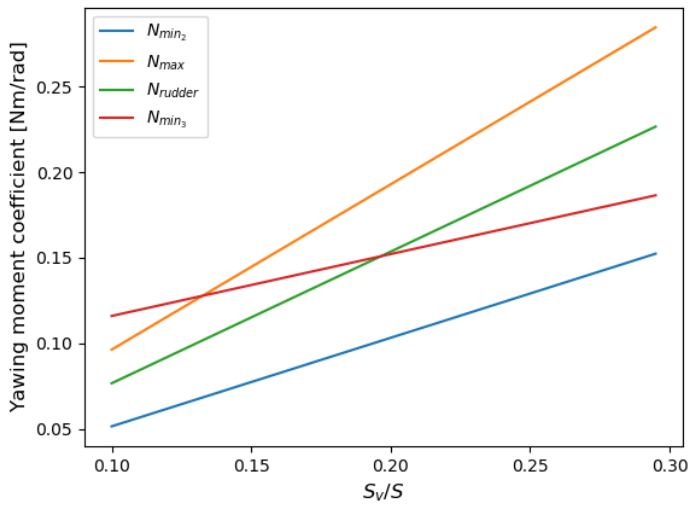

Figure 5.19: Vertical tail yawing moment coefficients boundary conditions

$$N_\zeta = -\overline{F}\left[\left(\frac{c_f}{c}\right)_R^{0.47} + 0.08\right]\left(\frac{l_F}{b}\right)\left(\frac{S_F}{S}\right) \tag{5.24}$$

This plot is created for a $\frac{C_R}{C_F}$ of 0.4. The goal is to design the vertical tail as small as possible, while still meeting the requirements stated above. Therefore, a $\frac{S_v}{S}$ of 0.19 was selected, as can be seen in Figure 5.19.

5.3.4. Results

The final design of the empennage and its control surfaces are summarised in Table 5.4 and Table 5.5.

Table 5.4: Final Design Parameters of the Empennage

	Horizontal Tail		*Vertical Tail*		
Parameter	**Symbol**	**Value**	**Symbol**	**Value**	**Unit**
Surface Area	S_h	14.27	S_v	13.29	m^2
Root Chord	c_{r_h}	2.52	c_{r_v}	4.16	m
Tip Chord	c_{t_h}	1.26	c_{t_v}	2.50	m
Mean Aerodynamic Chord	MAC_h	1.96	MAC_v	3.40	m
Taper Ratio	λ_h	0.5	λ_v	0.6	-
Span	b_h	7.56	b_v	3.99	m
Quarter Chord Sweep	$\Lambda_{c/4_h}$	15	$\Lambda_{c/4_v}$	30	deg
Aspect Ratio	A_h	4.0	A_v	1.2	-
Volume Coefficient	V_h	2.09	V_v	0.09	-

Table 5.5: Final design parameters of the empennage control surfaces

	Elevator		*Rudder*		
Parameter	**Symbol**	**Value**	**Symbol**	**Value**	**Unit**
Surface Area	S_e	1.78	S_r	1.96	m^2
Chord Ratio	C_e/C_h	0.376	C_r/C_v	0.4	-

5.4. Undercarriage Design

The position of the undercarriage is crucial to operate the aircraft safely on the ground. The longitudinal and lateral position of the undercarriage is determined to make sure that the aircraft can easily rotate during take-off and will not tip-over during loading and taxiing.

5.4.1. Longitudinal Position

The longitudinal position of the landing gear is determined by the load fraction on the wheels. It is desired to have 92% of the total load on the main landing gear and 8% of the total load on the nose landing gear [29]. For this calculation, the most aft centre of gravity is used. To avoid the aircraft from tipping over, the worst case scenario is used. Also, the loads on the main landing gear will be the largest in this case. The nose landing gear is placed in the nose cone of the fuselage. When this position is known, the position of the main landing gear can also be calculated by Equation 5.25. In this equation, x_{ml} and x_{nl} are the longitudinal position of both the main landing gear and nose landing gear, respectively. L_{nl} and L_{ml} are the load fraction on the nose landing gear and main landing gear, respectively.

$$x_{ml} = \frac{x_{nl}L_{nl}}{L_{ml}} \tag{5.25}$$

5.4.2. Height

When the longitudinal position is known, the undercarriage height can be determined. This is defined as the distance between the ground and the bottom of the fuselage. This distance is determined by the scrap angle and the longitudinal tip-over angle. The height constraint of the scrap angle can be found in Equation 5.26. As can be seen, the height is dependent on the distance between the main landing gear and the tail cone. The scrap angle is set to 8 degrees. This is based on the ATR 72 reference aircraft and the angle of attack needed to take-off and land.

$$h_{ml} = (l_{fus} - l_{tail} - l_{ml}) tan(\theta_{scrap}) \tag{5.26}$$

The tip-over angle can now be determined. It should be checked whether the tip-over angle is larger than the scrap angle. If this is true, it is certain that the aircraft will not tip-over during loading or accelerating. The equation for tip-over can be found in Equation 5.27. It is dependent on the longitudinal and vertical position of the main landing gear and centre of gravity. From this equation, it follows that the tip-over angle is 20 degrees. Hence, the aircraft will not tip over.

$$\theta_{tip} = tan^{-1}\left(\frac{l_{ml} - x_{cg}}{z_{cg}}\right) \tag{5.27}$$

5.4.3. Lateral Position

The last position that should be determined is the lateral position of the landing gear. The constraining factor for this position is the lateral tip-over angle (Ψ). The aircraft should not tip-over when turning during ground operations. The lateral position is dependent on the position of the main landing gear, position of the nose landing gear and the position of the centre of gravity. The lateral tip-over angle is set at 55 degrees, as this is suggested by Roskam [30]. The equation for the lateral position of the main landing gear can be found in Equation 5.28.

$$y_{ml} = \frac{(x_{cg} - l_{nl}) + (l_{ml} - x_{cg})}{\sqrt{\frac{(x_{cg} - l_{nl})^2 tan^2\Psi}{z_{cg}^2} - 1}} \tag{5.28}$$

From this equation, the lateral position of the landing gear is determined to be 1.49 meter from the centre line. It should be checked whether the aircraft will not tip over laterally when one of the tanks is removed. It was calculated that the centre of gravity will shift with a maximum of 0.6 m in the lateral direction when one of the tanks is removed. Since this is almost three times smaller than the lateral position of the landing gear, tip over should not be an issue.

5.4.4. Shock Absorber

It should be noted that these values do not include the length of the absorber stroke. The worst case scenario should be calculated and this is when the absorber is fully pulled in. The next step is to calculate the absorber stroke needed. This is done using Equation 5.29, found in Raymer [1]. It is assumed that the stroke will completely absorb the shock. This is done as a safety factor.

$$S_{stroke} = \frac{V_{vertical}^2}{2 g n_{gear} \eta} \tag{5.29}$$

In this equation, $V_{vertical}$ is the vertical approach speed. This is assumed to be 3.1 m/s, according to CS-25 regulations. The gear load factor (n_{gear}) is assumed to be 3, also according to CS-25 regulations. The stroke efficiency is assumed to be 0.75 [1]. From Equation 5.29, the stroke is calculated to be 0.22 m.

It is chosen to use steel as material for the undercarriage. Steel is widely used in the design of the undercarriage, because of its high failure stress. Furthermore, it is cheaper than titanium, which is the next best alternative.

5.4.5. Wheel Design

The tire pressure is determined by the lowest Load Classification Number (LCN) of the runways that will be used. For Aquila, this number is based on the reference airports. The design LCN is chosen to be 25. The tire pressure can be calculated with Equation 5.30.

$$p = 430ln(LCN) - 630 \tag{5.30}$$

From the chosen LCN, the tire pressure is calculated to be 7.54 kg/cm^2. The size of the wheels is determined by the load per wheel and the tire pressure. The size of the wheels can be found in Figure 5.20. From this figure, it was determined that the nose wheels have a diameter of 0.35 m and the main landing wheels have a diameter of 0.66 m. The nose landing gear consists of two wheels with one strut and the main landing gear of four wheels with two struts in total.

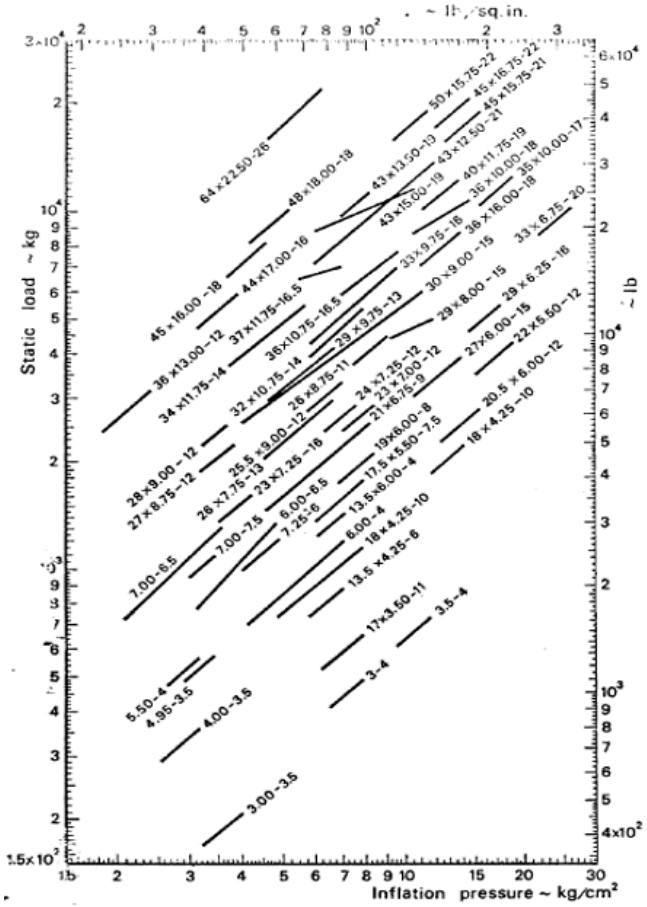

Figure 5.20: Determination of wheel size [31]

During landing a tire may fail, which could lead to the aircraft being not controllable and shooting of the runway. The aircraft however features two tires per strut for both the nose and main landing gear. Additionally, the aircraft is able to safely land and taxi with one tire per strut.

5.4.6. Results

The position of the nose landing gear and the main landing gear are calculated and summarised in Table 5.6. It should be noted that these are the values when the stroke is fully retracted, as this is the worst case scenario.

Table 5.6: Position of the Undercarriage

Parameter	Symbol	Value [m]
Nose Landing Gear		
Longitudinal Position	l_{nl}	2.00
Lateral Position	y_{nl}	0.00
Height	h_{nl}	0.79
Main Landing Gear		
Longitudinal Position	l_{ml}	10.94
Lateral Position	y_{ml}	1.49
Height	h_{ml}	0.79

5.4.7. Risk Assessment

The position of the centre of gravity is of great importance regarding the stability of the aircraft. During flight a sudden shift in the centre of gravity can occur due to cargo sliding in the cargo compartment for example. By increasing the minimum and maximum value of the c.g. location by 2% this risk is mitigated.

5.5. Material Characteristics

This section explains the reasoning behind the chosen materials for the design. One of the most important factors to take into account in the choosing the right materials, is the weight. Figure 5.21 shows the weight, as well as the requirements in terms of materials for different components that were considered during the design. This section discusses the different possibilities in terms of material choice.

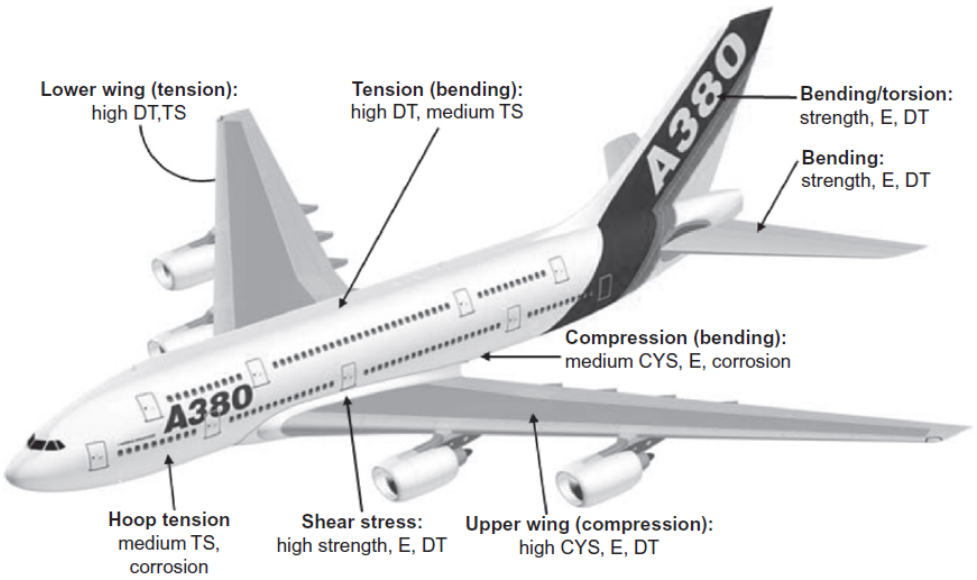

Figure 5.21: Typical load conditions and engineering property requirements for main structural areas of the Airbus A380: CYS = compressive yield strength; E = elastic modulus; TS = tensile strength; DT = damage tolerance properties (fatigue, fatigue crack growth, fracture toughness) [32].

5.5.1. Composite Materials

The use of composite materials in the aerospace industry has increased, with e.g. the B787 Dreamliner using up to 50% composite material by weight. Using composite materials allows a significant weight reduction [33], but introduces an increase in cost of both the material and production. In the long term, this may be countered by the savings in fuel as a result of the weight reduction, which can be 10-20% per part [32].

The resistance to corrosion and fatigue is another great advantage of the use of composite material, which greatly reduces the maintenance cost; in general, they are more durable than metals. In terms of structural

design, using composites increases the flexibility[5]. For example, a piece manufactured out of composite material can replace an assembly consisting of numerous metal parts.

However, using composite material also has some disadvantages. Even though on a laboratory scale level of the recycling of composites has been demonstrated, there still lies a big challenge in scaling these up to be economically viable [34], which is a disadvantage of using composites with respect to sustainability. Next to this, composites are more prone to impact damage and the related fatigue crack and delamination. This also became evident when the first flight of the Dreamliner was postponed by 6 months due to unexpected failure of the composite centre wing box [35]. Furthermore, legislation and manufacturing processes are not optimised yet to let the transition of using composites in aerospace applications accelerate further [35].

As the failure mode of composite structures is difficult to predict, the structure should be overdesigned, increasing the safety factor from 1.5, used for aluminium alloys, to 2 (on top of the critical conditions of load factor 2.5). Another failure mode of carbon fibre reinforced polymer (CFRP) arises due to the fact that they are poorer thermal and electrical conductors than aluminium alloys. Without the introduction of advanced materials as reinforcement like graphene, CFRP structures are susceptible to severe damage in case of a lightning strike [36].

Composites generally show larger variation in strength than metals, which affects the statistical B-basis design allowable (the value for strength that at least 90% of the materials exceed, with a confidence level of 95%), as shown in Figure 5.22. To find these design allowables, a research was performed in a PhD thesis which tests specimens at room temperature, hot-wet, and cold-dry conditions [37]. The mechanical properties of CFRP that were considered are the same as in the research that evaluates the design allowables, as shown in Table 5.7.

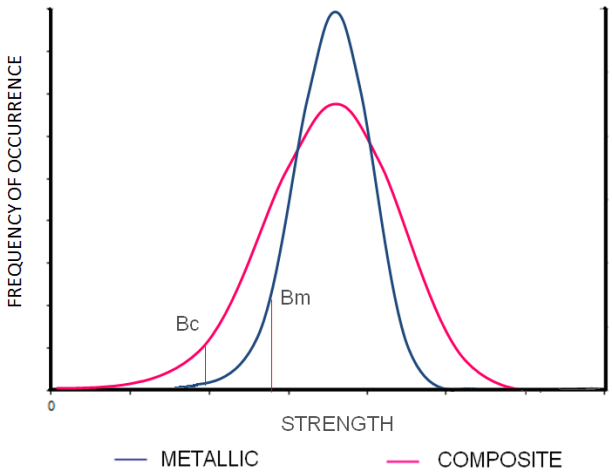

Figure 5.22: Illustration of the effect of the variation in strength between composites and metals on the B-basis design allowable [37].

5.5.2. Metals

The isotropic mechanical properties of alloys in general are an advantage with respect to composites, although this may vary per alloy. One of the flaws of the second generation of aluminium-lithium alloys was the anisotropic behaviour, which was minimised to an acceptable extent when developing the third generation [38]. As for aluminium alloys, the third and latest generation of aluminium-lithium (Al-Li) alloys offer weight savings with respect to older aluminium alloys having lower densities. Therefore, by having the same or even higher elasticity moduli, Al-Li alloys have 8-15% higher specific stiffness than conventional aluminium alloys. In addition, they are weldable, which reduces manufacturing cost, as it requires less steps, and increases the corrosion resistance due to the decrease in the amount of holes and gaps in the material [32].

[5]Retrieved from: http://compositeslab.com/benefits-of-composites/design-flexibility/ (consulted on 1-7-2019)

One of the flaws of the second generation of aluminium-lithium alloys was the anisotropic behaviour, which was minimised to an acceptable extent when developing the third generation [38]. Together with the increased specific properties, this already led to the use of the third generation aluminium lithium alloys in e.g. the Airbus A380-800 or Bombardier's Cseries[6].

For comparison of the mechanical material properties, titanium[7] was added, together with the relevant Al-Li alloys [32] and CFRP [35]. Table 5.7 only shows the raw material costs, where for the Al-Li alloys 2% of pure lithium was added, costing $16.5 per kg[8]. This results in a material cost of 2.55 USD per kg for the Al-Li alloys.

Table 5.7: Considered materials for the aircraft. A single value indicates the same tensile as compressive strength. (*) indicates a calculated or assumed value, as discussed in subsection 5.6.3

Material	**Density [kg/m^3]**	**Material cost [USD/kg]**	**Yield strength tensile/compressive [MPa]**	**E-modulus tensile/compressive [GPa]**	**Shear strength [MPa]**	**Fatigue strength [MPa]**
AA7075-T6	2810	2.3	503/503	71.7/73.1	331	159
AA2055-T84	2710	2.55	538/552	76.5/78.5	311	151
AA2195-T84	2700	2.55	500/510	78/79.4	331*	130
AA2099-T83	2630	2.55	490/476	78.6/82.1	448	130
AA2198-T8	2690	2.55	407	76.5	257*	130*
AA2060-T8E30	2720	2.55	488	72.1	300*	130*
Ti-6Al-4V	4430	20.85	880/970	113.8	550	240
QI CFRP	1600	42	511/509	115.9	70.7	-

5.6. Structural Design

In order to make sure that the aircraft can withstand all forces that act on it, the structure of the design has to be considered. The structural characteristics are defined in this section, comprising of analyses of the wing box, fuselage and implementation of the strut. First, the calculations of all of the forces are explained in subsection 5.6.1, followed by an explanation of how the stresses are calculated in subsection 5.6.2. After this, the possible failure modes of the structures are discussed in subsection 5.6.3. The structural characteristics of the wing box are presented in subsection 5.6.4. Next, the concept of aeroelasticity and its effect on the wing design is discussed in subsection 5.6.5. The structural design of the fuselage and strut are elaborated in subsection 5.6.6 and subsection 5.6.7 respectively. Lastly, the influence of the strut on the design and the risk of the structural design are presented in subsection 5.6.8 and subsection 5.6.9.

5.6.1. Calculations of Loading

In order to understand the loads and stresses that will act on the wing, all forces had to be analysed. First, the forces in the xy-plane were evaluated, after which the forces in the xz-plane were calculated. The wing was in both cases represented by a beam which is fixed at its root, where the wing meets the fuselage.

During the design of the wing box structure, several assumptions were made to ensure a less difficult design process, without compromising the design outcome too heavily. All assumptions regarding the calculations of the loading along the wing are listed below:

- The wing box can be modelled as a beam on which all loads act.
- The wing weight can be described as a distributed force.
- The engine weight, fuel weight and pod weight can be described as point forces.
- The wing box can be designed as a thin walled structure.
- The stringers in the wing box have no resistance against the shear flow.

[6] Retrieved from https://aluminiuminsider.com/aluminium-lithium-alloys-fight-back/ (consulted on 24-6-2019)
[7] Retrieved from: http://www.metalspiping.com/titanium-alloy-ti-6al-4v.html (consulted on 14-6-2019)
[8] Retrieved from: https://www.metalary.com/lithium-price/ (consulted on 17-6-2019)

- The angle of twist of the wing has a negligible effect on the loading calculations, and is covered by the safety factors.

Forces in the xy-plane

Figure Figure 5.23 shows a representation of the wing in the xy-coordinate system, together with all forces that act on the wing. The engine weight acts at 27% of the length of the wing, the strut at 50%, and the fuel pod at 55%. In this case the lift along the wing, the distributed weight of the wing, the weight of the engine and the weight of the pod were already known. The reaction forces in x- and y-direction, the moment around the z-axis and the force that the strut exerted on the wing were unknown.

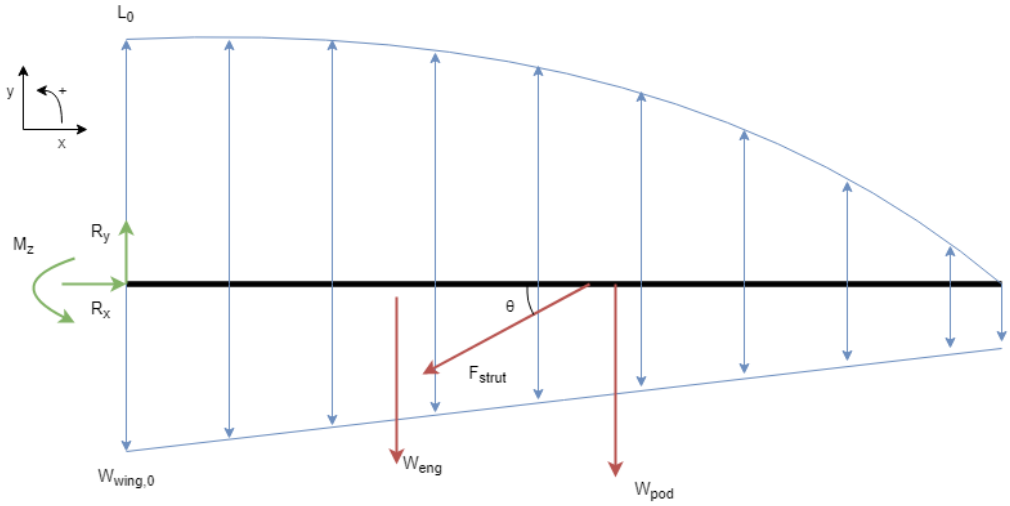

Figure 5.23: Beam representation of the wing in the xy-coordinate system.

Several equations were used to solve for these unknowns. Firstly, the sum of forces in both x and y have to be equal to zero. Furthermore, the sum of moments around the tip of the wing have to be zero. This yields the following three equations:

$$R_x - F_{strut} \cdot cos(\theta) = 0 \tag{5.31}$$

$$R_y - F_{strut} \cdot sin(\theta) - W_{engine} - W_{pod} - \int_0^{b/2} W_{wing}(x)dx + \int_0^{b/2} L(x)dx = 0 \tag{5.32}$$

$$M_z - W_{engine} \cdot (x_{tip} - x_{engine}) - F_{strut} \cdot sin(\theta) \cdot (x_{tip} - x_{strut}) - W_{pod} \cdot (x_{tip} - x_{pod}) - \int_0^{b/2} W_{wing}(x) \cdot (x_{tip} - x)dx + \int_0^{b/2} L(x) \cdot (x_{tip} - x)dx = 0 \tag{5.33}$$

In these equations, θ is the angle between the strut and the main wing, which has been quantified as: $\theta = arctan(d_{fuselage}/x_{strut})$. With the final aircraft layout parameters, this angle becomes 20 degrees.

With three equations and four unknowns, the system was still indeterminate. In order to solve for these unknowns an additional equation had to be set up. This extra equation came from the Euler-Bernoulli beam theory equation, shown in Equation 5.34, where $v_y(x)$ is the deflection of the beam at point x. $M_z(x)$ and $I_{yy}(x)$ are the bending moment and moment of inertia at point x [39]. This bending moment along the wing can be expressed using the Macaulay step function method [40]. Equation 5.35 describes the moment at each point x along the wing. As it was rather difficult to present the induced moment by the lift distribution and the wing weight distribution, these two force distributions were discretised into n sections to represent a large set of point forces along the wing. If the value between Macaulay brackets becomes negative for a certain value of x, it is left out of the moment computation for that point along the wing.

$$\frac{d^2 v_y(x)}{dx^2} = -\frac{M_z(x)}{EI_{zz}(x)} \tag{5.34}$$

$$M_y(x) = -M_z\langle x-0\rangle^0 + R_y\langle x-0\rangle^1 - W_{engine}\langle x-x_{engine}\rangle^1 F_{strut}\cdot sin(\theta)\langle x-x_{strut}\rangle^1 - W_{pod}\langle x-x_{pod}\rangle^1 + \sum_{i=1}^{n} L_i\langle x-x_i\rangle^1 - \sum_{i=1}^{n} W_i\langle x-x_i\rangle^1 \tag{5.35}$$

By integrating Equation 5.34 once, the angle of deflection that the beam makes with the horizontal can be found. If the equation is integrated once more, the actual deflection along the wing can be found. Since the equation which describes the moment of inertia was not exactly known at this stage of the design process, it was rather difficult to exactly integrate Equation 5.34. Therefore, the equation was discretised and numerically integrated twice which gave the following equations for deflection angle and deflection at any beam section i:

$$\theta_i = \theta_{i-1} + \frac{1}{2}\left(\frac{M_i}{EI_i} + \frac{M_{i-1}}{EI_{i-1}}\right)(x_i - x_{i-1}) \quad (i = 1,2\ldots n) \tag{5.36}$$

$$v_i = v_{i-1} + \frac{\theta_i + \theta_{i-1}}{2}(x_i - x_{i-1}) \quad (i = 1,2\ldots n) \tag{5.37}$$

In order to solve these, several boundary conditions had to be set. Since the wing box was approximated as a beam which is fixed at the root, the deflection as well as the angle at the root were zero. Next to this, the deflection of the wing at the position of the strut was also set to zero. This was set because deflection at this point would mean very high internal forces in the strut. The boundary conditions are summarised in Table 5.8.

Table 5.8: Boundary condition of the wing in the xy-frame

x-position	Boundary condition
x_{root}	$v_y = 0$
x_{root}	$\theta_y = 0$
x_{strut}	$v_y = 0$

By combining Equation 5.36 and Equation 5.37, the deflection at the strut can be expressed in terms of all forces and moments which act on the wing. This provided the fourth equation that was needed in order for the unknowns to be solved. The reaction forces are calculated for a load factor of 3.8, which includes a safety margin of 1.5 to ensure structural integrity of the wing. The forces in the xy-plane are then presented in Table 5.9.

Table 5.9: Reaction forces in the xy-plane

Unknown	Value	Unit
R_x	550.6	kN
R_y	-52.1	kN
F_{strut}	585.6	kN
M_z	9.2	kNm

Forces in the xz-plane

For the forces in the xz-plane a similar approach was used as for the computation of the forces in xy. Figure 5.24 shows a beam representation of the wing as viewed from the top. Again all moments and forces that act on the wing had to be calculated. The unknowns in this reference frame were the reaction force at the root, the z-component of the strut force and the moment at the root around the y-axis.

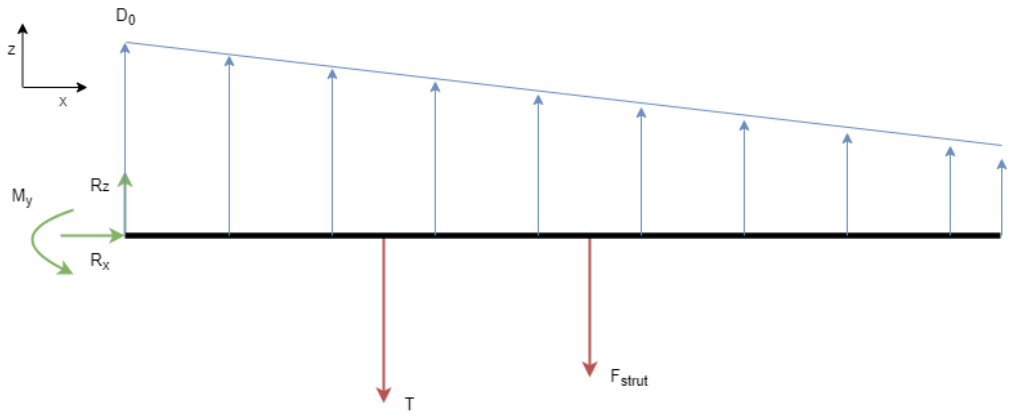

Figure 5.24: Beam representation of the wing in the xz-coordinate system.

The sum of forces in the z-direction, as well as the sum of moments around the y-axis provided the first two equations to solve for the unknown forces. The deflection of the wing, as described by Equation 5.38, provided the final equation.

$$\frac{d^2 v_z(x)}{dx^2} = -\frac{M_y(x)}{EI_{yy}(x)} \tag{5.38}$$

Table 5.10: Boundary condition of the wing in the xz-frame

x-position	Boundary condition
x_{root}	$v_z = 0$
x_{root}	$\theta_z = 0$
x_{strut}	$v_z = 0$

Again, using Equation 5.36 and Equation 5.37 together with the set boundary conditions in Table 5.10, the unknown forces in xz where determined to be:

Table 5.11: Reaction forces in the xz-plane

Unknown	Value	Unit
R_z	-25.1	kN
$F_{strut,z}$	-10.9	kN
M_y	65.9	kNm

Moment and Shear Diagrams

The calculated forces, as presented so far, allowed the generation of several shear force and moment diagrams as shown in Figure 5.25 up to Figure 5.28.

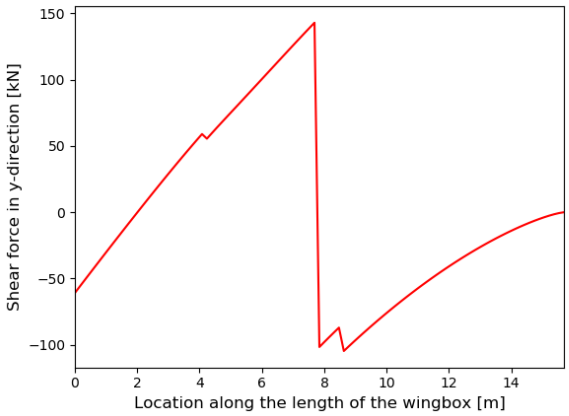

Figure 5.25: Shear force diagram of the wing box around the y-axis.

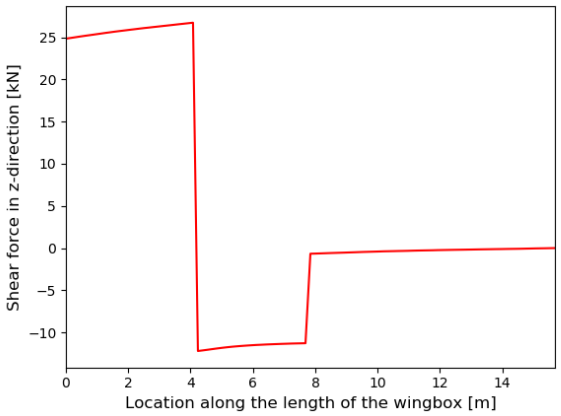

Figure 5.26: Shear force diagram of the wing box around the z-axis.

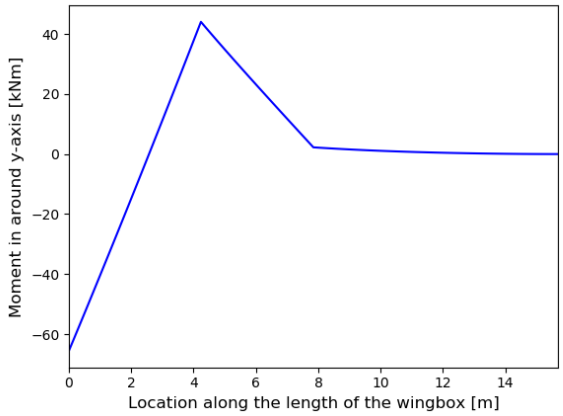

Figure 5.27: Moment diagram of the wing box around the y-axis.

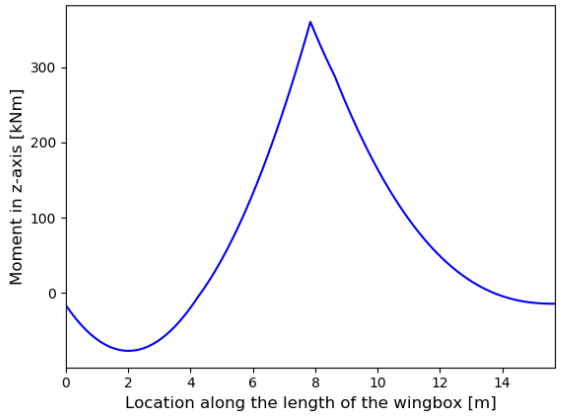

Figure 5.28: Moment diagram of the wing box around the z-axis.

Wing Deflection

Due to the bending moments presented above the wing is deflected. The resulting wing deflection in y- and z-direction are portrayed in Figure 5.29 and Figure 5.30. The positive values in Figure 5.29 represent upward deflection, whereas the negative values in Figure 5.30 represent backward deflection of the wing. It can be seen that due to the boundary conditions set in the design, the deflections at the root as well as at the strut are equal to zero. The total upward deflection is 8.3% of the wing half span.

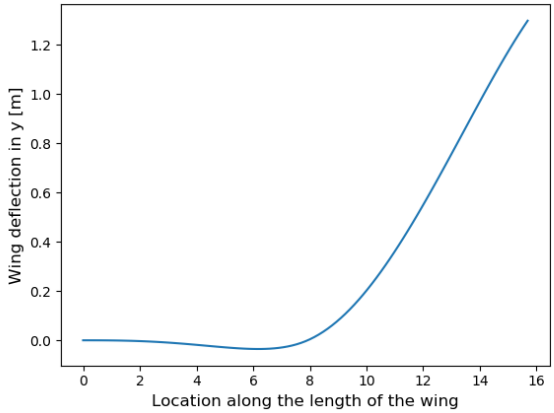

Figure 5.29: Deflection of the wing in y-direction

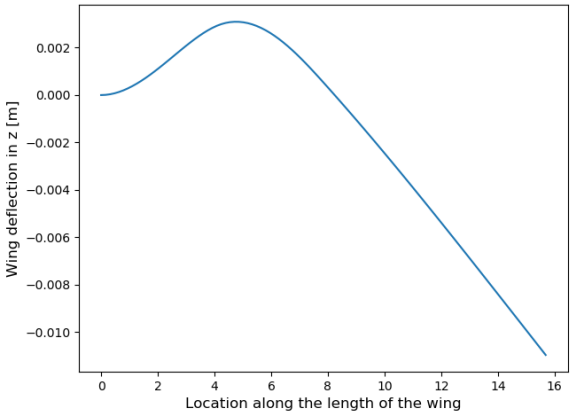

Figure 5.30: Deflection of the wing in z-direction

5.6.2. Stress Calculations

In order for the failure modes to be calculated in subsection 5.6.3, the stresses had to be calculated first. In this section, the normal and shear stresses are described.

Normal stress

The normal stress in the cross-section along the wing consists of three components: those due to the bending moment in y-direction, the bending moment in z-direction, and the normal force in x-direction. The number and type of stiffeners on the upper and lower skin might vary, which is why the neutral y-axis would most likely not be at 50% of the height of the wing box. To control the failure modes related to buckling, the spacing of the stiffeners was kept constant, resulting in a vertical plane of symmetry coinciding with the y-axis. Due to this vertical plane of symmetry, I_{yz} is zero. This leads to Equation 5.39, where the moment contributions have a negative sign due to the coordinate system, i.e. such that positive moments create positive stress in the positive quadrant.

$$\sigma = -\frac{M_y \cdot z}{I_{yy}} - \frac{M_z \cdot y}{I_{zz}} + \frac{N_x}{A} \tag{5.39}$$

The bending moments were available along the span of the wing, determined according to the method described in the previous section. A normal force in x-direction is only existing between the root and the strut. The other parameters, the distance in y and z, I_{yy}, I_{zz} and the cross sectional area A all vary along the span, and depend on the evaluated point in the cross section. The maximum normal stress occur at the maximum distances in y and z, i.e. at the corners of the wing box. In the critical flight condition, the upper skin of the wing box is in compression, and the lower skin is in tension, caused by the moment around the z-axis. Due to the moment around the y-axis, the wing is pulled backwards, causing the rear spar to be in compression, and the front spar in tension. In conclusion, the four corners experience the most extreme loads, which is why these were all evaluated.

Shear Stress

The shear stress at each section along the wing box can be expressed as Equation 5.40, where τ is the shear stress, q is the shear flow and t is the thickness of the wing box. This shear flow runs over the circumference of wing box skin and has two contributions; one being the shear flow due to the shear forces in y and z and the other being the torsional shear flow in the wing due to lift, drag and aerodynamic moment.

$$\tau = \frac{q}{t} \tag{5.40}$$

5.6.3. Failure Modes

Different kinds of failure modes were taken into account while setting up the wing box configuration. This section describes the methods that were used in order to determine the stress values at which the failure modes would occur. As the analysis of the behaviour of a stiffened panel under buckling conditions is both theoretically difficult and computationally intensive [41], the failure mode that was designed for is the yielding of the material at the skin. The failure modes due to aeroelasticity are discussed in subsection 5.6.5.

Yielding of the material

To test for yielding of the material, it is preferable to have high tensile and compressive yield strengths of the material. The Von Mises stress was calculated for the wing box to check for interference of the shear and normal loads that the material experienced by using Equation 5.41.

$$\sigma_y^2 = \sigma_1^2 + \sigma_2^2 - \sigma_1\sigma_2 + 3\tau^2 \tag{5.41}$$

In this equation, σ_1 and σ_2 are the normal stresses acting in the x and z direction, and τ the shear stress acting on the xz-plane.

Yielding of the material due to the shear stress is dependent on the shear yield strength of the material. In case a specific value was not found, it was taken according to the distortion-energy theory: $0.577 \cdot \sigma_y$ [42].

Fatigue

Fatigue is a result of the varying, cyclic loads that the structural components of an aircraft are subjected to every flight. 80% of the service-related failures are believed to result from fatigue, which not only include the cyclic loading fatigue, but also other forms like corrosion [32]. To simulate fatigue life conditions, a maximum load factor of 1.15 is taken during take-off. To increase the number of cycles, the wing box at the location of highest stress can be reinforced, in order to lower the experienced stress. The fatigue strength values in Table 5.7 were estimated based on previous generations Al-Li alloys. These strengths indicate the maximum stress amplitude for which no failure due to fatigue will occur for at least 500,000,000 cycles.

At this moment, fatigue data and diagrams for the third generation Al-Li alloys are not published yet. Therefore, in a later stage, research taking into account all factors that affect fatigue performance can be more conclusive about this matter. Considering corrosion fatigue specifically, the third generation of Al-Li alloys show superior performance over the established 7xxx-T6 and 2x24-T3 alloys [43]. As mentioned in section 5.5, CFRP outperform the Al-Li alloys in fatigue and corrosion [44].

Skin Buckling

For the stress at which skin buckling in between the ribs and stiffeners occurs, Equation 5.42 from Megson was used [39]. Here, C is the buckling coefficient, which depends on the ratio of the rib spacing over the stiffener spacing. As this concerns the skin, the E-modulus and Poisson's ratio of the skin material is used, as well as the thickness of the skin.

$$\sigma_{cr} = C\frac{\pi^2 E}{12(1-\nu^2)}\left(\frac{t}{b}^2\right) \tag{5.42}$$

Column Buckling

For column buckling, both the separate stiffeners and top panel as a whole were considered. Equation 5.43 was used for calculating the critical stress at which buckling occurs, where l_{eff} includes a correction factor based on the support of the analysed element.

$$\sigma = \frac{\pi^2 E I_{yy}}{A l_{eff}^2} \tag{5.43}$$

Stiffener Crippling

To analyse the stress at which the stiffener in compression would cripple, the method described during the lectures of the course *AE2135-II: Structural Analysis & Design* at the TU Delft were consulted [45]. Equation 5.44 was used to calculate the ratio of the crippling stress over the yield stress for all elements of the stiffener. α, n, σ_y, E and v are all material properties, whereas t and b depend on the geometry of the stiffener.

$$\frac{\sigma_{cc}^{(i)}}{\sigma_y} = \alpha \left[\frac{C}{\sigma_y} \frac{\pi^2 E}{12(1-v^2)} \left(\frac{t}{b} \right)^2 \right]^{1-n} \tag{5.44}$$

From the found ratios, the crippling stress of the stiffener as a whole was calculated with Equation 5.45.

$$\sigma_{cc} \frac{\sum \sigma_{cc}^{(i)} A_i}{\sum A_i} \tag{5.45}$$

Shear Buckling

Both local and global shear buckling may occur in the wing box. One advantage of the option of using hat stiffeners would be that the closed section that a hat stiffener creates, increases the resistance to local torsion, which increases the critical shear stress at which local shear buckling occurs. Research by NASA showed that for a hat-stiffened panel, local shear buckling is more critical than global shear buckling [46]. The reasoning behind the stiffeners is further explained in subsection 5.6.4. Calculating the local shear stress is a lot more complex than calculating the global shear stress (Equation 5.46 [39]). For that reason, the local shear buckling limit was determined by applying a safety factor to the global shear buckling limit. This safety factor was based on the found ratio in the NASA article: 4. In Equation 5.46, C_s is the shear buckling coefficient, again a function of the ratio of the rib- and stiffener spacing.

$$\tau_{cr} = C_s \frac{\pi^2 E}{12(1-v^2)} \left(\frac{t}{b}^2 \right) \tag{5.46}$$

5.6.4. Wing Box Configuration

Setting up the configuration of the wing box was an iterative process. The wing box covers 15% until 60% of the chord length. Due to the applied taper ratio, this results in the width of the wing box gradually going from 1.01 m at the root to 0.45 m at the tip. Its height decreases from 0.33 m to 0.076 m. Different types and numbers of stiffeners were considered, while varying the thickness of the spars and horizontal skins. After this, different kinds of material were applied in order to optimise for weight and cost. Ribs were placed to counter buckling, and the vertical flanges of the wing box act as the spars.

Stiffener Characteristics

By selecting the geometry of the stiffener, the different load cases for the top and lower skin were considered. A hat-shaped stiffener was selected for the top skin, whereas a Z-shaped stiffener was selected for the lower skin. The hat stiffener creates a closed section which increases the local resistance to torsion of the skin, as well as the effective sheet width, which increases the resistance to buckling of the skin. The upper vertical flange of the Z-stiffener adds area away from the neutral axis, increasing the moment of inertia. In the end, both the hat and Z-stiffeners increase the moment of inertia of the cross-section, allowing a thinner skin and ultimately a reduction in weight. The geometry of the stiffeners can be seen in Figure 5.31. Due to the taper of the wing, stiffeners are being cut off naturally along the span of the wing, as the chord length decreases. The spacing between the stiffeners maintains constant throughout the wing: 25 mm for the top stiffeners, and 55 mm for the lower stiffeners.

Configuration Trade-Off

The first configuration that was considered is a wing box without stiffeners and AA7075-T6 as skin material. Using this as a starting point, both the skin and stiffener material were varied, after which the number of stiffeners and ribs, and the skin thickness was adapted accordingly. This resulted in several configurations. The disadvantages of the use of composite material in this project outweigh the advantages, as described in section 5.5. Additionally, the 2055[9] and 2099[10] alloys have superior mechanical properties and perform better on fatigue and corrosion resistance in comparison with older aluminium alloys. The cost per configuration was calculated by multiplying the material cost by a factor 1.5 for the AA7075-T6, 2 for the Al-Li alloys, and 3 for the CFRP, based on the producability of the materials. From the configurations that were analysed, the configuration with 2055-T84 as skin material and 2099-T83 as stiffener material was selected.

Table 5.12 shows the results of the trade-off, using a constant skin thickness throughout the wing. Using a composite wing box results in a weight saving of 167.1 kg for two wings, resulting in a reduction of approximately 1% in fuel weight. When taking into account the additional factors that come into play as a result of using composites (as discussed in section 5.5) configuration 4 was chosen. The calculations of configuration 5 do not include the required lightning resistance reinforcements yet, which would increase both the cost and weight. In summary, it was found that the complications that come with using CFRP are recommended for further research, in order to verify and quantify the found difficulties as described in section 5.5.

Table 5.12: Analysed wing box configurations, with the number of stiffeners and ribs given per wing.

Parameter	**Config. 1**	**Config. 2**	**Config. 3**	**Config. 4**	**Config. 5**
Skin material	7075-T6	2195-T84	2195-T84	2055-T84	CFRP
Stiffener material	-	2099-T83	2024-T84	2099-T83	CFRP
Number of stiffeners	-	22	22	24	34
Number of ribs	20	10	10	10	6
Skin thickness [mm]	15	4	4.5	3.7	5.0
Weight [kg]	1,214.5	558.7	596.1	553.4	469.8
Cost [USD]	4,190.03	2,126.04	2,268.36	2,105.87	39,467.40

As expected, the highest stresses occurred at the strut. When simulating for fatigue, the maximum stress was found to be 171 MPa, which shows that the life time of the wing box at the current configuration is not endless. Exact fatigue numbers of the used Al-Li alloys are not published yet, so further research on this matter is recommended in a later stage, to get an impression of how much the wing box at the location of the strut has to be reinforced. Figure 5.31 shows the resulting cross section of the wing box at the root of the wing.

The critical load case for which the wing box was tested included the safety factor required by the authorities of 2.5, with an additional safety factor of 1.5, because of material uncertainties. It was found that under these conditions, the maximum stresses acted at the location of the strut. Table 5.13 shows the stresses that were found there. When comparing this with Table 5.7, the maximum tensile stress is about 82% of the yield strength AA2099: the material that was used for the stiffeners. The loading diagrams along the span of the wing are as shown in Figure 5.32 and Figure 5.33.

Table 5.13: Ultimate stresses along the wing box

Parameter	**Value**	**Unit**
Tensile stress	445.4	MPa
Compressive stress	-422.9	MPa
Shear stress	179.3	MPa
Von Mises stress	345.8	MPa

[9] Retrieved from: https://www.arconic.com/adip/catalog/AFE2055-factsheet.pdf (consulted on 12-6-2019)
[10] Retrieved from: https://www.smithshp.com/assets/pdf/2099-aluminium-lithium.pdf (consulted on 12-6-2019)

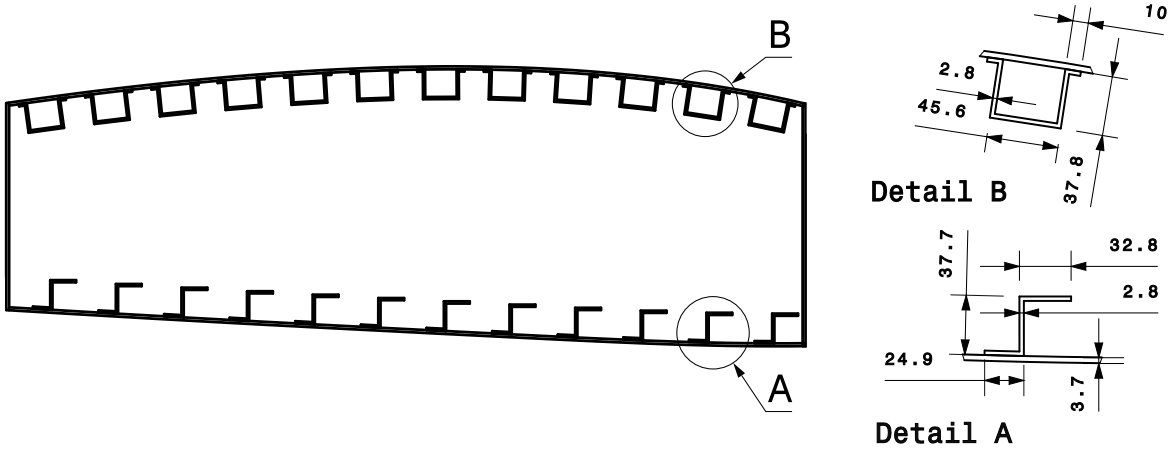

Figure 5.31: Cross section of the wing box at the root

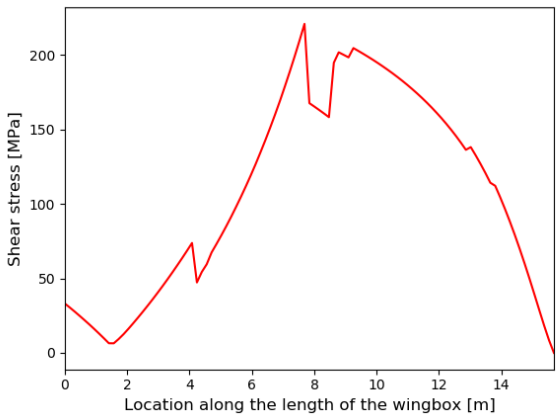

Figure 5.32: Shear stress diagram of the wing box.

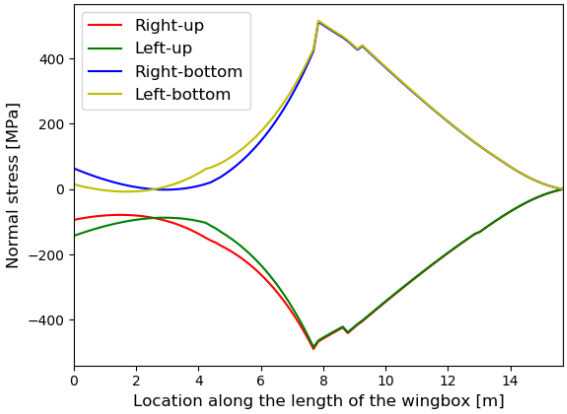

Figure 5.33: Normal stress diagrams of the four corners of the wing box.

Verification and Validation

The code was subjected to both code and calculation verification. As multiple people worked on the model, the code was checked on consistency, on for example the use of coordinate systems. For calculation verification, the input parameters were changed to that of a simple shape, 1 m x 1 m x 1 m, after which by hand the cross sectional properties and resulting stresses were checked with the results of the code. The influence of the stiffeners was also evaluated, by looking at the change in cross sectional properties when varying both the size and amount of stiffeners. To check the code for singularities, the effect of setting inputs to zero was evaluated. For validation, the use of software like Nastran of Abaqus can be used. Due to the limited available resources, this has to be further investigated in later research.

5.6.5. Aeroelasticity

Two forms of failure modes due to aeroelastic instability were considered: torsional divergence and flutter. Torsional divergence occurs when the aerodynamic forces, i.e. the dynamic pressure q, will become too large to be (out)balanced by the torsional resistance provided by the wing structure. When ignoring inertial effects, the dynamic pressure at which torsional divergence is prevented is as shown in Equation 5.47 [47]. Here, K_θ is the torsional stiffness, ec the distance between the aerodynamic centre and the elastic axis in meters and S the reference area per unit span. The elastic axis is the axis around which the wing twists, for

which the shear centre of the wing box was taken, considering the wing box was assumed to carry all of the loads. The torsional stiffness was calculated using Equation 5.48.

$$q \leq \frac{K_\theta}{C_{L_\alpha} ecS} \tag{5.47}$$

$$K_\theta = \frac{GJ}{L} \tag{5.48}$$

The analysis provided a boundary of altitude and velocity combinations before which torsional divergence would not occur, as shown in Figure 5.34. It can be seen that the velocities at which divergence will occur are all supersonic. This is due to the high torsional stiffness of the wing, for which it was assumed that only the sheet of the wing box carries torsional loads.

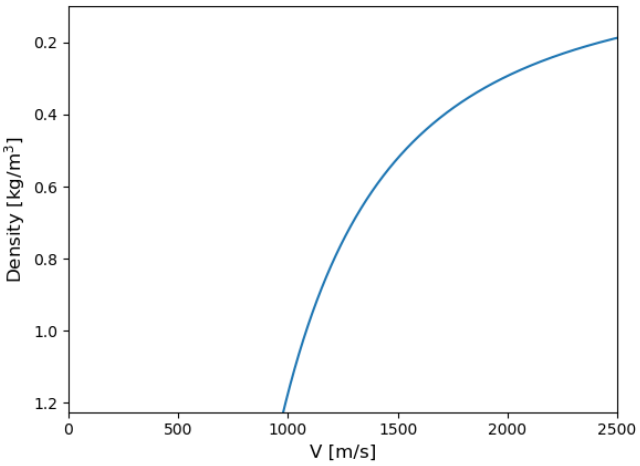

Figure 5.34: Boundary for torsional divergence

Flutter occurs as a result of a structure absorbing energy from the air flow that it is surrounded by. It only occurs above a certain velocity, after which the amplitudes of heave and pitch grow unbounded in a harmonic sense. This happens if on average, over a certain time period, the lift and motion of the wing are in the same direction, so work is done on the structure. If this happens the energy from the air will be transferred to the wing [47]. At that moment, the wing is on the boundary between a dynamically stable and unstable system, as illustrated in Figure 5.35 and Figure 5.36.

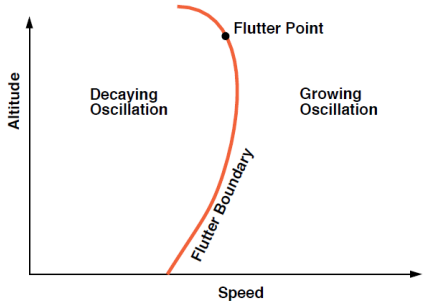

Figure 5.35: An example of a flutter boundary [47]

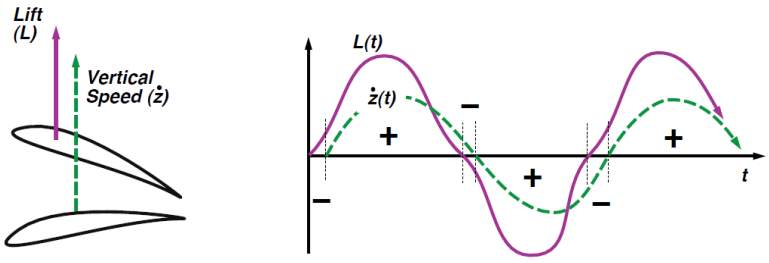

Figure 5.36: Timing of the force and motion of the wing [47]

To provide a preliminary analysis on the aeroelastic effects, only quasi-steady aerodynamics and two degrees of freedom (DOF) structural analyses were used. Figure 5.38 illustrates the DOF, by modelling springs to resist torsion and bending. Figure 5.37 shows the parameters for a typical wing section, as used in solving for a 2-DOF airfoil section.

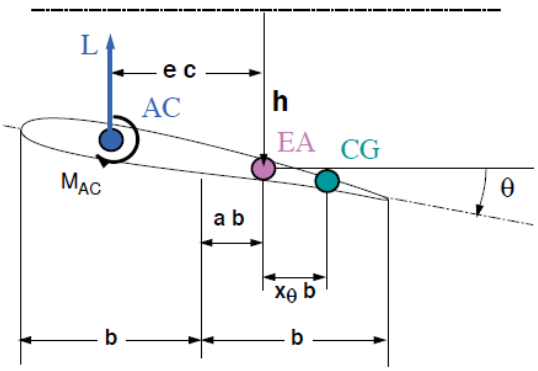

Figure 5.37: Typical section for solving the 2-DOF equations of motion [47]

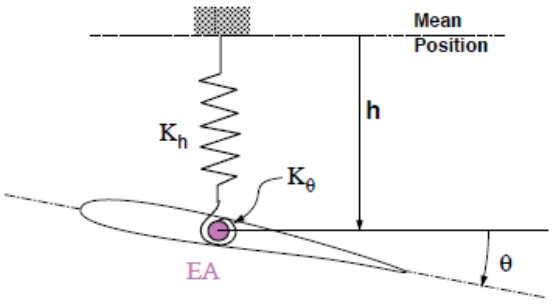

Figure 5.38: Structural model of the wing section [47]

Taking the moment about the elastic axis results in the following equations of motion:

$$[M]\ddot{\mathbf{x}} + ([K] - q[A_0])\mathbf{x} = \mathbf{0} \tag{5.49}$$

where

$$[M] = \begin{bmatrix} m & S_\theta \\ S_\theta & I_\theta \end{bmatrix} \tag{5.50}$$

$$[K] = \begin{bmatrix} K_h & 0 \\ 0 & K_\theta \end{bmatrix} \tag{5.51}$$

$$[A_0] = \begin{bmatrix} 0 & -SC_{L_\alpha} \\ 0 & 2SebC_{L_\alpha} \end{bmatrix} \tag{5.52}$$

Here, S_θ depends on the mass of the wing and the distance between the centre of gravity of the wing and the elastic axis, x_θ. I_θ is the mass moment of inertia and b represents the half-chord length.

For the analysis, the equivalent aerodynamic and structural characteristics were taken from 75% of the span. Taking the cross-sectional properties at this point for the entire wing made the analysis under-estimate the actual stiffness of the wing.

In order to solve the system, it was assumed that the solution is of the form $\mathbf{x} = \hat{x}e^{pt}$, which includes damped, diverging and neutral responses, both aperiodic and periodic. Plotting the roots p as a function of q results in the so-called flutter diagrams, with $p = \pm\sigma \pm i\omega$. The imaginary part of the roots corresponds with the frequency of the system, while the real part corresponds with the growth rate of the system. The flutter diagrams in Figure 5.39 and Figure 5.40 show the positive frequency branches to be separated until they co-ascend. The increase in growth rate coincides with the co-ascending of the frequency branches, which indicates the point for divergence. Although this is no proof for flutter, it usually is used as an indication of potential flutter problems [47].

The indicated dynamic pressure is far off from the experienced dynamic pressure during for example take-off (5.6 kPa) or cruise (7.5 kPa). One possible reason for this is the following. For this wing, the centre of gravity and elastic axis almost coincide, which makes the S_θ terms practically disappear from Equation 5.50. The result from this is that the bending and torsional frequencies are more or less uncoupled in this system, so the interaction between the motions is significantly lower, meaning the motions do not amplify each other. Increasing the distances to larger numbers therefore results in divergence occurring sooner, i.e. at lower dynamic pressures.

Another reason for the high divergence boundary, is that it is a result from the assumptions and simplifications that were made when using this method. Together with the resulting flutter diagrams, this encourages further research into the occurrence of flutter, by analysing the complete 6-DOF system, for which more complex tools and methods are required.

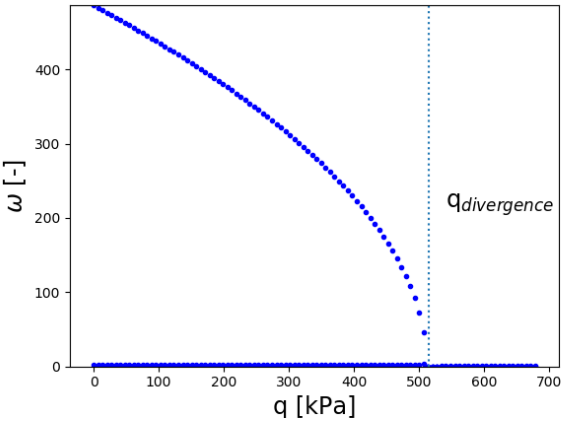

Figure 5.39: Imaginary components of the roots, corresponding with the frequency.

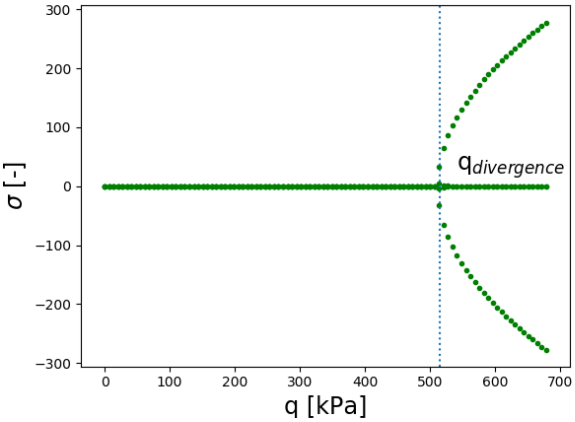

Figure 5.40: Real components of the roots, corresponding with the growth rate.

5.6.6. Fuselage

The predominant factor when determining the thickness of the fuselage, is the pressure difference between the air on the inside and outside of the fuselage. By rewriting Equation 5.53 and Equation 5.54 the required thickness could be calculated.

$$\sigma_{circ} = \frac{\Delta pR}{t} \tag{5.53}$$

$$\sigma_{long} = \frac{\Delta pR}{2t} \tag{5.54}$$

During flight the pressure inside the cabin is equivalent to the pressure at 1800 m (81200 Pa) and the minimum outside pressure is 35,000 Pa. The radius of the fuselage is 2.84 m. Plugging the values for the pressure in the equations above it was found that the required thickness for AA2198-T8 is equal to 0.38 mm and 0.27 mm for AA2060-T8E30. Composite materials are not taken into account due to various reasons which were discussed in section 5.5, and taking into account that the manufacturing of a fuselage would dramatically increase the production cost due to the size.

Due to the manufacturing and to include a safety margin, a fuselage skin with a thickness of 1.6 mm manufactured out of AA2060-T8E30 was chosen. In terms of corrosion resistance, this alloy outperforms previous generations, having a 140% increase in corrosion with respect to the AA2024-T351[11].
Once the required skin thickness was determined, the shear and moment diagrams could be analysed. It is assumed that weight of the aircraft is uniformly distributed along the length of the fuselage. The shear and moment diagrams can be found in Figure 5.41 and Figure 5.42.

Since the material already had been selected, the required moment of inertia and first moment of area could be determined using Equation 5.55 and Equation 5.56.

$$\sigma_z = -\frac{My}{I} \tag{5.55}$$

$$\tau = \frac{VQ}{It} \tag{5.56}$$

Calculations showed that the required moment of inertia and required first moment of area is equal to respectively 0.00113 m^4 and 5.47e-6 m^3. In order to achieve this value for moment of inertia and first moment of area, stringers will be attached to the fuselage.

[11] Retrieved from: https://www.constellium.com/sites/default/files/markets/airware_2198_t8_fuselage_sheet.pdf (consulted on 18-6-2019)

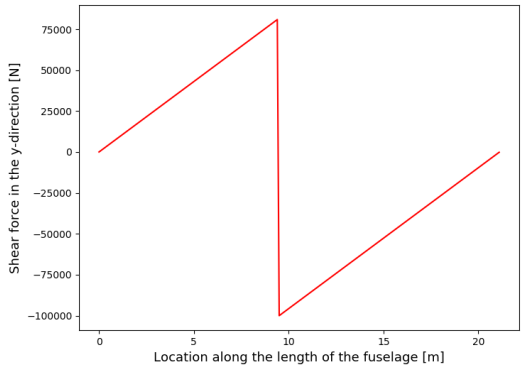

Figure 5.41: Shear diagram of the fuselage

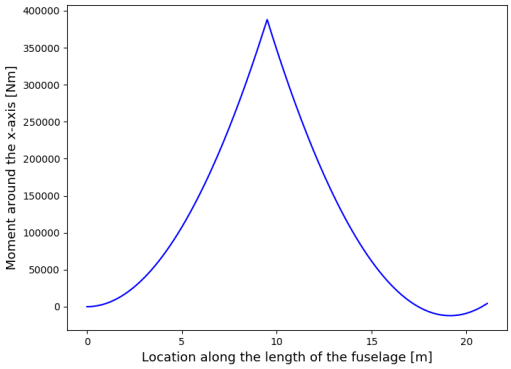

Figure 5.42: Moment diagram of the fuselage

5.6.7. Strut

One of key design features of this aircraft is the strut. In this section the sizing process of the strut will be discussed as well as other structural components which are necessary to implement the strut.

Strut Design

The structural part of the strut was designed to have a circular shape in order to transfer the loads as efficient as possible. Using the force in the strut calculated previously and the ultimate stress of the material, the required diameter could be calculated assuming that the strut is only in tension.

Table 5.14: Required diameter of the strut for different materials.

Material	Required Diameter [mm]	Mass [kg]
AA2198-T8	36	22.7
QI CFRP	46	18.7

As can be seen in Table 5.14, the carbon composite strut requires a larger diameter after applying the safety factor than the aluminium strut. However, the mass is much lower, so it was decided to produce the strut out of a carbon composite.
The diameter mentioned before is the required diameter if the strut would be solid. However, to improve manufacturing and the ability to fit an airfoil around the strut, the strut will be hollow. The outer diameter was set at 80 mm and the inner diameter at 69.2 mm. The length of the strut will be 8.34 m.

Strut box design

Once the strut was sized, the attachment of the strut could be analysed. Similarly as in the wing, a box transfers the loads to the fuselage. This box was placed below the floor and attached to the fuselage at two points. In order to design this box, external and internal loads had to be analysed as well as the cross-sectional properties.

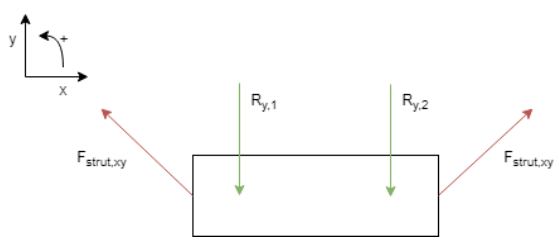

Figure 5.43: Free body diagram of the strut box in the xy-coordinate system.

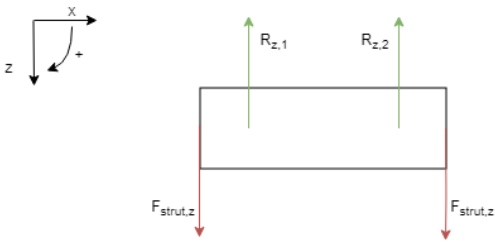

Figure 5.44: Free body diagram of the strut box in the xz-coordinate system.

In Figure 5.43 and Figure 5.44 the free body diagram of the strut box in the xy- and xz-plane can be found. Using these free body diagrams the shear and moment diagrams of the strut box could be constructed, which can be found in respectively Figure 5.45, Figure 5.46, Figure 5.47 and Figure 5.48.

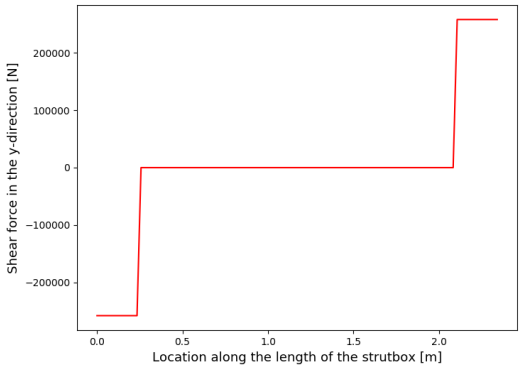

Figure 5.45: Shear force of the strut box in the y-direction.

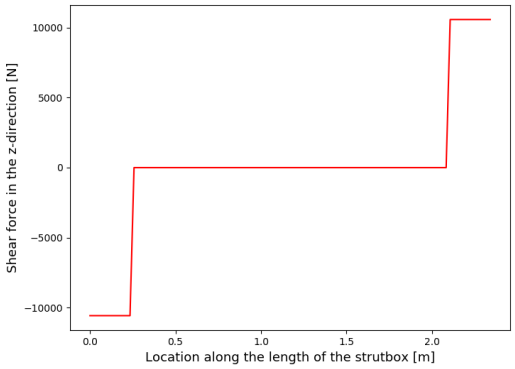

Figure 5.46: Shear force of the strut box in the z-direction.

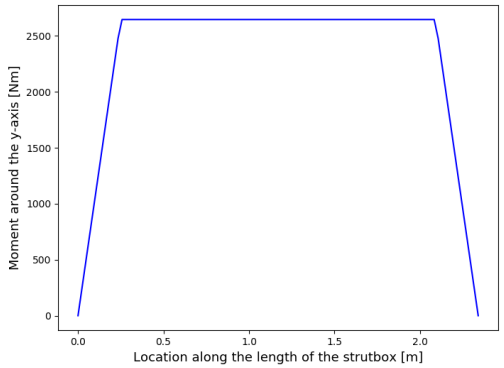

Figure 5.47: Moment of the strut box around the y-axis.

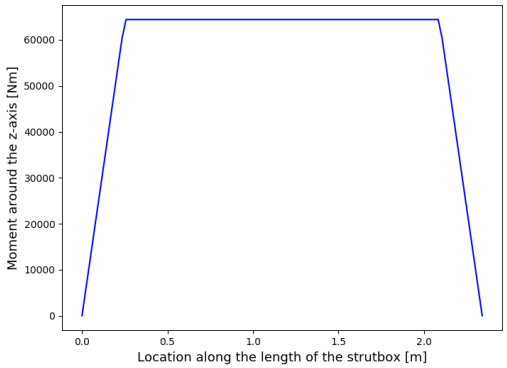

Figure 5.48: Moment of the strut box around the z-axis.

With the internal forces and moments known, the sizing of the strut box could start. By rewriting the shear stress equation, Equation 5.56, the required sheet thickness could be calculated. Next, from the moment diagrams the normal stress could be calculated with Equation 5.55. By manually altering the number and type of stringers, such that the strut box can withstand all the loads, a final design was obtained. The limiting failure mode is shear yielding which is discussed in subsection 5.6.3. Also note that the same stiffener geometry and material was used as in the wing box. In Figure 5.49 four lines can be distinguished, each representing the normal stress in a corner of the strut box.

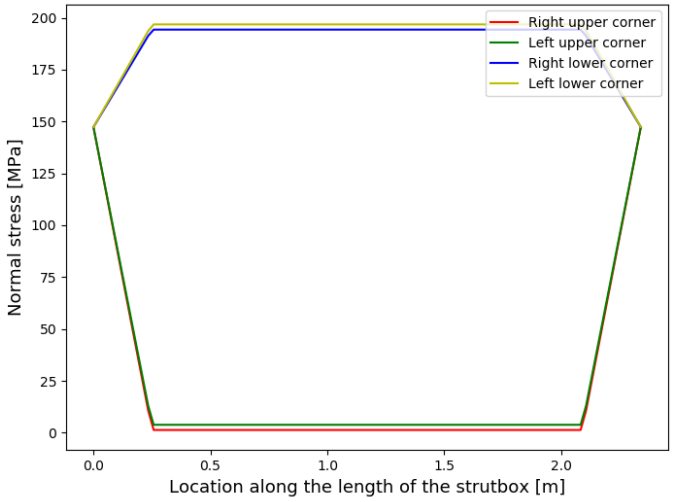

Figure 5.49: Normal stress at the corners of the strut box.

The stresses are predominantly positive, thus the strut box is loaded in tension. The deflection upwards of the strut box introduces compression into the upper skin and tension in the lower skin. However, the force of the strut in the x-direction almost completely cancels out the compression in the upper skin and greatly increases the tension in the lower skin. Additionally, due to the moment caused by the strut force in the z-direction, the corners on the left half of the strut box are experiencing a moderately higher normal stress. In Table 5.15 the final dimensions and weight of the strut box can be found.

Table 5.15: Final dimensions of the strut box.

Parameter	**Value**	**Unit**
Mass	51.75	[kg]
Cost	150	[USD]
Sheet thickness	3.0	[mm]
Skin material	AA2055-T84	[-]
Stiffener material	AA2099-T83	[-]
Length	2.34	[m]
Width	1.00	[m]
Height	0.36	[m]
Number of stiffener on top sheet	2 hat-stringers	[-]
Number of stiffener on bottom sheet	3 z-stringers	[-]

5.6.8. Influence of Strut on Wing Box Design

In order to confirm that the implementation of the strut was needed for the wing design for the Aquila aircraft, a comparison was performed for the aircraft with and without strut. First the critical stresses in the wing without strut were calculated and compared to the results from subsection 5.6.4, after which the wing tip deflection was also compared.

The procedures of calculating all reaction forces and stresses inside the wing were also performed for a case where no strut would be present. For these calculations the same conditions held as presented in subsection 5.6.1. Under the same aerodynamic forces and wing box layout, the stresses in the wing box for a wing without a strut were computed. The stresses in the wing box without the strut can be found in Table 5.16. Also the loading diagrams along the span of the wing are as shown in Figure 5.50 and Figure 5.51.

Table 5.16: Maximum stresses for wing without strut found at the root.

Parameter	Value	Unit
Tensile stress	936.6	MPa
Compressive stress	-841.7	MPa
Shear stress	170.7	MPa
Von Mises stress	810.9	MPa

When comparing this data with the data provided in subsection 5.6.4, it can be seen that under the same circumstances, the maximum stresses in the wing box heavily increase. Only the maximum shear stress is decreased slightly. However, this is not the most critical failure mode. Under the compressive load case, it was found that stiffener crippling occurs. In order to amend this, the thickness of the stringers was increased by 30%, which in term increased the total weight of the wing box by 13%.

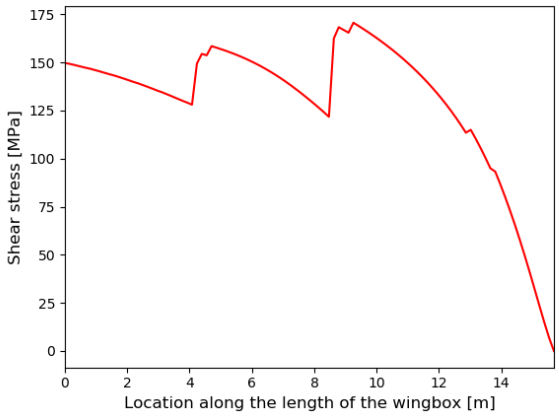

Figure 5.50: Shear stress diagram of the wing box without strut.

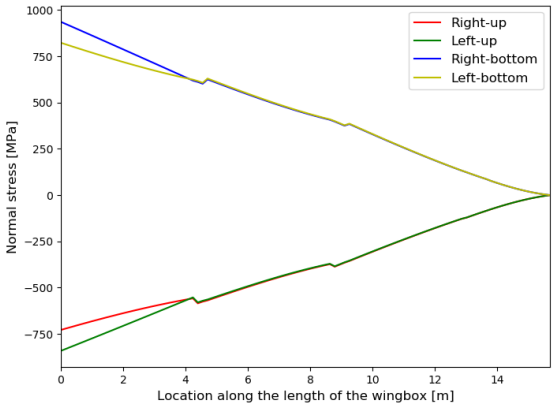

Figure 5.51: Normal stress diagrams of the four corners of the wing box without strut.

Apart from the stiffener crippling, the upward bending of the wing was also considered a problem. The upward wing bending before increasing the stiffener thickness is presented in Figure 5.52. The deflection at the wingtip is 35% of the half wing span, which is considered to be too much. As a comparison, the deflection of the wingtip with strut is only about 8.3% of the half span as can be seen in Figure 5.29. Therefore, in order to also get a wingtip deflection of 8.3%, the moment of inertia of the wing box was increased. Since the moment of inertia will mainly be increased by changing the stiffeners, the failure mode of stiffener crippling can easily be overcome by just improving the deflection performance of the wing. In order to get the same level of wing tip deflection without a strut, the average moment of inertia had to be increased by 430%. This would in term mean a total wing weight increase of 517%. It therefore becomes very apparent that for the long and slender wing setup for this aircraft it is of great importance to implement a strut.

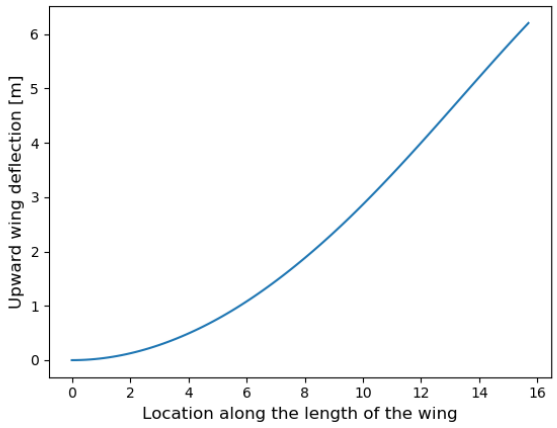

Figure 5.52: Upward bending of the wing without strut

5.6.9. Risk Management

The main risk when designing the structure of the aircraft is that it is not able to withstand the loads. Therefore the aircraft has to be designed for the highest theoretical load factor that the aircraft is able to achieve. Additionally, safety factors are applied which are different for different materials. The two main material types which are considered in the design of the aircraft are aluminium alloys and composite materials. The difference in safety factor is a consequence of the characteristics of the materials. Composites for example, are more prone to impact damage, which could be caused by a bird hitting the strut in-flight. Aluminium alloys are less prone to these failures. This, among other material characteristics, results in the safety factor being 1.5 for aluminium alloys and 2 for composites.

5.7. Propulsion System Design

The propulsion system is one of the most important systems of the aircraft and also one of the most expensive. The goal of the design team was to make significant improvements in terms of the fuel efficiency and reduce the emissions of the system. The engine was selected in subsection 5.7.1, followed by the sizing of the gearbox and propeller in subsection 5.7.2 and subsection 5.7.3, respectively. Some modifications to the engine had to be made, which were detailed in subsection 5.7.4. Similarly to the engine, the storage of LNG requires more attention than regular propulsion systems, this is addressed in section 5.7.7. The fuel feeding system architecture is discussed and sized in subsection 5.7.8.

5.7.1. Selection of Engine

The engine of the aircraft should be as efficient as possible in order to comply with the requirement of fuel efficiency as given in chapter 3. The most efficient and reliable engines that are in use today are the PW100 series. Several other engines are in development however. These engines were analysed to make a sound design choice. The engines that were deemed feasible by the design team were:

- The Pratt & Whitney Canada PW127G
- The General Electric Catalyst
- The General Electric T6E

Analysis of Real Brayton Cycle

In order to select the right engine an analysis was performed of the real Brayton cycle of each engine and a reference engine. To do this some input parameters were needed, which can be found in Table 5.17.

Table 5.17: Input values for the calculation of the real Brayton cycle.

Engine	Pressure Ratio [-]	Shaft Power [kW]
PW127G	14.7	2050
GE Catalyst	16	1190
GE T6E	17	1770

The real Brayton cycle was then used to calculate the fuel flow and Specific Fuel Consumption or SFC of each engine [48]. Methane was used as fuel, with the Lower Heating Value of 50 MJ/kg[12]. The performance of the PW127G running on kerosen was also calculated to validate the method by comparing with available data [49]. This analysis resulted in the outcomes as shown in Table 5.18.

Table 5.18: Output values for the calculations of the real Brayton cycle.

Engine	Fuel Flow [kg/s]	SFC [g/kW/h]	Weight [kg]
PW127G (Methane)	0.09	223	491
PW127G (Kerosene)	0.12	312	491
PW127G (Reference)	0.14	312	491
GE Catalyst	0.06	220	270
GE T6E	0.07	217	244

It becomes apparent that the engines have very similar SFC, but differ in general fuel flow, which can be explained by the different power levels. It should be noted that the weight of the GE T6E would increase as it does not come equipped with a gearbox, since it is primarily used as a turboshaft engine.

It was decided to use the GE T6E, since it offered the best compromise between power and weight and had the best fuel consumption characteristics.

5.7.2. Sizing of the Gearbox

As mentioned before The engine that was selected is the GE T6E, which is a turboshaft engine. As such it needs a gearbox to reduce the rpm of the engine. An estimation method from NASA was used to compute the weight in pounds of the gearbox, which can be found in Equation 5.57 [50], where Q is the torque in pound foot and GR is the gear ratio that is necessary. The necessary gear reduction ratio is equal to the turbine-to-propeller rpm ratio, which calculated to be equal to 18.3 [49].

$$m_{\text{gb}} = (0.0174Q + 45)\left[\frac{0.118}{GR}\right]^{0.5} \tag{5.57}$$

Using this equation, the mass for the gearbox was estimated to be 150.9 kg.

5.7.3. Selection of Propeller

The propeller that was selected for the Aquila is the 6-bladed Hamilton Standard 568F with a diameter of 3.93 m. This is the same propeller that is being used on the ATR 72 and offers high performance and a low weight of 165 kg [51]. It was chosen not to develop a new propeller, since the Hamilton 568F already offers an excellent performance and this would add unnecessary cost to the program.

5.7.4. Modifications

In order to let the engine run on methane/natural gas some modifications had to be made to the engine. These changes and the effect of these modifications are discussed in this subsection.

[12] Retrieved from: https://www.engineeringtoolbox.com/fuels-higher-calorific-values-d_169.html (consulted on 02/06/2019

Turbine

The thermal efficiency of the engine is determined by the amount of work that can be extracted from the heated air that flows through the engine. The amount of work that can be extracted is set by the difference in temperature between the compressor and the turbine blades. By using more heat resistant materials for the turbine blades, such as used in the GE Catalyst and the PW150, the temperature at the turbine can be increased and the thermal efficiency will increase [52].

Combustion Chamber

LNG is a different type of fuel than kerosene, but it requires no significant changes to the combustion chamber [53]. In fact methane has a lower adiabatic flame temperature than kerosene (2236 K vs. 2376 K), which would lower maintenance and wear on the turbine blades and the combustion chamber [54]. One concern, however, is that the combustion of methane should be complete, since methane is a greenhouse gas with an effect 30 times that of CO_2. Apart from the fact that methane is a more potent greenhouse gas, it is also important to reduce the amount of NO_x emissions. By using catalysts and by controlling the flame, the percentage of combusted methane can be increased and reduce the NO_x emissions. One of the most promising catalysts is a palladium catalyst [55]. These catalysts would be placed inside the combustion chamber, before the flameholder. They would be placed in the shape of a raster as not to disturb the airflow too much. Controlling the flame can best be done by the use of a swirl burners [56].

5.7.5. Nacelle and Wing Integration

The engine was placed under the wing between the fuselage and the strut, to minimise the yaw moment in case of an engine failure and to reduce the distance between the fuel tanks and the engine. To calculate the weight of the nacelles, the method of the class II weight estimation was used [1]. The result of this estimation was 357.38 kg for the nacelle of both engines.

5.7.6. Specifications

Below the specifications of the engine and nacelle group can be found. It must be noted that the weight of the engine was increased by 10% to account for oil and other substances that should be added to the dry weight for the engine to make it operative.

Table 5.19: Specifications of the modified GE T6E

Parameter	**Value**	**Unit**
Length	2134	mm
Width	660	mm
Height	850	mm
Diameter Propeller	3930	mm
Engine Weight (dry)	243.6	kg
Engine Weight	268.0	kg
Gearbox Weight	150.9	kg
Propeller Weight	165.0	kg
Nacelle Weight (per engine)	178.69	kg
Total Weight	762.1	kg
SFC (cruise)	217	g/kW/h
Power (maximum)	1770	kW

5.7.7. Fuel Containment System

As discussed in the Mid-Term Report, all the fuel is stored in two tanks suspended under the wing [12]. The total fuel stored for a normal mission profile, including the reserve fuel, is 1966 kg. Each fuel tank was designed to carry 1000 kg of LNG, with the surplus amount to account for trapped fuel. To store the

LNG at cryogenic temperatures, either an active or passive cooling system can be used. Early in the design phase it was chosen to discard active cooling, due to its major increase in weight, and the fact that even in space application, cryogenic fuel is only cooled actively if the mission duration exceeds several weeks [57]. Therefore a vacuum insulated tank was chosen for the design, due to its superior insulation characteristics, which allowed for a lighter design, as is common in industrial application.

Structural Design

The vacuum tank design consists of an inner shell, enclosed by an outer shell; the interstitial space is filled with microspheres at a pressure of 8 to 30 Pascals. The volume of the internal shell of the tank should provide additional space for ullage, contraction due to cooling, internal structures and equipment. These were taken into account by an extra factor for the volume, the allowance, which was set to 7% [58]. Combining the density of LNG (425 kg/m^3), the fuel weight and the allowance, resulted in an internal volume of 2.518 m^3 for a single tank.

The maximum pressure difference between the vacuum insulated space, the interior of the tank and the exterior of the tank is the dominant factor for the tank shell design. The maximum internal pressure is set to be 13.3 bar, which is explained in more detail in the next paragraph. The maximum pressure at which the aircraft operates was set to be 1 bar at sea level.

The internal shell was designed for tension, since the internal pressure would push in the outward direction, whereas the external shell was designed for buckling, since the outside pressure would push into the tank. The effect of the microspheres and fuel tank baffles taking up load was not taken into account. When considering a nominal cycle the internal pressure only rises to 1.2 bar in 8 hours ground time, due to evaporating LNG, and the pressure will decrease once fuel is pumped out of the tank. Abnormal ground time of the tank will lead to a maximum internal pressure of 8.7 bar, which is explained in more detail in the next section. The external pressure is set to 1 bar at sea level and the pressure decreases to 0.35 bar at cruise altitude, reducing the stress on the external shell. For both shells a safety factor of 1.5 was considered, to account for discrepancies and effects of fatigue, since the internal pressure build-up is only small compared to the maximum internal pressure, and a flight cycle will only reduce stress in the external shell.

The internal shell is made of an aluminium alloy 7075-T6 only, since in case of a leak of the outer shell and vapour barrier, the use of composites is not favourable at cryogenic temperatures in the vicinity of oxygen[13]. Furthermore, the characteristics of 7000 series aluminium alloys are well known at cryogenic temperatures and these alloys show little changes in properties [59]. The aluminium shell is 1.15 mm thick and was designed to yield at 13.3 bar, using equations similar to those used in section 5.6.6. Furthermore, any connections are welded to one another, these welds need to be vacuum tight. Steel was not considered due to its low specific strength.

The external shell is made of high-tech aramid fibres, which have a high specific modulus. Additionally, aramid is highly tolerant to impacts, which obviously is beneficial when working with LNG. Due to the high specific modulus, the required external shell thickness required is lower, resulting in a lighter design. The external shell was sized using equations set up by Windenburg and Trilling [60]. This resulted in a required thickness of the external shell of 6.2 mm, to counteract buckling at 1.5 bar difference.

Even small motions of the fuel tank can initiate large excursions of the LNG inside the fuel tank; this can cause serious stability and control issues. Fuel tank baffles are used to suppress the magnitude of fuel slosh, additionally they provide supplementary structural integrity [61]. Four equally spaced baffles are installed in the fuel tank. The geometry of the baffle includes a central orifice roughly 12 % of the tank cross-sectional area and 3 small slots at the outer radius that act like an equaliser on both the upper and lower part of the baffle. The equaliser ensures that no gas bubbles or fuel is trapped behind the baffles, multiple slots are required to allow movement of Boiled-Off Gas (at the upper part) or LNG (at the lower part) at different roll angles.

The fuel tank pylon was not designed in detail. However, next to the connection system to the wing, the fuel tank pylon houses the piping for the pumps and the vapour recovery line. Moreover, the fuel tank pylon

[13] This has shown to be the cause of the loss of AMOS-6 of SpaceX, retrieved from https://www.spacex.com/news/2016/09/01/anomaly-updates (consulted on 04-06-2019)

shall be able to withstand the dynamic loads with all possible fuel levels. The connection system consists out of 3 different couplings, out of which either combination of two are able to withstand all loads.

Tank Insulation

Boiled-Off Gas (BOG) in the tank is generated by evaporation of the LNG due to heat transfer during the transportation, local pressure changes due to sloshing, heat input during loading & unloading and other inherent disturbances. The most influential factor of boil-off in the fuel tank is due to heat penetration into the fuel tank [62]. To counteract the pressure increase, the gas can be vented into the air. Venting of BOG poses a possible safety and environmental hazard, since natural gas is flammable and a greenhouse gas. The time which the tank can hold the LNG without venting is called the holding time. Both the European and American authorities have set the minimum holding time to 5 days[14].

Since the concept of active cooling was discarded at an early stage of the design process, the fuel tank should be insulated adequately, to limit evaporation, such that the LNG and the BOG are contained. Vacuum insulation was the preferred option since it provided better weight characteristics, for instance compared to cryogels[15]. Besides vacuum conditioning, which will be addressed in the final paragraph, is relatively straightforward since the tanks are detachable.

The structure and insulation of the tank is designed to contain the LNG and the BOG for a minimum of 5 days. The insulation is filled entirely with glass fibre microspheres. The microspheres provide structural integrity to the vacuum section and keep the internal fuel tank in place, the added structural integrity has not been taken into account. However, during future analysis the weight can only decrease since the microspheres only benefit the structural integrity. Furthermore, the microspheres provide an open pore structure which is easily evacuated of air and the microspheres act like a gas at extremely low pressures, reducing the conduction heat transfer to a minimum. In between the vacuum section and the external shell, a vapour barrier is installed, since the aramid structure is not able to prevent air from coming in completely [63]. The vapour barrier is susceptible to damage, thus will be installed inside the aramid shell. The vapor barier is made of a bright colour to quickly discover a defect by inspection in the external shell. Additionally, the fuel tank will be painted with a reflective white polyurethane topcoat, to prevent additional heating of the tank.

As mentioned earlier, the boil-off rate is mostly determined by heat penetration into the tank. The heat penetration occurs via solid conduction (k_s), gaseous conduction (k_g) and radiation (k_r) [64]. The solid conduction depends on the structure and material properties of the core. The gaseous conduction by residual gases depends on the gas pressure which increases with time by infusion of atmospheric gases. Thermal radiation depends on the structure and optical properties of the core. This can be combined in the total effective conductivity (k_{eff}). For glass fibre microspheres this is 0.0028 W/mK for a pressure lower than 10 Pa [64]. However, an effective conductivity of 0.0032 W/mK was used since the pressure increases to 30 Pa in roughly 250 days time [65], provided the initial pressure is set at 8 Pa. The increase in pressure of the vacuum section is mostly dependent on the ambient pressure. The deterioration of the vacuum was determined with constant pressure at sea level, however the aircraft will spend a good amount of its lifetime in the air at lower pressure, thus the vacuum pressure will increase at a slower rate.

The effective conductivity was used to determine the heat penetration, or heat flux, into the tank. The thermal conductivity of the aramid shell was taken into account, although both the thermal conductivity is an order of magnitude higher and the thickness of the shell are an order of magnitude lower than the vacuum insulation. The total heat flux has been determined using the following formula [66]:

$$Q_{in} = A_{external} \cdot \frac{\Delta T}{t_{vacuum}/k_{eff} + t_{aramid}/k_{aramid}} \tag{5.58}$$

In which $A_{external}$ (m^2) is the external area of the fuel tank, t (m) the thickness of the element indicated in the subscript and k ($Wm^{-1}K^{-1}$) the thermal conductivity of the relevant insulation layer. The ΔT is the difference between internal temperature and external temperature [16].

[14] Regulations specified in: SAE J 2343

[15] Flexible insulation blankets made of aerogels designed by Aspen Aerogels

[16] Determined with an average outer temperature of 25 °Celsius, to simulate a normal hot day and night cycle

The boil-off rate (BOR) is determined using the following formula [67]:

$$BOR = \frac{Q_{in} \cdot 60}{\rho_{LNG} \cdot V_{LNG} \cdot \Delta H_{vap}} \tag{5.59}$$

In which Q_in (W) is the previously determined heat flux, ρ the density, V the volume and ΔH $(J\ kg^{-1})$ the enthalpy of vaporisation, or latent heat of vaporisation. Apart from the above relations, the relation between the bubble point and the pressure is used, for higher internal pressure, the LNG evaporates at a higher temperature[17].

Using the relations stated above, a simulation of the pressure build-up was made, using the Benedict-Webb-Rubin equation of state and a timestep of 30 seconds, for which the final results converged independently of the time step. The pressure build up can be seen in Figure 5.53. From this the maximum pressure before venting could be determined, which is 8.7 bar. Furthermore, the pressure only increases to 1.2 bar when the aircraft is non-operational for a period of 8 hours. It should be noted that the LNG will remain the majority of the time at the critical state.

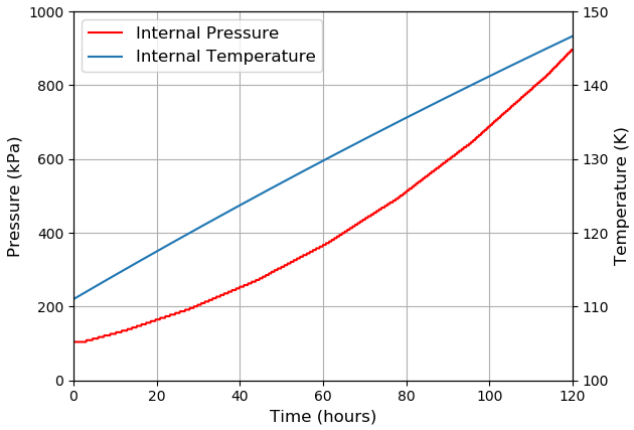

Figure 5.53: Results of the tank simulation, showing internal pressure and temperature as a function of time.

Tank Pumps and Plumbing

In order to transfer the fuel into the fuel system, the fuel is pumped out of the tank using booster pumps, of which two are located at each fuel tank. These are addressed in more detail in subsection 5.7.8.

Apart from refuelling the detached tank, the tank needs to be refuelled when attached to the aircraft. This is done via the refuelling valve located at the top aft part of the fuel tank.

Not only fuelling is required, the ability to defuel is both necessary in air and on the ground. This is enabled by an electric defuelling valve located at the bottom aft of the fuel tank. Either the electric valve can be operated remotely from the cockpit, such that the pilots can dump fuel in case of an emergency. Or engineers can operate the valve manually, to empty the tank on the ground.

The vaporisation of LNG results in an increase in volume 600 times greater than the original volume. Overpressurisation of the tank must be avoided at all costs to prevent rupture or explosion of the tank. This obviously poses serious safety and environmental hazards; large spills of flammable gas and flying shrapnel in the vicinity of the tank, and a large release of greenhouse gases in the air. This is counteracted by three pressure relief valves, which are stated in order of increasing valve pressure: the vapour recovery valve, the primary pressure relief valve and the secondary pressure relief valve. The vapour recovery valve operates at a pressure range of 1.5 to 5 bar and leads to the gaseous fuel system. This valve is only active when either one of the engines or the APU is operating. The primary pressure valve operates at a minimum pressure of 8.7 bar and the secondary 0.1 bar higher. The secondary pressure relief valve serves to indicate abnormal operation of the primary pressure relief valve or when the flow rate of the primary pressure relief valve

[17] Retrieved from the Dortmund Data Bank at http://www.ddbst.com/en/EED/PCP/VAP_C1051.php (consulted on 04-06-2019

alone is not sufficient. The primary and secondary pressure relief valve operate without any restrictions, apart from the minimum pressure, to prevent an over-pressurisation event even when the tanks are not monitored.

The LNG tanks require a system that prohibits the combustion of the fuel inside the tank, the inerting system. This can be done simply by deliberately feeding natural gas, which has been evaporated by the heat exchanger, back into the fuel tank, via the vapour feedback valve. This is only done when the pressure is below 1.1 bar to makes sure that the internal pressure is always higher than the ambient pressure, which will inhibit air from coming in. It should be noted that if the fuel system will not be able to feed the gas back into the tank, the normal heat flux will make sure the pressure does not drop below 1.1 bar if the fuel is not extracted by the pumps or dumped.

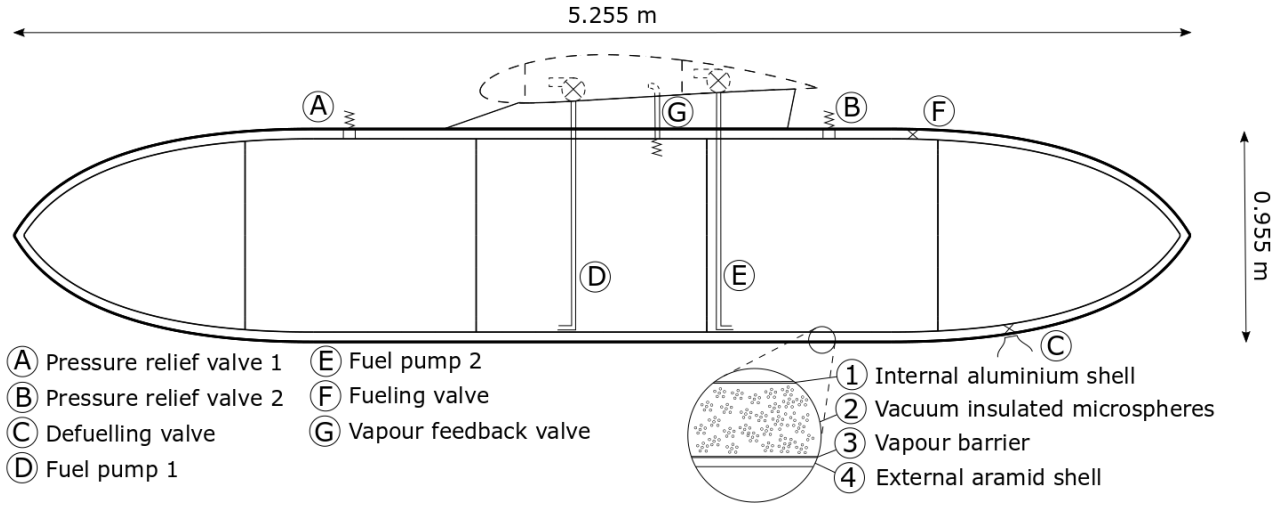

Figure 5.54: Schematic overview of the tank and major systems accompanied by the wing structure in dashed lines.

Tank Weight Estimation

The thickness of each pressure vessel, insulation layer and fuel sloshing plates were known. Combining this with the overall geometry and densities of each material, an accurate weight estimation could be made. For the tank accessories, data from equivalent systems was used [58]. Lastly, the weight of the tank pylon was estimated using data from engine pylons[18].

Table 5.20: Weight estimation of the components of a single fuel tank, and the percentage of the component weight with respect to the empty weight and full weight

Tank Component	Mass (kg)	Percentage EW	Percentage FW
Inner Shell	41,5	17,64%	3,36%
Insulation	33,8	14,36%	2,74%
Vapor Barier	16,5	7,01%	1,34%
Outer Shell	114	48,45%	9,23%
Fuel Sloshing Plates	2,8	1,19%	0,23%
Feulling Adapter	2,9	1,23%	0,23%
Defuelling Valve	2,4	1,02%	0,19%
Pressure Relieve Valve (2x)	3,6	1,53%	0,29%
Vapor Recovery Valve	2,3	0,98%	0,19%
Fuel Level Sensor (2x)	0,1	0,04%	0,01%
Pressure Sensor (4x)	0,4	0,17%	0,03%
Pylon	15	6,37%	1,21%
Total	235,3	100,00%	19,05%

[18] Retrieved from Voestalpine, https://www.voestalpine.com/blog/en/mobility/capabilities-that-aircraft-engine-mounts-must-possess/ (consulted on 16-06-2019)

Operations Regarding Fuel Tank

Several safety issues in the fuel tank design have already been addressed in the previous sections. However some issues have not yet been mentioned, such as those regarding refuelling and maintenance. The LNG is loaded at a pressure just above ambient pressure and at a temperature (105 K) a little under the evaporation point (111.7 K), to take into account the heat penetration during transport from the airport's fuel reservoir to the fuel tank. This is done to prevent air coming in the tanks if a leak is present or when refuelling operations are not carried out correctly, due to the overpressure in the tank. Furthermore, none of the adapters of the tanks shall be allowed to act as a hazard to equipment or personnel. The ingestion of ice, water or other contaminants shall not be able to occur during the refuelling process. The fuelling and defuelling adapter shall be designed to break away without rupture of the tank if the hose is pulled away without being properly disconnected. The adapter shall allow to be detached by manual handling in case of an emergency. Lastly, each adapter shall be designed different from one another, such that mating to the incorrect valve is not allowed.

When the fuel tanks are detached and stored with fuel, the tanks can be attached to a vapour recovery valve to capture BOG and liquefy the BOG at the fuelling terminal at the airport. The alternative is to drain the LNG via the defueulling valve, when the tanks are not in use. As previously mentioned, the tanks are only able to be detached by external operation by an engineer.

As discussed in the section Tank Insulation, the properties of the vacuum change over time, most notably because atmospheric gases and water vapour permeate through the vapour barrier, for instance at the attachment points of fuel pumps. Therefore vacuum conditioning is necessary, effectively resetting the pressure to initial conditions, namely 8 Pa. The tank is designed to contain the LNG with a thermal conductivity which has degraded for roughly 250 days. In order to increase the reliability of the thermal performance of the fuel tank, vacuum conditioning has to be performed every 6 months. The detachable tanks allow the aircraft to remain in operation while maintenance on the tank is done, or other defects on the tank are repaired.

5.7.8. Fuel Feeding System

The fuel feeding systems delivers the appropriate amount of LNG to the engines. It is more complex for this aircraft than for a conventional aircraft, as it deals with cryogenic liquids and high pressure gasses. Its architecture is therefore explained in more detail. After that the components and their masses are estimated. Finally a total mass estimation of the whole system is provided.

Fuel System Architecture

The system consists of two kinds of networks, a primary and a secondary. This can be seen in the schematic overview of the system in Figure 5.55.

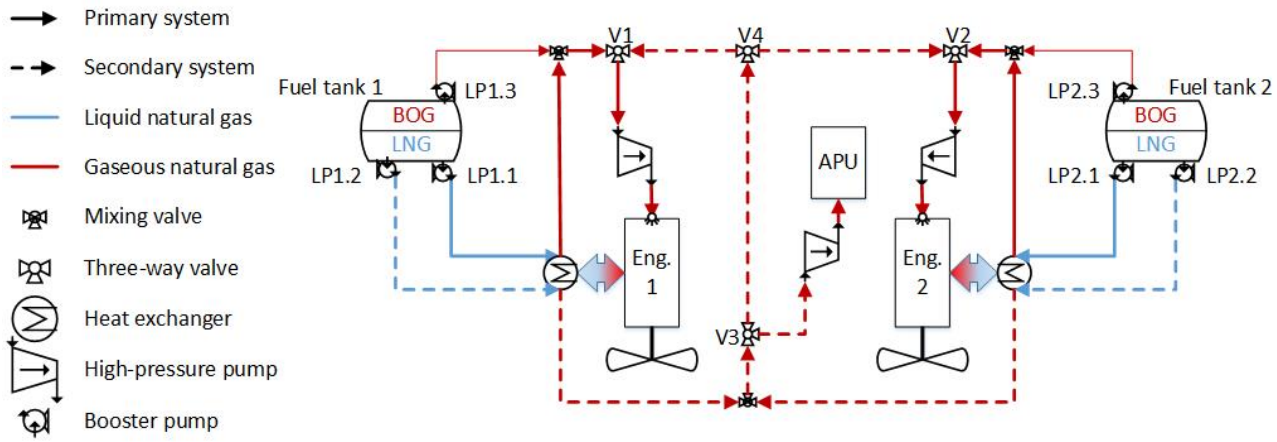

Figure 5.55: Schematic overview of the fuel system

For each tank, the primary (LP1.1 and LP2.1) and secondary (LP1.2 and LP2.2) booster pump can transfer the LNG to the engine heat exchanger. In the engine heat exchanger, the LNG is firstly heated by the high pressure bleed air. This cooled bleed air is used for air-conditioning in the cabin. The cooling of this high pressure air allows the air-conditioning units to require less low pressure bleed air to mix with it for a comfortable temperature. As bleed air decreases the performance of the engine, it is useful to minimise this as much as possible. After the LNG has been warmed in the A/C heat exchanger it is further heated by the heat of the exhaust gasses. The primary network then proceeds to a mixing valve, which mixes the heated gas with the Boiled-Off Gasses of the tank. It then enters three-way valve 1 for engine 1 or valve 2 for engine 2. These valves enable the switching between the primary and secondary network. After that it enters the high pressure pump to be ingested at the nominal pressure in the combustion chamber. After the secondary network of each tank passes the heat exchanger, it enters a mixing valve, which combines the fuel flows of tank 1 and tank 2. The flow then enters V3, which enables fuel flow towards the APU, if it is set RIGHT. If the valve is set to UP the natural gas flows towards V4, which enables the secondary network to switch between engine 1 and engine 2.

Although this system seems complex at first, it offers a good redundancy for different failures (see Table 5.21) and at the same time tries to minimise the number of heavy components, e.g. the heat exchangers.

Table 5.21: Pump and valve configuration for different scenarios

Condition	**LP1.1**	**LP1.2**	**LP2.1**	**LP2.2**	**V1**	**V2**	**V3**	**V4**
Nominal	ON	OFF	ON	OFF	LEFT	RIGHT	-	-
APU	OFF	ON	OFF	ON	-	-	RIGHT	-
Failure tank 1	OFF	OFF	ON	ON	RIGHT	RIGHT	UP	LEFT
Failure tank 2	ON	ON	OFF	OFF	LEFT	LEFT	UP	RIGHT
Failure LP1.1	OFF	ON	ON	OFF	RIGHT	RIGHT	UP	LEFT
Failure LP2.1	ON	OFF	OFF	ON	LEFT	LEFT	UP	RIGHT

Component sizing

It is difficult to size the whole system in detail as it is very complex and includes many gauges, sensors, safety valves and other components. Hence, only the main components were identified and sized. The first key components are the heat exchangers which heat up and vaporise the LNG. The masses of these components were taken from Daniel Brewer, who sized a similar system [58]. The mass for the exhaust heat exchanger was scaled for this turboprop engine with cross-sectional area. The low-pressure booster pumps were also taken from this source as they have similar mass flow and pressure characteristics. The masses for these pumps also include the necessary piping. Moreover, they run on 400 Hz AC, which is the same as the AC Essentials Bus. For the high pressure pump, it was more difficult to find real-world data as cryogenic pumps today are often only for very large mass flows. That is why a correlation between pump characteristics and mass had to be found from reference data. It was found that their was a strong correlation between mass flow and pump weight. This was used to make an estimation for this mass flow. Finally a weight estimation for the three-way and mixing valves was made. This is done using reference data from companies specialised in cryogenic valves. It was estimated that these valves weigh approximately 3 kg each. Since there are several smaller components that were not sized, an uncertainty factor of 1.1 was multiplied with the mass of this system. These components are a lot smaller than the components mentioned before, but still have to be accounted for, that is why 10 % seems like a decent approximation. In Table 5.22 a mass budget is provided.

Table 5.22: Fuel system mass budget

Part	**Mass [kg]**	**Number**	**Total mass [kg]**
Heat exchanger exhaust	38.8	2	77.6
Heat exchanger A/C	11.2	2	22.4
Booster Pump	44.0	2	88.0
HP pump	38.1	3	114.2
Three-way valve	3.0	4	12.0
Mixing valve	3.0	4	12.0
TOTAL	-	-	326.2
TOTAL + UNCERTAINTY FACTOR	-	-	358.8

5.7.9. Risk Assessment of Propulsion

The propulsion system is one of the most essential and delicate elements of the aircraft. The failure of this system may lead to a critical event which requires complicated operation to rescue the aircraft and its passengers. Possible failures of the propulsion system include a leakage anywhere in the system, complete fuel exhaustion, engine fire, engine damage, pump failure, fuel contamination, fuel system clogging, propeller blade separation, and fuel tank rupture. This can have multiple causes, or often a combination of several, like foreign option damage, part failure due to corrosion or fatigue, incorrect operation or refuelling, effects of icing, negligent maintenance, failing software, improper actions of the flight crew or even ingestion of volcanic ash[19]. The mitigation of nearly all of these risks is accounted for by authorities in terms of certification and training, which naturally Aquila will comply to.

Especially for Aquila, the risks concerning the use of LNG should be mitigated. LNG has a larger flammability range than that of kerosene (5.6 % - 15 % compared to 0.6 % - 4.7 %) [68]. As can be seen, LNG will only catch fire at a higher volume concentration than kerosene. LNG will evaporate in ambient temperatures, even at cruise altitude. Placing all systems and components containing LNG in a well ventilated area will decrease the likelihood of a build up of LNG or BOG. Furthermore the manufacturer is advised to set up in-house training facilities to train operators of Aquila in the handling of LNG specifically.

5.8. Aircraft System Design

The last part of the design process is the design of miscellaneous systems. This includes systems inside the aircraft, most of them not visible and integrated in the airframe. The first system that is discussed is the actuator system in subsection 5.8.1. After the actuator system, the electrical system is designed in subsection 5.8.2. Last of, the communications system is designed in subsection 5.8.3.

5.8.1. Actuator System

In each aircraft there are actuators performing different actions. These include actuators for flaps, control surfaces, spoilers, landing gear, etc. These can be powered in different ways: hydraulic, with the use of the shaft power of the engines to pressurise a fluid with a centralized pump; electro-mechanical with the use of the electric power generated from the APU and engines which is converted to mechanical energy; and electro-hydrostatic which is a hybrid solution that uses the electrical energy to power a pump for each actuator. Each of these systems has their advantages and disadvantages. In the following subsection each of these design options is discussed in detail.

Hydraulic Actuators

Hydraulic actuators rely on pressurisation of fluids in order to move a piston between the ends of a cylinder. Hydraulics have been widely used in aviation, because of their fast response, the large forces they can apply, the relatively low price and their good reliability. They require a centralised pump, a back-up electrical

[19] Retrieved from https://aviation-safety.net/database/databases.php, consulted on 20-06-2019

pump, a reservoir, directional valves, check valves, pressure relieve valves, selector valves, actuators, filters and an extensive piping system. This uses a lot of space and makes the system complex and difficult to install. These pipes can leak, which causes a loss of power in the system and as some hydraulic fluids are toxic can cause a hazard for people and the environment. These fluids can also become contaminated which can cause the system to fail, hence the focus for the maintenance of this system lies in checking the purity of the hydraulic oils. A hydraulic system requires the pump, which is connected to the engine shaft, to run continuously during operation to provide enough pressure at all time. This causes a continuous noise and causes the oils to heat up over time. These oils do therefore need to be (actively) cooled. Hydraulic fluids are far less compressible than gasses in for example a pneumatic system, but they can still be compressed a little. This makes the actuators more flexible than a rigid joint.

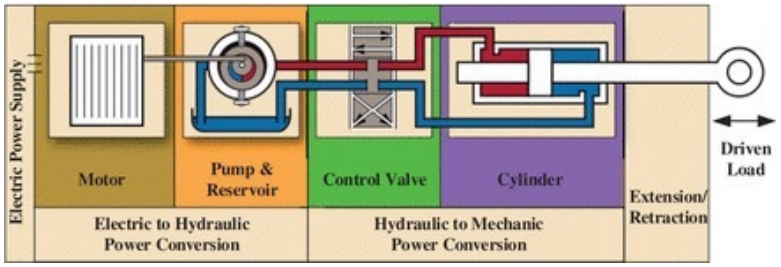

Figure 5.56: Hydraulic actuator [69]

Electro-Mechanical Actuators

Electro-mechanical actuators are actuators, which use electromotors and mechanical mechanisms. They are gaining ground in the aviation industry due to their lack of need for fluids and a complex piping system. Instead they only need wires for electricity. The system has the advantage to have 'Power on Demand', which means that it only consumes power when the systems move. Electro-magnetic motors produce less noise, can be locked in position, which causes the actuators to be very stiff, and are easy to install. They do, however, produce a lot of heat when running, which requires active cooling. Like the required mechanical connections, they also wear over time. Furthermore, they are rather expensive, especially for large forces as they are often not designed for this and therefore respond slowly. When jammed or when it overshoots its target, the whole system fails. This can be catastrophic for certain systems, e.g. the elevator. The immaturity of the technology and the lack of experience in Electro-Magnetic Interference (EMI) cause factors of uncertainty for this system.

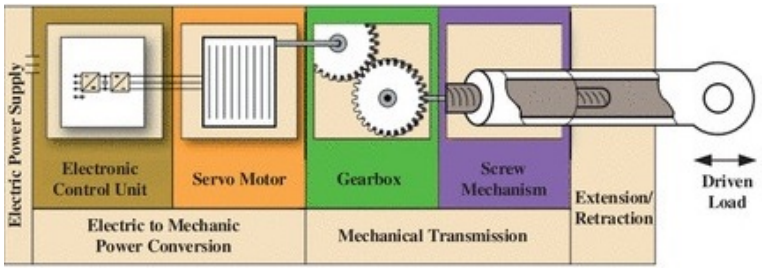

Figure 5.57: Electro-mechanical actuator [69]

Electro-Hydrostatic Actuators

Electro-hydrostatic actuators are a hybrid solution between hydraulic and electro-mechanical actuators. They use electrical power to power a pump which pressurises a fluid to move a piston. This eliminates both the need of a complex piping system and the inefficient mechanical parts. This makes it possible to create isolated units for different actuators. It combines the fast response, the large forces, the relatively low price and good reliability of hydraulics with the simple configuration for installation and maintenance of electrical systems. The pumps only need to be turned on when the actuator is moved. This consumes less power and produces less noise than a full hydraulic system. As it is partly hydraulic, the actuators are

less stiff and potentially toxic liquids have to be used. However, the risks for leaks is minimal due to the limited size of the system. As it has an electric motor, this has to be actively cooled. This type of systems is becoming more and more popular in aviation.

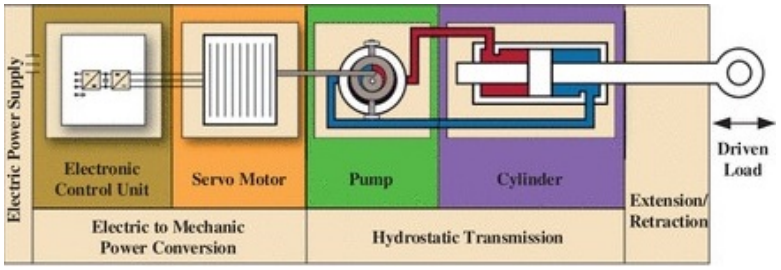

Figure 5.58: Electro-hydrostatic actuator [69]

As can be seen in Table 5.23, the EHA's are the better design choice mainly due to their better response in combination with their simpler design. The actuators necessary for the aircraft are for the flaps, control surfaces, speedbrakes, wheel braking, cargo door, landing gear, bay doors. For each of these actuators, a back-up actuator is installed for redundancy. The primary system is connected to the Essentials AC Bus and the back-up system is powered by the RAT Bus, this is explained in detail in subsection 5.8.2.

Table 5.23: Actuator System Trade-Off

	Hydraulic (HA)	Electro-Mechancial Actuators (EMA)	Electro-Hydrostatic Actuators (EHA)
Speed	Fast	Slow	Fast
Force	Strong	Weak	Strong
Reliablilty	Good	Less reliable	Good
Maturity	Mature	Least mature	Less mature
Redundancy	Good	Jamming causes failure	Good
Stop protection	Yes	No	Yes
Complexity	Large piping network	Only wiring necessary	Isolated units
Power use	Continously	Only when used	Only when used
Maintenance	Focussed on purity fluid	Focussed on wear of mechanical parts	Low
Installation	Complex	Easy	Easy
Stiffness	Compressible fluids	Stiff	Compressible fluids
Environment	Potentially toxic fluids	No toxic fluids	Potentially toxic fluids
Noise	High (constant pump)	Low	Lower (switching off pump)
Cooling	Oil cooling	Active motor cooling	Active motor cooling
Price	Cheap	Expensive	Cheap
Other	Loss of power due to leakage	EMI	EMI

Legend	Good	Mediocre	Bad

5.8.2. Electric system

Various subsystems require electricity in order to operate. Some of these are crucial for the integrity of the flight. That is why it is important for the electrical system to have sufficient power and enough redundancy. The electrical systems consist of different power sources, busses and loads. These are discussed in the following subsections.

Power sources

The main power source for the aircraft are 2 Integrated Drive Generators (IDG's). These generators use the mechanical power of the engines to produce Alternating Current (AC). They only produce electricity when the engines are turned on and run on a sufficient rpm. The Auxiliary Power Unit (APU) is used to start the engines and provide electrical power in AC when the engines are not running. The APU can in turn be started with the APU battery, which runs on Direct Current (DC). Finally one external AC power receptacle in the nose and one for DC under the left wing is available in the aircraft. They are placed on different places

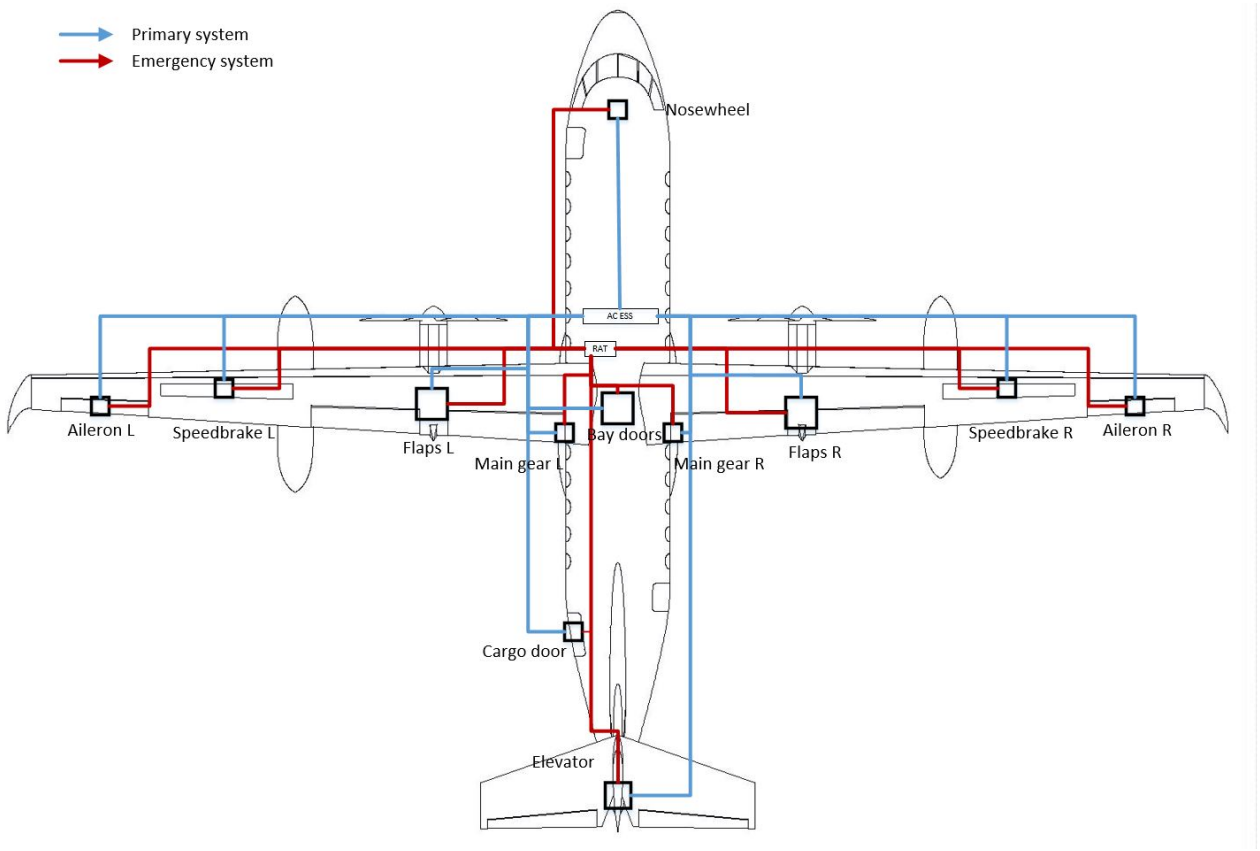

Figure 5.59: Actuator system

to avoid confusion. These can be connected with the ground power. This power can be used to power the systems and charge the batteries when the plane is idle. The aircraft is also equipped with a Ram Air Turbine, which uses the air stream to power the electrical systems in flight in case of a failure of the electrical system.

Electrical Bus

All electronic systems are connected with busses. These ensure that the right power can be provided to the right load. There are two kinds: AC busses and DC busses.

The 7 AC busses on board run on 115V rms 400 Hz current [70]. They are powered by the generators of the engines, the APU, the RAT and/or the external AC source. AC Bus 1 & 2 can be powered by the different engines respectively, the APU and the external AC source. Their main purpose is to power the main AC loads and other busses on the aircraft. Both are connected with the AC Essential Bus, which connects all vital systems necessary for a safe flight. The Essential Bus is also connected to the RAT Bus, which is responsible for powering the emergency hydraulic system. The RAT Bus is connected to the RAT and has priority over the AC Essential Bus if all electrical power sources would be lost during flight, as it is the last lifeline to power the control surfaces and flaps. The AC Essential Bus can also be powered by the main batteries through a power inverter. AC Bus 1 & 2 are also connected to Utility Bus 1 & 2 respectively. These power the on-board facilities for passengers and cabin crew, like for example the galley. The Service Bus is connected to the AC Bus 1. This bus enables the ground crew to perform basic operations like cleaning the aircraft without having to energise the whole system.

The DC systems run on 28V [70]. Just like the AC system, it also consists of several busses. In analogy with the AC system there are DC Bus 1 and DC Bus 2, which provide energy to the main DC loads in the aircraft. These are located aft in the plane. These busses are powered by the external DC power source or the rectified current from AC Bus 1 & 2. Current can be rectified by a Transformer Rectifier Unit (TRU). The current from AC Bus 1 & 2 can rectified by TRU 1 & 2 respectively. DC Essential Bus is in comparison to the AC system not directly connected to DC Bus 1 & 2. Instead it is connected with TRU Essential to AC Essential and with TRU 2 to AC Bus 2. In analogy to the AC system there are two utilities busses and one Service Bus connected

with their respective TRU's. The Battery Bus is connected to DC Bus 1 & 2 and handles the charging and discharging of the batteries. There are two main batteries on board which can power DC Essential Bus and AC Essential Bus through a power inverter and the APU battery, which starts the APU.

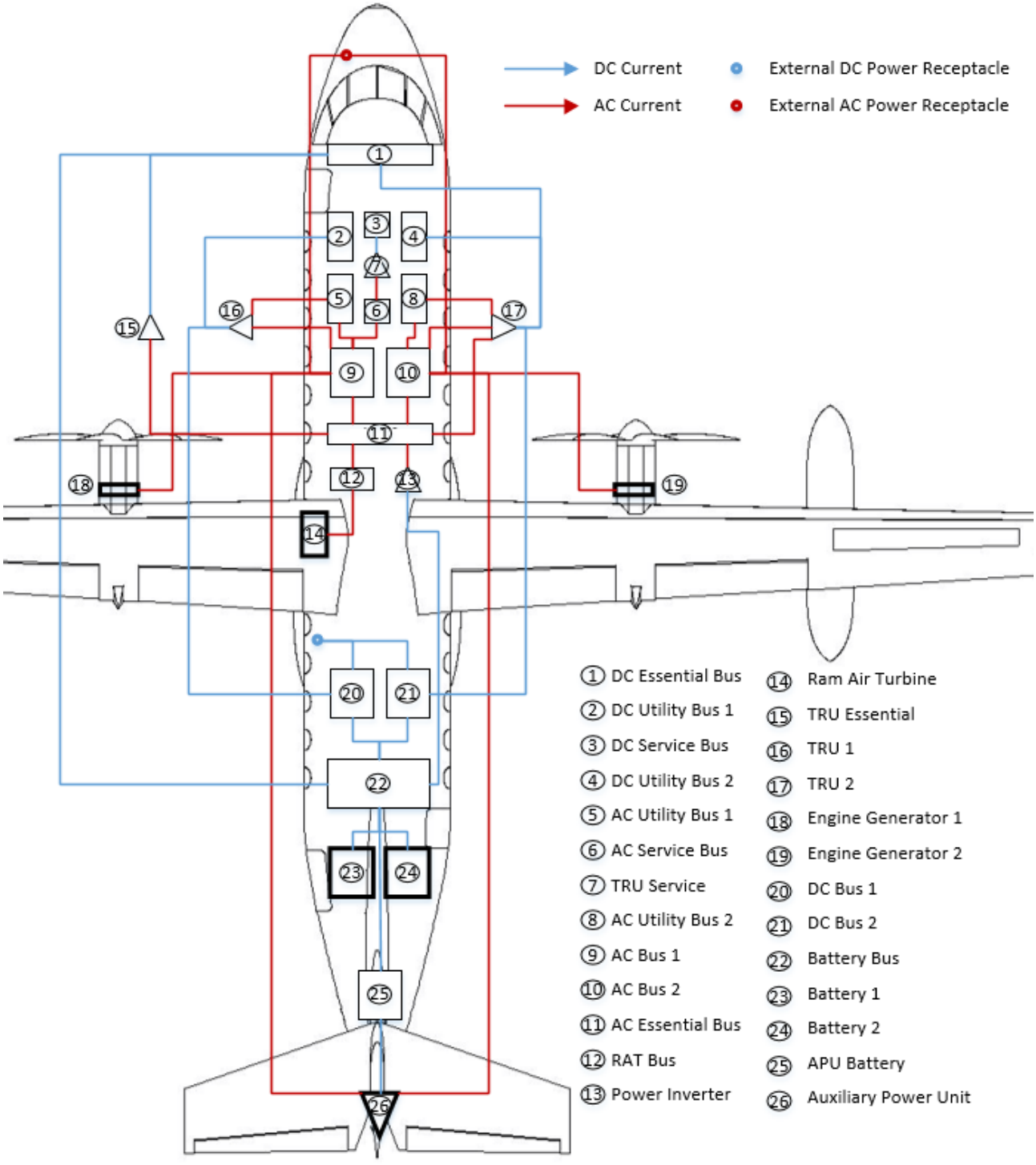

Figure 5.60: Electrical system

Bleed Air System

Some systems need pressurised air in order to operate. This bleed air or pneumatic systems consists out of several components.

Two pressurised tanks are situated in a compartment beneath the cabin. These tanks are connected and can supply each other with air if a valve is opened if necessary. However, in nominal conditions, pressure tank 1 is connected to engine 1 and pressure 2 is connected to engine 2.

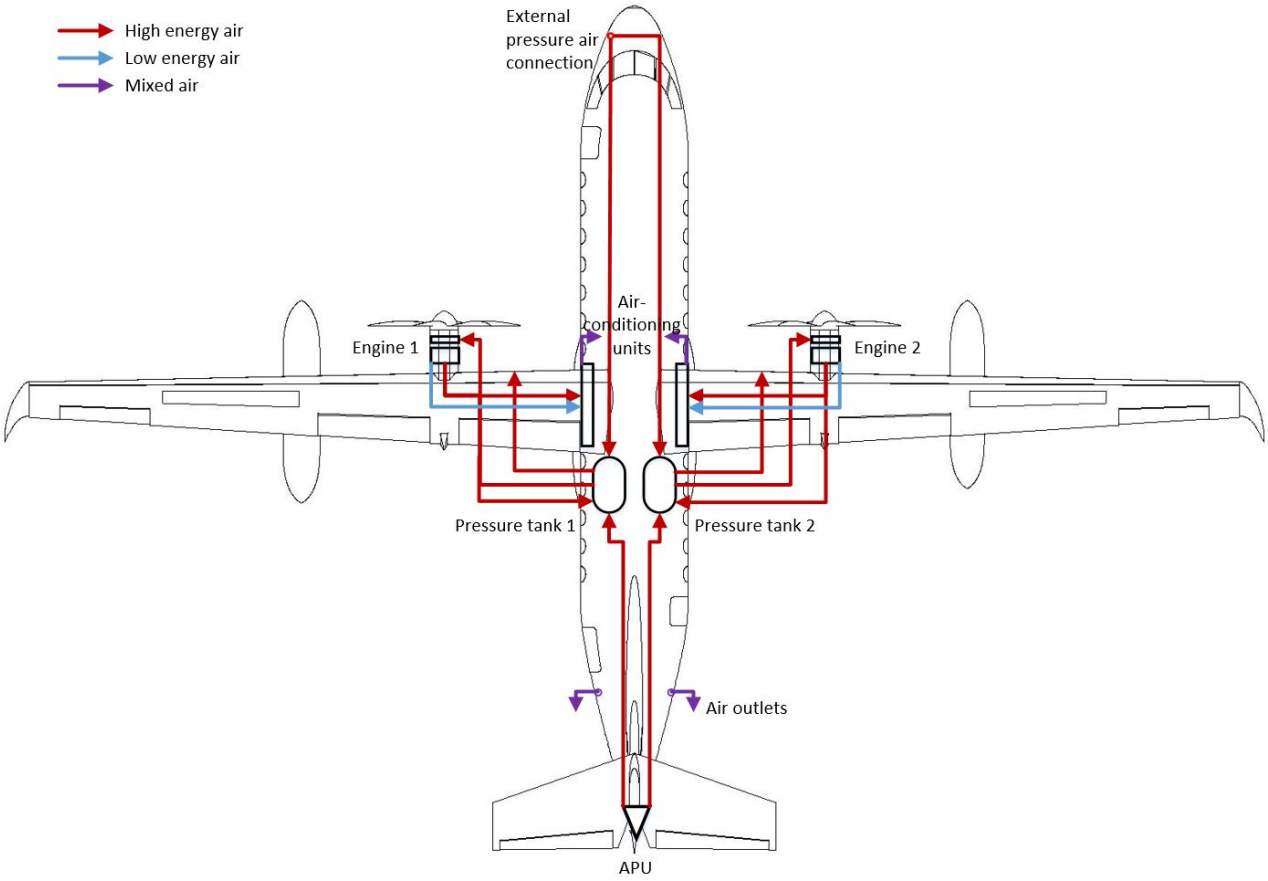

Figure 5.61: Bleed air system

External pressure air connection allows the filling of the tanks of pressurised air from the ground service. This port is situated in the nose and is mainly used to re-supply the pressure tanks if necessary.

Both the engines and the APU can provide the system with high energy air, which is bled off from the HP compressor section. In addition to that, the engines can also provide low energy air which is bled off before the air enters the compressors and is used for the air-conditioning. The main purpose of the pressurised air provided by the APU is to power up the engines. The APU itself is started with electrical cranking through the batteries.

The air-conditioning units provide the right temperature and pressure in the cabin. They use high and low energy air, which comes directly from the engines and mix it with the recirculated air from the cabin. At the back of the cabin two air outlets allow for sufficient venting in the cabin. No specific air-conditioning unit is chosen, but it is expected that the requirements on pressure, ventilation and temperature (AQ-OPS-03, AQ-OPS-04, AQ-OPS-05) can be met.

De-icing system

De-icing boots are present at the leading edge of the wing. They are powered by the pressurised air from the tank and allow for the removal of ice on the wings. Ice build-up decreases the performance of the aircraft and must therefore be avoided.

5.8.3. Communication System

Operating an aircraft requires various ways of communication. Not only contact with the external world is important, but the internal communication between crew members must be ensured as well. Next to this, there are various other systems using radio communication such as navigation and weather monitoring.

ATC communication Communication with the Air Traffic Control can be divided in short range communication and long range communication. Long range communication is mainly used for transatlantic flights and thus is not important for Aquila. The short range communication between the cockpit and ATC uses a VHF (118-151 MHz) wave connection. This connection is ensured by 2 VHF antennas.

Satellite Communication SATCOM can be used for a wide variety of applications in aviation. Aquila uses the Thales FlytLINK SATCOM system. FlytLINK is a recently developed SATCOM system which makes use of the Iridium satellite network. Its main advantage is the fact that it allows the airline to combine its logistical operations with the aircraft's in-flight operations. This is done by combining service logging, flight crew scheduling and aircraft monitoring with real-time weather info and even GPS navigation.

On-board Communication The communication between the cockpit and the cabin crew is done through an intercom telephone system. The flight crew communicates with each other by use of the cockpit's local radio system.

Other systems

Weather Radar The weather is placed in the aircraft's nose, which is the conventional position. It uses radio waves with a UHF range between 5 GHz and 10 GHz[20].

Traffic Collision Avoidance System The TCAS warns the pilots in case of a mid-air collision danger, by reporting the presence of other aircraft in their vicinity. The system uses a transponder, which detects the presence of similar transponders on different aircraft.

ILS (Instrument Landing System) Detection System The ILS system detects the ILS localizer and glideslope and guides the autopilot down this path. The glide slope detection system is situated in the aircraft's nose, together with the weather radar. The localiser detector is situated on top of the vertical tail.

Emergency Location Transmitter The goal of the ELT is to broadcast an emergency signal in case of an accident, allowing the aircraft to be located by any external parties. In commercial aviation, the flight data recorder must contain an underwater ELT. The Aquila is equipped with two different ELTs; one on the back of the aircraft, the other one is a part of the flight recording system. Both transponders have impact monitors which are activated by g-forces during an accident.

VHF Omni-Directional Range The VOR is an alternative type of navigation, using short-range radio waves. It helps the pilot to stay on course by sending VHF waves which are captured by an antenna on the aircraft, after which the navigation system determines the aircraft's position with regards to the VOR radio beacon.

The position of these systems/antennas are shown in Figure 5.62.

[20] Retrieved from https://www.aircraftsystemstech.com/2017/05/weather-radar.html (Consulted on 06/06/2019)

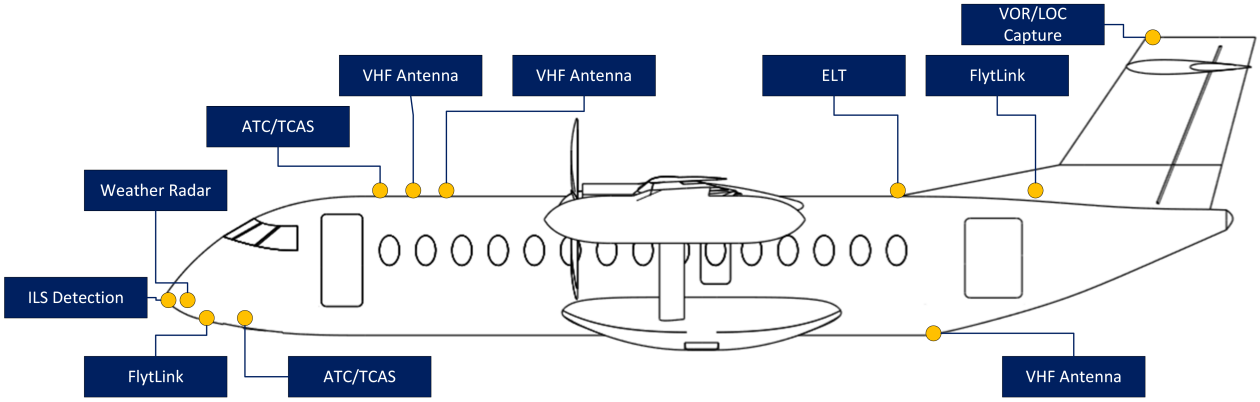

Figure 5.62: Aquila antenna locations

External Communication Diagram

The main parties in aircraft operation are the airline, the airports, air traffic control and of course the aircraft. Communication is crucial to ensure a smooth operating process. The communication system for the Aquila fleet is presented by Figure 5.63.

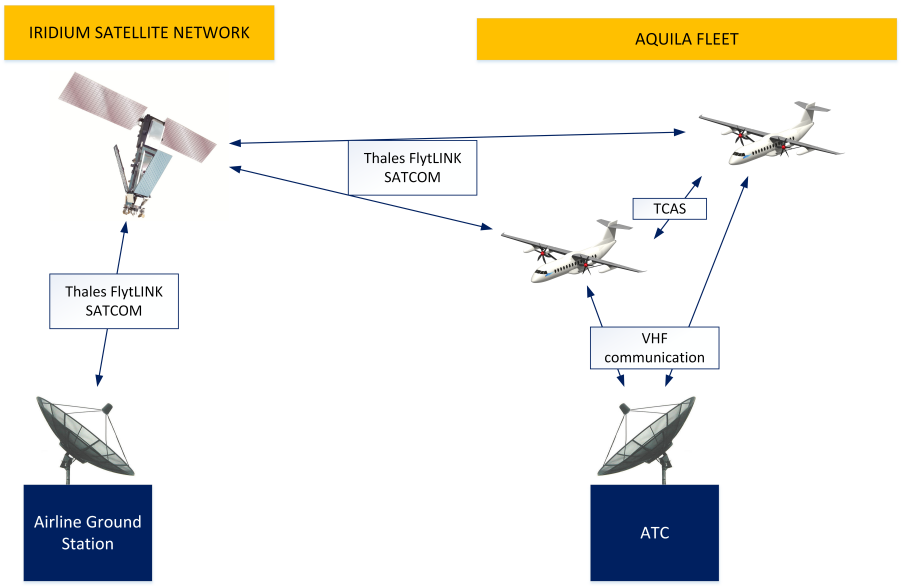

Figure 5.63: Air to ground connection diagram

5.8.4. Risk Assessment

The aircraft contains multiple complicated systems with varying levels of importance. In this section the risks introduced by these systems and their mitigation is discussed. The systems are divided in four categories, namely the actuator system, electric system, communication system and other systems.

Actuator System Risk Assessment

As explained in subsection 5.8.1, the aircraft uses electro-hydrostatic actuators. This kind of actuator minimises the risk for leaks due to the limited size of the system. Additionally, every actuator utilises its own pump, therefore it is unlikely that multiple actuators fail at once. However, if an actuator does fail, a back-up pump and actuator is switched on. Every actuator has a back-up in order to minimise the risk that systems controlled by the actuator can not be operated. This is crucial since systems such as the ailerons are de-

pended on these actuators, which means that in case of complete failure, the aircraft is uncontrollable.

Electrical System Risk Assessment

The electrical system consists of multiple busses which are powered by different sources. In case of failure of a bus or power source a back-up can be switched on. However, the failure of some busses has a larger impact than others. The essential bus for example is vital; a complete failure of this system would mean that the aircraft is uncontrollable. Hence this system can be powered by all available power sources with the addition that the hydraulics can also be powered by the RAT.

The routing of the cables of the electrical system is done in such a way that there is no location in the aircraft where all cables come together. By doing this, there are no critical points in the electrical system which limits the risk of failure of multiple busses.

Communication and Other Systems Risk Assessment

The aircraft contains various communication systems with ranging levels of importance. In case of failure of the most important systems such as the ATC communication system or the TCAS, a back-up system switches on. The same holds for the remaining other systems.

5.9. Conclusion

A preliminary sizing of the system was performed, of which the results can be found in Table 5.24. Designing them in more detail is considered to be part of a later phase of the design. This has to be done by experts in the specific fields. AQ-OPS-04 and AQ-OPS-05, which concern the cabin climate can not be validated at this moment. However, the necessary infrastructure is in place to be able to install the right system and it can therefore be said with confidence that this will not lead to problems in the future.

Table 5.24: Specifications of the Aquila 60 aircraft.

Parameter	**Value**	**Unit**
Wing		
Span	32.65	m
Area	49.21	m^2
Aspect Ratio	20.0	-
Empennage		
Horizontal Tail Area	14.27	m^2
Aspect Ratio Horizontal Tail	4.0	-
Vertical Tail Area	13.29	m^2
Aspect Ratio Vertical Tail	1.2	-
Fuselage		
Length	21.45	m
Diameter (outside)	2.84	m
Cabin Pressure	81200	Pa
Propulsion		
Engine	GE T6E	-
Take-off Power	1775	kW
Specific Fuel Consumption (Cruise)	217	g/kWh/h
Mass		
Operational Empty Weight	10270.3	kg
Maximum Take-off Weight	18536.1	kg
Maximum Payload Weight	6600	kg
Maximum Zero Fuel Weight	16870.3	kg
Maximum Fuel Weight	2000	kg

6
Operations

In this chapter, the most important operational procedures for the aircraft are outlined. First, section 6.1 explains how the aircraft shall be loaded and how passengers can board the aircraft. It also describes the procedures related to the fuel system, which are quite different than for regular aircraft flying on kerosene. In section 6.2, the most relevant emergency procedures are discussed, with a focus on flying with LNG on board. Finally, the risks of the procedures that are described in this chapter are assessed in section 6.3.

6.1. Passenger- and Fuel-Related Procedures

This section describes the procedures that are related to the passengers and fuel system. First, the aircraft loading procedures are outlined in subsection 6.1.1. As the aircraft also needs to be cleaned, subsection 6.1.2 provides a brief description of procedures related to the cabin replenishment. The logistics of LNG are a key aspect of the operations of the aircraft; therefore, these are described in subsection 6.1.3. This allows for a description of the refuelling procedures in subsection 6.1.4. Finally, subsection 6.1.5 provides a brief overview of the time required for the average turnaround procedure.

6.1.1. Loading

For airlines, flexibility during loading is key to a short turnaround time and thus high efficiency of aircraft use. As it plays an important role in how much revenue an airline can obtain, designing for such flexibility can make the aircraft more competitive on the market. Hence, the aircraft is designed to allow for loading in any order; that is, it does not matter whether passengers board first, or cargo is loaded before the passengers. The same holds for the attachment of the fuel tanks, which can theoretically happen at any moment during the turnaround (even though the fuelling normally takes place when there are no passengers aboard, as is explained later in this chapter). The additional flexibility in this design is particularly interesting for low cost carriers, which are expected to be the major customers of the aircraft.

Focusing on the loading of the passengers, the airline can choose between three options: boarding via the main exit at the left front of the aircraft or via the (equally large) secondary exit at the right back of the aircraft. Either of these options is possible at a small regional airport, as none of the exit doors require stairs to be brought to the aircraft. These doors can rotate and contain fixed steps, as is common in business jets.

With a full-economy cabin layout as seen in Figure 6.1, consisting of 60 seats with a 4-seat abreast configuration, the expected boarding time using one door is 7.5 minutes. This is based on an arrival rate of ten passengers per minute, estimated by Boeing[1]. Half a minute is added to this time to account for the start-up and close-out of the process. Furthermore, one minute is reserved for the storing of luggage by the passengers who board the aircraft last. Higher arrival rates can lead to queues of passengers in the aisle waiting to get seated and would thus not significantly reduce the boarding time [71].

For the deboarding of passengers, a higher passenger flow can be achieved since there is no need to check boarding passes. According to Boeing, the number of passengers leaving the aircraft during this process can be estimated to be 16 per minute, leading to a deboarding time of four minutes.

As most boarding procedures are likely to use one door, the expected time required for a full boarding and deboarding process is 11.5 minutes. Since the loading of cargo or luggage can be done simultaneously with

[1] Retrieved from http://www.boeing.com/commercial/aeromagazine/aero_01/textonly/t01txt.html (Consulted on 12/06/2019)

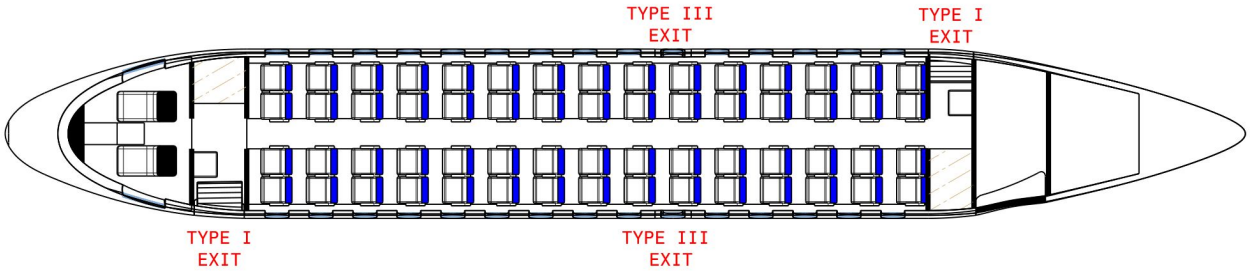

Figure 6.1: Cabin layout in full-economy configuration: exit types according to CS 25.807 [72]

the refuelling process, this is not a limiting factor for the turnaround time.

6.1.2. Cabin Replenishment

There are three types of cabin cleaning services: a quick transit, a layover and deep cleaning [73]. The first type is most common and takes place before every flight. It involves cleaning activities that are necessary to provide a comfortable, safe and hygienic travel experience for passengers and crew. There are seven main activities which can be requested within this service: seat cleaning, seat pocket cleaning, galley cleaning, toilet cleaning and replenishment, floor cleaning and blanket distribution. The exact services can differ per flight, as there are both standard and 'on request' cleaning operations [74]. For example, the distribution of blankets on short-range flights is unlikely to occur. For small aircraft like the Aquila, this cleaning process usually takes between 12 and 20 minutes.

6.1.3. LNG Logistics

Using a new fuel brings technical challenges, but also logistical challenges, which are discussed here. Conveniently for the project, LNG is already being produced on a large scale and the production is still increasing, with more and more LNG being used for road vehicles, ships and power generation. The infrastructure for LNG distribution is already present in a large part of the world, but is mainly focused on ports and terminals that are near the sea. Some airports, such as Brussels Airport and Schiphol Airport also offer LNG fueled transport busses. These facilities could be used to store LNG for LNG powered aircraft.

In Europe there are already over 100 LNG stations that are being used by LNG powered cars and busses [75]. These facilities could be used to fuel tank cars that can be used as an intermediate solution for small airports, which do not have LNG facilities themselves. A single-tank car such as the ST-16300 would be able to transport and provide 22861 kg of LNG. This would be sufficient to supply fuel for over 11 flights of Aquila for the design payload and range. A welcome development is that the number of tank stations is rapidly increasing and it is expected that also more airports will choose for LNG facilities, which would negate the need for tank cars and decrease cost.

One point of concern is that the quality of LNG is preferably over 99% methane. This is primarily an environmental concern, since impurities in the LNG will lead to higher emissions of NO_x and SO_x. This risk can be mitigated by checking the quality of LNG before use.

When biomethane becomes economically viable, it is advised to use fuel trucks to bring the fuel to airports to allow for even more CO_2 reduction. For larger airports, it might even be viable to make larger storage tanks for this.

For LNG containers that do not make use of active cooling or vapour recovery systems, it is advised to either return the vented gas to the natural gas pipes or, if that is not possible, to use the vented gas to produce electricity which can be used to return power to the grid or run systems at the airport.

Since LNG is a cryogenic fuel, proper training needs to be given to the ground personnel. Improper handling of the fuel can lead to frostbite or other accidents. Proper gear needs to be handed out such as gloves and facial protection. This should ensure that the number of incidents purely related to the type of fuel used is minimised.

6.1.4. Refuelling

Refuelling the aircraft with LNG adds some challenges, which can be mitigated by changes in the operations. The aircraft can be fuelled in two different ways: refuelling while the tanks are attached to the aircraft and refuelling while the tanks are detached from the aircraft. In either case, the refuelling process shall occur when there are no passengers aboard the aircraft. This is to fully guarantee their safety. However, the safety hazards are so limited that cabin replenishment and cargo handling can be done during the refuelling process.

The removable fuel tank is one of the key features of the Aquila. It allows for a highly adaptable aircraft and flexible operations. The fuel tanks can be refuelled in a hangar and attached to the aircraft while it is on the ground.

When the airline chooses to change the fuel tanks, they must make sure that there is equipment available to lift the fuel tanks to a height of approximately 3.1 metres from the ground. Here, it should be taken into account that each fuel tank has a maximum mass of 1250 kg. A normal forklift truck should be able to lift this weight without problem. In order to make sure that the fuel tank does not fall off the truck a jig should be used to hold the tank in place and protect it if it does hit the ground. The changing time depends on whether the aircraft can be connected to ground power or not. When this is possible, both fuel tanks can be replaced simultaneously. The required time to swap these tanks, provided that the airport services are fully prepared and standing within the vicinity of the aircraft, is estimated at 10 minutes. If no ground power is available, the tanks shall be replaced one by one, as the aircraft must run its APU. This system requires fuel to run on, and thus needs to be connected to at least one of the tanks. In this case, the procedure takes approximately 20 minutes.

The time required for refuelling of the aircraft while the tanks are attached to the aircraft is limited by the maximum fuel flow of the fuel system at the local airport. This depends on the available equipment. Using a reference pump for LNG which can be placed on airports, a first estimation was found. The Artika 2S [2] has a rated flow capacity of 430 litres per minute and can apply a maximum pressure of 25 bar, which is more than ten times as high as required for the fuelling of the tank. The internal volume of the tanks is 2500 L, so it would take 5.8 minutes to fuel one tank or the whole aircraft if both tanks are filled at the same time.

6.1.5. Conclusion

In conclusion, the minimal turnaround time of the Aquila comes at just under 20 minutes; this is the case when boarding processes takes place via both doors, both fuel tanks can be replaced simultaneously and the cabin replenishment is finished within 12 minutes. The minimum turnaround time in the most likely scenario is expected around 32 minutes, when only one door is used for the boarding process and both tanks need to be topped up with fuel consecutively. Hence, the flexibility of the Aquila offers a short turnaround time and therefore improves its competitiveness on the regional aviation market.

6.2. Emergency Procedures

In this section, the emergency procedures are outlined. The focus lies on those procedures that are different for the Aquila compared to conventional aircraft. This has mainly to do with the use of LNG. In subsection 6.2.1, depressurisation and engine failure procedures are briefly described. Although there is little adaptation required for the use of LNG, they were deemed important and are therefore discussed here. Then, the procedures that must be followed in case of fire or an emergency landing are described in subsection 6.2.2 and subsection 6.2.3, respectively.

6.2.1. Depressurisation and Engine Failure Procedures

Emergencies such as mid-air depressurisation and engine failure are severe and need to be treated in a safe and efficient manner. However, since they are standard procedures, they are only discussed here briefly. The use of LNG does not significantly change these procedures.

[2] Retrieved from http://www.vanzettiengineering.com/automotive.php (Consulted on 13/06/2019)

Depressurisation of the cabin can lead to critical situations and is a very serious hazard, especially when flying at high altitudes. In case of such an event, oxygen masks will drop and passengers shall breath through these. As the oxygen supply is limited and will likely last no longer than 15 minutes, the pilots need to perform an emergency descend to 10,000 feet or the minimum safe altitude, whichever is lowest[3].

When there is an engine failure, the pilots shall start the procedures for an emergency landing. If the failed engine cannot be restarted, it should be left switched off and disconnected from the fuel system. Cross-feeding shall be enabled to allow for high thrust-level operations using the remaining engine and stabilisation using fuel pumps. In the unlikely event that the engine failure is caused by an event that could also damage the fuel tank, the defuelling valves shall be opened to let the LNG escape.

6.2.2. Fire Procedures

In the event of an on-board fire, the location of the fire shall be identified first. If it is in the aircraft interior, the crew shall try to extinguish it, if it is safe to do so. Independent on the outcome of this action, an emergency landing shall be attempted. Oxygen masks will also drop from the ceiling to facilitate safe breathing of the passengers. In case of a fire in the engine or fuel system, the fuel system shall be isolated from the source of the fire using control valves and pumps. Emergency systems shall cross-feed the fuel if required. In the worst case scenario, the fuel shall be released and a gliding descent needs to be initiated. However, the likelihood of this event is extremely low, as LNG is not flammable unless mixed with air in the right proportions. Even if this happens, the size of the affected area is limited to the direct surroundings [76].

6.2.3. Evacuation Procedures

In case of emergencies, an evacuation is often necessary. The evacuation of an aircraft is different for emergency landings on the water or on land.

During an emergency landing on land, passengers and crew shall be seated in a brace-position. After impact, passengers seated at the emergency exits behind the wing shall remove the exits and deploy them. Lights along the cabin floor lead people to the nearest exit. Cabin attendants shall help people to exit the aircraft. In addition, slides need to be activated at the main exits. This is discussed further in subsection 7.4.4. Once the aircraft has been evacuated, passengers and crew need to get at a safe distance. Although the likelihood of leakage in the fuel tanks is very low, it can cause a hazard if it occurs. Leaking gasses can evaporate and create a ‘smoke curtain’ in the area. This might become flammable if the concentration of methane in air is between 5.3% and 15% (at sea level conditions) [68].

In case of an emergency landing on water, similar procedures are followed as described above. However, upon leaving the aircraft, passengers need to receive life jackets for infants. These flotation devices shall be inflated only after one has left the aircraft. The slides, activated at the main exits, can be used as rescue rafts.

6.3. Risk Assessment

In this section the risk assessment of the operations is described. The operations can be divided into four categories which are the risks regarding passenger procedures, fuel procedures, emergency procedures and maintenance.

6.3.1. Passenger-Related Procedures Risk Assessment

When embarking or disembarking the aircraft, the passengers are exposed to many risks which could lead to a delay of the flight. When embarking the aircraft by means of the built-in stairs for example, the passenger could slip and fall which could result in a delay. This risk is mitigated by equipping the built-in stairs with an anti-slip coating and handrails. Another cause of delay could be a person with a physical disability. By giving these people priority when boarding it can be assured that the aircraft will depart on time.

[3] Retrieved from https://www.skybrary.aero/index.php/Pressurisation_Problems:_Guidance_for_Flight_Crews (Consulted on 20/06/2019)

6.3.2. Fuel-Related Procedures Risk Assessment

The refuelling procedures for the Aquila aircraft are vastly different than for conventional aircraft as stated in subsection 6.1.4. Since LNG is a cryogenic fuel, it is of the utmost importance that the person operating the refuelling system wears protective clothing and has proper training. This is done to limit the risk of injuries. Additionally, the refuelling area has to be blocked to prevent unauthorised people injuring themselves.

In order to fuel the aircraft, the LNG has to be stored in a tank, which will be relatively large on large airports. This could impose the risk of explosion which could have catastrophic effects. However, this risk is already mostly mitigated by the characteristics of LNG. LNG is only flammable when the concentration in air becomes between 5.3% and 15% [68]. Therefore LNG should always be handled and stored with caution and care.

6.3.3. Emergency Procedures Risk Assessment

During an emergency situation, it is crucial that the emergency systems work correctly. If normal power fails, there are backup systems that can provide power in an emergency as described in subsection 5.8.2. Since all emergency situations are different, it is difficult to perform an adequate risk assessment. For some emergency situations however, the risk can be assessed and mitigated. The aircraft rafts for example need to work in every condition, therefore the deployment should not be dependent on other systems. Also, it should always be possible to deploy the raft manually. Another emergency situation that could occur, is an engine fire. This kind of emergency has a low likelihood and will always result in an emergency landing with possible critical consequences. Therefore, to handle this critical situation as well as possible the engines are equipped with fire extinguishers. If, despite the mitigations, multiple failures occur simultaneously, accidents can not be ruled out.

7
Design Analysis

Now that the design is completed, it is necessary to analyse the design. The purpose of the analysis is to check whether the design meets all the requirements that were set earlier. Firstly, the detailed mass budget is given. After that, both the ground and flight performance of the aircraft are analysed. Next, the sensitivity of the design is assessed. Then the RAMS characteristics of the aircraft are analysed. The chapter is concluded with a validation of the analysis methods.

7.1. Design Mass Budget Breakdown

To have a better overview of the mass budget of the aircraft, the maximum take-off weight is broken down into its several components. Also the empty mass is broken down into the different subsystems it consists of. The mass budget can be used in a later phase of the design process to investigate whether weight can be saved in systems that are heavier than reference values.

Figure 7.1 shows the budget breakdown of the maximum take-off weight of the aircraft. As visible in the pie chart, most of the weight is allocated to the operational empty weight. The rest of the maximum take-off weight is allocated to the payload and fuel. The payload consists of 60 passengers including their luggage for which a value of 105 kg per passenger is used to estimate the payload mass. The fuel weight is determined by calculating the amount of fuel needed for the design range of 1850 km. Adding these weights brings the MTOM of the aircraft to 18,536.1 kg.

The operational empty weight can also be divided in different systems. This is visualised in Figure 7.2. Most of the empty weight is allocated to the wing and to the fuselage. This seems logical, since these are also the largest systems on the aircraft. Comparing the fractions to a conventional aircraft, the engine and fuel system seem to stand out. Because of the innovative LNG propellant, heavier system parts are required. This includes the pressurised fuel tanks under the wing, but also the heat exchanger and high pressure pumps are causing the weight to increase.

The control system consists of the hydraulics and actuators which are needed to control the aircraft. Furthermore, the electrical system consists of all electrical components in the aircraft. Both these systems are explained elaborately in section 5.8. All the components in the pie chart can be added to get to the empty mass of the aircraft, which accumulates to 9824.3 kg.

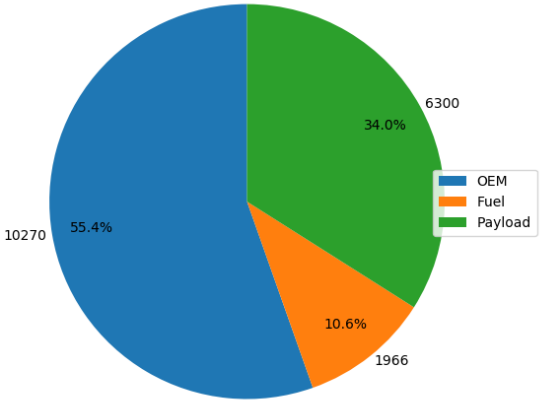

Figure 7.1: Masses as percentage of MTOM

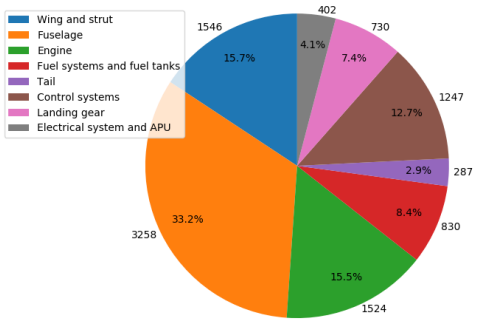

Figure 7.2: Component masses as percentage of empty mass

7.2. Performance Analysis

In this section, Both the ground and flight performance of the aircraft were assessed. The ground performance consists of the manoeuvrability of the aircraft on the ground. The flight performance consists of both take-off and landing field length. In this section, also climb and descend performance is assessed. Performance of the cruise phase consists of the payload-range diagram, the flight envelope and the flight profile. At last, the sustainable performance of the aircraft is investigated. This includes the noise and emission performance of the aircraft.

7.2.1. Ground Performance

As the aim of the aircraft was to be operable on small airports, it needs to be able to manoeuvre in small spaces. Because of the high aspect ratio, this was something that required extra attention. This section discusses the performance of the aircraft from gate to runway.

Turning performance on ground

Because of the slender wings of the aircraft, it is possible that the turning radius during ground operations exceeds the maximum allowable radii for regional airports. The aircraft shall therefor be able to make a turn with a minimum radius of 19.74 meters, as specified in section 3.1. Therefore, it was investigated whether the aircraft is able to achieve the required turning radii for small airports. In Figure 7.3, the definitions of the different turning radii are given. For the Aquila aircraft, the wing radius, nose landing gear radius and outer gear radius are most constraining. The nose landing gear is able to turn with a maximum angle of 70 degrees, but several different turning radii were investigated. First the landing gear radii were calculated to ensure the space needed on the paved runway is sufficient. Next, the radii of the wing tip, the horizontal tail and the nose of the aircraft were investigated to see what the ultimate turning radius of the entire aircraft would be. In Table 7.1, the values of the radii for different steering angles are given. It is concluded that, when the nose landing gear is at maximum steering angle, the requirement can be met. Also the minimum pavement width for a 180^{o} turn is shown in Table 7.1, as this can also be an important factor for operations on small airports.

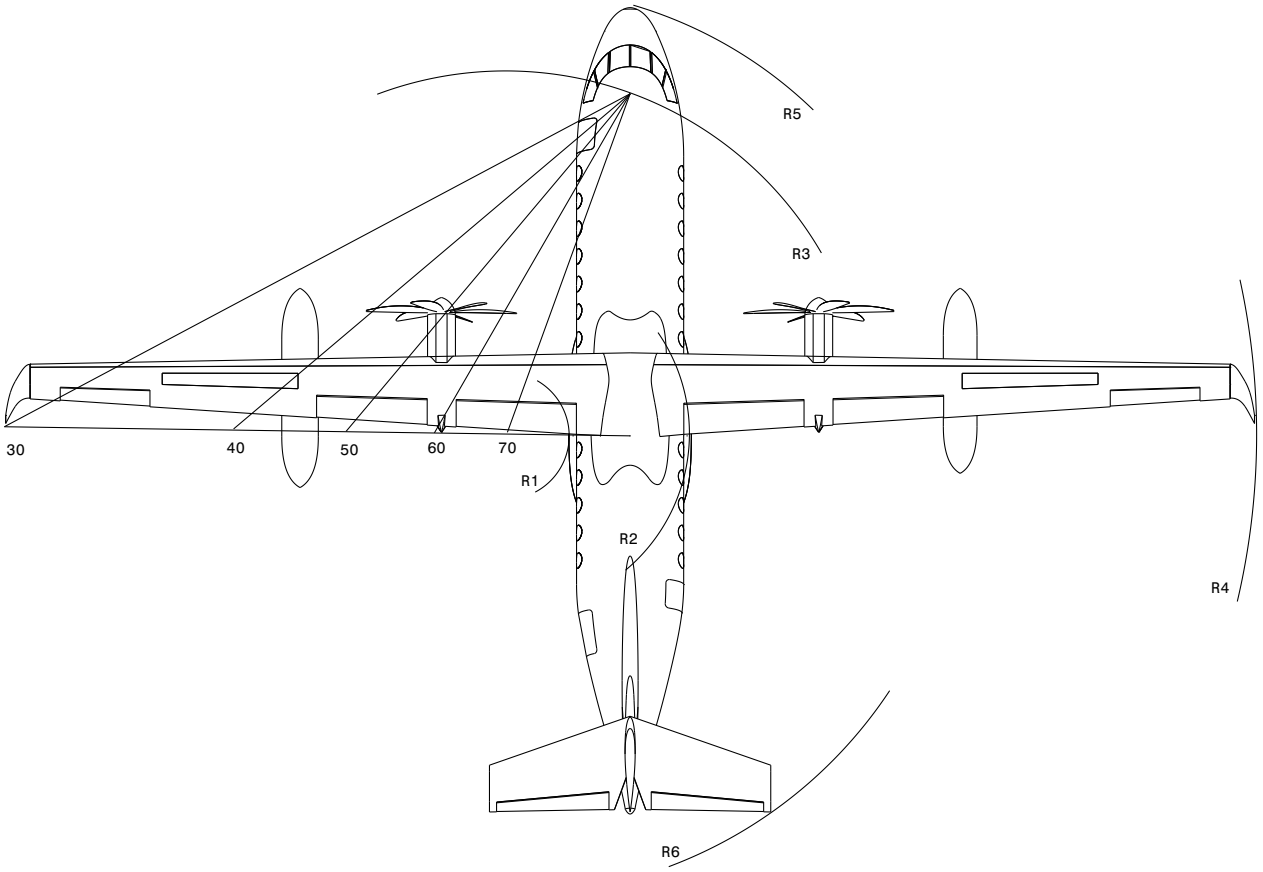

Figure 7.3: Turn radii during ground taxiing

Table 7.1: Turning radii of crucial aircraft components for different steering angles.

Steering angle [deg]	**R1 Inner Gear [m]**	**R2 Outer Gear [m]**	**R3 Nose Gear [m]**	**R4 Wing Tip [m]**	**R5 Nose [m]**	**R6 Tail [m]**	**Minimum Pavement Width [m]**
30	13.22	16.20	16.98	30.39	18.06	21.03	33.18
35	10.64	13.62	14.80	27.81	16.03	18.82	28.42
40	8.63	11.61	13.21	25.80	14.57	17.17	24.82
45	7.00	9.98	12.01	24.18	13.50	15.88	21.99
50	5.63	8.61	11.08	22.81	12.68	14.87	19.70
55	4.45	7.43	10.36	21.63	12.06	14.03	17.80
60	3.41	6.39	9.80	20.59	11.58	13.34	16.20
65	2.47	5.45	9.37	19.65	11.21	12.75	14.82
70	1.60	4.58	9.03	18.78	10.94	12.25	13.62

7.2.2. Take-Off Performance

The take-off performance of the aircraft consists of two phases: the ground take-off and the climb. Firstly, the required length of the runway is calculated (TOFL). Once the aircraft is off the ground, it is desired to climb to cruise altitude as fast as possible. This is calculated after the TOFL is known. Lastly, the methods are validated.

Take-Off Field Length

The TOFL was calculated as described by Ruijgrok [77]. As can be seen in Figure 7.4, it consists of three different phases; the ground roll, the rotation and the initial climb. The take-off manoeuvre is finished when the aircraft is 50ft above the ground (also known as the screen height).

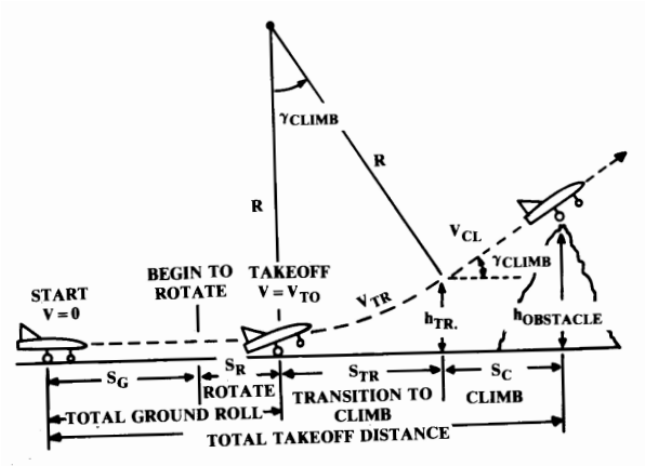

Figure 7.4: Take-Off Field Length [1]

The ground distance is calculated using the acceleration of the aircraft until the lift-off speed V_{LOF} (or V_{TO} in Figure 7.4) is reached. The equation for the acceleration can be found in Equation 7.1. In this equation, the mean thrust, mean drag and mean ground friction force are used. The mean forces are calculated at a speed of $\frac{V_{LOF}}{\sqrt{2}}$. The lift-off speed was determined to be 1.05 times the stall speed.

$$\bar{a} = \frac{g}{W}(\bar{T} - \bar{D} - \mu(W - \bar{L})) \tag{7.1}$$

The ground roll distance can then be calculated. This was done by integrating the distance covered between 0 and lift-off speed. The integration can be found in Equation 7.2.

$$s_{gr} = \int_0^{V_{LOF}} \frac{VdV}{a} = \frac{V_{LOF}^2}{2\bar{a}} \tag{7.2}$$

The distance needed for the rotation depends on the load factor during the rotation and the desired path angle. The radius of the rotation was calculated using Equation 7.3.

$$R = \frac{V_{LOF}^2}{(n_{LOF} - 1)g} \tag{7.3}$$

The horizontal distance covered during the rotation can be calculated using Equation 7.4. This is the distance between a path angle of 0 and a path angle of γ.

$$s_r = Rsin(\gamma) \tag{7.4}$$

The last phase in the take-off is the distance between the rotation and when the screen height (50ft) is reached. This is the initial climb phase and can be calculated using Equation 7.5. The vertical distance covered during the rotation is subtracted from the screen height.

$$s_{ic} = \frac{h_{screen} - R(1 - cos(\gamma))}{tan(\gamma)} \tag{7.5}$$

Climb performance

Once the aircraft is off the ground, the climb to cruise altitude starts. The maximum climb rate the aircraft can achieve is determined by available excess power. The equation for the rate of climb is given in Equation 7.6. As the altitude increases, the amount of excess power decreases. Also, the velocity at which the aircraft must fly to reach this maximum climb rate increases. When the aircraft has no excess power left, the flight ceiling is reached.

$$RC_s = \frac{P_a - P_r}{W} \tag{7.6}$$

In Figure 7.7, the power available vs power required at sea level is visualised. The lower limit is, in this case, the stall speed. The upper limit is the intersection between the two lines. The efficiency of the turboprop engine varies with velocity. This variation is simplified as can be seen in Figure 7.5. The red line is the simplified turboprop efficiency and the black line is the real turboprop efficiency.

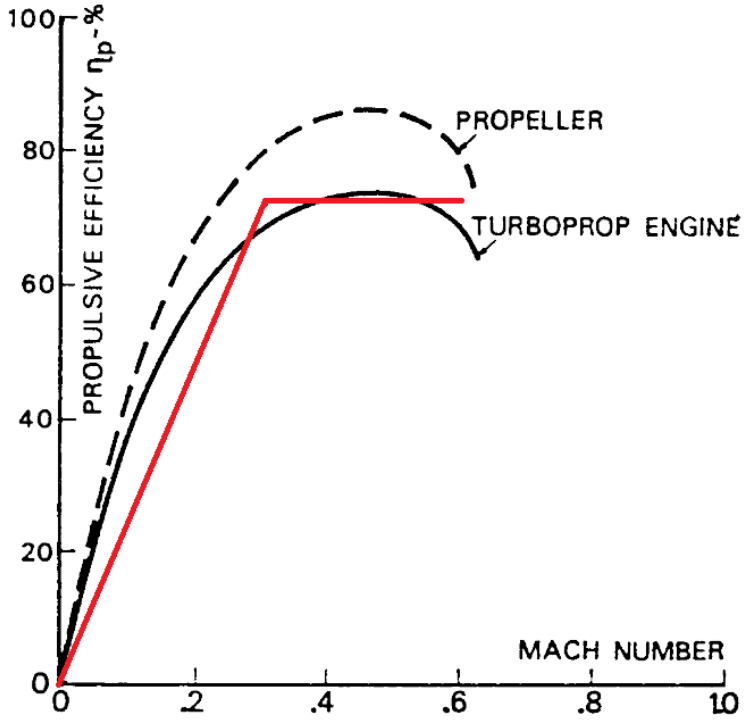

Figure 7.5: Turboprop efficiency vs airspeed [31]

With the equation above, the steady rate of climb was calculated. As can be seen, the velocity at which the aircraft must fly to achieve maximum rate of climb increases with altitude. This also means that the aircraft must accelerate when climbing. Part of the excess power is used for this and hence, the aircraft cannot use this power to climb. According to Ruijgrok [77], the rate of climb ratio can be calculated with Equation 7.7. This equation only holds in the troposphere (altitudes lower than 11 km).

$$\frac{RC}{RC_s} = \frac{1}{1 + 0.567M^2} \tag{7.7}$$

When the maximum rate of climb at every altitude is known, this can be integrated to determine the time that is needed to reach the cruise altitude. The integral is given in Equation 7.8.

$$t_{climb} = \int_0^{h_{cruise}} RC(h)dh \tag{7.8}$$

in Figure 7.6, the velocity limits of the aircraft at different altitudes is given. When the aircraft is flying on one of these lines, it is not possible to climb. The area between the lines means that a positive rate of climb can be achieved. Therefore, any point outside the lines means the aircraft is losing altitude. From this figure, the theoretical flight ceiling can be determined. It can be seen that the ceiling is at 12,500 m. It should be noted, however, that this is a theoretical value based on a simplified mode. In reality, it is probably not possible to reach this altitude.

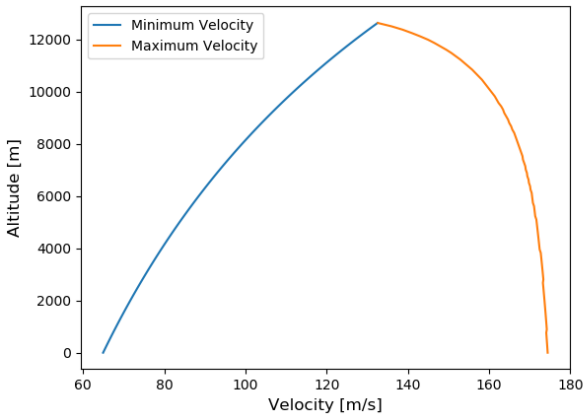

Figure 7.6: Velocity limits of the aircraft

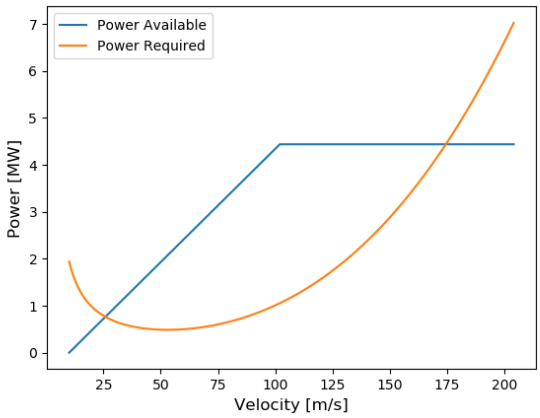

Figure 7.7: Power available vs Power required at sea level

Results

The results of both take-off and climb can be found in Table 7.2. Because of the TOFL of 1213 m, requirement AQ-PERF-08, as described in chapter 3, is met.

Table 7.2: Results of Take-Off and Climb

Parameter	Value	Unit
Take-Off Field Length	1213	m
Maximum ROC	18.611	m/s
Flight Ceiling	12,500	m

Validation

The equations used for take-off performance are validated using the ATR 72 aircraft. Available parameters of the ATR 72 were used as input for the python script and the results were compared with the data from ATR. This was done for both the take-off and climb data.

As can be seen in Table 7.3, the take-off distance from the python script is extremely close to the data given by ATR. The difference between the two numbers is 0.54%. It can be concluded that the calculation of the take-off distance is accurate and can be used for the Aquila aircraft.

Table 7.3: Validation of the take-off performance

Parameter	Simulation	Reference Data
Take-Off Distance [m]	1181	1175

In Table 7.4, the climb parameters from both the python script and ATR data are given. It can be concluded that the python script overestimates both the climb rate and the flight ceiling. The equations used in this chapter are based on ideal, theoretical climb rates. In real life, this will not be the case. This should be taken into account when using the script for the Aquila aircraft.

Table 7.4: Validation of the climb performance

Parameter	Simulation	Reference Data
Maximum ROC [ft/min]	2573	1800
Flight Ceiling [ft]	29000	25000

7.2.3. Landing Performance

The landing performance of the aircraft consists of the descend from cruise, as well as the landing procedure of the aircraft which will determine the landing field length.

Descend performance

The descend of the aircraft is the next stage in the mission profile. It starts at cruise altitude, from which the aircraft has to drop down towards the runway to make a safe landing. For this procedure it is assumed that the aircraft will descend with a constant rate of descend (ROD). This means that due to the constant change in flight level, the aircraft's airspeed as well as the pitch down angle will change slowly during descend. Typical descend rates of the ATR 72-200 vary between 1000 ft/min at high altitudes, to 1500 ft/min at lower altitudes[1]. This translated approximately to rates between 5 and 8 m/s. In this analysis it is assumed that a constant ROD is maintained during the entire descend. The airspeed and downward path angle during descend is plotted against altitude for four different ROD's, which is shown in Figure 7.8 and Figure 7.9 respectively. These plots give insight on the attitude and airspeed that the pilot needs to maintain from cruise till approach.

For each of the evaluated ROD's the elapsed time and distance during descend can be calculated. From this, an airline can choose what type of descend run is most favourable for that specific airline. A lower ROD, for instance, will be more pleasant for the passengers, but it will take longer. The elapsed time and the ground distance of the descend, for a descent from an altitude of 9000 m, are presented in Table 7.5. From this table, the different choices in descend rate are presented. However, when used in the computation of other calculations in the remaining of this report, the nominal rate of descend of 7 m/s is used.

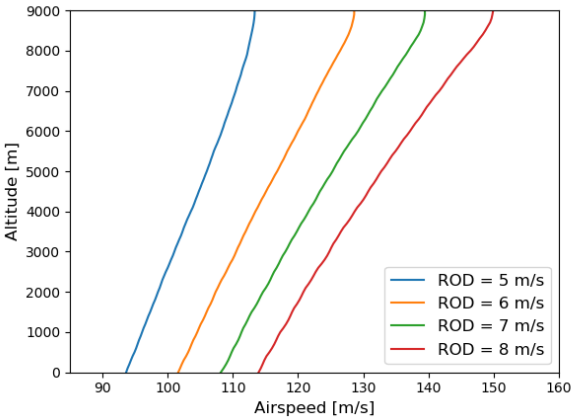

Figure 7.8: Required airspeed during descend

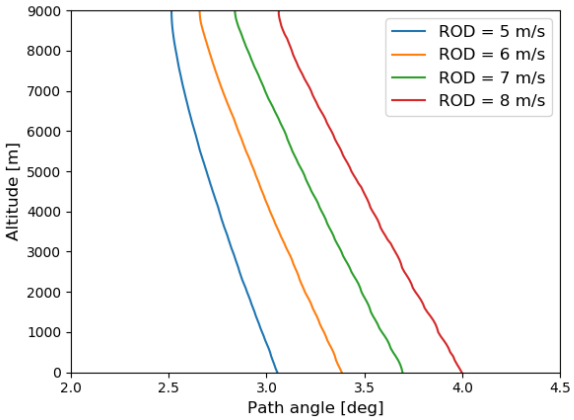

Figure 7.9: Required downward path angle during descend

Table 7.5: Duration and ground distance of descend

Rate of descend [m/s]	Duration of descend [min]	Ground distance [km]
5	30.0	187.7
6	25.0	172.7
7	21.4	158.9
8	18.8	147.4

Landing Field Length

After the descend, the approach and landing procedure of the aircraft has to be evaluated. The landing performance of the aircraft will determine the landing field length (LFL) of the aircraft. The method used in this section is described by Ruijgrok [77]. It suggests that the landing manoeuvre consists of four different

[1] Retrieved from: https://doc8643.com/aircraft/AT72 (Consulted on 14/06/2019)

sections: the approach, the flare, the ground run before braking and the ground run during braking up till standstill. This is visualised in Figure 7.10.

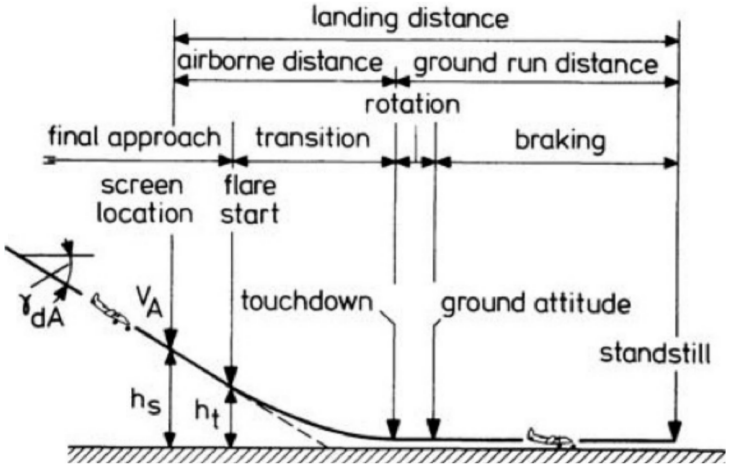

Figure 7.10: Landing manoeuvre [77]

The approach section is considered as the part of the landing manoeuvre between the screen location and the start of the flare. Airworthiness regulations state that the steady approach speed shall not be less than 1.3 times the stall speed at landing configuration. Additionally, the screen height is equal to 50 ft. The horizontal approach distance can be calculated by Equation 7.9.

$$s_{approach} = \frac{h_s - h_t}{\gamma_{dA}} \tag{7.9}$$

The flare section is the section in which the aircraft pitches up in order to level with the runway. This motion is considered circular with a certain radius of curvature R. The horizontal flare distance is described in

$$s_{flare} = R \cdot \gamma_{dA} = \frac{V_A^2}{(n_A - 1)g} \cdot \gamma_{dA} \tag{7.10}$$

The total ground run is taken as the distance from touchdown to standstill. This consists of first a section of just ground roll before braking, and subsequently a section with braking. This is due to the fact that the touchdown speed may be too high for braking without danger of skidding. The total distance can be found by evaluating Equation 7.11 step by step. However, in order to get an analytical answer of the total LFL, the equation was divided into two parts. Equation 7.12 describes the distance before braking, where $Z = (C_{Dg} - \mu C_{Lg})/(\mu C_{LT})$. In this section the friction coefficient of the wheels μ only account for the resistance of the tarmac on the wheels. The section during actual breaking is described in Equation 7.13. The subscript T stands for the condition during touch down, whereas the subscript B suggest a condition during braking. C_{Lg} and C_{Dg} represent the lift and drag coefficient on the ground.

$$s_{ground} = \int_{V_T}^{0} \frac{V dV}{a} \tag{7.11}$$

$$s_{ground,1} = \frac{V_T^2}{2g\mu Z} \cdot ln\left[\frac{1+Z}{1+Z\frac{V_B^2}{V_T^2}}\right] \tag{7.12}$$

$$s_{ground,2} = \frac{W}{C_{Dg}\rho g S} \cdot ln\left[\frac{\frac{1}{2}C_{Dg}\rho V_B^2 S}{D_{g,max}} + 1\right] \tag{7.13}$$

Results

The total landing length that now has been calculated is basically the shortest length in which the aircraft can land. This value is commonly multiplied by a factor of 10/6 as a safety factor to account for operational variances such as different pilots or uncertainties during the landing manoeuvre. The LFL at sea-level for MLW was calculated to be equal to 1082.5 meters.

Validation

For the landing field length calculations a comparison with the LFL of the ATR 72 was made. When importing the reference data of the ATR 72 as input parameters, a LFL of 1193.8 m was calculated. The actual LFL of the ATR 72 is equal to 1210 m. This means only a difference of 1.3% was found for this calculation.

7.2.4. Effect of Runway Altitude

The altitude at which the aircraft has to take-off or land has a major influence on the TOFL and LFL. This is due to the variance of air density with altitude. The change in density can be calculated with Equation 7.14. The effect on the runway length for the Aquila can be found in Figure 7.11.

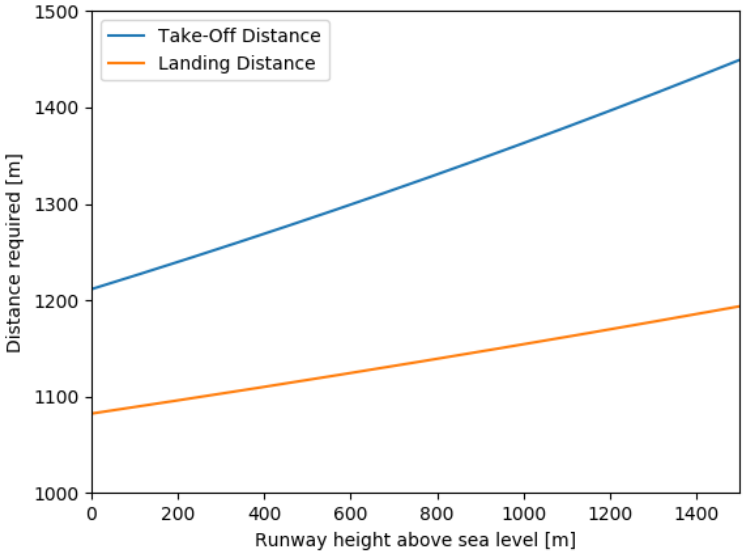

Figure 7.11: Field Length as a function of runway height

$$\frac{\rho}{\rho_0} = \left[1 + \frac{\lambda H}{T_0}\right]^{-\frac{g_0}{R\lambda}} \tag{7.14}$$

It can be seen from Figure 7.11 that both the take-off distance and landing distance increase with an increase in runway altitude. At runway altitudes higher than 1220 m, the calculated TOFL becomes more than 1400 m, which means that the TOFL requirement will not be met.

7.2.5. Cruise Performance

Most of the flight, the aircraft will be in cruise flight. This is also the phase in which the most fuel is burned. Therefore, optimising the cruise flight will result in the largest decrease on the fuel burn. In this section,the payload-range diagram, flight envelope and flight profile will be given.

Payload-Range Diagram

The payload-range diagram shows the envelope of the achievable range for every possible payload mass. The diagram is shown in Figure 7.12. The design point is indicated with a dotted line. This point is a 1850 km flight with 60 passengers. It is possible to carry more payload in terms of cargo. This, however, influences the maximum achievable range possible. When the cargo compartment is completely filled, the range of the aircraft is 1281 km. As can be seen in the figure, the ferry range of the aircraft is 4112 km. Because of the high lift-over-drag ratio of the aircraft, it is able to achieve more than double the design range when no payload is carried on-board.

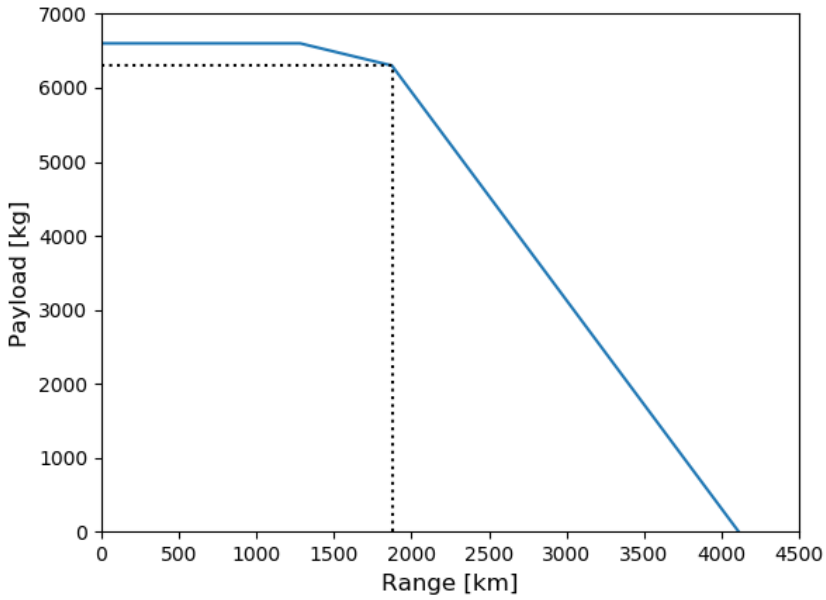

Figure 7.12: Payload-Range Diagram

Flight Envelope

The flight envelope shows the capability of the designed aircraft in terms of its flight velocities and corresponding load factors. The procedure to create this flight envelope is taken from CS-25, amendment 3 [78]. It consists of two parts; the manoeuvring envelope and the gust envelope. The manoeuvring envelope consists of the aircraft boundaries in clean configuration and flap down configuration. For the clean configuration the boundary load factors were calculated to be +3.8 and -1.5.

The gust envelope consists of several lines which depict the influence on the load factor of sudden changes in airspeed due to gusts. The reference gusts that were used to calculated the load factors were set at 50 ft/s at cruise speed and 25 ft/s at diving speed [78]. The full flight envelope is portrayed in Figure 7.13.

When the manoeuvring envelope and the gust envelope are combined, and also the absolute stall limit is implemented, the service flight envelope is created. The service envelope for the flight profile is shown in Figure 7.14. The full line basically shows the total limits in which the aircraft can operate. Outside these limits, hazards such as stall and structural failure are more likely to occur.

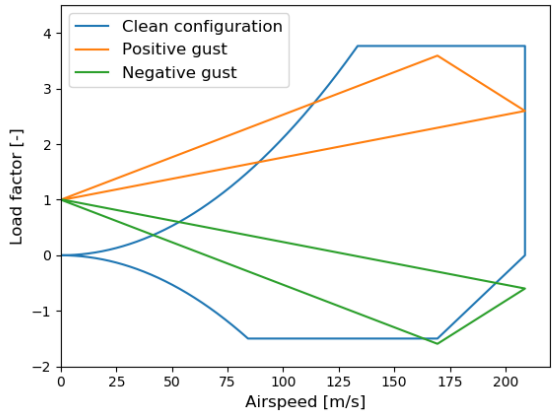

Figure 7.13: Total flight envelope including both manoeuvring loads and gust loads

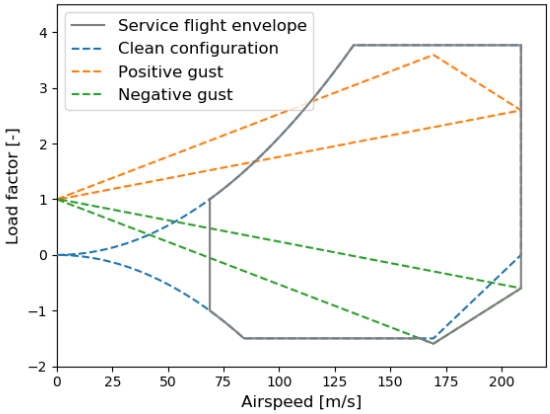

Figure 7.14: Service flight envelope

Flight Profile

The flight profile shows the corresponding ground distance for each phase of the flight. The total distance needed should be equal to the design range of the aircraft. The climb and descend rate given in previous sections result in a horizontal distance needed for both climb and descend. The remaining part of the range will be in cruise.

As can be seen in Figure 7.15, the cruise altitude does not remain constant. As the aircraft becomes lighter, the optimal altitude will increase. This will happen gradually during cruise. Because of the crowded airspace, this happens in steps and not gradually. In the figure, one step in altitude is given, as this is usual for this range.

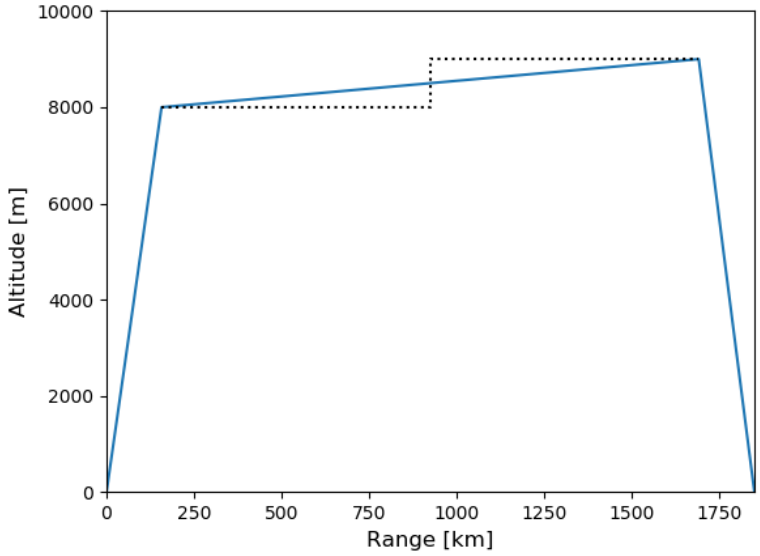

Figure 7.15: Flight Profile

7.2.6. Noise

One of the requirements of Aquila is to comply with the noise regulations that are set by the ICAO. The goal is to not only meet these requirements, but to improve on them, thereby beating the competition. In this section an estimation and explanation of the noise calculations has been provided as well as recommendations to further improve the design.

Regulations

Noise requirements are regulated by the ICAO and stipulated in CS-36. These noise requirements are given in EPNdB, which stands for Effective Perceived Noise in decibels. This takes into account that not all sounds are registered the same way by the human ear and is the standard for noise measurements. The regulations that are currently in use by the ICAO and that apply for Aquila are:

- A maximum noise of 94 EPNdB during lateral at 450 m.
- A maximum noise of 89 EPNdB during fly-over at 1022 m.
- A maximum noise of 98 EPNdB during approach at 120.5 m.

The height for the fly-over was determined by calculating the altitude the aircraft would have after flying for 6 km. In order to better visualise the way these requirements are implemented a graphic representation has been provided in Figure 7.16.

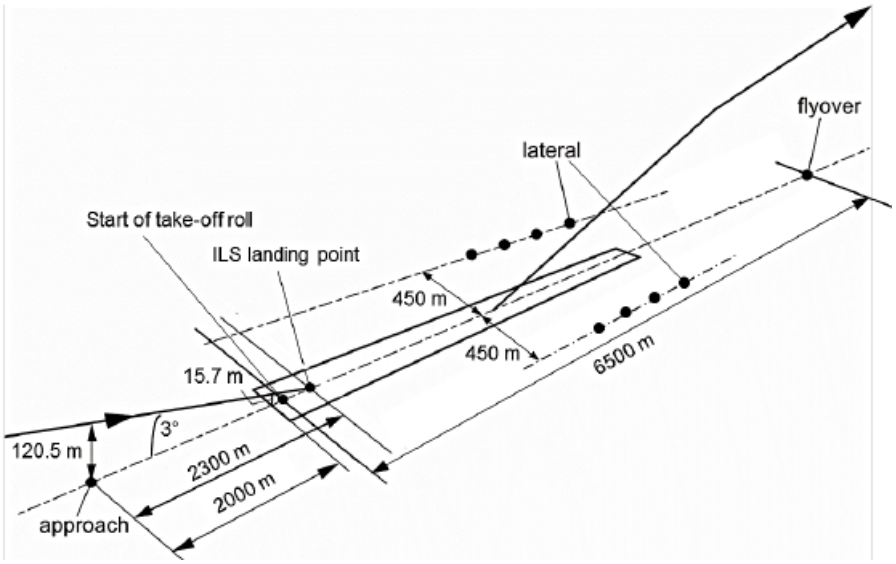

Figure 7.16: Positions of noise measurements.[79]

Estimation Method

To estimate the noise that the aircraft generates during operations one has to divide the aircraft into multiple pats that generate sound. Broadly spoken this can be divided into two main components that generate the majority of noise: Airframe and Engine. The noise estimation calculations were performed using Excel.

Airframe

For the airframe the ANOPP method was used, developed by NASA [3], which provides an empirical method for calculating the sound pressure level (SPL) of the several components that together make up the airframe. The SPL of every component can be calculated with Equation 7.15, where p_e is the pressure generated by the component and p_{ref} is the hearing threshold of the human ear, set at $2 * 10^{-5}$ Pa.

$$SPL = 10 \log \frac{p_e^2}{p_{e_{ref}}^2} \tag{7.15}$$

The pressure generated by the component can be described by Equation 7.16, where p_∞ is the air density, c is the speed of sound, P is the power generated by the component, D is the directivity function, F is the spectral function, r is the distance between the observer and the component, M is the Mach number and θ is the polar directivity angle.

$$p_e^2(f,\theta,\phi) = \frac{\rho_\infty c P D(\theta,\phi) F(S)}{4\pi r^2 (1 - M\cos\theta)^4} \tag{7.16}$$

The power function as shown in Equation 7.17 describes the power of each component. K is an empirical constant and a is a power coefficient. G is describes the effect of the geometry of the aircraft component and b_w is the span of the wing.

$$P_i = K\left(M_\infty\right)^a G \rho_\infty c_\infty^3 b_w^2 \tag{7.17}$$

The spectral function F uses the Strouhal number which has been determined for every component and can be found in Equation 7.18. f is the frequency at which one is evaluating the sounds and L is the characteristic dimension of the component noise source.

$$S = \left(1 - M_\infty \cos\theta\right) \frac{fL}{M_\infty c_\infty} \tag{7.18}$$

To determine the total airframe noise one has to calculate the SPL of every component and sum these up. This has been done for frequencies ranging from 10 Hz to 10000 Hz.

$$SPL_{\text{total}} = 10\log \sum_{i=1}^{N} 10^{SPL_i/10} \tag{7.19}$$

Engine

Engine noise is mainly created by the propeller of the aircraft. To estimate this a method for noise estimation from JPL and NASA [2]. This method uses the shaft power of the engine to get an initial estimate for the noise of the engine and uses empirical relations to correct for several factors. The steps to estimate the far field noise are given below:

1. Obtain the reference level L_1 from Fig B-2.
2. Calculate the correction factors for diameter and number of blades of the propeller.
3. Obtain the correction factor for the tip speed of the propeller.
4. Obtain the correction factor from Fig B-8, this accounts for directional characteristics of the propeller. For these calculations they were assumed to be maximum.
5. Correct for distance to the propeller.
6. Sum the factors from step 1 to 5.
7. Determine the harmonic distribution of the noise.
8. Combine the harmonic levels using the chart in Fig B-7 to derive the octave band levels.
9. Correct for molecular absorption using Fig B-9.

In order to calculate the EPNdB it is important to correct for the 'perceived' loudness. This is for the fact that higher frequencies are deemed 'louder' and lower frequencies as 'softer', therefore they require an additional correction, which is specified in Equation 7.20 and Equation 7.21

$$R_A = \frac{12194^2 \cdot f^4}{\left(f^2 + 20.6^2\right)\sqrt{\left(f^2 + 107.7^2\right)\left(f^2 + 737.9^2\right)}\left(f^2 + 12194^2\right)} \tag{7.20}$$

$$A = 20\log\left(R_A\right) + 2.00 \tag{7.21}$$

7.2.7. Cabin Noise

According to AQ-OPS-02 the average noise in the cabin during cruise should be less than 78 dB. After doing research it was decided that it would be outside the scope of this project to accurately model the noise in a cabin during cruise. It is therefore recommended to start doing research and build a full scale model to determine the cabin noise. Given the fact that the Aquila overall produces less noise than the ATR 72 and has a engine with a lower power output, thus it is likely that the cabin noise on the Aquila is lower than on an ATR 72.

Results

In order to estimate the total noise of the aircraft the engine noise was added to the airframe noise for every frequency using Equation 7.19. The results for the various settings have been provided in Figure 7.17, Figure 7.18 and Figure 7.19

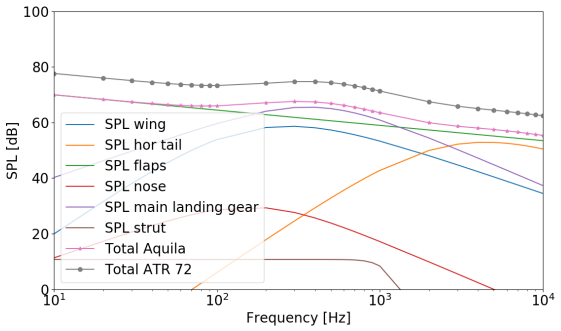

Figure 7.17: Approach noise from Aquila and ATR 72.[79]

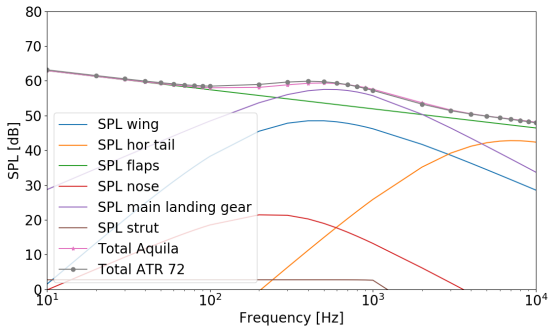

Figure 7.18: Fly-over noise from Aquila and ATR 72.[79]

It can be seen that during approach the flaps are the main contributor to noise, followed by the main landing gear. The large difference between the ATR 72 and the Aquila can best be explained by the difference in approach speeds, which is lower for the Aquila. The difference between the ATR 72 and the Aquila are smaller during fly-over.

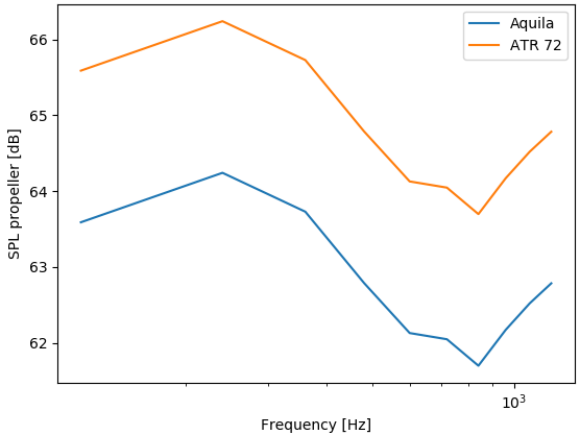

Figure 7.19: Lateral (propeller) noise from Aquila and ATR 72.[79]

The propeller of the Aquila produces less noise than the ATR 72, which is mainly attributed to the lower power output of the GE T6E engine of the Aquila.

To estimate the noise that is heard from all the frequencies simultaneously they should be added by using Equation 7.15. This resulted in Table 7.6, which shows the maximum noise for each of the three situations.

Table 7.6: Maximum noise of the Aquila and the ATR 72

Situation	Aquila	ATR 72	Limit
Lateral [EPNdB]	71.1	73.1	94
Approach [EPNdB]	85.8	89.1	98
Fly-over [EPNdB]	72.9	73.5	89

It can be seen that the Aquila outperforms the ATR 72 in all categories, especially during approach, which is the noisiest situation. This reduction in noise can primarily be attributed to the lower approach speed and the smaller wing area.

Verification and Validation

The methods that were used to determine the noise during several setups are empirical methods and as such are only an approximation of what the noise would be. Verification and validation were therefore performed to ensure that the results are consistent and meaningful.

Verification of the noise estimation was done by changing input values and see if the solution of the estimation was consistent and stable. This was done and the results converged and were thus deemed verified.

From EASA the certification noise levels of several aircraft were found, including the ATR 72 [80]. Since the dimensions and input data of the ATR 72 are known and its certification noise levels as well a comparison can be made between the estimated noise levels and its actual values. This can be found in Table 7.7

Table 7.7: Validation of the noise estimation model.

Situation	**ATR 72 (calculated)**	**ATR 72 (from data)**
Lateral [EPNdB]	73.1	82.2
Approach [EPNdB]	89.1	92.2
Fly-over [EPNdB]	73.5	79.0

It can be seen that for all situations the model estimates the noise to be lower than the actual tested values. At this point it cannot be determined if this would also be the case for the Aquila. It is recommended to do a further analysis by using a more extensive method such as described Antonio Fillipone in research done at the University of Manchester [81]

7.2.8. Emissions

The emission of greenhouse gases is one of the main causes for climate change and as such it was the goal for Aquila to reduce the environmental impact as much as possible. To estimate the impact in terms of greenhouse gas emissions one first needs to take a look at the fuel that the aircraft is using. An overview of the emissions for the two types of fuel that were considered has been provided below.

The fuel use of Aquila and the ATR 72 have been analysed for a flight of 1000 km, both with 60 passengers. This means that the ATR is not flying at full capacity. It is assumed that they loiter for 15 minutes before they are able to land. The results can be found below in Table 7.8. It is concluded that the requirements regarding emissions are met.

Table 7.8: Emissions of CO_2 and NO_x for kerosene and LNG [2, 3]

Parameter	**Aquila (LNG)**	**ATR 72 (Kerosene)**
CO_2 (kg/kg fuel)	2.75	3.00
NO_x (kg/kg fuel)	0.001	0.003
Fuel used (kg/1000 km flight)	1494.1	2159.0
CO_2 (kg/1000 km flight)	4108.7	6477.0
NO_x (kg/1000 km flight)	1.5	6.5
CO_2 (kg/pax/1000 km flight)	68.5	83.0
NO_x (kg/pax/ 1000 km flight)	0.025	0.108

It can be seen LNG offers some benefits over kerosene in terms of CO_2 and a large improvement in terms of NO_x emission reduction. It must be stated that the emissions for LNG are even better compared to kerosene when one factors in that LNG has 25% more energy per kg than kerosene.

There are also other greenhouse gases and emissions that are preferably avoided. A group of these is sulphur-oxides (SO_x, of which SO_2 is the most common. This gas is one of the causes of acid rain and can cause discomfort for people if the concentration becomes too high. These emissions are caused by

[2] Retrieved from: https://www.engineeringtoolbox.com/co2-emission-fuels-d_1085.html (Consulted on 21/06/2019)
[3] Retrieved from: https://www.engineeringtoolbox.com/nox-emission-combustion-fuels-d_1086.html (Consulted on 21/06/2019)

small contents of sulphur present in kerosene. This sulphur content has been decreasing over the years, thereby reducing the emission of these sulphur-oxides, falling below 0.01% by weight in 2007 [4]. The sulphur content in LNG is significantly lower, being below 5 ppm [5]. Using LNG as fuel should thus also decrease the emission of sulphur-oxides significantly.

7.3. Sensitivity Analysis

To check how sensitive the design is to changes in parameters, a sensitivity analysis was performed. It was investigated what impact changing one of the requirements would have on the design. Also, it was checked how sensitive the design is when the mass of a system is estimated incorrectly and changes in a later stage.

In the sensitivity analysis, three parameters were varied. The first parameter is the number of passengers, followed by the design range of the aircraft. These two parameters are both dependent on the client's requirements. Lastly, the weight of the fuselage was analysed for sensitivity. This parameter is varied for the sake of estimation errors in the preliminary design phase. The outputs that are investigated for all three parameters are the total block fuel burned on a 1000 km trip, the OEM, and the TOFL. These parameters were deemed most important, taking the driving client requirements into account.

7.3.1. Change in Requirements

For the number of passengers, Figure 7.20 shows that the OEM is the least sensitive output. The boundaries of this sensitivity analysis are such that they correspond with the capacity of the ATR 42 and the ATR 72. An increase in the number of passengers to 70 (equivalent of an ATR 72) would increase the TOFL by almost 20%. Because of the less powerful, more efficient engines on the aircraft, the TOFL would become even larger than the TOFL of the ATR. Though, an increase in the amount of passengers would result in the design still outperforming the ATR 72 in terms on sustainability. Decreasing the number of passengers would allow the aircraft to be operable at even smaller airports. Although, inevitably the fuel efficiency would go down in terms of fuel burned per passenger.

Figure 7.21 shows that the sensitivity of the output when varying the range is minimal. The most sensitive output is the TOFL, which still only is increased by 4%, or 50 meters. The OEM and fuel burned per passenger show almost no variation by a change in the design range. From this analysis, it can be concluded that adapting the design range would require a minimal amount of redesigning, based on the varied inputs.

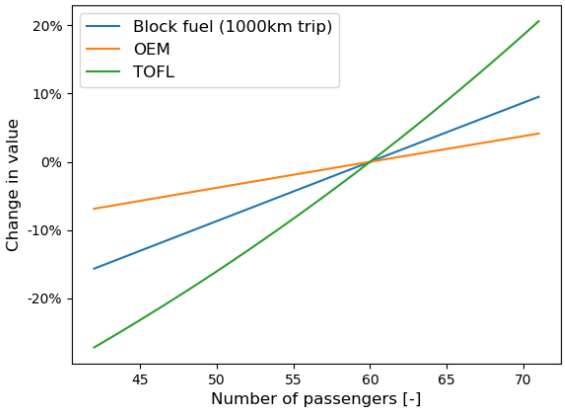

Figure 7.20: Sensitivity analysis of the number of passengers

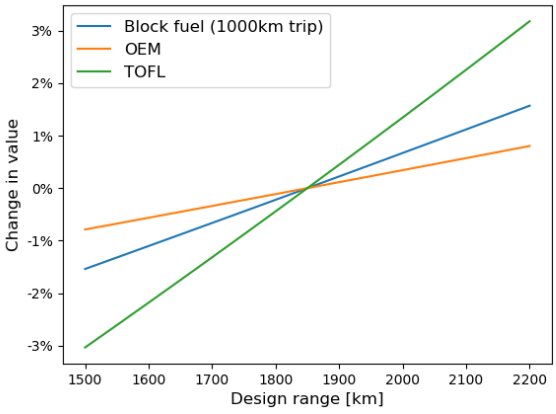

Figure 7.21: Sensitivity analysis of the design range

[4] Retrieved from: http://www.ec.gc.ca/doc/energie-energy/1088/sul/sul-eng.htm#fig4-12 (Consulted on 19/06/2019)
[5] Retrieved from: https://aai.solutions/applications/lng-liquefied-natural-gas-analysis (Consulted on 19/06/2019)

7.3.2. Estimation Errors

One of the main components of the OEW is the fuselage. In this phase of the design process, the detailed mass estimation of the fuselage has not been carried out yet. Even though an extensive class II estimation was made to predict the mass of this system, it is very likely that the mass will either increase or decrease. To avoid any surprises later on, a sensitivity analysis of the fuselage mass was made. As can be seen in Figure 7.22, the biggest impact on an increase in fuselage weight is in the TOFL needed. A 5% increase in fuselage weight already results in more than 2% increase of the TOFL.

The other main component of the aircraft frame is the wing. Though a more extensive structural analysis was performed on this component, it is still possible that the weight changes. For example, when a new high-level material is discovered in the future. In this case, it can be investigated what the influence of a lighter or heavier structure of the wing is on the entire aircraft. It is visible in Figure 7.23 that the design is much less sensible to a change in wing weight than to a change in fuselage weight.

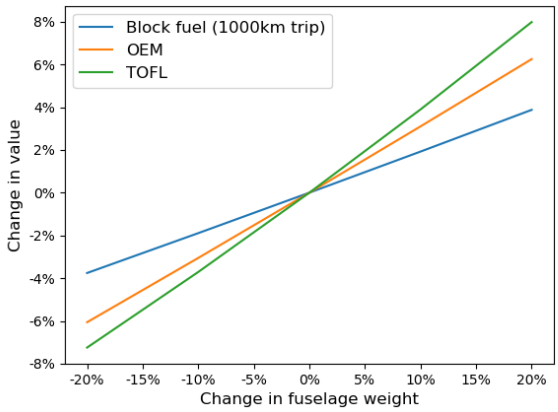

Figure 7.22: Sensitivity analysis of the fuselage weight

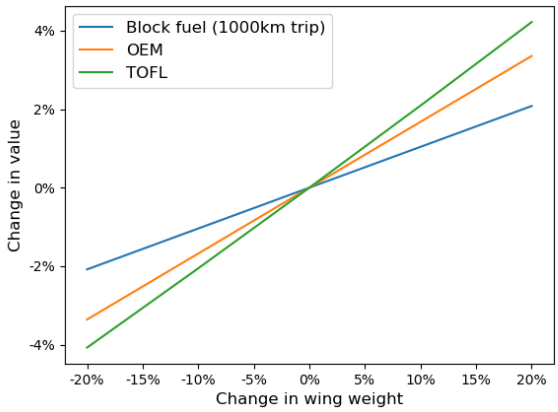

Figure 7.23: Sensitivity analysis of the wing weight

7.4. RAMS Analysis

In this section, an analysis of the reliability, availability, maintainability and safety of the Aquila will be performed. These parameters all characterise the final design and are important tools to analyse the overall performance of the product.

7.4.1. Reliability

Reliability is a crucial factor of the design, as failure can be very catastrophic. The reliability of the aircraft depends on the reliability of its subsystems and their individual parts. It will influence the type of maintenance and the time interval between two consecutive checks.

The biggest challenge for Aquila in terms of reliability results from the fact that for several systems there exists few to none technical experience at this point. These systems are mainly the fuel system and the high AR wing including the strut. In order to check the reliability of these systems, exhaustive testing and simulation must be performed, as described in section 12.3.

For the remaining (sub)systems, data from already operating aircraft can be used to analyse the reliability of the design.

7.4.2. Availability

Monitoring the aircraft's flight performance is key when increasing the availability of the aircraft. Aquila is equipped with an electronic flight bag (EFB). This EFB system will monitor and transmit both in-flight and ground data measured by several sensors. The data can be analysed in order to plan maintenance as efficient as possible, reducing the out-of-service time of the aircraft and thus increasing the availability.

Aquila is designed to be in-service for at least 300 days a year. The block time on a 1000 km mission will be 2.17 hours. So for these trips the aircraft will fly up to 5 times a day. This results in a total amount of 1500 flight cycles a year. If the airline chooses to operate the aircraft over shorter distances, the amount of daily flight cycles will increase accordingly.

7.4.3. Maintainability

Maintainability is defined as "the ability to undergo modifications and repairs" [82]. In order to make these processes as efficient as possible, the maintainability aspect was kept in mind during the design face of Aquila.

Maintenance Documentation

In order to provide sufficient information to the airline regarding to the maintenance of Aquila, some documents will be provided by the manufacturer:

- The **Airline Maintenance Manual** is the document covering all of the information with regards to operation and maintenance of the aircraft. It explains the functions of all of the (sub)systems together with the maintenance and service actions the operator must conduct.
- The **Illustrated Parts Catalogue** is a list of all the parts of the Aquila equipment. The parts are numbered and accompanied by diagrams.
- The **Maintenance Planning Document** provides an extensive list of maintenance and service actions depending on the aircraft age.
- The **Master Minimum Equipment List** sets the degradation limit of Aquila's systems. This is used as a guideline for the flight crew.

Types of Maintenance

Maintenance can occur in two different cases: scheduled maintenance and unscheduled maintenance resulting from a check or in-flight error. The goal of the design team was to minimise the occurrence of unscheduled maintenance, as they will result in additional costs and delays.

There exist different types of maintenance. The main three are explained below:

- **Line maintenance**: performed at the airport (tarmac) on in-service flights. **Transit checks** are visual checks performed by the flight crew and ground crew. **48-hr checks** are performed by maintenance crew for around 12 hours per aircraft per week. Here, the landing gear, brakes, APU and emergency systems are tested.
- **Hangar maintenance**: scheduled maintenance performed on an out-of-service aircraft. There exist three types of hangar maintenance, A, C and D checks[6]. **A checks** happen every 8 to 10 weeks and take between 6 and 24 hours to complete. The filters will be changed and the control surfaces are lubricated. **C checks** are planned every 18 months to 2 years, and will take around 3 weeks to complete. They are further subdivided in 4 types (C1, C2, C3, C4) with increasing level of maintenance. During these C checks, inspection for corrosion, structural defects and cables are performed. The last type of hangar maintenance are the **D checks**. These will be performed every 10 years. The aircraft will be stripped from its interior and engines. The material conditions will be thoroughly checked, and reparations will be performed. The D checks will take 3 to 6 weeks each.
- **Shop maintenance**: These are performed in repair shops. The focus lies on the repair of equipment removed from the aircraft during hangar maintenance.

Spare parts

Aquila consists of many parts, each with their specific functions. To ensure the availability of the aircraft, these parts must be present in case of maintenance. The type of maintenance depends from part to part. The different types are listed below.

[6] Retrieved from http://newsinflight.com/2018/11/03/types-of-aircraft-maintenance/ (consulted on 17/06/2019).

- **Rotable** components can be economically restored in an overhaul shop. Their life is equal to the aircraft/ engine life. The main rotable parts on Aquila are the flaps, control surfaces, fuel pumps, hydraulic pumps, transmission and other expensive components.
- **Repairable** components can be economically repaired limited amount of times over their life. Their life is shorter than the life of the aircraft.
- **Recoverables** are components that are being refurbished one or more times. Their life is longer than the aircraft life. These are for example batteries or avionic computers.
- **Expendables** are spares of which the cost of repair is higher than the unit cost. They are not authorised for repair and are replaced at the end of their life. Some examples of expendable parts in Aquila are fire extinguishers, switches, ashtrays and temperature sensors.

7.4.4. Safety

Aquila consist of many systems, ensuring the safety of the passengers and crew, as well as the environment. In section 6.2, the emergency procedures are explained. In order to facilitate these procedures, some emergency systems were implemented in the Aquila design.

Warning System

The goal of the Aquila emergency warning system is to instantly signal the flight crew in case of any malfunction. This is achieved by a warning sequence consisting of the following steps.

1. A malfunction is detected by a sensor and/or control unit
2. A warning system is sent to the central warning panel
3. Visual and sound signals are triggered to inform the flight crew about the malfunction
4. Flight crew silence the warning and read the caption on the warning panel
5. Flight crew performs the necessary corrective action

Emergency Oxygen

In case of cabin pressure loss, the flight crew will conduct a steep descent in order to regain pressure in the cabin. The pilots will fit masks linked to a pressurised oxygen bottle. In the cabin, oxygen masks will be deployed from the rack above the seats. The cabin crew will inform the passengers about this procedure in the beginning of every flight.

Flight Recorder

During the flight, the critical flight parameters and cockpit audio are recorded by the flight recording system beneath the cockpit. After a crash, the recorder gets ejected from the aircraft and will broadcast an emergency signal. The data from the recorder will enable a detailed crash investigation and will provide useful data in order to prevent similar events in the future.

Emergency Exits

The EASA CS 25.807 regulations state that an aircraft for 60 passengers must contain at least one *Type I* and one *Type III* emergency exit on each side of the fuselage[7]. The Type I exits shall be converted into life-rafts in case of an emergency landing on water, and have a capacity of 32 people each. In the Aquila design, the Type I exits are situated on the left front and the right back of the aircraft. The Type III exits are situated right behind the wing. The location of these exits will be presented to the passengers by the cabin crew in the beginning of the flight.

[7] Retrieved from https://www.easa.europa.eu/sites/default/files/dfu/CS-25%20Amdt%2012.pdf (Consulted on 07/06/2019).

8

Production Plan

The production of Aquila is of key importance to the client. It is required that 5 Aquila aircraft will be produced each month, with an option to increase the production rate to 10 aircraft a month. This chapter starts by highlighting the general production considerations in section 8.1 and gives an overview of the part manufacturing in subsection 8.2.1. Then the assembly process of the aircraft is discussed in subsection 8.2.3 after which the strategy on how the sustainability of the production process can be increased is explained in section 8.3. To end the chapter, the possibility to increase the production rate is discussed in section 8.4..

8.1. General Production Considerations

Due to the fact that this project requires a large investment in advance, production can be distributed along different manufacturers. On the one hand this allows for the spread of the risk of the project and the outsourcing of components or subassemblies to other skilled parties in the industry [83], on the other hand this increases project complexity and requires more transport. Instead of outsourcing the manufacturing of components, the components can be made in-house. This decreases the dependency on other manufacturers and tends to reduce the purchases of material inputs while maintaining sales and final outputs [84]. However, this requires expertise on more aspects of the manufacturing process which could increase costs. Therefore, a combination of outsourcing and in-house manufacturing will be used when the aircraft goes in production.

Production of an aircraft can be organised in several different structures. Other manufacturers have shown that an assembly line is the best method in terms of efficiency. With this method, the assembly is divided into stations for subsystems, which are subdivided into work packages. Every station has a team working on a specific work package, while every station is led by a foreman, who is responsible for the various teams that are working at different work packages at that system. By using the same workers for a station, the crew's experience speeds up the production process and increase efficiency in terms of time and revenue.

The final lay-out and work distribution of the stations will be determined in later stage of the Aquila project. However, next to the nominal production operations, designers should take additional adverse factors into account. Such as work stoppages, absenteeism and managerial span of control.

A work stoppage is defined as any event that temporarily stops or significantly slows down the operation of a station, which naturally spreads to downstream stations. Work stoppages can occur for various reasons, for instance: worker injury, machine failure, tool breakage, shortage of parts or fasteners, mending a defect, preventive maintenance, temporary absence of a worker and external events [85].

Absenteeism reduces quality and throughput of the production, since the replacing worker is usually not as proficient as the absent worker. Absenteeism can be reduced by offering attendance bonuses, sending warning letters or requiring counselling for habitual absentees. The effects of absenteeism can be reduced by continuously educating standby workers for several tasks during production [86].

The foreman gives managerial and relief service to all engineers of the station, since management and supervision is necessary at every assembly line. The more workers are under supervision of the foreman, the less the assembly station is resistant to adverse effects. The foreman's span of control is also affected by absenteeism, since substitute workers need more help, which overloads the foreman more frequently [85].

8.2. Top Level Production Plan

The production process can roughly be divided in three phases, namely the general assembly phase, propulsion assembly phase and product completion phase. A flow diagram of the production process can be found in Figure 8.1. Each block represents a process which takes 4 days of work, except for the installation of the AP and the installation of the fuel systems in the fuselage, which both take 2 days of work. Setting the station time to 4 days allows a production rate of 5 aircraft per month, including weekend days off. In the flow diagram, the first block representing the part manufacturing is not included in one of the three phases. This was done on purpose, since the part manufacturing process is a parallel process. In this section the part manufacturing and the assembly phases are discussed in further detail.

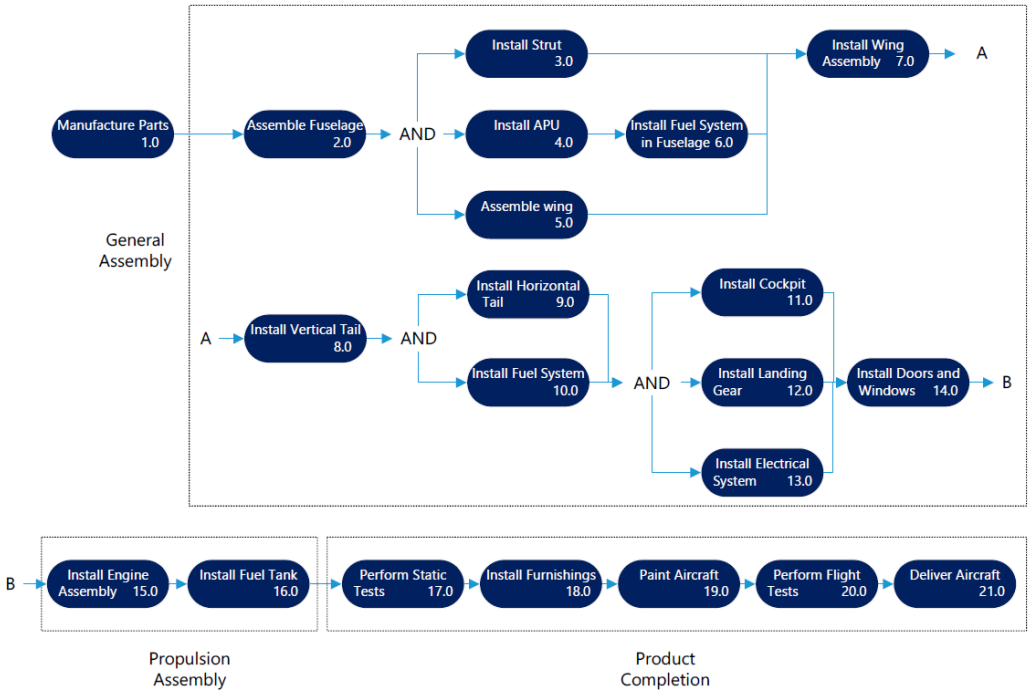

Figure 8.1: Top level of the production flow diagram.

8.2.1. Manufacturing of Components

The manufacturing of components is the first step of production after the acquisition of materials. Some subsystems require special materials or employ special manufacturing techniques, which are explained here.

Additive manufacturing will be used to decrease weight and costs for components that are used in small quantities on the aircraft. This will primarily be done on metal components, such as the landing gear. The type of additive manufacturing that will be primarily used is powder bed infusion as it allows for a high quality. It does, however, come at a higher cost than other manufacturing methods [87].

The strut will be made out of carbon composites and is one of the low-series production parts of the aircraft. The production method to produce the struts will be resin transfer moulding or RTM for short, as only two struts are needed for the aircraft. This method is well suited for small production series since it provides a high quality of parts [88].

The fuel tanks are made of two shells, the inner shell is made out of aluminium and will be formed out of three parts that are welded together. The outer shell is made out of aramid composite and will be made out of two halves that are formed using RTM or Vacuum Infusion depending on the available equipment, RTM is preferred. Special tools are required for the handling of Aramid composites, since the fibres are hard to work with.

A majority of the parts of the aircraft are made out of metal, these parts are made with the use of various

manufacturing processes, such as pressing, milling and forming. Care must be given with the aluminium lithium alloys, since they are harder to process. To join larger structures made out of the material friction stir welding is the preferred method. The primary structure which will use this method is the fuselage.

8.2.2. Transport of Components and Subassemblies

As will be made clear in the next section, final assembly will be done at one facility. Supposing that the manufacturer divides the production among different subcontractors, subassemblies can be made externally. The dimensions of the produced components and subassemblies should allow for simple transport. Assuming that a component will never exceed the maximum dimension of a subassmbly, only the transport of subassemblies is highlighted in this report. The following subassemblies are able to be transported by container[1] [12 x 2.6 x 2.3][2]:

- Strut [7.3 x 0.1 x 0.6]
- Wing Fairing [4.5 x 0.8 x 2.1]
- Horizontal tail [7.4 x 2.5 x 0.4]
- Center wingbox [2.5 x 0.4 x 2.3]
- Flaps [3.2 x 0.8 x 0.2]
- Ailerons [2.4 x 0.4 x 0.1]
- Engine [2.2 x 0.9 x 0.7]
- Propeller blade [1.8 x 0.2 x 0.2]
- Fuel tank [5.3 x 1.0 x 1.0]
- Landing gear [1.0 x 0.6 x 0.7]
- Windows & doors [-]
- Furnishings [-]

Intuitively, not all subassemblies fit in a container. The length of the total wing does not even allow for exceptional road transport in the Netherlands, therefore, the wing is assembled at the same location as the final assembly. Subassemblies that are allowed for continuous exceptional road transport are[3] [27.5 x 4.25 x 3.5] m:

- Front fuselage [7.8 x 2.8 x 2.8]
- Center fuselage [8.4 x 3.2 x 3.2]
- Aft fuselage [5.3 x 2.8 x 2.8]
- Right wing [15.1 x 0.4 x 2.3]
- Left wing [15.1 x 0.4 x 2.3]
- Vertical tail [7.2 x 4.0 x 0.5]

Mass of the subassemblies are not an issue for road transport, since the maximum mass for a container is 28 tons and for exceptional road transport 100 tons. In comparison the MTOM of Aquila is approximately 18.5 tons.

8.2.3. General Assembly

To support the description of the general assembly, the general assembly is illustrated in figure 8.2.

The general assembly starts with the assembly of the different parts of the fuselage. Once the fuselage is assembled, the strut will be installed to the bottom part of the fuselage.

At the wing assembly station, the wing will be brought in from a separate wing assembly line, which is located perpendicular to the general assembly line. This enables the wing to be installed in one simple operation. Without complex turning operations of the long wing. After the installation of the wing the fuel systems in the fuselage can be done and the vertical stabiliser can be installed.

[1] Retrieved from RDW at https://www.maersk.com/-/media/ml/special-cargo-container-specifications-18.pdf?la=en, consulted at 17-06-2019

[2] The dimensions are given in meters [length x heigth x width], rounded up one decimal and do not account protective cases required for transport

[3] Retrieved from RDW at https://www.rdw.nl/-/media/rdw/rdw/pdf/sitecollectiondocuments/ontheffingen-tet/themasite-ontheffingen/handleidingen/2-b-1097b-overzicht-maten-en-gewichten.pdf, consulted at 17-06-2019

Once the vertical stabiliser has been installed, all the control surfaces can be joined by completing the electrical system. This is accompanied by the installation of the cockpit and installation of the landing gear. When the cockpit has been installed, engineers are able to perform software tests on the aircraft and subsystems. The last station of the general assembly will install all the windows, emergency doors and doors. This finalises the general assembly and the aircraft can be transported on its own wheels to the engine installation hangar.

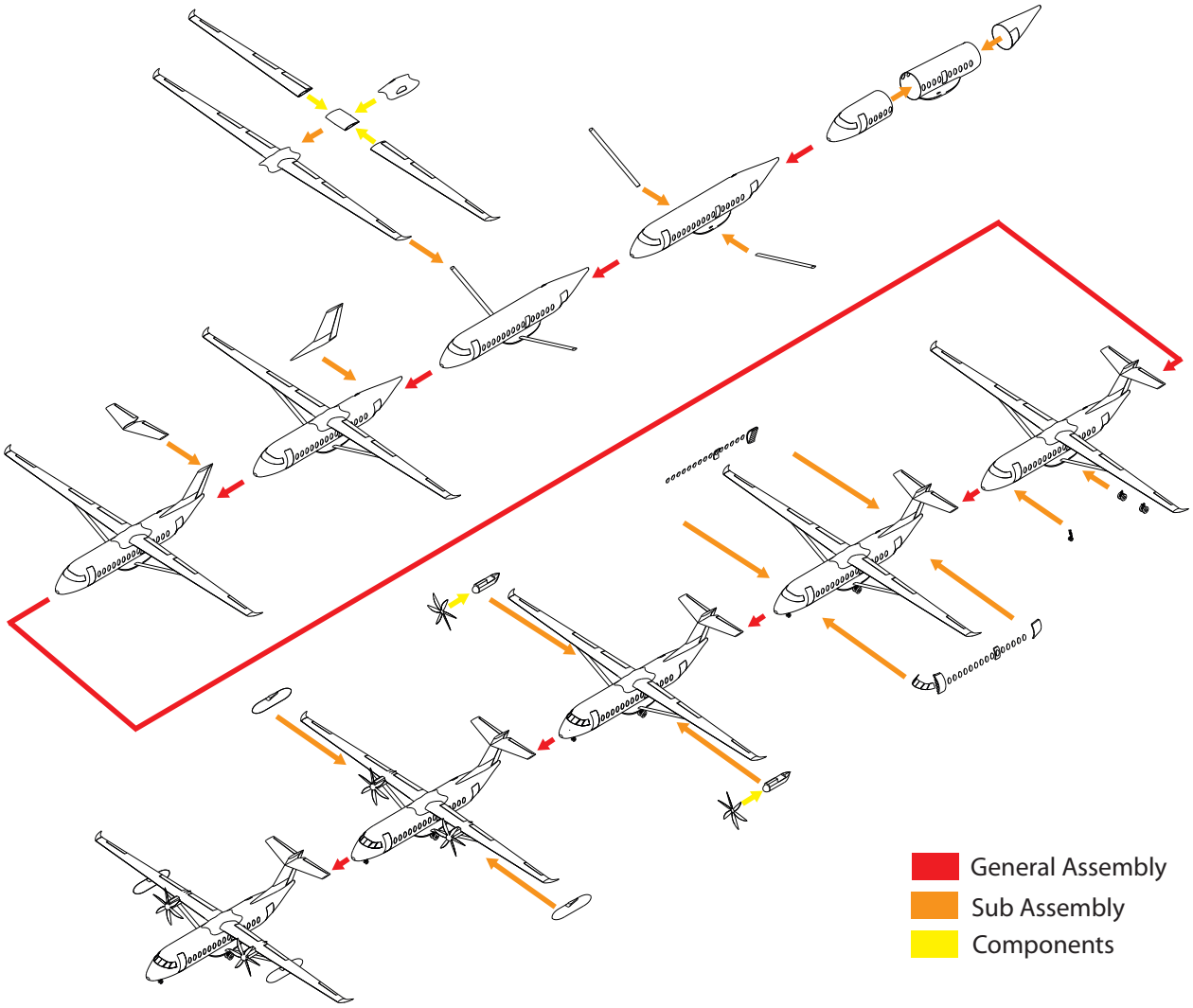

Figure 8.2: Overview of the main assembly line

8.2.4. Wing Assembly

Before the wing can be installed onto the fuselage, the wing subassembly has to be made. The wing subassembly consists of the wing box, the leading and trailing edge, high lift device, ailerons and other systems, like the pneumatic system, the actuator system, the electrical system and the fuel system. These will be built on site or at other facilities. Once all the parts have arrived at the final assembly location, the wing subassembly can be assembled at the wing assembly line. The embedded systems will be installed when the wing is assembled. Since this is complex and time-consuming, four wings (two right and two left) will be assembled in parallel, as the small slender wing does not allow multiple engineers to work simultaneously in a limited space. This ensures that the wing assembly is not a limiting factor for the main assembly in terms of throughput. Once a left and right wing are assembled, they are joined together and the fairing is installed. When both the fuselage and wing are in place, the wing can be installed.

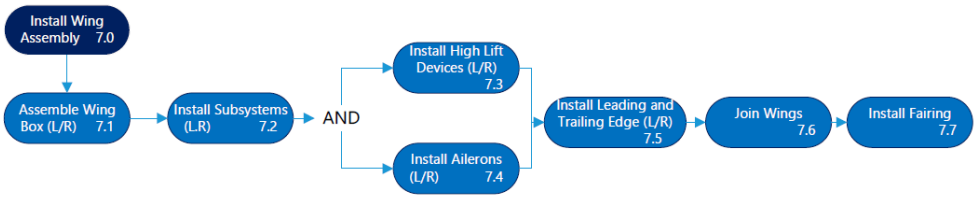

Figure 8.3: Detailed flow diagram of the wing installation process.

8.2.5. Propulsion installation

Since the propulsion group is the most valuable element in terms of cost of the aircraft, this is done at the final stage of the production of the aircraft. The propulsion group will be installed in a different hangar, which is specialised for propulsion installation only and allows the option for the client to install different engines, during a later stage of the project. This also allows for different versions of the aircraft to be developed. A version with an extended cabin for example would require a different engine than the original version. The propulsion installation will start with the attachment of the engine core to the wing, followed by installation of the propeller blades and completed with the installation of the engine cowling. After all the systems have shown to be gas-tight, the fuel tanks are attached. It may be obvious that concise fuel management is necessary if the aircraft is loaded with LNG, for all subsequent steps.

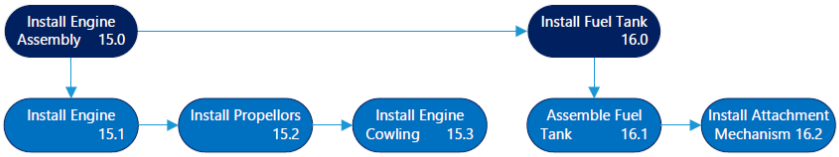

Figure 8.4: Flow diagram of the propulsion system installation process.

8.2.6. Product Completion and Delivery

When the general and propulsion assembly is finished, the completion of the aircraft can start. This first step in this process is to perform static tests. It is crucial to perform them in this stage of the production process in order to allow for ease of access to systems if defects become apparent through testing. When the tests have been completed, the interior is installed which consists of the seats, galley, instruments, etc. Next the aircraft is painted to protect the aircraft from external effects of the environment, in the correct livery. By painting the aircraft in the factory, the correct weight and centre of gravity can be ensured. Finally, the flight tests are performed. When these tests are completed, the aircraft is ready to be collected by the buyer.

8.3. Production Sustainability

Aircraft manufacturing requires the use of various materials and processes. These processes require energy and material and as such have an effect on the environment. The choice of material use in the aircraft has a direct environmental impact in terms of energy used and emitted greenhouse gases. The part manufacturing and assembly add more energy and waste to the production of the aircraft.

8.3.1. Material Manufacturing

The energy use to produce a ton of a type of material was gathered to estimate the effect that the use of materials have in the production of aircraft. The energy cost for a list of materials and their CO_2 equivalent according to average emissions per kWh have been provided below [89].

As can be seen in the table, metals need less energy to produce than composites and when recycled, the

Table 8.1: Energy needed to produce 1 ton of material

Material	Energy Needed [kWh/ton]	CO_2 equivalent [kg/ton]
Aluminium (from ore)	63,000	30,744
Steel (from ore)	7,000	3,416
Carbon Fibre Composites	301,000	146,888
Titanium (from ore)	250,000	122,000
Aluminium (recycled)	3,500	1,708
Steel (recycled)	2,500	1,220
Plastics (from crude oil)	24,000	11,712
Fiberglass	4,510	2,201

energy needed for metal is reduced drastically. It is therefore advised to try and use recycled metals for the aircraft as they significantly reduce the energy needed for production and reduce cost.

8.3.2. Part Manufacturing and Assembly

The materials that are used in an aircraft can be made in a sustainable manner, but they should also be used in a sustainable manner. During the manufacturing of parts one inevitably wastes some of the material (through milling, pressing or other manufacturing processes). When using metals, it is important to gather the 'wasted' parts, so that it can be reprocessed and reused for further parts.

Because the subassemblies of the aircraft will be produced as close as possible to each other, the need for special transport is reduced and with that extra costs and energy. Only subassemblies which do not require special transport will be produced on external locations other than the main assembly line.

8.3.3. Factory Sustainability

Sustainability inside the factory can be increased by making the building itself more sustainable. This can be done by lowering the waste of energy by for example insulating the factory and thereby reducing the amount of energy needed to heat or cool the building. Further gains can be made by installing solar panels on the roof and create a green roof by using the roof as a garden, insulating the building even more. This has been done in recent years by the Ford Motor Company. By making the factory run on green electricity one can reduce the carbon footprint of the factory and the production of the aircraft even more.

8.3.4. Employee Well-Being

Healthy employees work better and make less mistakes, it is therefore important to ensure the well-being of the employees during production. Not only from a production perspective, but also a moral one. Proper gear for handling toxic and dangerous materials will be available according to regulations and the use of these materials shall be limited.

With regard to assemblies, the jigs shall be positioned such that employees have easy access to parts and do not have to take a stressful posture. Bikes shall be provided to allow for easy access between factory buildings and minimise energy and material use.

8.4. Production Increase

In order to make Aquila more economically viable it might be wise to increase production so that the break-even-point can be reached. There are two ways to increase this production, more assembly lines can be created or the same assembly line can be used for more hours during the day. Since the original assembly line is not used throughout the whole day the design team opted for increasing the number of shifts to two shifts a day to increase production. These first shift would start early in the morning and end in the afternoon after which the second shift start which would last until the evening. This effectively reduces the station time to 2 days, on the contrary to the initial 4 days per station. A night shift was deemed unnecessary

and less productive than the day shift and would also lead to negative health for the employees.

While increasing the amount of shifts is the easiest solution to increasing the production rate it also makes the main bottleneck of production worse, which is finding the man-hours. It is hard to find a skilled workforce and increasing the size of that workforce. This was a problem during the early stage of the production of the Boeing 787 dreamliner[4]. A way to solve this is to increase the wages of the employees or by promoting working at the company through the use of ads.

Subcontractors are also used so it should be investigated if they can also increase the production of the parts that they produce. If they are not in a position to do this, new suppliers should be found in time for the extra needed parts.

If these bottlenecks can be solved the increase of production rate should not meet significant obstacles and the break-even-point can be reached sooner.

8.5. Production Risk Management

In order for the production to become a success, the cost, the throughput and the quality of the product is paramount. Obviously, these will be affected by certain risks involved. In the previous sections, some risks were already taken into account for different aspects of production and in this section these risks are elaborated on. Regarding production risks, this section starts off with the most important risk, namely the safety and well-being of the employees, followed by the risks involving quality and lastly the logistical risks, risks involving costs are addressed in chapter 9.

8.5.1. Safety Risks

The need for a safe working environment is apparent. However, working with advanced equipment is not always beneficial for safety. For instance working with composites, chemicals and machinery comes with inherent risks. To prevent a decline in the well-being of the employees, correct training and instruction of the employees is needed. Furthermore, appropriate safety measures are necessary, for instance the correct attire like safety shoes, goggles, gloves and masks, hard hats, welding goggles and earmuffs, but also the prevention of stress related illnesses. In addition to prevention, the manufacturer should be prepared for the worst case scenario by providing and installing safety equipment, for example a fire alarm and containment system, gas detectors, first-aid kits, emergency showers and eye washers. Even regular housekeeping increases safety, by not letting combustible dust accumulate to dangerous levels or letting tools lie around the assembly hall, over which a worker could trip.

8.5.2. Quality Risks

In the end, the quality of the product determines the safety of the users of Aquila. Quality can be decreased by faults in the production instruction, faults of the employees, impurities of materials, issues with the subcontractor and the omission of quality control. Besides the adequate training of the employees, quality can be increased by quality controls. If quality control reveals a defect, this should be resolved as quickly as possible, otherwise it will affect the logistics.

8.5.3. Logistical Risks

Usually airlines take an aircraft in use directly after delivery to increase revenue, therefore time management of the production is of great importance. By the use of an assembly line the status of completion is directly related to the position in the assembly line. A halt of the assembly line is a critical event which reduces production rate considerably, therefore troubleshooting teams are necessary to resolve an issue, while regular production can go on, even to the next station or further, while the defect is still an issue.

[4]Retrieved from https://www.reuters.com/article/us-boeing-dreamliner/boeing-struggles-with-787-production-bottlenecks-idUSBREA1A06T20140211 (Consulted on 17/06/2019)

9
Financial Analysis

Besides defining the next advancement in the regional aircraft, the Aquila project also aims at making a profit. This can be measured with the return on investment (ROI) of the project. In order to calculate this, the revenue and the costs are estimated. Revenue comes from the sale of aircraft and to be market competitive, the retail price has to be determined based on what the competitors ask for their products. This is done in section 9.1. In section 9.2, a cost breakdown for the rest of the project is made in order to determine the further investments that have to be made. Knowing this, the gross profit of the project is estimated and the ROI is calculated. One of the key selling points of this project is a low operating cost. That is why it is estimated and compared to the ATR 72-600 in in section 9.3. The financial risk is assessed in section 9.4, after which a sensitivity analysis is performed in section 9.5. In last section of this chapter,section 9.6, the financial analysis is coupled back to the cost requirement and conclusions are drawn.

9.1. Market Price

For a new product to be a success, it has to be price competitive with the competitors in the market. That is why it is important to determine a market-oriented retail price. As stated before in chapter 2, the three direct competitors in the market are the ATR 42-500, ATR 72-600 and Bombardier Q400. These three aircraft dominate the regional turboprop market based on their open orders and total deliveries. Other commercial turboprop aircraft own a market share which is too small or are not in production anymore, therefore they have not been used as reference aircraft.

Different price-determining parameters had to be found in order to determine the market-oriented retail price for the Aquila aircraft. The two main parameters in aviation, which determine the retail price, are seat capacity and range. These parameters were plotted for the different aircraft against their list price.

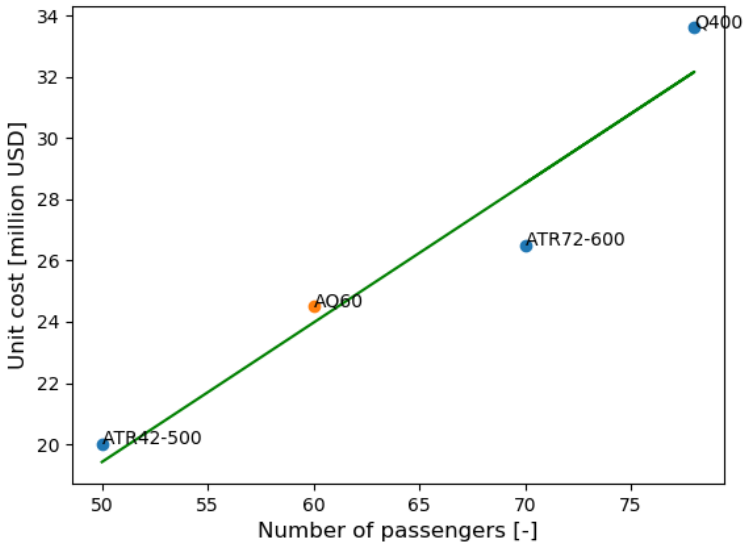

Figure 9.1: Aircraft market price trend

It was found that there is no correlation between range and retail price for regional turboprop aircraft. An explanation for this could be that due to their limited speed, an increase in range is not beneficial as they

would be too slow to compete against jets. There was, however, a strong correlation between seat capacity and list price. This correlation can be seen in in Figure 9.1. A regression of this made it possible to determine market-oriented retail price of the Aquila. This was set on 24.5 million USD.

9.2. Cost Breakdown Structure

This report is part of one of the first phases in this project, after which the development continues. The further development requires an investment of time and resources. As this is a significant investment, it is valuable to make a breakdown of the costs. This can be seen in Figure 9.2. For this analysis Roskam's [90] method was used, which mainly uses empirical relations. The costs can be divided into two categories: Research, Development, Testing and Evaluation (RDTE) phase (non-recurring costs) and production phase (recurring costs).

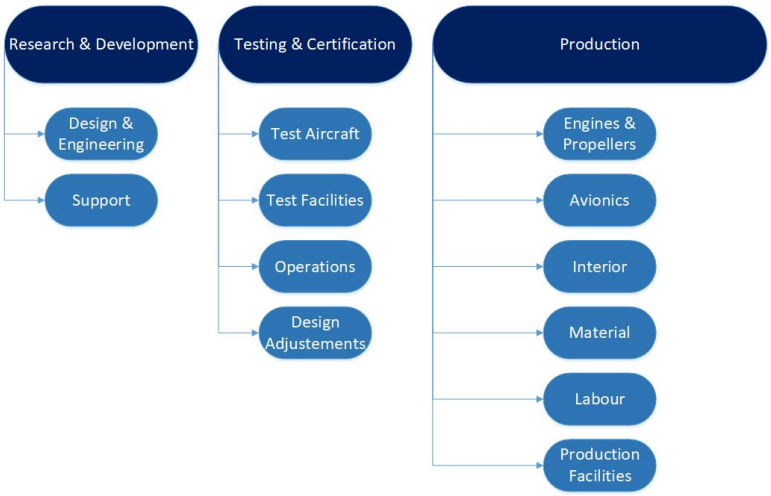

Figure 9.2: Cost Breakdown Structure

9.2.1. Research, Development, Testing and Evaluation Costs

This report is the kick-off for the R&D phase. It is mostly focused on concept assessment, concept design and preliminary engineering. The coming months and years will focus on developing this concept further and designing the systems in detail. The cost breakdown of this phase can be seen in Figure 9.3. The engineering and design costs come from the salary of the engineers. The Aquila concept uses innovating technologies, which require a bigger investment for the development than for a more conventional aircraft. This is accounted for by a complexity factor during the whole cost estimation process. The rest of the costs for R&D is for support, which includes for example buildings, small scale tests and software.

After R&D, the testing and certification can begin. The main cost contributors to the testing and certification phase are the test aircraft that will be build. A total of five test aircraft will be build of which only three are equipped with engines, the rest will be used for static tests. These test aircraft could later be sold with a discount to an airline, but this assumption was not made in these calculations. These aircraft have to be operated, which also induces costs. Certain test facilities have to be used for certification. As the manufacturer is a new player in the aviation industry, it is assumed that the company does not posses these facilities.

The manufacturer has to take a loan to finance this project, which also creates costs in the form of interests. These are the extra costs to finance the RDTE phase and are estimated to be 10 %, as estimating this in more detail goes beyond the scope of this report. All these costs sum up to a total of 782 million USD (2019) and the breakdown can be seen in Figure 9.3.

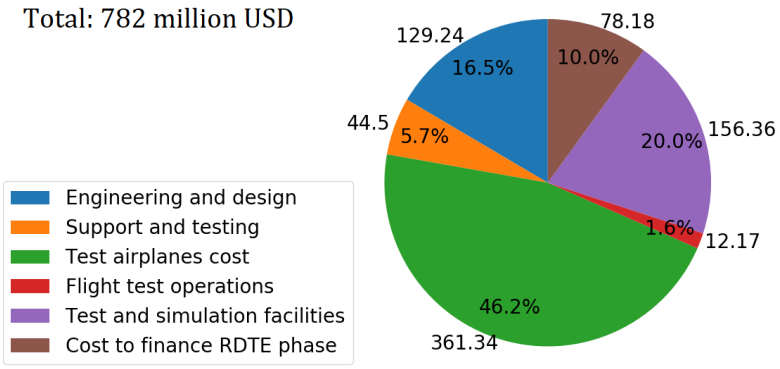

Figure 9.3: Development cost in million USD

9.2.2. Production Costs

After certification the aircraft can be build to production standard. The divison of costs needed to build one Aquila aircraft are given in Figure 9.4. The engines and propellers are bought from third parties. The same goes for the avionics, which is the second most expensive parts, after the engines. The airframe is build by the manufacturer by combining its production facilities with raw materials and human labour. It is assumed that the manufacturer already owns the required facilities and machines. The complete aircraft is delivered with a complete flight-ready interior. This interior is only a small portion of the whole aircraft. Finally, as with the RDTE, loans have to be taken out in order to finance the project. This brings the total cost to produce 1 of the 630 aircraft to 21,660,000 USD. The market-oriented retail price is set on 24,500,000 USD, which means that the aircraft has an ROI of 13%. For the entire program this would mean a gross profit 1,790,859,000 USD.

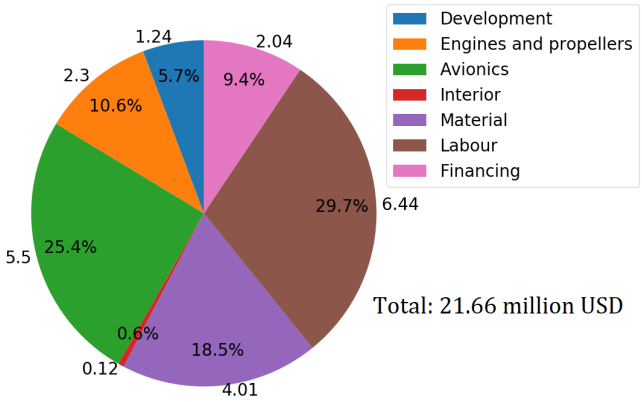

Figure 9.4: Unit cost breakdown of the Aquila in million USD

9.3. Operational Cost

One of the key drivers in the Aquila design is to reduce operational costs. That is why it is important to quantify these costs. The estimations for the direct operational costs (DOC), are made using empirical equations from Roskam. For verification and comparison the same equations are used to estimate the operational costs of the ATR 72-600. The results can be seen in Figure 9.5 and Figure 9.6.

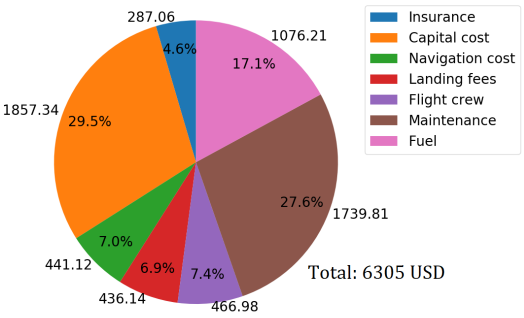

Figure 9.5: Operation cost Aquila on 1000 km trip

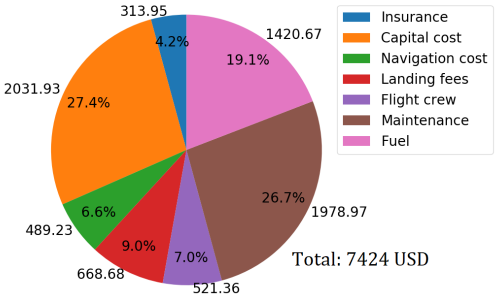

Figure 9.6: Operation cost ATR 72-600 on 1000 km trip

The lower list price of Aquila leads to a lower insurance premium and lower capital costs. The latter are the costs for paying off the aircraft itself to the manufacturer, which also includes interest on the loans. Both the navigation and the landing fees are also lower due to the lower MTOW of the Aquila. In contrast to the other costs, an estimation from Airbus was used for these costs instead of Roskam as this is more recent and reliable.

Another cost on a 1000 km trip that is lower for the Aquila aircraft compared to the ATR is the crew cost. This is caused by the higher cruise speed of Aquila. This reduces the block time and therefore the flying hours for which the pilots need to be paid. The reduction of maintenance for the Aquila aircraft is caused by the smaller airframe and the lighter engines. The most significant cost reduction comes from the fuel. LNG has a higher price per kg at the distribution station than kerosene, but the energy density is higher, which outweighs the increase in price per kg. This in combination with more efficient engines leads to a very big cost reduction.

All these things combined make a 1000 km trip with the Aquila aircraft more than 1000 USD cheaper than the ATR 72-600, with the ATR costing 7424.78 USD per 1000 km trip and the Aquila 6304.67 USD. Not only the total cost is significantly less, but the CASK, which is the cost for the airline for each passenger per kilometer, is also lower as it is 0.106 USD for the ATR 72-600 and 0.105 USD for the Aquila. This makes the Aquila not only a more flexible, but also a cheaper solution for regional airlines.

The direct operational cost give a good estimation of the LCC as all the parts from development to operations are included. By multiplying the DOC, which is calculated for block miles flown, with the expected block miles that are flown in a life cycle, the LCC can be found. The disposal cost at the end of life has to be added to this. This is hard to predict in detail at this point, which is why this was set at 2% of the LCC. This brings the LCC to 274,708,000 USD [91].

9.4. Risk Assessment

The biggest risk regarding the financial aspect of the project is that the costs are higher than initially thought. This increase in costs could be due to various reasons. A few possible reasons are: delays in the future development process, the aircraft shows defects during testing and certification or changing in regulation. If some of these things occur the increase in costs will result in a lower return on investment. Therefore, a buffer has to be built in the theoretical return on investment.

9.5. Sensitivity Analysis

In order to sketch how much the cost of the aircraft varies with the mission's main requirements, a financial sensitivity for the Aquila project has been conducted. Both the DOC and the aircraft unit price were analysed as a function of the change in number of passengers and design range respectively. This is represented in Figure 9.7 and Figure 9.8.

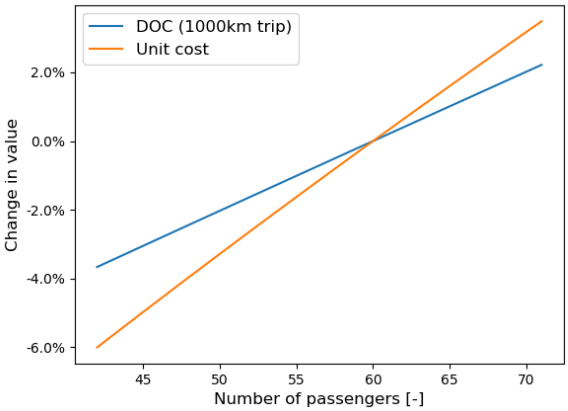

Figure 9.7: Sensitivity of DOC and unit cost to number of passengers

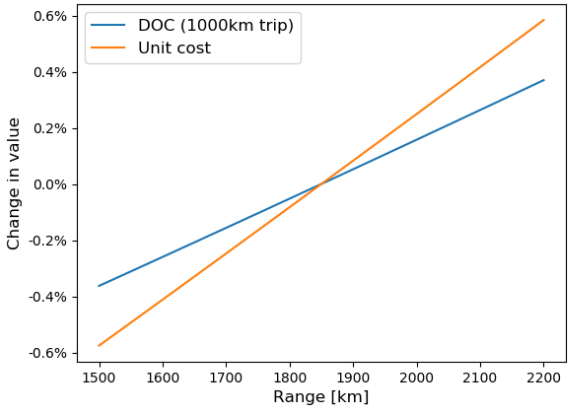

Figure 9.8: Sensitivity of DOC and unit cost to design range

It can be concluded that the unit price is more sensitive to a change in number of passengers and design range than the DOC. This is due to the fact that the unit costs is more sensitive for a bigger MTOW, which increases with an increasing number of passengers or design range, while the DOC also includes factors which are not correlated to MTOW.

9.6. Conclusion

During the development of the project some requirements concerning costs seemed less relevant. AQ-COST-01, which states that the retail price of the aircraft shall be 30% of the LCC, is not met. This would mean that the retail price of the aircraft should be 65,150,000 USD or that the life time should be way shorter. This is of course unfavourable as it would make the aircraft a lot less attractive to potential buyers. This discrepancy between the requirement and the results is potentially caused by the fact that when the requirements were drawn, it was not clear if a jet or a turboprop would be designed and values for Life Cycle Cost for jets were used. Jets are a lot more expansive in retail price than props, but their operational costs are significantly lower. This makes their portion of acquisition price of the Life Cycle Cost a lot bigger than for turboprops. This also has an impact on AQ-COST-03, which states that the monthly operational cost shall be less than 56% of the Life Cycle Cost. It was already tried to keep the operational costs as low as possible, but due to the low retail price this requirement can not be met. A erroneous approach was taken when setting up the cost requirements by expressing certain costs as a percentage of the LCC. Due to a lack of absolute numbers at that time, cost requirements were set up using relative numbers. However, if one of these parts is decreased another increases by definition, even though the total LCC would be decreased. That is why it is suggested to remove these requirements from the list and add new ones expressed in absolute values.

AQ-COST-02 states that the production price shall be less than 80% of the retail price. With a production price of 21,660,000 USD and a suggested retail price of 24,500,000 USD, the production price is 88% and therefore the requirement is not met. However, it is estimated that the project would give an ROI of 13.1%. This should be compared with the two main players in the aviation industry, Airbus and Boeing, which respectively have an ROI for the last 5 years of 4.39% and 16.3% [1]. This big difference in ROI is caused by Boeing's efforts to reduce operating costs by reducing administration costs and interest and debt expenses, while the administrative costs of Airbus only increased. At the same time Boeing has managed to sell more of the very profitable wide body aircraft than Boeing [92]. The ROI of Aquila falls in between, this makes a good first estimate. If requirement AQ-COST-02 would be met, the ROI would soar to 25% which is unrealistically high for the industry. It would mean that impossible savings would have to be made or that the retail price should be set to 27,000,000 USD, which is more expensive than the ATR 72-600, which can carry 10 passengers more than Aquila. For these reasons it is strongly advised to revise this requirement.

[1] Retrieved from https://www.investing.com (Consulted on 22/06/2019)

AQ-COST-04 states that the End-Of-Life (EOL) cost shall be less than 4% of the LCC. Although some attention is spend in this report on the EOL, a detailed cost analysis was not made on this subject due to the insufficient amount of detail at this stage and the lack of time. This should further be investigated in a more detailed design phase.

AQ-COST-05 says the CASK shall be less than 0.106 USD. The estimation for the CASK of the Aquila is 0.105 USD, so this requirement is met.

All these costs are first estimations and should only be used as reference point for a further, more detailed financial analysis. It has, however, shown a first indication for a potential profit. These values will shift over time when the aircraft is developed, but as the main objective of this project was to make a price-competitive aircraft, this analysis should be made in every step of the design, even in the preliminary design.

10
Sustainability and Risk Assessment

In the beginning of this report the goals and design philosophy behind the sustainability and risk was determined. This chapter will analyse and assess if these goals were met and how they can be improved upon even further. The sustainability will be analysed first and compared to the main competitor: the ATR 72. This is done by first analysing the life of the aircraft in section 10.1, investigating the economic and social sustainability in section 10.2 and the final assessment in section 10.3. Finally, as pointed out in section 4.2, risk has been addressed during the design process and in section 10.4, an overview of the most important risks and their related mitigation is given.

10.1. Life Cycle Assessment

A life cycle assessment or LCA is a tool to estimate the environmental impact of a product. It is useful to gain insight in the total impact and not just look at the emissions for the operational phase. The section on LCA starts with the production phase, followed by the operational phase and the end-of-life.

10.1.1. Production

In chapter 8 it was shown that not every material has the same environmental impact. To estimate the total environmental impact in terms of CO_2 emissions, the total used material weight of each material was multiplied by the CO_2 emissions per ton of each material. This table can one find below in Table 10.1.

Table 10.1: Total CO_2 emissions during production of the Aquila and ATR 72 aircraft.

Material	**CO_2 AQ-60 (rec.) [kg]**	**CO_2 AQ-60 [kg]**	**CO_2 ATR 72 (rec.) [kg]**	**CO2 ATR 72 [kg]**
Aluminium	8293	149,276	10,282	185,072
Steel	1256	3518	1731	4846
Composites	38,778	38,778	376,768	376,768
Titanium	24,400	24,400	33,612	33,612
Plastics (from oil)	5856	5856	8067	8067
Fiberglass	440	440	606	606
Unaccounted	2775	2775	2257	2257
Total mass	9824	9824	13,500	13,500
Total CO_2	79,024	231,818	431,066	608,971

As can be seen, the Aquila with recycled materials has an environmental impact 1/5 the size of the ATR 72, which is mainly due to the fact that less composites are used. It should be noted that the estimations for the material weights of the ATR 72 were estimated using a weight factor of the materials of the Aquila and a calculation for the carbon composites based on the fact that it was known that the ATR 72 uses a carbon composite wing box.

10.1.2. Operations

During the lifetime of the aircraft it will fly thousands of flights. To estimate the total impact on the environment, the amount of flights that the aircraft flies over its lifetime has to be estimated first. It was assumed

that the aircraft would fly 5 flights per day for an average of 300 days per year over the course of 30 years. This amounts to 45,000 flights over the lifetime of the aircraft. The total environmental impact of both the Aquila and the ATR in terms of CO_2 and NO_x was calculated and can be found in Table 10.2

Table 10.2: Operational Emissions over the lifetime of both aircraft

Parameter	**Aquila**	**ATR 72**
Fuel used (1000 km trip 60 pax) [kg]	1,496	2,159
CO_2 (1000 km trip 60 pax) [kg]	4,488	6,477
NO_x (1000 km trip 60 pax) [kg]	1.496	2.159
Lifetime CO_2 [kg]	185,130,000	291,465,000
Lifetime NO_x [kg]	67,430	291,465
Percentual difference CO_2 compared to ATR 72 [%]	-36.5	0
Percentual difference NO_x compared to ATR 72 [%]	-76.9	0

It can clearly be seen that the Aquila outperforms the ATR 72 both in terms of fuel, CO_2 and NO_x. If biomethane is used for the Aquila the emissions from the operations can be reduced by another 97%.

10.1.3. End-of-Life

The end-of-life assessment shall be done based on the amount of material of the aircraft that can be usefully recycled. On average about 85% of the weight of aircraft is currently being recycled [93]. However, most aircraft that are recycled today are made out of aluminium, which is relatively easy to recycle. Modern aircraft use more advanced materials which are harder to recycle. That is why the focus of the Aquila project is to recycle not just the conventional materials, but also make an effort to recycle these advanced materials.

In order to estimate the recyclability of the aircraft, a comparison was made between the Aquila and the ATR 72. This was done by calculating the estimated recyclability for every material and applying the mass fraction. It must be emphasised that this is only an estimation and real recyclability also depends on the airliner. The main improvement with regard to recycling is the recycling of materials that were not ordinarily recycled, in this case titanium and composites.

Titanium was previously very hard to recycle because of the high temperatures needed to process it. Recently a factory in France has started to recycle titanium, which can also reduce production cost of titanium and give Europe a steady supply of titanium [1]. Up to 93% of the recycled titanium can be recovered and reused [94]. Another development in recent years has been the recycling of carbon composites, in particular the carbon fibres themselves [93]. For plastics, the average value for plastics recycling in the Netherlands was taken, which is 50% [2]. The recyclability for each material and the plane as a whole, based on the empty mass of Aquila and the ATR 72, is given in Table 10.3.

[1] Retrieved from: https://medium.com/eib-connect/titanium-recycling-gives-europe-a-valuable-new-metal-supply-27d9fe0e836d (Consulted on 19/06/2019)

[2] Retrieved from: http://www.europarl.europa.eu/news/en/headlines/society/20181212STO21610/plastic-waste-and-recycling-in-the-eu-facts-and-figures (Consulted on 19/06/2019)

Table 10.3: The recyclability of Aquila and the ATR 72

Material	**Recyclability [%]**	**Aquila (recyclable weight) [kg]**	**ATR 72 (recyclable weight) [kg]**
Aluminium	98	4758.3	5899.4
Steel	98	1009.2	1390.2
Composites	30	79.2	769.5
Titanium	93	186	256.2
Plastics	50[3]	250	344.4
Fiberglass	0	0	0
Total Recycled Mass	n.a.	6282.7	8659.7
Total Wasted Mass	n.a.	766.5	2583.4
recyclability [%]	n.a.	89.1	77.0

It must be stated that this is only an estimation of what the recyclability of Aquila could be; these results are all highly dependent on the choices of the airline. However, it is the view and ambition of the design team to assist where possible in this process to make sure that the Aquila lives up to its recyclable potential.

10.2. Economic and Social Sustainability

Throughout this report it was shown that the Aquila was designed with sustainability in mind with respect to the environment, but this is not the only aspect with respect to sustainability that was considered.

In terms of economic sustainability it was shown that the Aquila has lower operational costs than its best competitor and would thus be the ultimate choice for low-cost carriers in terms of regional aviation. If the likely rise in kerosene prices, either due to market forces or because of (inter)governmental initiatives, is factored in, the difference in operational costs between Aquila and competitors is likely to increase even more.

From the perspective of the manufacturer, the Aquila also offers a promising outlook. The aircraft can be produced for 21.66 million USD and will be sold for 24.5 million USD. Over the lifetime of the project this would result in a gross profit of 1.79 billion USD, paving the way for new investments or allow the company to grow in a different way.

Aquila also offers a renewed and positive image of aviation and regional aviation sin particular. Over the last few years the demand from the public for a more sustainable aviation industry has been on the rise. This is due to the growing awareness for climate change and the role that the aviation industry plays in this issue. Aquila offers a short-term solution to comply with the Paris Climate Agreement, by using LNG (fossil fuel) and offers also solutions for long-term CO_2 reductions by using biomethane (renewable fuel) to eventually make regional aviation carbon neutral.

10.3. Assessment and Future Development

In order to better visualise the improvements that have been made with the Aquila project, a spider diagram was made to show the comparison in terms of sustainability between the ATR 72 and the Aquila. CO_2, NO_x, Noise, DOC, Unit Cost and recyclability have all been quantified, the other factors have been qualitatively analysed. They were all scored from 1 to 5, with 1 being the worst score in the center of the diagram and 5 being the best score.

[3] Retrieved from: http://www.europarl.europa.eu/news/en/headlines/society/20181212STO21610/plastic-waste-and-recycling-in-the-eu-facts-and-figuresrecyclingofplastic,addasfootnote (Consulted on 18/06/2019)

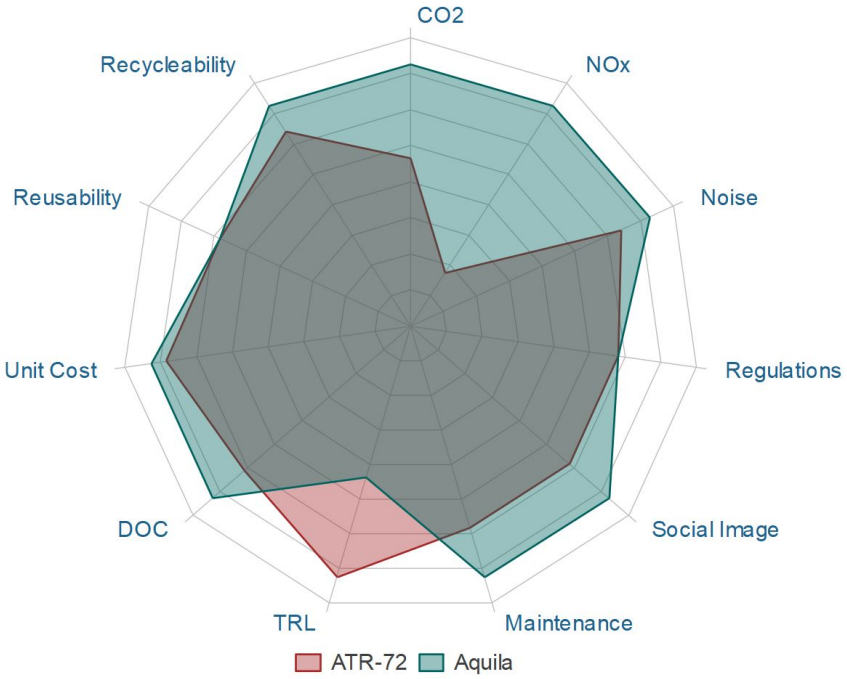

Figure 10.1: Spider diagram of the sustainability comparison between the ATR 72 and the Aquila.

Throughout the life cycle assessment it can be seen that the Aquila outperforms the ATR 72 in terms of sustainability, with the ATR 72 being the "greenest" aircraft in the regional aviation market. Aquila offers a short-term solution to the need for sustainability in the regional aviation, but the sustainable development does not stop here. The design that has been proposed so far offers an economically viable and sustainable design, but can be improved even more. By using biomethane the operational CO_2 emissions can be reduced by another 97%. Through the usage of natural gas to power the grid, the emissions during production of materials and the emissions for production can be reduced by 50% and can be reduced even more by switching to renewable energy sources. When recycling techniques for glass fibre become cheaper and recycled glass fibre can compete with new glass fibre in terms of pricing, this material can also be recycled effectively.

This aircraft presents a step in the right direction for aviation in general and should be a stepping stone towards true sustainable flight, which is the ultimate goal. By using these methods a sustainable future can be realised without compromising on the qualities of flight and the connectivity of modern society.

10.4. Overview of Project Risk Assessment

Throughout the report, risk assessment and mitigation is conducted. In this section an overview of the most important risks concerning Aquila is shown. Followed by a graphical representation in the form of a risk map. Then an overview of the mitigation of these risks is given. Finally, the updated risk map is presented, showing the effects of the mitigation and most importantly, which risks require more attention in the continuation of this project.

Table 10.4: Risk register

Identifier	Risk	Cause	Impact
AQ-RISK-DES-1	Wing is not able to provide sufficient lift	Failure of the high lift devices	Aircraft not able to land in a controlled way
AQ-RISK-DES-2	Decrease in stability and controllability	Shift in c. g. location, for instance due to sliding cargo	Rescue of the aircraft becomes extremely unlikely or results in a crash
AQ-RISK-DES-3	Tire fails during landing	Puncture due to items on runway or excessive wear	Possible decrease in controllability on the ground
AQ-RISK-DES-4	Failure of structure	Aircraft experiences larger forces than anticipated	Emergency landing or crash
AQ-RISK-DES-5	Engine fire	Failure in engine	Emergency landing or crash
AQ-RISK-DES-6	Pump failure	Failure of component or electrical system due to improper maintenance	Emergency landing
AQ-RISK-DES-7	Fuel tank rupture	Design flaws or foreign object damage	Emergency landing or crash
AQ-RISK-DES-8	Explosion of the LNG	Combustion of gas which has build up in a confined space, for instance due to a leak	Emergency landing or crash
AQ-RISK-OP-9	Ground operator gets injured while refuelling	Human or technical error while refuelling	Injury of the worker and LNG spillage
AQ-RISK-OP-10	Unauthorised people get injured by LNG	Refuelling area is not blocked	Injury or death
AQ-RISK-OP-11	Faulty emergency system	Emergency system receives no power, for instance due to the RAT not deploying	Emergency situation can not be contained
AQ-RISK-PROD-12	Injury of employee during production	Misuse equipment or carelessness	Absence due to recovery or death
AQ-RISK-PROD-13	Fire in production facility	Misuse of equipment or carelessness	Injury or death of employees and damage to factory
AQ-RISK-FUT/FIN-14	Increase in certification time	improper certification process	Increase in development costs and time
AQ-RISK-FUT/FIN-15	Aircraft shows defects during testing	Mistakes during design process	Increase in development costs and time, possible redesing needed
AQ-RISK-FUT/FIN-16	Change in legislation	Decisions by government or failing aircraft lobby	Increase in operation cost

The above risks are graphically presented in the following risk map. Please note that this risk map focuses on the risks that were identified before and during the design process, thus without the effect of mitigation. The combination of the consequence and likelihood result in a colour, the colour indicates the required risk management needed. Red (the top right) indicates unacceptable risk and should be mitigated before continuation of the project. Orange indicates that extensive risk management is required. Yellow indicates that the risk is significant but manageable. Green (the bottom left) indicates that the risk requires no extra mitigation.

Table 10.5: Risk map

Likelihood \ Consequence	Negligible	Marginal	Moderate	Critical	Catastrophic
Very High					
High				14	
Medium			6, 9, 12, 16	7, 8, 15	
Low			1, 3	2, 4, 5, 10, 11	13
Very Low					

Table 10.6: Risk mitigation of the production phase

Identifier	Risk	Mitigation
AQ-RISK-DES-1	Wing is not able to provide sufficient lift	Aircraft lands at higher speed
AQ-RISK-DES-2	Decrease in stability and controllability	Safety margin in c.g. location
AQ-RISK-DES-3	Tire fails during landing	Aircraft is able to land with one tire per strut
AQ-RISK-DES-4	Failure of structure	Apply safety factors
AQ-RISK-DES-5	Engine fire	Maintenance, fire detection and extinguishing system
AQ-RISK-DES-6	Pump failure	Back-up pumping system, maintenance
AQ-RISK-DES-7	Fuel tank rupture	Sacrificial device for valves, safety factor, maintenance
AQ-RISK-DES-8	Explosion of the LNG	Place systems containing LNG in a well ventilated area
AQ-RISK-OP-9	Ground operator gets injured while refuelling	Provide protective clothing and proper training
AQ-RISK-OP-10	Unauthorised people get injured by LNG	Block refuelling area
AQ-RISK-OP-11	Faulty emergency system	Emergency system is indepent; manually operable
AQ-RISK-PROD-12	Injury of emplyee during production	Provide correct clothing and training
AQ-RISK-PROD-13	Fire in production facility	Install smoke detectors and fire containment system
AQ-RISK-FUT/FIN-14	Increase in certification time	Extensive time management
AQ-RISK-FUT/FIN-15	Aircraft shows defects during testing	Buffer built in the theoretical return of investment
AQ-RISK-FUT/FIN-16	Changes in legislation	Buffer built in the theoretical return of investment

Below the updated risk map can be seen, which shows the effect of the mitigation that was carried out, and and the same time shows the outliers that need more concise risk management.

Table 10.7: Updated risk map

Likelihood \ Consequence	Negligible	Marginal	Moderate	Critical	Catastrophic
Very High					
High					
Medium		16	15	14	
Low		3, 6	4, 5, 9	7, 1, 8, 12	
Very Low			1, 11, 12	2, 10, 13	

The risks that show the need for more management are the ones involving certification. This result is to be expected due to the new application of LNG as fuel and the new design regarding the strutted wing.

In chapter 12 some risks will be addressed which concern processes between the end of this project and the final implementation of Aquila into the market. Furthermore, a strategy is presented to extend the detail of the risk management for future development.

11
Compliance Matrix

Now that all aspects of the design have been looked at, the development team has to revise the requirements to see whether these are met. The compliance of the design with the requirements has been evaluated in this chapter.

At this stage of the design it has to be checked whether the requirements of section 3.1 have been met. Tables 11.1 to 11.6 summarise the compliance of all requirements and in which sections each particular requirement is discussed. If necessary, it also presents some extra comments on the status of compliance of the requirements. A check-mark (✓) grants that the requirement is definitely met. A tilde (~) shows that the design still needs some evaluation to state that it fully complies with the requirement, but that there already has been some analysis about it in the report. A cross (×) states that the requirement definitely has not been met and specific focus has to be put on this part for future development.

Table 11.1: Compliance matrix of performance requirements

Identifier	**Description**	✓/~/×	**Relevant Sections or Comments**
AQ-PERF-01	The aircraft shall have a design range of 1850 km for nominal payload.	✓	section 3.2 & subsection 7.2.5
AQ-PERF-02	The fuel burn of the aircraft on a 1000 km trip shall be less than 1943 kg.	✓	subsection 7.2.8
AQ-PERF-03	The aircraft shall produce a maximum of 94 dB during take-off.	✓	subsection 7.2.6
AQ-PERF-04	The aircraft shall produce a maximum of 89 dB during cruise.	✓	subsection 7.2.6
AQ-PERF-05	The aircraft shall produce a maximum of 98 dB during landing.	✓	subsection 7.2.6
AQ-PERF-06	The emissions of the aircraft shall comply to the ICAO regulations for 2020-2050.	✓	subsection 7.2.8
AQ-PERF-07	The aircraft shall be able to take-off on a runway of 1400 m at sea level at MTOW.	✓	subsection 7.2.2
AQ-PERF-08	The aircraft shall be able to land on a runway of 1400 m at sea level at MLW.	✓	subsection 7.2.3
AQ-PERF-09	The number of passengers shall be in the range of 60-65 passengers.	✓	section 3.2

Table 11.2: Compliance matrix of production requirements

Identifier	**Description**	✓/~/×	**Relevant Sections or Comments**
AQ-PROD-01	The production factory of the aircraft shall be able to produce 5 aircraft per month.	✓	section 8.2
AQ-PROD-02	The production shall have an option to increase to 10 aircraft a month.	✓	section 8.4
AQ-PROD-03	The system shall be manufactured according to the lean manufacturing philosophy.	✓	section 8.3

Table 11.3: Compliance matrix of operations requirements

Identifier	Description	✓/~/×	Relevant Sections or Comments
AQ-OPS-01	At least 2 cabin seating configurations shall be designed for the aircraft.	~	It is possible to change the layout of the cabin, but this has not been done in this design phase.
AQ-OPS-02	The average noise in the cabin during cruise shall be less than 78 dB.	~	subsection 7.2.7
AQ-OPS-03	The cabin pressure shall be at least 75.3 kPa during cruise operation.	✓	subsection 5.6.6
AQ-OPS-04	The nominal CO_2 concentration in the cabin shall be less than 1000 ppm.	~	section 5.9 It is unclear whether this requirement is met. More extensive sizing and research is needed.
AQ-OPS-05	The cabin temperature shall be in the range of 15-30 ^{o}C in nominal flight.	~	section 5.9 It is unclear whether this requirement is met. More extensive sizing and research is needed.
AQ-OPS-06	There shall be at least one toilet on board.	✓	section 5.1
AQ-OPS-07	There shall be at least one galley on board.	✓	section 5.1
AQ-OPS-08	The MTOW shall not exceed 28,000 kg.	✓	section 7.1
AQ-OPS-09	The minimum turning radius for ground manoeuvres for the point furthest from the pivot point shall be less than 19.74 m.	✓	subsection 7.2.1
AQ-OPS-10	The wing span shall be less than 36 m.	✓	subsection 5.2.1
AQ-OPS-11	The tail height shall be less than 13.5 m.	✓	subsection 5.3.3
AQ-OPS-12	The turnaround time shall be less than 45 min.	✓	subsection 6.1.5
AQ-OPS-13	The aircraft shall be able to perform 72,000 flight cycles.	~	subsection 5.6.3: Fatigue calculations of the aluminum alloy used in the wing box is still rather premature.
AQ-OPS-14	The passengers shall be able to board the aircraft without the use of external stairs.	✓	subsection 6.1.1
AQ-OPS-15	The aircraft shall have at least 5.2 m^3 cargo volume.	✓	section 5.1

Table 11.4: Compliance matrix of cost requirements

Identifier	Description	✓/~/×	Relevant Sections or Comments
AQ-COST-01	The retail price of the aircraft shall be 30% of the LCC.	×	Needs to be revised, see section 9.6.
AQ-COST-02	The production price shall be less than 80% of the retail price (after inflation).	×	Needs to be revised, see section 9.6.
AQ-COST-03	The monthly operational cost shall be less than 56% of the LCC.	×	Needs to be revised, see section 9.6.
AQ-COST-04	The EOL cost shall be less than 4% of the LCC.	~	section 9.6.
AQ-COST-05	The CASK shall be less than 0.106 USD (2019).	✓	section 9.6.

Table 11.5: Compliance matrix of schedule requirements

Identifier	Description	✓/~/×	Relevant Sections or Comments
AQ-SCHED-01	The aircraft shall be operational in 2027.	✓	section 12.4
AQ-SCHED-02	The certification shall take 5 years or less.	✓	section 12.3

Table 11.6: Compliance matrix of PESTLE requirements

Identifier	**Description**	✓ / ~ / ×	**Relevant Sections or Comments**
AQ-PESTLE-01	The aircraft shall comply with the current FAA regulations.	✓	subsection 12.3.6
AQ-PESTLE-02	The aircraft shall comply with the current EASA regulations.	✓	section 12.3
AQ-PESTLE-03	The aircraft shall include at least two innovations (yet to be certified technologies).	✓	The implementation of the high aspect ratio wing with the strut and the use of LNG as fuel are both innovations.

12
Project Development

This chapter discusses the future of Aquila. Upon completion of the DSE project, the aircraft will not be ready to fly yet. A brief overview of the tasks and planning is provided in section 12.1. In section 12.2 the first period after the end of the DSE is discussed. Next, section 12.3 describes how the Type Certificate can be obtained. Then, section 12.4 explains the distribution process and the service provided by the manufacturer throughout the programme's lifetime. The risks that lie ahead in the future are assessed in section 12.5. Finally, section 12.6 provides ways to further improve on sustainability in the future.

12.1. Project Planning

As mentioned before, the aircraft is not finished yet. Therefore, a schematic overview of the tasks that still lie ahead can be useful to see how the project will develop further. Figure 12.1 shows a flow diagram outlining the major development phases that still need to come. It can be seen that the testing and production phases are shown in parallel; the production of aircraft can start as soon as the static tests show that the aircraft is airworthy. The other tests, especially those including fatigue and endurance, can be performed while the first commercial aircraft are already in production.

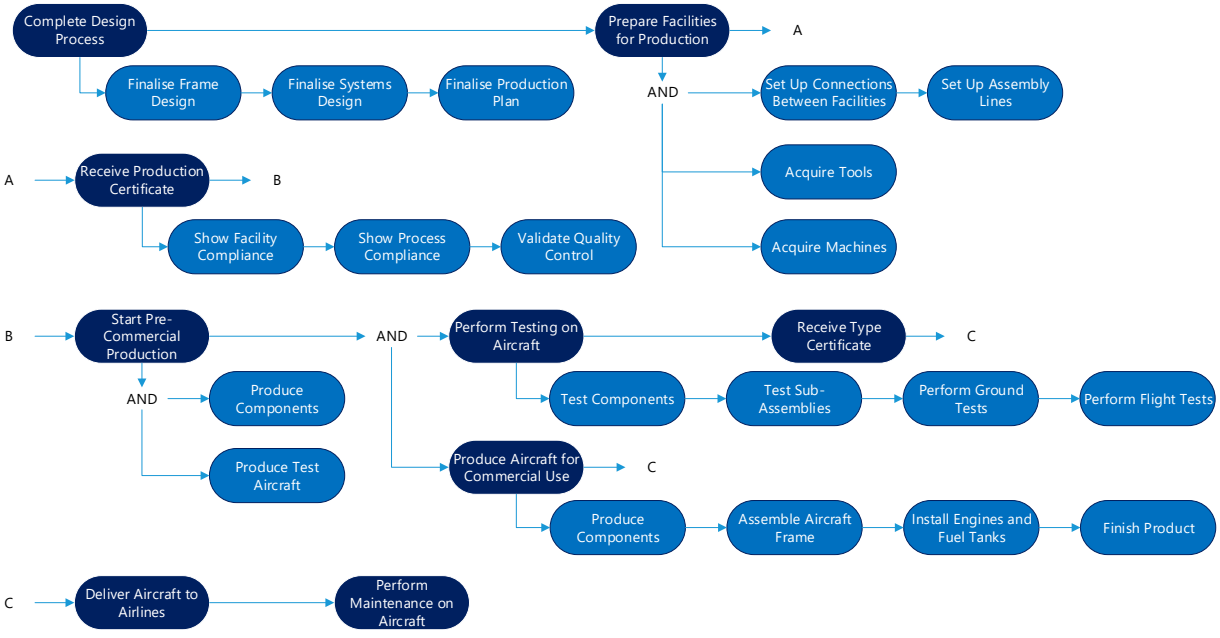

Figure 12.1: Project Design and Development Logic

To obtain a better overview of the time frame of these tasks and development phases, a Gantt Chart is provided below. This timeline does not include the operational phase for clarity. However, this phase will be briefly discussed in section 12.4. Furthermore, the full-scale flight tests are performed while the first aircraft will already be produced and delivered. The tests that will not be finished before the delivery of the first aircraft are meant to show the ageing of the aircraft and are only critical for the last decade of the lifetime of the aircraft. This is in accordance with CS 21 [95].

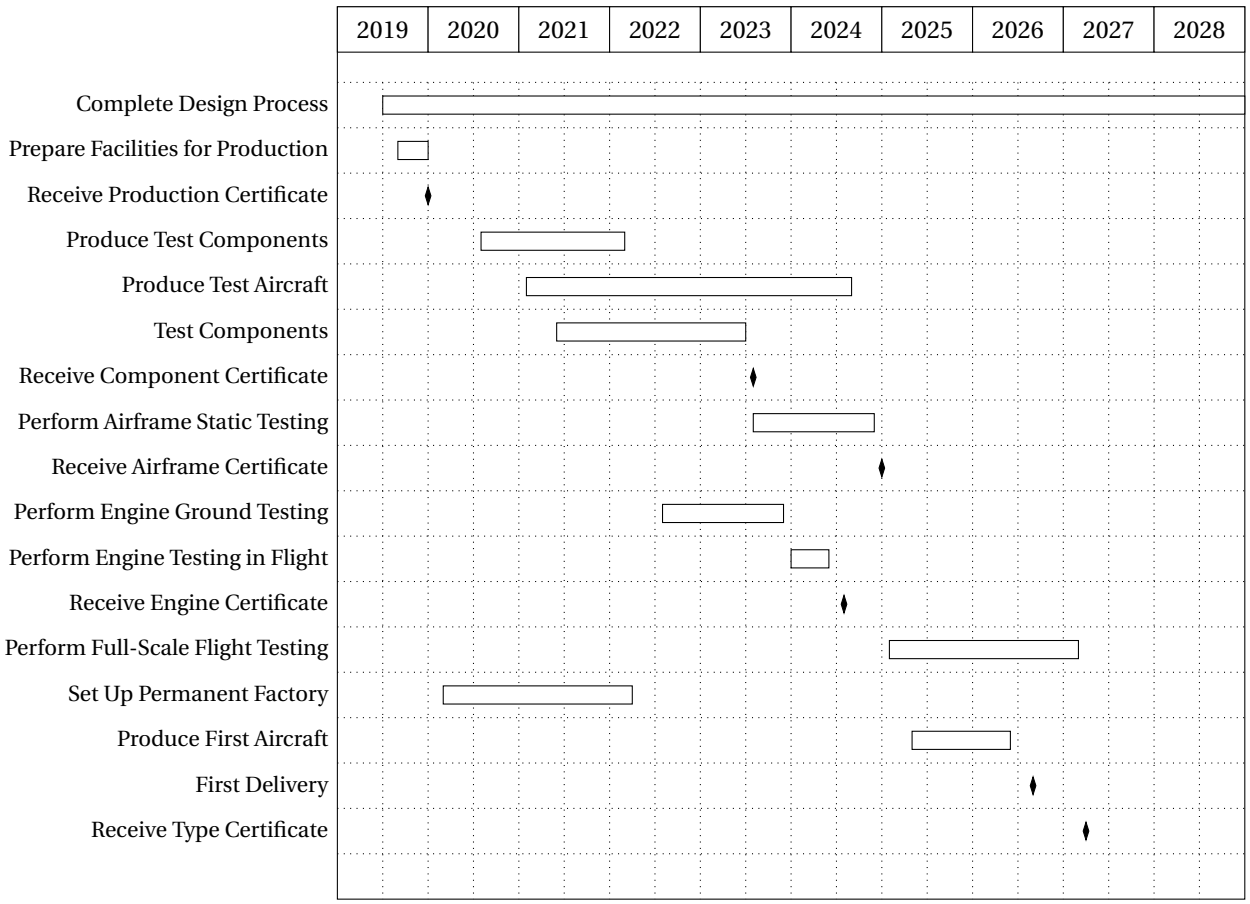

12.2. Early Project Phases

The exact duration of each phase in the Gantt Chart is not completely defined yet. However, together with Figure 12.1, this timeline gives a first indication of what the development looks like. In subsection 12.2.1, it is described what still needs to be done in terms of designing. In subsection 12.2.2, an explanation is provided on how to develop the production facilities according to the industry standards.

12.2.1. Closing of Design Process

In June 2019, the Design Synthesis Exercise is finished. During the DSE, the design has been completed on a high level and all systems have been determined. However, there are still tasks left to finalise the design on a very detailed level. This final design process starts after the DSE is finished. Finally, as shown in Figure 12.1, a detailed production plan shall be developed. As a large team will be employed to complete these last steps, this design phase is estimated to take 21 months. This is based on a workforce of 500 employees and a work load of 1.8 million man hours for a complete aircraft design[1] [90]. The main design phase shall thus be closed in March 2021. However, the design is never completely finished; even as aircraft are already flying, there might be changes required to implement in the design. Therefore, the design process in the Gantt Chart continues until the end of 2028.

12.2.2. Production Facilities and Certification

This section describes the phase in which the production facilities will be set up and test aircraft will be built. First, it is mentioned why and how the test aircraft are produced in existing facilities. Then, it is described how the permanent production hall will be established. Finally, a brief summary of important requirements on the facilities and organisation is provided as a base for certification.

[1] The reference uses 3.5 million man hours for a wide-body aircraft. It is assumed that for the Aquila, the number of man hours is roughly half of that for this reference aircraft.

Production of Test Aircraft

As shown in the Gantt Chart, a period of two years is required to set up the factory which will be used to build the aircraft. However, in order to meet requirement AQ-SCHED-01, the aircraft shall be available for operations by 2027. This requirement would not be met if the test aircraft were to be produced only after the factory is completed. Hence, existing facilities, already available to the manufacturer, will be used for these aircraft. Since they are able to produce only three aircraft at once, they would not suffice for the production of the commercial aircraft. Therefore, the development of these facilities that will be used throughout the rest of the programme are discussed next. With the existing facilities, the first test aircraft can be produced within two years time. For all subsequent aircraft, a period of 1.5 years is scheduled for their production. As will be explained in subsection 12.3.3, five complete aircraft need to be built for certification. Since three aircraft will be produced at once, 3.5 years are reserved for the production of test aircraft.

Development of Facilities

To create aircraft production facilities, an efficient planning and building process is required. It is estimated that it will take two years to create an assembly hall that meets the requirements for production facilities, as stated in CS 21 (subpart G) [95]. In case an existing building can be used, this time may be reduced to 1 or 1.5 years. The turnover process from a regular factory hall to a high-quality aircraft manufacturing facility requires the installation of stations in the different sections. Furthermore, proper connections between sections along the assembly line must be established.

In addition to the development of the work environment, as mentioned above, the facility upgrade includes the acquisition of tools and machines. These shall all be ordered in due time and positioned at the right stations in the hall. There shall be spare tools in case one breaks, and the facility manager shall investigate whether it is required to order spare machines as well, depending on their reliability.

Production Certification

Before the production of aircraft can start, a manufacturer is required to obtain a Production Certificate [82]. In case of Aquila, this is issued by EASA and follows the guidelines as outlined in CS-21. In order to receive this certificate, Aquila shall show compliance with the requirements on various aspects, including:

- **The quality system.** This includes a description of the control procedures.
- **The organisational structure.** The structure and responsibilities within the organisation shall be outlined in a clear and concise manner.
- **The data management system.** All data from production, testing and certification shall be available for inspection.
- **Obligations of the holder.** The manufacturer shall deliver a product up to standards as requested by EASA. This is not limited to the aircraft, but also includes standards related to the working environment.

The manufacturer will set up a specialised team to organise the production of the aircraft. This team will implement a quality control system to check all procedures followed in the facility and all steps taken throughout the process. Tasks will be specialised on a managerial level, which results in clear responsibilities for each position.

12.3. Type Certification

The type certification process for civil aircraft consists of four main steps[2]:

- Provision of technical overview and Certification Basis.
- Establishment of certification programme.
- Demonstration of compliance.
- Technical closure and issue of Type Certificate.

[2]Retrieved from https://www.easa.europa.eu/easa-and-you/aircraft-products/aircraft-certification (Consulted on 13/06/2019)

From the Gantt Chart, it is visible that the certification process of the entire aircraft is estimated to last from 2023 until the start of 2028, provided that all necessary parts have been produced before the start of this process. In the following sections, each of the certification steps will be explained and applied to the Aquila project.

12.3.1. Technical Overview and Certification Basis

At the start of the certification process, the project shall be presented to the primary certificating authority. For Aquila, this is the EASA as the design is developed in Europe. Furthermore, the certification team and the guidelines for the certification process are established. This is called the Certification Basis and remains the same for five years for aircraft and three years for engines. This is a constraint for the time frame of the certification process; if the aircraft can be certified within five years, and the engines within three years, there is no need to enter a second Certification Basis. According to the current estimations and the Gantt Chart, both requirements will be met.

12.3.2. Certification Programme

Once the Certification Basis is determined, the EASA and Aquila need to define and agree on the methods that will be used to determine how to demonstrate compliance of the Aquila with every requirement of the Certification Basis. This will most likely be a combination of analysis (for non-crucial elements or effects that cannot be tested in an organised manner), ground tests (on levels ranging from components to assemblies) and flight tests (for the propulsion system and the complete integrated aircraft system).

12.3.3. Compliance Demonstration

When the methods have been agreed upon, Aquila shall demonstrate compliance of the aircraft with all requirements established by EASA. As mentioned before, these demonstrations include analysis, ground tests and flight tests. Compliance demonstration by analysis does not require significant resources apart from man hours and is therefore not discussed here. The ground tests are discussed first in the subsequent text. It is followed by a description of the flight tests.

12.3.4. Ground Tests

For this particular aircraft, the tests related to the propulsion system and wing structure are the most critical. This is caused by the novel technology that is implemented in the design. Concerning the engine certification, the following tests are required [96]:

- **Tests concerning main rotating parts.** These include tests regarding compressor and turbine blade failure, rotor integrity, compressor, fan and turbine shafts.
- **Tests concerning certification of engine limitations and functioning.** These tests include endurance, over-torque, maximum engine over-speed, exhaust gas over-temperature, engine acceleration, starts (cold, hot and false), relighting in flight and engine bleed.
- **Tests concerning certification of ingestion aspects by the engine.** These look at the effects of rain and hail ingestion, as well as bird strike and ingestion.
- **Tests concerning performance in ice-forming conditions.** These tests are performed in a climate-controlled chamber and include both duration and short intensity tests.
- **Tests concerning over-temperature for both the turbine rotor and the complete engine.** These are used to test the engine performance if operating in extreme conditions or to simulate a one-engine failure, resulting in a higher power requirement for the other engine.

Apart from extensive engine tests, the aircraft shall also undergo structural static tests[3]. Especially those related to the structural integrity of the wing are important, as the high-aspect ratio wing with struts is a novel concept in commercial air transport. These tests include a Flight Test Installation (FTI) calibration test, as well as tests for the maximum wing bending at limit load. Furthermore, the functioning of ailerons

[3] Retrieved from https://www.airbus.com/aircraft/how-is-an-aircraft-built/test-programme-and-certification.html (Consulted on 14/06/2019)

and spoilers shall be tested during maximum wing bending, a fuselage pressure test must be conducted, and fatigue tests and flight cycles simulation are performed. Depending on costs and availability, adverse weather conditions can also be simulated in a climate-controlled hangar. The performance in these conditions, however, also needs to be tested in real-flight. Finally, ground emergency tests such as an evacuation simulation shall be performed as well, to ensure that the aircraft optimises safety during emergency situations.

Concerning the timeline of the process, the fatigue test is the most critical. Testing the aircraft up to 15,000 cycles will take approximately 15 months[4]. This number of cycles is three times higher than strictly required for certification, according to Airbus[5]. These tests are all conducted in existing testing facilities. During the ground tests, one aircraft will be used for fatigue testing, and one for non-destructive and, later on, destructive testing. Hence, two complete aircraft need to be built for this phase. Furthermore, several smaller sections will be produced for specific testing. After these tests have been completed successfully, the performance during flight needs to be demonstrated.

12.3.5. Flight Tests

Upon completion of the engine ground tests, the propulsion system shall be tested on an existing test aircraft with a four-engine propeller configuration. This allows for safe operations in the unlikely event of a failure of the new engine.

After excessive engine testing, the propulsion system can be placed on the aircraft itself. Then, test aircraft will take off for the first time for a series of flight testing. Tests regarding airfield performance, such as taxiing, water ingestion trials, manoeuvring and low-speed take-off tests can be performed. Furthermore, the performance during rejected take-off and landing shall be demonstrated.

Other tests regarding general handling qualities, operational performance and airfield noise emissions shall be set up. Besides system operational tests in normal flight conditions, failure scenarios and emergency situations must be simulated. The test aircraft shall also fly through extreme weather conditions. For example, this route could start in northern Scandinavia to simulate cold and icy conditions; then continue to Nepal for high altitude evaluations and finish in the United Arab Emirates in extreme hot and dry air. One aircraft will be produced to conduct these tests. Finally, an endurance test will be conducted, up to a total of 1800 flight hours, which is equivalent to 70% of the Airbus A350 XWB testing programme. Upon scaling the time required by Airbus, it was determined that two more aircraft need to be built for these tests, resulting in a total of three test aircraft for flight tests.

12.3.6. Route-Proving Tour and Type Certificate Issue

Once all testing has been successfully completed, one final step remains before the Type Certificate is issued. The aircraft fleet shall visit various airports around the world to show airport compatibility. During some of these flights, employees will act as passengers and a full crew is employed, to simulate real operating conditions. Upon a successful compliance demonstration by Aquila, the EASA will close the investigation and issue a Type Certificate. Consequently, the FAA and other authorities can validate the results from EASA and issue certification in their own countries, which is scheduled for 2027.

12.4. Aircraft Delivery and Maintenance Programme

In 2026, the first aircraft are expected to be delivered. The customisation of the aircraft will happen in the manufacturing hall, such that the aircraft are completely ready to use once they are finished. The customisation includes the furnishing of the aircraft interior, painting of the exterior and installing optional features, such as entertainment systems and adjusted galleys.

With a ferry range of more than 3750 km, the Aquila can be delivered to any airport in Europe by a single

[4] Assuming that one cycle takes 11 minutes, which was also the case for the Airbus A380.

[5] Retrieved from https://www.airbus.com/newsroom/press-releases/en/2006/07/airbus-a380-fatigue-test-reaches-15-000-flight-cycles.html (Consulted on 14/06/2019)

flight. For delivery to American airlines along the east coast, the route will be divided into two segments, with a stop-over in Iceland or the Azores. For delivery to the west coast of the United States, three or four segments are required.

The minimal aircraft lifetime was set at 30 years. Hence, the Aquila programme will run for this period after the cease of production. Since the exact number of aircraft that will be ordered is unknown at this point, the duration of the production phase is not entirely fixed yet. However, a preliminary estimation is provided. Based on an average production rate of five aircraft per month and a total volume of 630 aircraft, the production phase is estimated to last for 11 years, starting in 2025. When the manufacturer would increase their production rate, the production phase is likely to last shorter. Therefore, the production is likely to cease in 2036 or earlier and the last aircraft will be removed from service in 2066. This means that until that time, the manufacturer will provide maintenance services as described in subsection 7.4.3.

12.5. Risk Assessment

Most risks concerning future development are due to possible delays. There is a possibility that the factory is not ready in time, that the certification process takes longer than expected due to possible defaults in the aircraft or that there are problems with the delivery of the engine. Nevertheless, it is crucial that the test aircraft are built with a high level of precision to limit the possibility of defaults during testing. In the Gantt Chart, it can be seen that there is a buffer of approximately one year before the implementation time requirement is not met.

Some risks may become apparent as future studies extend the detail of the design. Whenever these risks show to be significant, adequate countermeasures should be taken. Future designers may express risk for their particular part of the design, creating a more thorough analysis. Furthermore, risk managers may express these risks in different ways. For instance, likelihood may be expressed in event per flight hour; along with the impact, it may be specified on which field the risk has the most impact: the schedule time, the cost, the safety or the technical performance of the product. Once all the possible mitigation has been performed, the legal department of the client will cover those that are left which are still significant.

12.6. Continued Sustainability

In this phase of the project, already a 36% reduction in CO_2 emissions is achieved compared to the ATR 72, which is already a step in the right direction to make flight more sustainable. This is however not the true definition of sustainability. This is defined as:

"Sustainability is the process of people maintaining change in a balanced environment, in which the exploitation of resources, the direction of investments, the orientation of technological development and institutional change are all in harmony and enhance both current and future potential to meet human needs and aspirations." [6]

To achieve the true goal of sustainability, the already low emissions of the aircraft must significantly decrease. This can be done by redesigning the aircraft or by reducing the impact of the fuel that it is using. Changing the footprint of the fuel would be the most viable option. Methane can be produced as a renewable energy source with the use of different processes.

12.6.1. Biomethane

Biomass can be used to generate methane. This can range from biomass from plants or other green "waste", to sewage waste; as long as it is organic material. Through the use of anaerobic or thermal gasification, the waste can be processed into methane, which can then be used for other purposes, such as powering aircraft. This principle has already been put to use in several powerplants, with a converting efficiency (in terms of potential energy) of 65-70%. In Sweden such a powerplant has been operational by converting biomass waste to methane[7]. Alternatively, the Sabatier reaction can be used to produce methane out of CO_2 and

[6] Retrieved from: https://www.globalfootprints.org/sustainability/ (Consulted on 20/06/2019)

[7] Retrieved from: https://www.goteborgenergi.se/om-oss/vad-vi-gor/forskning-utveckling/gobigas (Consulted on 21/06/2019)

hydrogen by processing it with pressure and heat through the use of a catalyst. This would however only be economical if renewable energy is cheap and available. By using these processes and method the net CO_2 emissions due to the usage of fuel can be reduced up to 97% [97].

12.6.2. Renewed Design

All these innovations with regard to sustainability and performance can be implemented throughout the lifetime of the aircraft. New engines will reduce the fuel consumption and emissions and reduced maintenance will also reduce the amount of work and number of parts that are necessary. This can be achieved by using new materials to improve the turbine blades, allowing higher temperatures at the turbine and improving the thermal efficiency of the engine, thereby increasing fuel efficiency. Renewable natural gas can provide a long term solution to the sustainability issues of aviation, by effectively reducing the net carbon dioxide emission footprint of the aviation industry.

12.6.3. Improved Production Methods

The production of the aircraft can be improved in multiple ways. By using renewable energy in the factory for both production of the materials as well as the assembly itself, the impact of production on the environment can be reduced tremendously. By increasing the use of recycled materials, by also using recycled titanium and recycled carbon fibres for the composites, a theoretical recyclability of around 90% can be achieved for the aircraft.

13
Conclusion and Recommendations

The aim of this project was to outperform the current competitors, by coming up with an innovative, sustainable design. The innovations prove their value, especially when combined with the latest developments in already proven technologies. Findings in this report suggest the Aquila is able to form serious competition for current competitors in regional aviation, in particular the popular ATR 72. Furthermore, incorporating sustainability throughout the design showed significant improvements when comparing it with the ATR 72, which currently is the best in its class in terms of sustainability. By increasing the focus on sustainability even more in further research, the Aquila might only just be the beginning of making aviation fit in the environmentally friendly future that the world is yearning for.

Keeping in mind that regional airports are becoming more popular, the optimal number of passengers may turn out to be different for Europe and Asia. Even though the focus was put on the market in Europe, the Asian market cannot be neglected. The landscape of distant regions that are to be connected to the aviation network may turn out to be unfriendly in terms of altitude and runway length. Varying the number of passengers affects the TOFL the most, which is therefore a result of the sensitivity analysis that should be further evaluated.

The focus during the design process has been on proper implementation of the innovations, i.e. the peculiarities. The fuselage is in principle not different from conventional designs, like the ATR 72, which is why the fuselage must be worked out in more detail when continuing this project. This might introduce changes which may require adaptions to other subsystems as well.

The strut was able to allow a lighter construction of the wing with an acceptable amount of aerodynamic interference with the wing. The entire wing construction can potentially be made even lighter by increasing the use of composite material, although this highly depends on the outcome of research in the near future, as well as advancement in terms of recycling. Next to changing the material, extensive computational tools such as Abaqus or Nastran might allow further optimisation in terms of weight saving. Using such tools may also provide a more conclusive aeroelastic analysis, as the simplified method that was used did not provide a solid conclusion on this matter, and did not include non-classical forms of flutter due to the limited resources and high complexity of such analyses.

The use of LNG shows very promising results in terms of sustainability, although in terms of feasibility it highly depends on regional airports to install the required facilities and train the ground personnel. Authorities will have to take the initiative in promoting the use of LNG, by stimulating the airports that are hesitant and help the airports that do not have the resources to implement the required adaptions. Allowing a removable fuel tank might also interest other aircraft manufacturers. Low cost carriers like Ryanair will most likely be very interested in decreasing their turnaround time and increase the time-efficiency of their resources.

Another aspect that needs further evaluation to be able to start using LNG, is development of engines. For this innovation to be certified and implemented as soon as possible, it is essential that engine manufacturers will start to see the opportunities that lie in LNG, and start designing engines that run as efficient as possible on LNG. Additionally, the fuel tank requires more research on the behaviour of the LNG within the tank itself, like the weathering process and the impact of radiation. Furthermore, the exact interaction of the vacuum microspheres on the structural integrity and the impact of tank accessories on the insulation need to be analysed in more detail.

Bibliography

[1] D. P. Raymer, *Aircraft Design: A Conceptual Approach*. 370 L'Enfant Promenade, S.W., Washington D.C. 20024: American Institute of Aeronautics and Astronautics Inc., 1992.

[2] J. E. Made, "A Review of Aerodynamic Noise From Propellers, Rofors, and Liff Fans," tech. rep., NASA, 1970.

[3] A. K. Sahai, *Consideration of Aircraft Noise Annoyance during Conceptual Aircraft Design*. PhD thesis, Aachen University, 2016.

[4] M. Mehta, "Global Aviation Summit 2019: Vision 2040 for the Civil Aviation Industry in India," tech. rep., Federation of Indian Chambers of Commerce & Industry, 2019.

[5] Bombardier, *Market Forecast*, 2017.

[6] C. Hoyle, "Slow climbers." World Airliner Directory, 2018.

[7] ATR, *Turboprop Market Forecast 2018-2037*, 2018.

[8] Eurocontrol, "European Aviation in 2040: Challenges of Growth," tech. rep., Eurocontrol, 2018.

[9] Airports Council International, *European Regional Aircraft*, 2017.

[10] P. Bijl, R. Coenen, B. Harrison, B. van Manen, R. Nelen, S. Nolet, E. Peeters, T. Stolk, M. Torsij, and V. Vloeberghs, "Project Plan," tech. rep., Delft University of Technology, 2019.

[11] P. Cirillo, "Risk Management Lecture 1." Lecture slides, 2018.

[12] P. Bijl, R. Coenen, B. Harrison, B. van Manen, R. Nelen, S. Nolet, E. Peeters, T. Stolk, M. Torsij, and V. Vloeberghs, "Mid-Term Report," tech. rep., Delft University of Technology, 2019.

[13] B. W. McCormick, *Aerodynamics, Aeronautics and Flight Mechanics*. John Wiley & Sons, Inc., second ed., 1995.

[14] Dr. R. Vos and ir. J.A. Melkert, "Wing and Propulsion System Design." Lecture slides, 2018.

[15] A. Elham, "Aircraft Aerodynamic Analysis - Fundamentals." Lecture slides, 2016.

[16] Dr. J. Roskam, *Aircraft Design - Part II: Preliminary Configuration Design and Integration of the Propulsion System*. DARcorporation, 1985.

[17] A. Elham, "Aileron Design." Lecture slides, 2016.

[18] V. Holmén, "Methods of Vortex Identification," Master's thesis, Lund University, 2012.

[19] ir. J. A. Melkert, "AE1110: Introduction to Aerospace Engineering - Aerodynamics Lecture 7." Lecture slides, 2018.

[20] G. Ananda, R. Deters, and M. Selig, "Propeller-Induced Flow Effects on Wings of Varying Aspect Ratio at Low Reynolds Numbers," *32nd AIAA Applied Aerodynamics Conference*, 2014.

[21] L. Veldhuis, *Propeller Wing Aerodynamic Interference*. PhD thesis, Delft University of Technology, 2005.

[22] Dr. F. Oliviero, "AE3211-I: Systems Engineering and Aerospace Design." Lecture slides, 2019.

[23] Dr. R. Vos, "AE4240: Advanced Aircraft Design I." Lecture slides, 2019.

[24] M. H. Sadraey, *Aircraft Design: A Systems Engineering Approach*. Wiley, 2013.

[25] P. Barua, T. Sousa, and D. Scholz, "Empennage Statistics and Sizing Methods for Dorsal Fins," Master's thesis, Hamburg University of Applied Sciences, 2013.

[26] E. Torenbeek, *Advanced Aircraft Design*. The Atrium, Southern Gate, Chichester, West Sussex, PO19 8SQ, United Kingdom: John Wiley & Sons Ltd, jun 2013.

[27] D. Howe, *Aircraft Conceptual Design Synthesis*. Wiley India Pvt. Ltd., 2014.

[28] Prof. A. in 't Veld, "AE3212-I: Aerospace Flight Dynamics - Lateral Stability and Control in Steady Flight." Lecture slides, 2019.

[29] ir. J. A. Melkert, "AE1222: Aerospace Design and Systems Engineering Elements." Lecture slides, 2019.

[30] Dr. J. Roskam, *Aircraft Design - Part IV: Layout Design of Landing Gear and Systems*. DARcorporation, 1986.

[31] E. Torenbeek, *Synthesis of Subsonic Aircraft Design*. Delft University Press, 1976.

[32] R. Wanhill, *Aluminium-Lithium Alloys*. Butterworth-Heinemann, 2014.

[33] M. Kalanchiam and M. Chinnasamy, "Advantages of composite materials in aircraft structures," *International Journal of Aerospace and Mechanical Engineering, Vol:6, No:11*, 2012.

[34] Dr. G. Leeke, "Composites recycling: Where are we now?," tech. rep., Composites UK, 2016.

[35] S. Rana, *Advanced Composite Materials for Aerospace Engineering: Processing, Properties and Applications*. Woodhead Publishing, 2016.

[36] C. Karch and C. Metzner, "Lightning Protection of Carbon Fibre Reinforced Plastics," *33rd International Conference on Lightning Protection (ICLP)*, 2016.

[37] P. R. Spendley, *Design Allowables For Composite Aerospace Structures*. PhD thesis, University of Surrey, 2012.

[38] R. J. Rioja and J. Liu, "The Evolution of Al-Li Base Products for Aerospace and Space Applications," *The Minerals, Metals & Materials Society and ASM International*, 2012.

[39] T. Megson, *Aircraft Structures for Engineering Students*. Elsevier, fifth ed., 2013.

[40] W. H. Macaulay, "A note on the deflection of beams," *Messenger of Mathematics*, vol. 48, p. 129, 1919.

[41] L. Qi, *A Study of the Buckling Behaviour of Stiffened Panels under Compression and Lateral Pressure*. PhD thesis, Delft University of Technology, 2018.

[42] R. Budyanas, *Shigley's Mechanical Engineering Design*. McGraw-Hill, 9th ed., 2008.

[43] J. P. Moran, F. S. Bovard, J. D. Chrzan, and P. Vandenburgh, "Corrosion Performance Of New Generation Aluminum-Lithium Alloys For Aerospace Applications," *ICAA13 Pittsburgh*, 2012.

[44] A. A. R. Broer, "Fatigue Life Prediction Of Carbon Fibre-Reinforced Epoxy Laminates Using A Single S-N Curve," Master's thesis, Delft University of Technology, 2018.

[45] Dr. C. Rans and ir. J.A. Melkert, "AE2135-II: Structural Analysis & Design - Lecture 10." Lecture slides, 2018.

[46] W. Ko, "Shear Buckling Analysis of a Hat-Stiffened Panel," *NASA Technical Memorandum 4644*, 1994.

[47] S. J. Hulshoff, "Course ae4930: Aeroelasticity," 2011.

[48] ir. J.A. Melkert, "AE2230-II: Propulsion & Power - Slides." Lecture slides, 2019.

[49] Jane's, "Jane's All The World's Aircraft," 2019.

[50] R. M. Plencner, P. Senty, and T. J. Wickenheiser, "Propeller Performance And Weight Predictions Appended To The Navy/NASA Engine Program," tech. rep., NASA Lewis Research Center, 1983.

[51] A. Filippone, "Advanced Aircraft Flight Performance," *Cambridge University Press*, 2012.

[52] S. Gavali, "Review of Cooling of Gas Turbine Blades," *International Journal of Applied Engineering Research*, vol. 13, pp. 43–48, 2018.

[53] R. W. Graham, "Some Advantages Of Methane In An Aircraft Gas Turbine," tech. rep., NASA Lewis Research Center, 1980.

[54] W. M. Haynes, *CRC Handbook of Chemistry and Physics*. CRC Press, 96th edition ed., 2015.

[55] W. J. Kuper, " Catalytic Combustion Concept For Gas Turbines ," *Catalysis Today*, 1999.

[56] A. Guessab, A. Aris, M. Cheikh, and T. Baki, "Combustion of Methane and Biogas Fuels in Gas Turbine Can-type Combustor Model," *Journal of Applied Fluid Mechanics*, vol. 9, pp. 2229–2238, 2016.

[57] D. Plachta and P. Kittel, "An Updated Zero Boil-Off Cryogenic Propellant Storage Analysis Applied to Upper Stages or Depots in an LEO Environment," tech. rep., NASA, 2002.

[58] D. Brewer, *Hydrogen Aircraft Technology*. CRC Press, first ed., 1991.

[59] J. L. Christian and J. F. Watson, "Properties of 7000 Series Aluminum Alloys at Cryogenic Temperatures," *Advances in Cryogenic Engineering*, vol. 6, pp. 604–621, 1961.

[60] J. P. Kamperveen and M. P. N. Spruijt and J. E. A. Reinders, "Heat load resistance of cryogenic storage tanks – Results of LNG Safety Program," tech. rep., TNO, 2016.

[61] T. Kandasamy, S. Rakheja, and A. K. W. Ahmed, "An Analysis of Baffles Designs for Limiting Fluid Slosh in Partly Filled Tank Trucks," *The Open Transportation Journal*, vol. 4, pp. 23–32, 2010.

[62] H. Jeong and W. Shim, "Calculation of Boil-Off Gas Generation," *Polish Maritime Research*, vol. 24, pp. 100–114, 2017.

[63] D. S. et al., "Preparation and characterization of thermally stable polyimide membranes by electrospinning for protective clothing applications," *Textile Research Journal*, 2015.

[64] J. S. Kwon, C. H. Jang, H. Jung, and T. H. Song, "Effective thermal conductivity of various filling materials for vacuum insulation panels," *International Journal of Heat and Mass Transfer*, vol. 52, pp. 5525–5532, 2009.

[65] H. S. et al., "Permeation of Different Gases Through Foils used as Envelopes for Vacuum Insulation Panels," *Journal of Thermal Envelope and Building Science*, vol. 28, pp. 293–317, 2005.

[66] E. Lisowski and W. Czyzycki, "Transport and Storage of LNG in Container Tanks," *Journal of KONES Powertrain and Transport*, vol. 18, 2011.

[67] D. Dobrota, B. Lalic, and I. Komar, "Problem of Boil-off in LNG Supply Chain," *Transactions of Maritime Science*, vol. 02, pp. 91–100, 2013.

[68] Groupe International des Importateurs de Gaz Naturel Liquéfié, "Basic Properties of LNG." LNG Information Paper No. 1, 2013.

[69] G. Qiao, G. Liu, Z. Shi, Y. Wang, S. Ma, and T. Lim, "A review of electromechanical actuators for more/all electric aircraft systems," *Proceedings of the Institution of Mechanical Engineers, Part C: Journal of Mechanical Engineer-*

ing Science, 12 2017.

[70] Airbus, "A319/A320/A321 Flightdeck and systems briefing for pilots." Lecture slides, 1998.

[71] M. Schultz, T. Kunze, and H. Fricke, "Boarding On The Critical Path Of The Turnaround," tech. rep., Technische Universität Dresden, Dresden, Germany, 2013.

[72] E. A. S. Agency, *European Aviation Safety Agency Certification Specifications and Acceptable Means of Compliance for Large Aeroplanes CS-25*. 2018.

[73] S. S. M. Yeung, I. T. S. Yu, and K. Y. L. Hu, "World at work: Aircraft cabin cleaning," *Occupational and environmental medicine*, pp. 58–60, feb 2005.

[74] World Health Organization, Geneva, *Guide to Hygiene and Sanitation in Aviation*, 3rd ed., 2009.

[75] N. Europe, "LNG Transport Catalogue," 2017.

[76] Dr. G. A. Melhem, Dr. A. S. Kalelkar, Dr. S. Saraf, and H. Ozog, "Managing lng risks: Separating the facts from the myths." ioMosaic Corporation, aug 2006.

[77] J. J. Ruijgrok, *Elements Of Airplane Performance*. Delft Academic Press, second ed., 2009.

[78] European Aviation Safety Agency, "Certification Specifications for Large Aeroplanes CS-25, Amendment 3," 2007.

[79] U. Michel, "Correlation of Aircraft Certification Noise Levels EPNL with Controlling Physical Parameters," *19th AIAA/CEAS Aeroacoustics Conference*, 2013.

[80] EASA, "Heavy Propeller Driven Aeroplanes Noise Database." EASA Database, 2019.

[81] A. Fillipone, "Aircraft noise prediction." Article, 2014.

[82] Dr. ir. W. Verhagen, "AE4468: Airline Maintenance Operations." Lecture slides, feb 2017.

[83] J. R. Passarella, "The Value of Strategically Sourced Sub-Assembly," tech. rep., Exothermic Molding, Inc., 2012.

[84] I. B. Tucker and R. P. Wilder, "Trends in Vertical Integration in the U.S. Manufacturing Sector," *The Journal of Industrial Economics*, vol. 26, pp. 81–94, 1977.

[85] Y. Cohen, "Assembly Line Segmentation: Determining The Number Of Stations Per Section," *Journal of Manufacturing Technology Management*, vol. 24, pp. 397–412, 2013.

[86] D. E. Blumenfield and R. R. Inman, "Impact of Absenteeism on Assembly Line Quality and Throughput," *Production and Operations Management*, vol. Vol. 18 No. 3, pp. 333–343, 2019.

[87] ir. J. Sinke, "AE3211-II: Lecture Notes: Additive manufacturing." Lecture notes, 2019.

[88] ir. J. Sinke, "AE3211-II: Processes for Thermoplastic (TP) and Thermoset (TS) Composites." Lecture slides, 2019.

[89] Low Tech Magazine, "How much energy does it take (on average) to produce 1 kilogram of the following materials?." Low Tech Magazine Database, 2019.

[90] Dr. J. Roskam, *Aircraft Design - Part VIII: Airplane Cost Estimation: Design, Development, Manufacturing and Operating*. DARcorporation, 2002.

[91] Prof. Dr. R. Curran and Dr. W. Verhagen, "Concurrent Engineering & Design for Lifecycle." PowerPoint slides, 2019.

[92] D. A. I. Kumaranayaka, "Financial Analysis - Boeing and Airbus," tech. rep., London School Of Commerce, 2016.

[93] E. Asmatulu, M. Overcash, and J. Twomey, "Recycling of Aircraft: State of the Art in 2011," *Hindawi*, 2012.

[94] IFW Universität Hannover, "Processing and recycling titanium waste." Hannover University, 2016.

[95] EASA, "AMC and GM to Part 21 - Issue 2," oct 2012.

[96] Ecole Nationale de l'Aviation Civile, "IENAC16_OPS: Certification of aircraft engines." Lecture slides, 2019.

[97] M. Burston, T. Conroy, L. Spiteri, M. Spiteri, C. Bil, and G. E. Dorrington, "Conceptual design of sustainable liquid methane fuelled passenger aircraft," *20th ISPE International Conference on Concurrent Engineering*, 2013.

A
Work Division

In this appendix, the responsible authors per chapter are noted. Because of the size of the design and analysis chapters, a separate table is made for these chapters. In these tables, the responsible authors per section are given.

Chapter Work Division

Chapter	**Authors**	**Chapter**	**Authors**
Executive Overview	Robert	Analysis	See below
Introduction	Bas	Production Plan	Toon, Mathijs & Pieter
Market Analysis	Robert & Victor	Financial Analysis	Victor
Mission Analysis	Stijn & Bas	Sustainability Assessment	Pieter
Sustainable Development Strategy	Pieter	Risk Assessment	Toon & Mathijs
Risk Strategy	Toon	Compliance Matrix	Stijn & Erik
Design	See below	Project Development	Rick
Operations	Rick	Conclusion and Recommendations	Robert

Design & Analysis Work Division

Design	**Authors**
Wing	Rick & Erik
Empennage	Benjamin & Bas
Undercarriage	Bas
Materials	Robert
Structures	Matthijs, Stijn & Robert
Propulsion	Victor, Pieter & Toon
A/C Systems	Benjamin & Victor
CAD Model	Rick
Ansys	Erik

Analysis	**Authors**
Resource Allocation	Benjamin & Bas
Performance	Stijn, Pieter & Bas
Sensitivity	Benjamin & Bas
RAMS	Benjamin